DMHCA, A NOVEL SYNTHETIC LIVER X RECEPTOR AGONIST, PROTECTS FROM ATHEROSCLEROSIS IN MICE

DI Adelheid Kratzer

Institute of Molecular Biology and Biochemistry,

Center of Molecular Medicine, Medical University of Graz

Dissertation submitted at the Medical University of Graz for the degree of Doctor of medical science (Dr. scient. med.)

Graz, May 2009

1 Content

1 CONTENT I

2 ACKNOWLEDGEMENT IV

3 SUMMARY VI

4 ZUSAMMENFASSUNG VII

5 INTRODUCTION 1

5.1 MONOCYTES AND MACROPHAGES 1

5.2 VASCULAR SMOOTH MUSCLE CELLS 3

5.3 CARDIOVASCULAR DISEASE AND ATHEROSCLEROSIS 4

5.4 CHRONIC KIDNEY DISEASE 8

5.5 CHOLESTEROL METABOLISM 9

5.5.1 Cholesterol biosynthesis and hereditary defects 10

5.5.2 Regulation of cholesterol biosynthesis 14

5.5.3 Lipoprotein metabolism and reverse cholesterol transport 16

5.6 FA METABOLISM 19

5.7 CURRENT AND FUTURE TREATMENTS OF ATHEROSCLEROSIS 19

5.7.1 Preventive sanctions 19

5.7.2 Mechanical interventions (angioplasty and bypass) 20

5.7.3 Statins 20

5.7.4 Fibrates 20

5.7.5 BA sequestrants 20

5.7.6 Niacin 21

5.7.7 Ezetimibe 21

5.7.8 Angiotensin converting enzyme (ACE) inhibitors 21

5.7.9 LXR 21

5.8 NUCLEAR RECEPTORS 21

5.8.1 Coactivators and corepressors 25

5.8.2 Posttranslational modification 27

5.8.3 RXR 28

5.8.4 LXR 28

5.8.5 LXR and its influences on metabolism and disease 31

5.8.6 Agonists for LXR and their structural requirements 32

5.9 ATHEROSCLEROTIC MOUSE MODELS 34

5.10 NOVEL NON-INVASIVE MICROSCOPY TECHNIQUES 36

6 AIMS OF THIS DOCTORAL THESIS 41

7 MATERIALS AND METHODS 42

7.1 LIST OF CHEMICALS 42

7.2 BUFFER AND SOLUTION PREPARATION 43

7.2.1 Isolation medium for MPM 43

7.2.2 Phosphate buffered saline (PBS) 44

7.2.3 Solutions for Western blotting 44

7.2.4 Gel electrophoresis 44

7.3 PRIMER LIST 44

7.4 SYNTHESIS OF N, N-DIMETHYL-3β-HYDROXYCHOLENAMIDE (DMHCA) 46

7.5 CELL CULTURE 46

7.5.1 RAW264.7 (ATCC Number: TIB-71) 46

7.5.2 HepG2 (ATCC Number: HB-8065) 46

7.5.3 Caco-2 (ATCC Number: HTB-37) 46

7.5.4 Mouse peritoneal macrophages (MPM) 46

7.5.5 THP-1 monocytes (ATCC Number: TIB-202TM) 47
7.5.6 Human peritoneal macrophages (hPM) 47
7.5.7 Perinuclear blood mononuclear cells (PBMC) 47
7.5.8 Treatment of cells with agonists 47
7.6 RNA ISOLATION, REVERSE TRANSCRIPTION AND QUANTITATIVE REAL-TIME PCR 47
7.7 QUANTIFICATION OF NUCLEIC ACID CONCENTRATIONS 48
7.8 WESTERN BLOT 49
7.9 IMMUNOFLUORESCENCE 49
7.10 MICROARRAYS 49
7.10.1 ABI Mouse Genome Survey Arrays hybridizations 49
7.10.2 Data analysis of microarrays 50
7.11 DETECTION OF LXRE 50
7.12 ANIMALS AND DIETS 51
7.12.1 Mice for non-invasive microscopy 52
7.13 DISSECTIONS, CRYOSECTIONS AND STAININGS 52
7.13.1 Cryosectioning 53
7.13.2 Preparation of histological sections and lesion analysis 53
7.13.3 En face analysis of aortas 53
7.13.4 Oil red O staining 53
7.13.5 Nile red staining 54
7.13.6 Von Kossa staining 54
7.14 LIPID QUANTIFICATION AND MEASUREMENT OF ENZYMES RELATED TO LIVER INJURY 54
7.14.1 Lipoprotein profile 55
7.14.2 Neutral lipid extraction from tissues 55
7.14.3 Fecal bile acid determination 55
7.14.4 Quantification of cholesterol and triglycerides by gas chromatography 55
7.15 CHOLESTEROL BIOSYNTHESIS 56
7.16 MICROSCOPY TECHNIQUES 57
7.16.1 Two photon excitation 57
7.16.2 Second harmonic generation 57
7.16.3 Description of the system for the nonlinear multimodal imaging 58
7.17 BIOAVAILABILITY ANALYSIS OF DMHCA BY LIQUID CHROMATOGRAPHY AND TANDEM MASS SPECTROMETRY (LC-MS/MS) 59
7.18 2-D-GEL ELECTROPHORESIS 59
7.18.1 LC-MS/MS-analysis 60
7.19 STATISTICS 61

8 RESULTS 62
8.1 SYNTHESIS OF N,N-DIMETHYL-3-β-HYDROXY-Δ5-CHOLENAMIDE (DMHCA) 62
8.2 GENE REGULATION BY DMHCA IN COMPARISON WITH OTHER LXR AGONISTS IN DIFFERENT CELL LINES 66
8.2.1 Influence of time and concentration 66
8.2.2 Gene regulation in different cell lines 67
8.2.3 Microarrays and verifications 68
8.2.4 DMHCA reduces mRNA expression of inflammatory genes in mice 83
8.3 CHOLESTEROL BIOSYNTHESIS IN MPM 86
8.4 REGULATION OF PROTEINS IN LIVERS AND MACROPHAGES BY DMHCA TREATMENT 87
8.5 SHORT-TERM TREATMENT WITH DMHCA 88
8.5.1 Intraperitoneal injection of DMHCA in comparison with T0901317 88
8.5.2 High and low doses of DMHCA and T0901317 within the diet 91
8.6 BIOAVAILABILITY OF DMHCA 105
8.7 IMPACTS OF DMHCA ON ATHEROSCLEROSIS AND CHOLESTEROL METABOLISM 107
8.7.1 Chronic treatment with DMHCA 107

8.8 NON-INVASIVE MICROSCOPY TECHNIQUES: ALTERNATIVE TO CONVENTIONAL STAINING TECHNIQUES? 114
8.8.1 Traditional staining of aortas and heart valves from ApoE-/- and LDLR-/- mice.....116
8.8.2 Second harmonic generation/two photon excitation and coherent anti-Stokes Raman scattering (SHG/TPE and CARS) 118
9 DISCUSSION.....124
10 ABBREVIATIONS AND ACRONYMS.....140
11 BIBLIOGRAPHY 143
12 SUPPLEMENTAL DATA.....159
12.1 MICROARRAY DATA 163
12.1.1 Gene regulation in DMHCA-treated macrophages versus control-treated macrophages.....163
12.1.2 T0901317-treated macrophages versus control-treated macrophages.....176
12.1.3 Treated (combination of DMHCA and T0901317) macrophages versus control-treated macrophages 182
12.2 DMHCA-TREATED MACROPHAGES VERSUS T0901317-TREATED MACROPHAGES 188
12.3 ADDITIONAL LXRE.....196
12.4 PROTEIN DETERMINATION BY TWO DIMENSIONAL GEL ELECTROPHORESIS.....199

2 Acknowledgement

First of all, I want to express my gratitude to Prof. Dr. Gerhard M. Kostner and Prof. Dr. Dagmar Kratky who enabled me to perform my doctoral thesis in their laboratory at the Institute of Molecular Biology and Biochemistry, Center of Molecular Medicine, Medical University of Graz, Austria. This doctoral thesis was financed through the GEN-AU GOLD C6/II project, which was supported by the Federal Ministry of Education, Science and Culture of Austria. Moreover, I want to thank Dr. Moshe Levi for giving me the possibility to spent one year in the Department of Medicine, Division of Renal Diseases and Hypertension, located at the University of Colorado Health Sciences Center in Denver, Colorado, USA. Additionally, I want to thank Dr. Levis collaborators Dr. Bruce Tromberg and Dr. Eric Potma at the Beckman Laser Institute from UC Irvine, California, USA. This year was possible within the project in form of a mobility program.

I also want to thank my colleagues in Graz and Denver for the good and amicable working climate and interesting and fruitful discussions. My special thanks go to Marlene Buchebner and Anton Ibovnik for their help and assistance in several experiments.

Special thanks to my family and friends,

for their encouragement, motivation, help and support.

Friends are angels who lift our feet when our

own wings have trouble remembering how to fly.

In remembrance of my father.

It is through science that we prove, but through intuition that we discover (*Jules H. Pincare*).

3 Summary

Atherosclerosis is the main cause of cardiovascular disease (CVD) such as stroke or heart attack. Activation of the nuclear liver X receptors (LXR) has been shown to reduce atherosclerotic plaque formation, but the known agonists have the unfortunate side effect of inducing liver steatosis and hypertriglyceridemia. N,N-Dimethyl-3β-hydroxy-Δ^5-cholenamide (DMHCA) showed promising results and I decided to synthesize this steroidal compound and study its effects in different mouse models and its impact on atherosclerosis. I investigated differences in gene and protein regulation in mouse peritoneal macrophages, liver and other tissues upon treatment with DMHCA compared to the non-steroidal synthetic LXR agonist T0901317. However, the latter not only activates LXR, but also the farnesoid X receptor and the pregnane X receptor. Applying cDNA microarrays revealed significant differences in gene regulation between DMHCA- and T0901317-treated mouse peritoneal macrophages. Verification with real-time PCR proved the different regulatory mechanism of DMHCA, from which the downregulation of genes from cholesterol biosynthesis was the most striking effect of DMHCA. Furthermore, I investigated the effects of DMHCA on the development of atherosclerosis, liver steatosis and hypertriglyceridemia in wild type, apolipoprotein E (ApoE-/-) and low density lipoprotein receptor (LDLR-/-) knockout mice. I could show that DMHCA reduced atherosclerotic plaque formation in ApoE-/- mice without induction of liver steatosis or hypertriglyceridemia.

The second part of my thesis is assigned to chronic kidney disease (CKD) and its involvement in CVD. In fact, CKD leads not only to plaque development, but also to vascular calcification. The aim was the detection of atherosclerotic plaques and vascular calcification within the aorta in different models of renal failure in male ApoE-/- mice using state-of-the-art microscopy techniques compared to traditional staining techniques. Second harmonic generation (SHG) / two photon excitation (TPE) and coherent anti-Stokes Raman scattering (CARS) techniques were applied. SHG was used for identification of the structural protein collagen and TPE for detection of autofluorescence signal from elastin. CARS allowed detection of lipids and calcium-hydroxyapatite within atherosclerotic plaques. This approach was compared to standard staining techniques such as oil red O for lipids and von Kossa for calcium deposits. The non-invasive *in vivo* imaging with SHG/TPE and CARS techniques allows studying atherosclerotic plaque development at any stage of disease or intervention.

4 Zusammenfassung

Atherosklerose ist hauptverantwortlich für die Entstehung von kardiovaskulären Erkrankungen wie Schlaganfall oder Herzinfarkt. Die Aktivierung der nuklearen Liver X Rezeptoren (LXR) war erfolgreich in der Verminderung von atherosklerotischen Plaques. Leider führt LXR Aktivierung auch zur Entstehung von Lebersteatose und Hypertriglyzeridämie. N,N-Dimethyl-3β-hydroxy-Δ^5-cholenamide (DMHCA) zeigte diesbezüglich erfolgsversprechende Resultate, woraufhin wir diesen Agonisten synthetisierten und seine Eigenschaften in verschiedenen Mausmodellen untersuchten. Erforscht wurden die Unterschiede in der Gen- und Proteinregulation zwischen DMHCA und dem vielfach verwendeten, synthetischen nicht-steroiden LXR Agonisten T0901317, welcher nicht nur LXR, sondern auch den Farnesoid X Rezeptor und den Pregnane X Rezeptor aktiviert. Durch die Verwendung von cDNA Microarrays konnte ich einen signifikanten Unterscied in der Genregulation von DMHCA- und T0901317 behandelten Mausmakrophagen zeigen. Verifizierung mittels real-time PCR bestätigte diese Ergebnisse, wobei die Hinunterregulierung von Genen der Cholesterinbiosynthese am auffälligsten war. Ich untersuchte die Effekte von DMHCA auf die atherosklerotische Plaqueentwicklung in einem atherosklerotischen Mausmodell, den Apolipoprotein E-defizienten (ApoE-/-) Mäusen, und konnte eine deutliche Reduktion derselbigen durch DMHCA in ApoE-/- Mäusen feststellen, ohne Entwicklung von Lebersteatose oder Hypertriglyzeridämie.

Der zweite Teil meiner Dissertation befasste sich mit chronischer Nierenerkrankung, welche die Entstehung von Atherosklerose unterstützt und zu Kalzifizierung der Plaques führt. Ziel war die Erforschung von atherosklerotischen Plaques und und deren Kalzifizierung in ApoE-/- Mäusen mit eingeschränkter Nierenfunktion. Anwendung fanden second harmonic generation (SHG) / two photon excitation (TPE) und coherent anti-Stokes Raman scattering (CARS). SHG wurde zur Detektion des Strukturproteins Kollagen verwendet und TPE zur Erfassung der Autofluoreszenz von Elastin. CARS fand Anwendung in der Lipid- und Kalziumdetektion. Diese moderenen Mikroskopietechniken wurden mit konventionellen Standardfärbetechniken verglichen (Ölrot O für Lipide und von Kossa für Kalzium). Nicht-invasives Mikroskopieren ermöglicht das Erforschen von atherosklerotischen Plaques und deren Kalzifizierung sowie die Kontrolle der Wirksamkeit eines potentiellen plaquereduzierenden Medikamentes zu jedem beliebigen Zeitpunkt.

5 Introduction

Cardiovascular diseases (CVD) are aftereffects of atherosclerosis. They comprise coronary heart disease such as heart attack, cerebrovascular disease including stroke, raised blood pressure (hypertension), peripheral artery disease, rheumatic heart disease, congenital heart disease, and heart failure. CVD are the number one cause of death worldwide and are estimated to remain in this leading position. In 2005, 17.5 million people died from CVD, representing 30 % of all global deaths. If current trends are allowed to continue, by 2015 an estimated 20 million people will die from CVD, mainly from heart attacks and strokes. These data are derived from http://www.who.int/mediacentre/factsheets/fs317/en/index.html by the World Health Organization facts sheet. In fact, risk for cardiovascular events start already in childhood and early adolescence. Children that suffer from obesity or diabetes are at high risk to develop early atherosclerosis, but precautionary actions can help preventing this fate (1).

The main cause for CVD is atherosclerosis from athero (soft, gruel-like deposit) and sclerosis (hardness). Atherosclerosis is defined by the deposition of fats, cellular metabolites, cholesterol, calcium, and various other substances on the inner lining of the artery (2). Atherosclerosis is described as a chronic inflammatory disease characterized by abnormal thickening and hardening of the arterial walls with resulting loss of elasticity. It is characterized by plaque deposits and fibrosis of the inner layer of the arteries (3).

5.1 Monocytes and macrophages

The mononuclear phagocyte system has been defined as a family of cells comprising bone marrow progenitors, blood monocytes, and tissue macrophages (4). Their developmental procedure is shown in Figure 1. Macrophages play an important role in different metabolic pathways and are supposed to represent the “policemen” of the mammalian body that work against exogenous or endogenous protruders, which are phagocytosed by “big eater” cells (macro=big, phagos=eat). Macrophages belong to the most versatile cells of the body. Heterogeneity arises as macrophages differentiate from monocyte precursors and is determined by the genetic background as well as by specific tissue-related and immune-related stimuli [5]. Depending on their location as well as the kind of stimulus macrophages can exert a lot of different functions and play a role in inflammation, wounding, tissue repair, bone remodeling, and malignancy (5).

Macrophages are resident cells within many different tissues where they exhibit different functions depending on their environment. They might also be recruited upon a certain external

stimulus such as inflammation or bacterial infection and become so-called "activated" macrophages (4). Yet, also resident macrophages can become activated which is the case in certain diseases, for example in multiple sclerosis or other neurodegenerative diseases (6). Depending on the tissue we distinguish between blood monocytes, peritoneal macrophages that are recruited in the peritoneum after any inflammatory stimulus, Kupffer cells in the liver, splenic macrophages, pulmonary macrophages with three subpopulations (alveolar, interstitial and intravascular), pleural macrophages, microglia in the brain, macrophages of the gastrointestinal mucosa, and endocrine macrophages, kidney and synovial macrophages. Testicular, ovarian and uterine macrophages play important roles in the reproductive organs (4).

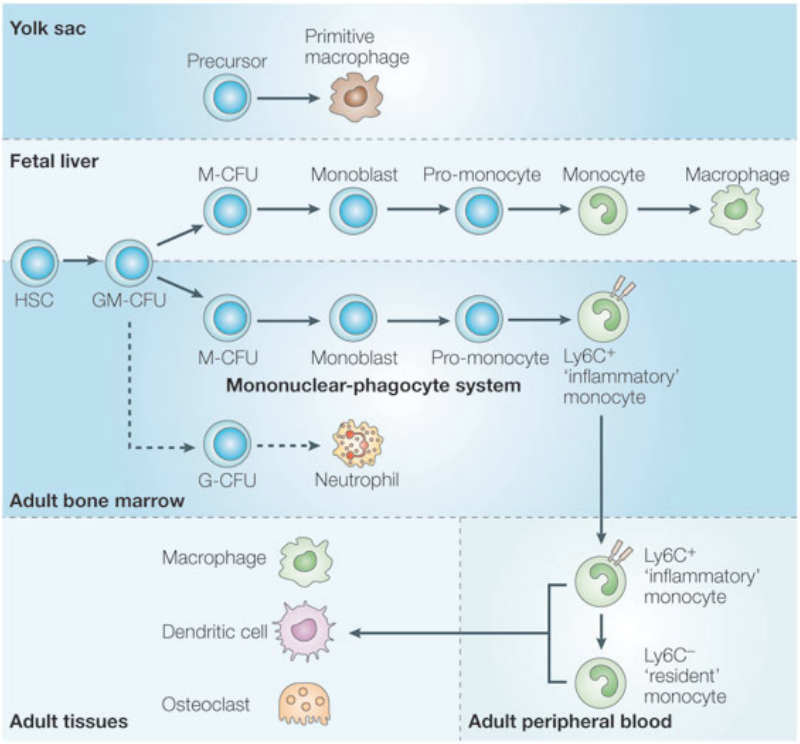

Figure 1. Development and differentiation of monocytes and macrophages (5)
Macrophages are first found in the yolk sac, showing morphological characteristics and expression of macrophage markers such as colony-stimulation factor-1 receptor (c-fms), CD11b, and the mannose receptor. Later, haematopoiesis in the fetal liver, which defines the formation and development of blood cells, becomes a source of macrophages that resemble those present in adults. Haematopoiesis in the liver generates a large amount of macrophages, which are present in most organs. Although monocytes can be precursors for the replacement of tissue-resident macrophages, many of them might be derived from local proliferation in the adult rather than from recruited peripheral monocytes. When bone-marrow monocytes are released into the peripheral blood, they have a Ly6C+ phenotype and are defined as the so-called 'inflammatory' monocytes, belonging to the M1 state. They are thought to differentiate into a phenotypically distinct (Ly6C-) cell subset, which is also called 'resident' monocyte or M2 state. Both subtypes can differentiate to either macrophages, dendritic cells or osteoclasts (5).

A crucial step in atherogenesis consists of the infiltration of monocytes into the subendothelial space of large arteries, where monocytes differentiate into macrophages or dendritic cells (7). Macrophages are a heterogeneous cell population that adapt and respond to a large variety of microenvironmental signals (8). The activation state and function of mononuclear phagocytes are highly affected by cytokines and microbial products. While Th1 cytokines such as interferon gamma (IFNγ) and interleukin-1beta (IL-1β), or lipopolysaccharide (LPS) induce a "classical"

activation profile, also defined as M1 state, Th2 cytokines (e.g. IL-4 and IL-13) induce an "alternative" activation program (M2) in macrophages (Figure 1). Moreover, macrophages are plastic cells because upon specific signals they can switch from an activated M1 state back to M2 state and vice versa (9). M1 macrophages are potent effectors that kill microorganisms and produce primarily proinflammatory cytokines, for example tumor necrosis factor alpha (TNF-α), IL-6, and IL-12 (10). In contrast, M2 macrophages dampen these inflammatory and adaptive Th1 responses by producing anti-inflammatory factors (IL-10, transforming growth factor beta (TGF-β), and IL-1 receptor antagonist (IL-1Ra)), scavenging debris, and promoting angiogenesis, tissue remodeling, and repair (11). Thus, inflammatory diseases such as atherosclerosis may be caused not only by a sustained proinflammatory reaction but also by failure of anti-inflammatory control mechanisms. It is difficult to distinguish between the two types of macrophages as well as to study the mechanisms that control the switch from one state to the other (12, 13).

5.2 Vascular smooth muscle cells

Another type of cells that play an important role in the development of atherosclerosis, specifically calcification, comprises the vascular smooth muscle cells (VSMC). VSMC are plastic cells, which respond to different growth factors. They are responsible for a variety of functions in the arterial intima. In fact, they can proliferate and endoreduplicate (dublicate their genome without undergoing mitosis), undergo hypertrophy, or apoptosis (14). VSMC are responsible for contractility and maintenance of structural integrity by synthesizing collagen, elastin, and proteoglycans. Moreover, similar to macrophages, they are able to remove lipids by the expression of low density lipoprotein receptor (LDLR) and/or by phagoytosis (15).

Among the mechanisms utilized by VSMC to mediate these varying cellular responses are autocrine and paracrine signaling pathways. An autocrine growth mechanism is one in which the individual cell synthesizes and/or secretes a substance that stimulates the same cell type to undergo a growth response. A paracrine growth mechanism is one in which the individual cells respond to growth factors synthesized and/or secreted by neighboring cells of another cell type (14). Most smooth muscle cells are found in the media, but also a significant number of these cells are present in the intima. These areas are conserved areas and known as places of "intimal thickenings", which are often found in arterial branchpoints and areas of increased blood flow (16). These locations are also correlated with advanced lesions at later stages of atherosclerosis.

Unfortunately, no rodent animal model that develops intimal thickening exists so far (15). One well studied situation in which VSMC growth occurs is after blood vessel injury. The pattern of events that lead to vessel repair and intimal thickening is likely similar in different species and

different types of arteries. Many candidate molecules that regulate VSMC growth have been studied in the rat carotid injury model by use of pharmacological and gene therapy approaches (17). Results suggest important roles for the renin-angiotensin system, catecholamines, endothelin-1, natriuretic peptides, thrombin, platelet derived growth factor, TGF-β and other activins, fibroblast growth factor, oxidative stress, nitric oxide, and the estrogen receptor. Vascular remodeling is a physiological response to alterations in flow, pressure, and atherosclerosis (14). Medial VSMC express mainly proteins that have contractile function such as α-actin, whereas intimal VSMC generally express extracellular matrix proteins, proteases and cytokines (synthetic state). Depending on the atherosclerotic stimuli these cells can switch from the "contractile" to the "synthetic" state and produce more collagen (18).

VSMC are known to play important roles in advanced stages of atherosclerosis such as atheroma building and calcification. Yet, they can have similar functions as macrophages in earlier stages of atherosclerosis. The expression of receptors for LDL and very low density lipoprotein (VLDL) confirms the fact that VSMC might become lipid-laden (19). Moreover, they also express relevant genes for promoting the reverse cholesterol transport (RCT), which will be described in 5.5.3 (20). VSMC also show antiapoptotic effects on monocytes and macrophages. Together with cytokine production and extracellular matrix production, which attract monocytes from the blood, the abilities of VSMC indicate their important role in the early stage of atherosclerosis (16). VSMC have currently been shown to be responsible for vascular calcification, which is similar to bone mineralization. The calcification is referred to as the deposit of calcium hydroxyapatite and the presence of components related to bone morphogenesis such as plasma phosphate levels (21, 22). Vascular calcification is an important factor in the increase of late stage atherosclerosis and cardiovascular morbidity. Calcification of the heart valves and the aortic vessel walls is associated with aging, diabetes, and uremia (23).

5.3 Cardiovascular disease and atherosclerosis

Initiating events of atherosclerosis may be different under distinct circumstances, but endothelial dysfunction is one of the major initiating events. This dysfunction may arise due to many factors including vessel injury and collagen exposure, metabolite deposition in the vessel wall (increase in lipids, such as cholesterol), or change in vascular reactivity due to change and rate of the blood flow (24). However, the initial cause of atherosclerosis is not known. There are many environmental and risk factors, which are known to accelerate atherosclerosis: cigarette smoke, obesity, diabetes, chronic kidney disease (CKD) (25), lack of physical activity, lipid- and glucose-rich diets as well as stress and alcohol. Altered nitric oxide production, lipid accumulation and chemokine release by the endothelium leads to upregulation of the endothelial cell adhesion molecules and receptors (Figure 2) (26).

Monocytes adhere to the endothelium with the help of specific adhesion molecules such as vascular cell adhesion molecule (VCAM) or intracellular adhesion molecule (ICAM). The macrophage chemoattractant protein (MCP-1) binds to its chemokine receptor CCR2 and helps migration of monocytes to the sub-endothelial space. Once monocytes are in the endothelium, they differentiate into macrophages. Macrophages belong to the defense machinery of the body against bacteria, viruses or toxic substances such as oxidized lipids. There are several uptake mechanisms for lipids in macrophages such as receptor-mediated or receptor-independent endocytosis.

As soon as macrophages are activated by a stimulus such as macrophage colony stimulating factor (M-CSF) or modified lipids, they start taking up different forms of lipids such as minimally modified low-density lipoprotein (mmLDL), acetylated (acLDL) and oxidized LDL (oxLDL) (27) as shown in Figure 2. They can also take up cholesterol esters (CE) from high density lipoprotein (HDL) via scavenger receptors. Those scavenger receptors are for example macrophage scavenger receptor A (MSR-A), scavenger receptor lass B type I (SR-BI) or fatty acid translocase (FAT), also called CD36. CE, associated with the plasma membrane, are captured by ApoE and internalized by cells in a mechanism that involves the LDL receptor-related protein. Assuming that both macrophages and adipocytes express this pathway, suggests that this mechanism has a function in selective high-density lipoprotein (HDL) CE uptake in SR-BI-deficient cells (28).

Once macrophages have taken up external lipids, they start secreting inflammatory mediators such as cytokines (INFγ, CD40), which attract smooth muscle cells (SMC). Consequently, the SMC also start migrating into the intima and contribute to the formation of a fibrous plaque by proliferating and secreting extracellular matrix proteins. The building of a fibrous cap is also supported by an increase in collagen and fibrin, which usually takes place at a later stage of atherosclerosis (15).

Macrophages interact with other cells in the endothelium including T helper cells (Th) and VSMC via various receptors and cytokines, such as IL. This causes an enhanced inflammatory response (29), however, certain anti-atherogenic mediators are also released. One of those is IL10, which was shown to have a protective role in atherosclerosis (30). Macrophages cannot always deal with the huge amount of endocytosed lipids or non-lipid material. Therefore, they start undergoing apoptosis inside the endothelium, leading to their phagocytic clearance. Necrotic death of macrophages and VSMC leads to accumulation of insoluble lipids and other cellular material such as calcium hydroxiapatite, a characteristic of atherosclerosis and calcification in advanced lesions (Figure 2) (31).

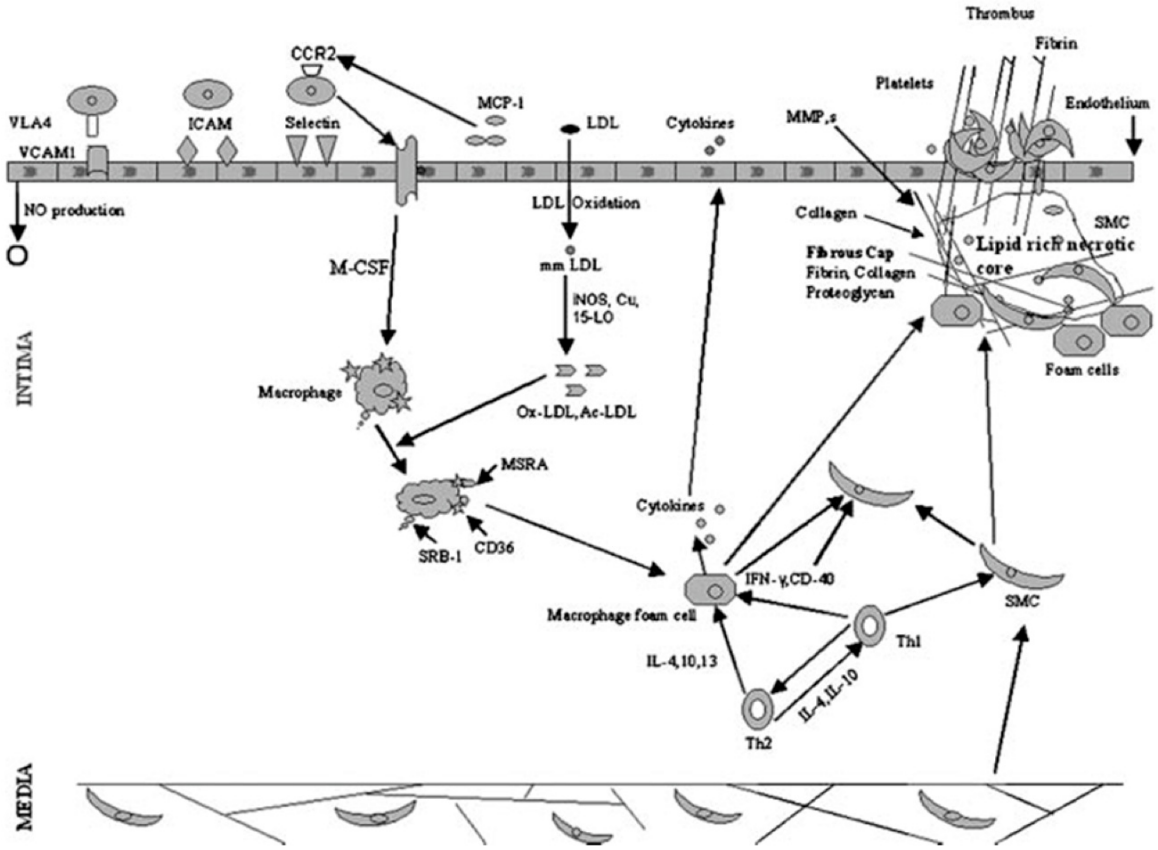

Figure 2. Description of plaque development (31)

Initial events in atherosclerosis include altered nitric oxide production, endothelial dysfunction, secretion of inflammatory cytokines, and monocyte activation and recruitment. Monocytes adhere to the endothelium via cell adhesion molecules like VCAM, ICAM, and selectins. MCP-1 binds to its receptor CCR-2 and facilitates monocyte activation and adhesion to the endothelium. LDL, taken up by the endothelium, gets converted to mmLDL and further to oxLDL and acLDL by the action of free radical-generating enzymes like inductible nitric oxide synthase (iNOS), lipoxygnases, nicotinamide adenine dinucleotide phosphate (NADPH) oxidase, and also metal ions such as copper (cu). Inside the endothelium, monocytes differentiate into macrophages in presence of MCS-F. Subsequently, these differentiated macrophages accumulate oxidized lipids via their scavenger receptors, especially SR-A and CD36. Accumulation of LDL-derived cholesterol esters leads to formation of macrophage foam cells. Interaction of these foam cells with T helper cells (Th1 and Th2) within the endothelium leads to release of various cytokines including IFNγ, CD40 and various interleukins. Cytokine release is followed by proliferation of VSMC, which migrate from media to the intima and accumulate along with the macrophages. Cell-cell interaction between the macrophages, Th cells and VSMC leads to further secretion of inflammatory mediators. Necrotic death of macrophages and VSMC leads to accumulation of insoluble lipids and other cellular components. This also leads to the development of a lipid- rich necrotic core, while fibrin, collagen, and proteoglycans form the fibrous cap, which keeps the plaque stable. Macrophage apoptotic death also leads to the release of matrix metalloproteinases (MMP), which degrade the extracellular matrix proteins. This degradation and concomitant neovascularization cause plaque instability and rupture. As a consequence, blood and tissue factor get exposed to each other and provoke activation of the coagulation cascade. Fibrin gets deposited, platelets get activated and thrombi can form (31).

In atherosclerosis, macrophages are likely recruited to early plaques to phagocytose oxidized lipids and apoptotic cells. However, within the vessel wall, macrophages contribute to lesion growth and plaque rupture by secreting growth factors and proteolytic enzymes. It has been difficult to distinguish the ‘‘good’’ from the ‘‘bad’’ macrophages in plaques and to identify molecular mechanisms that control their conversion from one state to the other (13).

Cholesterol accumulation and endoplasmatic reticulum (ER) stress promotes the unfolded protein response (UPR) which is supposed to help cells withstanding ER stress. Yet, persistent imbalance of the ER stress and the UPR leads to apoptosis and death of macrophages and consequently to increased plaque formation (32). Insulin resistance is also correlated with atherosclerosis. Insulin-resistant macrophages have impaired phagocytic clearance, leading to apoptosis and necrosis within the atherosclerotic plaque (33). Death of macrophages leads to release of inflammatory metalloproteinases (MMP), which degrade the fibrotic cap of the plaque resulting, together with neovascularization, in instability, vulnerability, and plaque rupture (34). Both macrophages and VSMC undergo apoptosis and it is still not clear if apoptosis is more pro- or antiatherosclerotic. While apoptosis in endothelial cells and VSMC is detrimental for plaque stability, apoptosis of macrophages in early stage disease might be beneficial for plaque stability. Since lipid lowering causes a decrease in macrophage accumulation in the plaque it might be interesting if apoptosis induction of macrophages shows the same result. Depending on the outcome of such studies, the development of apoptosis-inducing drugs could be used for atherosclerosis prevention (35).

The plaque development within the aorta and its arteries is site-specific and mostly takes place in the branches of the vessels, especially where intimal thickening takes place. In fact, those locations of advanced atherosclerotic lesions are the heart valves, the aortic arch, the coronary arteries (innominate artery (IA), left common carotid artery (LCC) and left subclavian artery (LSA)), and the renal arteries (36, 37). The main cause for that is restricted blood flow according to natural bending and turning of the aorta. In general, first plaque development takes place proximally and only later distally. Figure 3 reflects the structure of an aorta.

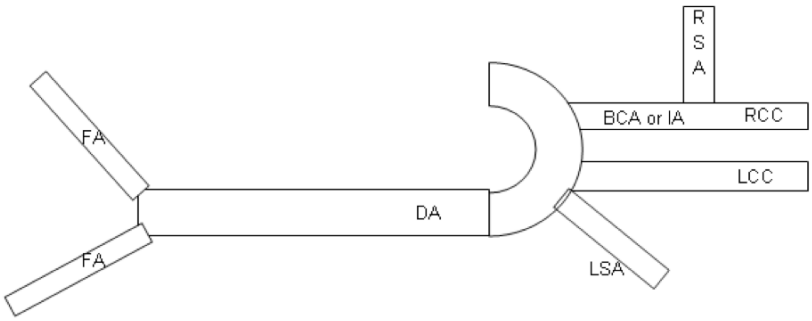

Figure 3. Sketch of an aorta
FA…femoral artery, RSA…right subclavian artery, RCC…right common carotid artery, LCC…left common carotid artery, LSA…left subclavian artery, DA…descending artery, BCA…brachiocephalic artery, IA…innominate artery

There are usually six stages in the development of atherosclerosis (Figure 4). Phase I defines the migration of monocytes into the intima upon any kind of inflammation. These monocytes then differentiate into macrophages, which ingest excessive lipids to form the so-called foam cells. At this stage the formation of fatty streaks in the arterial wall takes place (phase II). Then, increased intracellular lipid levels are accompanied by an extracellular lipid accumulation, which causes the formation of a lipid core. These stages of atherosclerosis are called

intermediate lesion and atheroma formation (phase III and IV). Further accumulation of lipids and other cellular material leads to several lipid cores together with fibrosis and calcific layers (phase V or fibroatheroma). The late stage, which equals phase VI, is defined as complicated lesion, where unstable plaques can undergo rupture, hemorrhage, and thrombosis (38).

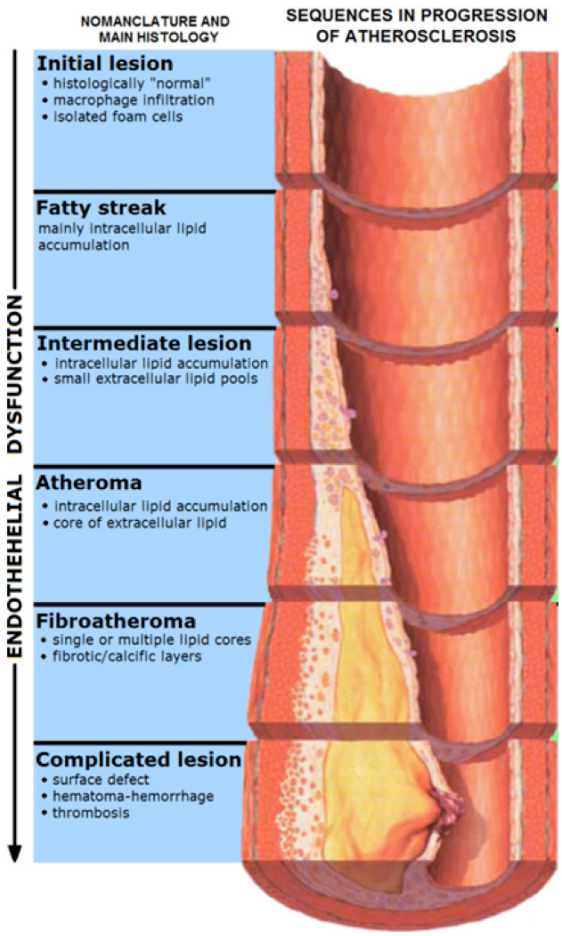

Figure 4. Characterization of the different stages in atherosclerosis (37) Atherosclerosis timeline, showing the underlying role of endothelial dysfunction in the progression of atherosclerosis from initial lesion to complicated lesion. There are six different stages until the lesion becomes dangerous and close to instability and rupture (37, 39).

There are several cells involved in atherosclerotic development, such as endothelial cells, neutrophilic granulocytes, macrophages derived from monocytes (5.1), and VSMC (5.2).

5.4 Chronic kidney disease

Chronic kidney disease (CKD) increases and accelerates the incidence of CVD, but the mechanism of how CKD is related to CVD is not yet fully understood. Usually, CKD patients in late stage develop hyperphosphatemia, which results in vascular calcification. In fact, CKD patients show increased cardiovascular morbidity compared with the general population and usually die before they reach the end-stage kidney disease with renal replacement (40). In these patients mineralization of soft tissue, including the vasculature, are observed.

Vascular calcification leads to increased pulse, increased cardiac work, left ventricular hypertrophy, and decreased coronary artery blood flow. Phosphorous (Pi) is implicated in the

change of gene transcription of VSMC proteins involved in osteoblast function, bone formation (41) and stimulating matrix mineralization (42, 43). The Pi pool in the body consists of intracellular Pi, to a lesser extent of the skeletal mineralization front and less than 1% of serum Pi. Part of the Pi is excreted by the kidney, another part by the intestine and some skeletal Pi removal also takes place. In CKD, the Pi balance is impaired leading to hyperphosphatemia. The reservoir function of the skeletal is blocked, leading to bone disorders as well as deposits in soft tissue organs such as the vasculature. Vascular calcification in CKD can occur both in atherosclerotic neointimal plaques as well as in the arterial media, the latter being the most important factor for vessel stiffness (40). Phosphate-calcium, namely calcium hydroxyapatite, and calcite crystals deposit in the atherosclerotic plaque, both in the intima and media. Calcification takes place at any developmental stage but is certainly higher at the late stage of atherosclerosis and much more pronounced in chronic renal failure, in fact as early as 6 weeks post uremia creation. Increased collagen content is also related to vascular calcification (44) and von Kossa staining can easily identify calcification. The mechanistic explanation of vascular calcification is not yet fully understood, but it certainly involves differentiation of VSMC into bone cells.

Surgical interventions that mimic the influence of CKD on atherosclerosis were performed by total or partial removal of the kidneys, where one kidney is removed (uninephrectomized mice) or the 5/6 nephrectomized mice, where one kidney and 2/3 of the second kidney are removed.

5.5 Cholesterol metabolism

The name cholesterol is derived from the Greek chole- (bile) and stereos (solid), and the chemical suffix -ol for an alcohol. François Poulletier de la Salle first discovered it in 1769 in solid form in gallstones. However, it was only in 1815 that chemist Eugène Chevreul named the compound "cholesterine"(45)

Cholesterol is a lipophilic, waxy alcohol with a steroidal structure (Figure 5). The definition sterol derives from a combination of **ste**roid and alcoh**ol**. Together with phospholipids (PL) cholesterol builds up cellular membranes. Cholesterol is required for membrane fluidity and is the precursor for sex hormones (46). The cholesterol content of a human body is about 0.2% of its body weight. Cholesterol is taken up with the diet in a quantity of about 100-500mg per day, depending on the diet. Cholesterol is also synthesized in all cells and tissues of the body, most highly in the brain, which synthesizes almost all of its cholesterol itself and cannot take up cholesterol from the circulation (47). The intestine, adrenal glands and reproductive organs follow the liver. In fact, about 1.5-2g per day is produced by *de novo* synthesis in the liver (48). There, cholesterol is either transported to peripheral tissue or converted to bile acids (BA) and

further transported to the intestine. Intestinal cholesterol absorption efficiency in humans is about 60%, but varies in healthy subjects (49, 50). Since cholesterol is a lipophilic molecule and insoluble in blood, it is transported in the circulatory system within hydrophilic blood lipoproteins. Cholesterol is essential for each cell, but accumulation of unesterified "free" cholesterol (FC) or cholesterol esters (CE) is the main cause of atherosclerosis.

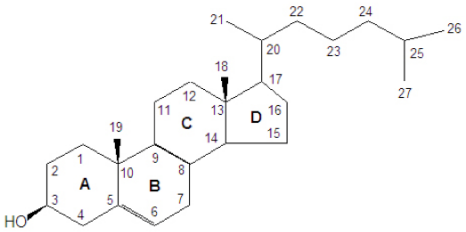

Figure 5. Chemical structure of cholesterol
The chemical name is cholest-5-en-3β-ol. Cholesterol is a polycyclic alcohol that belongs to the group of sterols within the steroids and is designated a lipid, although it doesn't belong to the group of fats. The basic structure is a sterane, which consists of three hexamerous rings and one pentameric ring.

5.5.1 Cholesterol biosynthesis and hereditary defects

Cholesterol belongs to the isoprenoids and the synthesis starts with acetate that is converted to acetyl-CoA. It involves a complex set of about 30 enzymatic reactions, where the C_{27}-sterol is build up from C_2-components. The four most import steps are synthesis of 1) mevalonate, 2) the "active isoprene" isopentenyl-diphosphate, 3) polymerization to squalene, and 4) cyclization to cholesterol (51-54) (highlighted in Figure 6).

The first seven enzymes of cholesterol biosynthesis are soluble proteins with the exception of 3-hydroxymethyl-3-methylglutaryl-CoenzymeA reductase (HmgCoAr). HmgCoAr is the key enzyme of cholesterol biosynthesis and is regulated by a negative feedback mechanism from sterols or non-steroidal metabolites derived from mevalonate and from excessive cholesterol uptake by the diet. Insulin and thyroxin stimulate the enzyme and glucagon inhibits it. The inactive form of the enzyme is phosphorylated. As far as its key role in cholesterol biosynthesis is concerned, pharmacological interventions take place here. Statins block the enzyme and therefore help reducing plasma cholesterol, which is taken up by receptor-mediated endocytosis. Reactions generating mevalonate can also take place in the peroxisome and its conversion to farnesyl-pyrophosphate is exclusively peroxisomal. The remaining reactions of cholesterol biosynthesis take place in the ER with membrane-bound enzymes and substrates (51).

The first sterol intermediate, lanosterol, is formed from squalene and then further converted to cholesterol, which involves a lot of different steps such as reduction of C-24 double bond, removal of three methyl groups, and migration of the C-8(9) double bond. The saturation of the C-24 double bond of lanosterol takes place at different points and creates two immediate precursors for cholesterol, desmosterol and 7-dehydrocholesterol (DHC7) (51). The abundance

of cholesterol varies among tissues, whereas desmosterol is present in the developing mammalian brain (55).

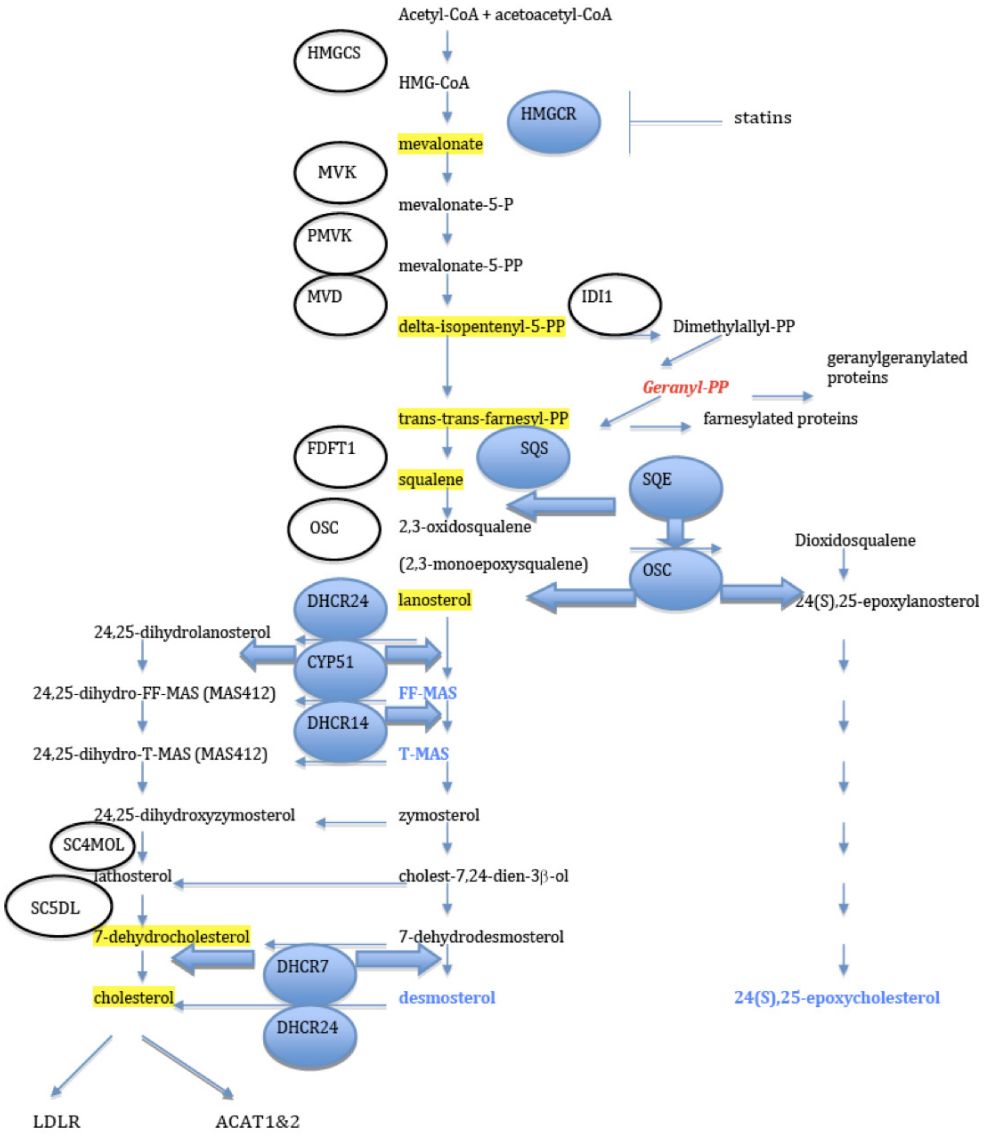

Figure 6. Cholesterol biosynthetic pathway
Intermediates and products of liver X receptor (LXR) agonism are highlighted in blue whereas geranylgeranyl-pyrophosphate, a LXR antagonist, is marked in red. Many intermediates in the synthesis of 24(S),25-epoxycholesterol from 24(S),25-epoxylanosterol have not yet been studied concerning LXR agonism and are not shown. Intermediates that have important roles in synthesis of further components are highlighted in yellow. The represented enzymes are: 3-hydroxy-3methylglutaryl-coenzyme A reductase (HMGCR), squalene synthase (SQS), squalene epoxidase (SQE), oxidosqualene:lanosterol cyclase (OSC), 3-β-hydroxysterol Δ^{24}-reductase (DHCR24), lanosterol 14α-demethylase (sterol 14-demethylase) (CYP51), sterol 14α-reductase (DHCR14), 7-dehydrocholesterol reductase (DHCR7), mevalonate kinase (MVK), phosphomevalonate kinase (PMVK), mevalonate (diphospho) decarboxylase (MVD), isopentenyl-diphosphate-δ-isomerase 1 (IDI1), farnesyl diphosphate synthetase (FDPS), squalene epoxidase (SQLE), lanosterol synthase (LSS), sterol-C4-methyl oxidase-like (SC4MOL), NAD(P)-dependent steroid dehydrogenase like (NSDHL), sterol-C5-desaturase-like (SC5DL), low density lipoprotein receptor (LDLR), acyl-CoA:cholesterol acyltransferase (ACAT) (53, 54).

Figure 6 shows a summary of the most important enzymes in cholesterol biosynthesis, highlighting important intermediates that are necessary for the synthesis of other compounds.

The isoprenoid intermediates serve as precursors for isopentenyl tRNAs involved in protein synthesis as well as dolichol, ubiquinone, and heme A (51). Derivatives of lanosterol and lathosterol have meiosis-stimulating activities (56) and accumulate in the ovary and testis. 7-deoxycholesterol is the precursor of vitamin D synthesis. Cholesterol itself is important for BA and steroid hormone synthesis and can, together with other intermediates, be converted to oxysterols that are able to act as regulatory signaling molecules and activate nuclear receptors such as LXR (57). All intermediates, which have been shown to have LXR activating potential, are highlighted in blue (Figure 6). Moreover, hedgehog signaling molecules, which are involved in a number of developmental processes, can be modified by cholesterol (58).

Impaired cholesterol content in the blood leads to hypercholesterolemia, which might be the consequence of other diseases such as diabetes, kidney disease, hypothyroidism, anorexia nervosa or family history. Actually, the familial hypercholesterolemia is a genetic disorder due to a mutation in the LDLR.

There are a lot of genetic disorders known which are related to dysfunction of cholesterol biosynthesis, mainly downstream of mevalonate. If there is a defect in e.g. mevalonate kinase (MVK), the synthesis of cholesterol and isoprenoids cannot take place. A patient suffering from this rare disease called mevalonic aciduria is not able to grow. The disease is very rare and most patients decease in infancy and early childhood (59).

There are six disorders related to defective enzymes in the post-squalene cholesterol biosynthesis: desmosterolosis, X-linked dominant chondrodysplasia punctata, CHILD syndrome, lathosterolosis, hydropsectopic calcification-moth-eaten skeletal dysplasia and the most common cholesterol biosynthetic disorder, Smith–Lemli–Opitz syndrome. All of them show major developmental malformations that are unusual for metabolic disorders (51). The development of knock out mouse models allows studying these rare diseases.

Smith–Lemli–Opitz syndrome (SLOS) was the first described disease related to malfunction in cholesterol biosynthesis and identified in 1993 (60). The disease results from enzymatic deficiency in DHC7 reductase (DHCR7) and shows characteristics such as microcephaly, ptosis, a small nose with anteverted nares and micrognathia, growth and mental retardation, poor feeding in infancy often requiring placement of a gastrostomy tube and many more. Treatment of SLOS is usually performed by cholesterol supplementation in form of eggs and oils. This therapy can improve growth and developmental defects but not mental retardation since brain cholesterol has to be synthesized *in situ*. Two DHCR7 knockout (Dchr7-/-) mouse models have been reported so far. The pups of both homozygous Dhcr7-/- models die shortly after birth, do

not suckle and show immature tissue development (51). Selective reconstitution of liver cholesterol biosynthesis did not prevent neonatal lethality in the Dhcr7-/- mice (61).

Desmosterolosis is an autosomal recessive disorder, which results from mutations or deficiencies in the 24-dehydroxycholesterol reductase (DHCR24). DHCR24 catalyzes the conversion of desmosterol to cholesterol. So far, only two patients have been reported with this disease. One female, who died 1 hour after birth, showed similar facial features and malformations as in SLOS and high plasma desmosterol levels, whereas the second patient showed much less severe syndromes (51, 62). In order to better understand this severe disease, Dhcr24-/- mice were created. In one study, knockout mice died shortly after birth and their skin was wrinkleless, movement was restricted, and they could not suckle. Examination of the skin showed lethal restrictive dermopathy, suggesting that DHCR24 was necessary for normal skin development (63). In the second study, a different group reported that the Dhcr24-/- mice were viable with minor abnormalities, but are not able to reproduce. Lack of this enzyme was shown to be compatible with life indicating that desmosterol can replace cholesterol in a lot of membrane-related functions, but severe abnormalities in sterol homeostasis take place (64, 65). Moreover, desmosterol was shown to activate LXR, which was also the case for several other sterol intermediates in the cholesterol biosynthesis (highlighted in blue in Figure 6) (64, 66). Furthermore, DHCR24, was described to mediate the neuroprotective effects of estrogens in addition to its own protective role in Alzheimer's disease (67).

X-linked dominant chondrodysplasia punctata (CDPX2, also called Conradi–Hunermann or Happle syndrome) is a rare X-linked disorder with skeletal, skin and ocular manifestations and presumed male lethality. The reason for this disease is suggested in mutations of the gene encoding the Δ^8, Δ^7 sterol isomerase emopamil-binding protein (EBP). A knockout mouse mouse model, the tattered (Td) mouse, with an X-linked semi-dominant mutation with prenatal male lethality has been described recently. These mice showed a significant accumulation of steroid precursors such as 8-dehydrocholesterol and 7-dehydrocholesterol in plasma and tissues. Heterozygous Td female mice had severe malformations, whereas male hemizygous embryos died shortly before or after birth, depending on the genetic background. In Td^{Ho} male embryos, diminished expression of embryonic globin genes was detected as well as increased apoptosis of fetal yolk-sac-derived erythrocytes. This result supported the assumption that defective erythropoesis might contribute to male embryonic lethality (51).

CHILD syndrome (congenital hemidysplasia with ichthyosiform erythroderma or nevus and limb defects) is another X-linked male-lethal disorder. Mutations in the NADH steroid dehydrogenase-like (NSDHL) gene are characteristic for this disease. NSDHL is an enzyme encoding a sterol dehydrogenase or decarboxylase that is part of the C-4 sterol demethylase

protein complex and precedes the sterol-Δ^8–Δ^7-isomerase step in the cholesterol biosynthetic pathway. A mouse model with allele mutations of NSDHL is called bare patches (Bpa) mouse, carrying an X-linked male lethal mutant with features very similar to those described in Td heterozygotes. Milder Bpa alleles, called striated (Str), were originally thought to reside at distinct loci and were indistinguishable from wild type littermates until day 12–14 (51).

Lathosterolosis shows a similar phenotype as SLOS with an abnormal accumulation of lathosterol in the plasma, implying a defect in sterol-C5-desaturase (SC5D). Krakowiak et al have created a Sc5d-/- mouse model (68). Scd5-/- mice showed severe malformations, increased lathosterol levels and decreased cholesterol concentrations in serum and tissues. Increased survival within humans might be due to hypomorphic alleles having still some enzyme activity.

Hydropsectopic calcification-moth-eaten (HEM) or Greenberg skeletal dysplasia is a uniformly lethal disease with consanguineous abnormal calcification and severely disorganized chondrogenesis. This disease showed elevated levels of cholesta-8,14-dien-3β-ol and cholesta-8,14,24-trien-3β-ol. Two human candidate sterol-Δ^{14}-reductase enzymes have been identified The first, transmembrane 7 superfamily 2 (TM7SF2), encodes a ubiquitously expressed ER transmembrane protein that is linked to the DHCR7 locus. The second is the lamin B receptor (LBR), a nuclear membrane protein whose C-terminal site of ~400 amino acids contains eight putative transmembrane domains with homology to sterol-Δ^{14}-reductases from a variety of eukaryotes. No mutations were detected in the TM7SF2, whereas the LBR showed mutation in its C-terminus. Thus, the ichthyosis mouse (*ic/ic*) might be a good model to study this defect since it also showed mutations in the LBR (51).

Antley–Bixler syndrome (ABS) is a heterogeneous malformation. Based on the presence of ambiguous or underdeveloped genitalia in some cases of ABS and the presence of a similar phenotype in four infants exposed in utero to fluconazole, an antifungal medication that inhibits lanosterol-14α-demethylase (CYP51), it has been suggested that some cases of ABS may be caused by mutations in CYP51 or a related gene involved in this cholesterol biosynthesis syndrome (51).

5.5.2 Regulation of cholesterol biosynthesis

Brown and Goldstein et al showed that cellular cholesterol exerts negative feedback on cholesterogenic enzymes and LDLR via sterol regulatory element-binding protein (SREBP) transcription factors (69). SREBP are synthesized as large inactive precursor proteins that are inserted into the ER (70). Each SREBP precursor is organized into three domains: (A) an N-terminal domain containing the basic helix-loop-helix-leucine zipper (bHLH-Zip) region for binding DNA, (B) two hydrophobic transmembrane-spanning segments interrupted by a short

loop, and (C) a C-terminal domain that is necessary for the regulatory function (71). In the ER, the C-terminus interacts with SREBP cleavage-activating protein (SCAP), which functions as a sterol sensor (72). If cells are depleted of cholesterol, SREBP are transported from the ER to the Golgi complex via SCAP. In the Golgi two membrane-associated site 1 (S1P) and site 2 (S2P) proteases liberate transcriptionally active fragments of SREBP at the N-terminus, which can enter the nucleus (Figure 7). While S1P is a membrane-bound subtilisin-related serine protease that cleaves the hydrophilic loop of SREBP, projecting into the ER lumen, S2P is a hydrophobic protein zinc metalloprotease. This cleavage is unusual because it takes place within a membrane-spanning domain of SREBP.

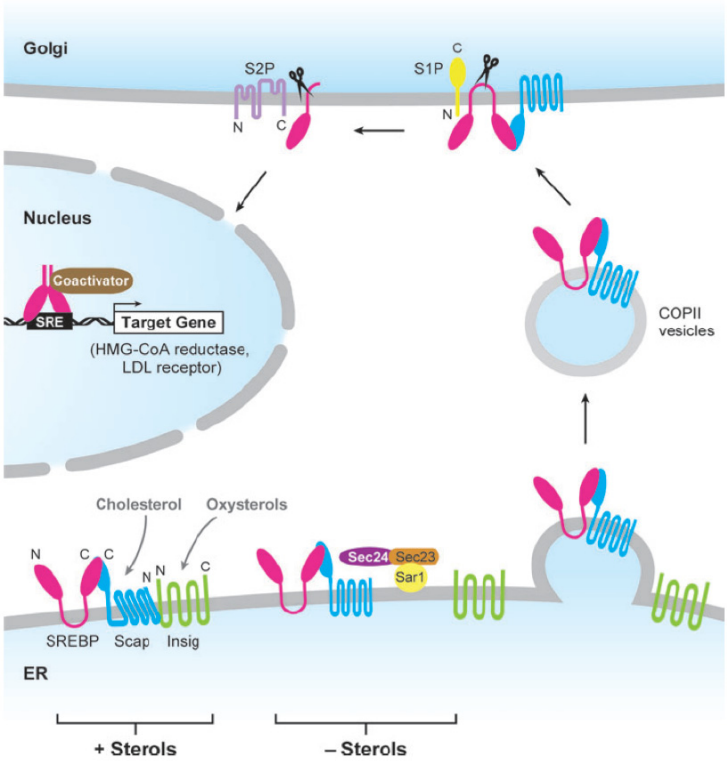

Figure 7. Sterol-mediated proteolytic release of SREBP from membranes and processing via SCAP and INSIG (73)
Cellular sterol and TG levels control the SREBP transcription factor activity. The SREBP (pink) are synthesized as inactive precursors in the ER. They build a complex with SCAP (blue) and INSIG proteins (two isoforms, INSIG-1 and INSIG-2) (green). In the presence of sterols an interaction between SCAP and INSIG retains the SCAP/SREBP complex in the ER. When sterol levels are low, SCAP undergoes a conformational change and is released from INSIG. The SREBP/SCAP complex is incorporated into COPII-coated vesicles through interaction with the proteins SEC23/24 and SAR1, which fuse with the Golgi apparatus. This is the initial step in SREBP activation. In the Golgi a two-step proteolytic cleavage of the 120kDa precursor SREBP takes place, involving the Golgi-specific S1P and S2P proteases and a 60–70kDa N-terminal domain is released. This mature, transcriptionally active bHLH fragment is subsequently translocated to the nucleus where it activates expression of genes involved in cholesterol and fatty acid (FA) biosynthesis via binding to their sterol response element (SRE) (73).

After translocation to the nucleus the active elements can bind to the promoters of SREBP target genes, including target genes of cholesterol and FA synthesis and metabolism (74). If cholesterol is build up in the ER, the SREBP/SCAP complex is retained in the ER and proteolytic cleavage cannot take place and, consequently, target gene expression is inhibited. Moreover, the active transcription factor (TF) is degraded by ubiquitination in the nucleus.

In fact, also HmgCoAr is sterol-dependently regulated, similar as SCAP, via sterol-sensing domains (SSD) within its transmembrane domains. As far as SCAP is concerned, cholesterol directly binds to the SSD, which leads to a conformational change (75). Consequently, the

SREBP/SCAP complex cannot interact with the COPII proteins and are not incorporated into COPII-coated vesicles, which bud from ER membranes and fuse with the Golgi. The inhibition of SCAP binding to the COPII proteins is enhanced by two related ER anchor proteins called insulin induced gene 1 and 2 (INSIG-1 and INSIG-2) (76). These Insig proteins enhance the response to cholesterol by supporting the binding of cholesterol to SCAP and possibly compete with COPII proteins for SCAP binding.

SREBP directly activate the expression of more than 30 genes responsible for the synthesis and uptake of cholesterol, FA, TG, and PL, as well as NADPH required to synthesize these molecules. The mammalian genome encodes three SREBP isoforms, namely SREBP-1a, SREBP-1c, and SREBP-2. SREBP-1a can activate all SREBP-responsive genes, including those that mediate the synthesis of cholesterol, FA, and TG. The roles of SREBP-1c and SREBP-2 are more restricted than that of SREBP-1a. SREBP-1c preferentially enhances transcription of genes required for FA but not cholesterol biosynthesis. Like SREBP-1a, SREBP-2 has a long transcriptional activation domain, but it preferentially activates cholesterol synthesis (Figure 6). SREBP-1a and SREBP-2 are the predominant isoforms in most cultured cell lines, whereas SREBP-1c and SREBP-2 predominate in the liver and other tissues (71, 74).

5.5.3 Lipoprotein metabolism and reverse cholesterol transport

Liver can synthesize cholesterol itself and take up excessive cholesterol from peripheral tissues by the reverse cholesterol transport (RCT). There are several lipoproteins involved in the transport of cholesterol, named after their size and density. VLDL transport cholesterol, PL and TG from the liver to peripheral tissues that have low amount of these substances, and then convert to intermediate and low density lipoproteins (IDL and LDL) after release of FA by the action of lipoprotein lipase (LPL). In contrast, HDL transport excess cholesterol from peripheral tissues back to the liver. The brain is an exceptional organ since it synthesizes all the cholesterol it needs de novo, because cholesterol itself cannot cross the so-called blood brain barrier. The conversion of cholesterol to 24(S)-hydroxycholesterol is used as an effective mechanism for cholesterol excretion (77). In the liver cholesterol is esterified by a acyl-CoA:cholesterol acyltransferase (ACAT) 2 for storage in cytoplasmic lipid droplets and avoidance of cytotoxicity. To get rid of high amounts of cholesterol the liver produces and secretes VLDL particles and it converts cholesterol to bile acids (BA), which are transported to the bile and further to the intestine, where cholesterol can be reabsorbed and transported back to the liver or together with BA excreted by the feces (Figure 8) (78).

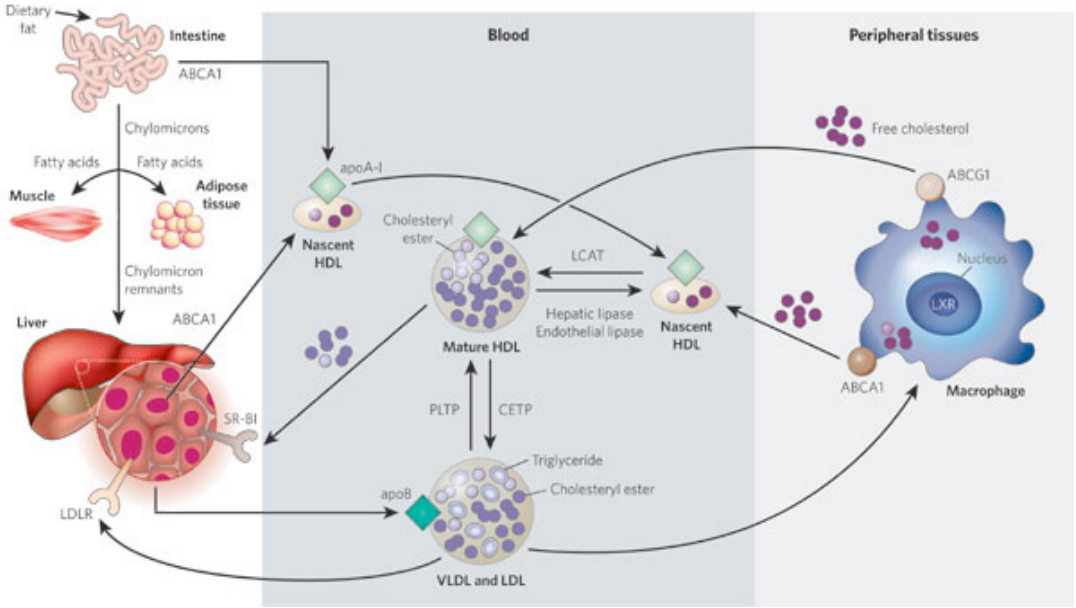

Figure 8. Reverse cholesterol transport (79)
RCT involves the transport of lipids, particularly cholesterol and TG, in the blood. The intestine absorbs dietary fat and packs it into chylomicrons, which are transported to peripheral tissues through the blood. In muscle and adipose tissues, LPL breaks down chylomicrons, and FA enter these tissues, while chylomicron remnants are taken up by the liver. The liver loads lipids onto apolipoprotein B (APOB) and secretes VLDL, which undergo lipolysis by LPL to form LDL. LDL are then taken up by the liver through binding to the LDLR. HDL are generated by the intestine and the liver through the secretion of lipid-free apoA-I, which recruits cholesterol from these organs by ABCA1, forming nascent HDL. In peripheral tissues, nascent HDL promote the efflux of cholesterol from tissues and cells, including macrophages, through the actions of ABCA1. Mature HDL also promote this efflux but through the actions of ABCG1. The FC in nascent HDL is esterified to CE by LCAT, creating mature HDL. HDL cholesterol is returned to the liver both directly, through uptake by the receptor SR-BI, and indirectly, by transformation to LDL and VLDL through CETP. The lipid content of HDL is changed by hepatic lipase and endothelial lipase as well as CETP and phospholipid transfer protein (PLTP) (79). ApoE is an effective ligand for LDLR and uptake of cholesterol in the liver takes place upon binding of APOE to the hepatic LDLR (80).

When cholesterol concentration exceeds normal levels in macrophages, muscle and fat cells, the RCT removes excess cholesterol. These cell types cannot form lipoproteins or metabolize cholesterol extensively. Therefore, stored CE are cleaved by cholesterol ester hydrolases and the resulting FC is effluxed from the cells by specific transporters. These transporters are activated not only by excessive cholesterol but also by oxysterols. Oxysterols activate LXR, which induces target gene transcription of efflux pumps from the adenosine triphosphate (ATP) binding cassette transporter (ABC) family such as ABCA1 or ABCG1 (81). Once cholesterol is removed from the cell, nascent HDL takes it up. Cholesterol becomes esterified by lecithin cholesterol acyltransferase (LCAT), leading to mature HDL particles, which are transported in the blood back to the liver. HDL are generated by the intestine and the liver through the secretion of lipid-free apolipoprotein A-I (APOA-I). APOA-I then recruits cholesterol from these organs through the actions of ABCA1 forming nascent HDL. This protects APOA-I from being rapidly degraded in the kidneys. HDL cholesterol (esterified or not) is taken up directly by SR-BI or indirectly by LDLR from LDL and VLDL. These low density lipoproteins are derived from HDL by the action of

cholesteryl ester transfer protein (CETP), which is missing in rodent models (79). Since HDL is claimed to be the primary acceptor for cholesterol efflux from the cell, it is defined as the "good" cholesterol. Yet, this might be an oversimplification and the concept of RCT needs re-definition. There are new proteins found to play a role in RCT such as ABC transporters and nuclear receptors (82).

CETP-deficient species are particularly resistant to diet-induced elevations in plasma cholesterol levels, demonstrating that they possess an effective RCT pathway in the absence of CETP. APOE-enriched HDL accomplishes this. High HDL concentrations and resistance to atherosclerosis are also consistent with the inverse correlation between HDL levels and risk of atherosclerosis observed in humans (83). Since APOE is an effective ligand for LDLR, APOE-enriched HDL can deliver cholesterol acquired from the periphery to the liver via hepatic LDL receptors (84).

Cholesterol, which is transported back to the liver, is converted by specific enzymes (mostly cytochrome P450 enzymes (CYP) to BA, which are excreted together with FC into the bile. These enzymes insert a hydroxyl group in the molecule and BA formation starts with a 7α-hydroxylation of cholesterol by CYP7A1 in the liver. The "acidic" pathway starts with a hepatic or extrahepatic 27-hydroxylation by CYP27A1 (85).

After conversion to BA, cholesterol is further transported to the intestine. One part of cholesterol is excreted via feces, consisting of half BA and half neutral sterols, while the other part is absorbed in the intestine together with dietary cholesterol by proteins such as Niemann-Pick C1 like 1 (NPC1L1) (86) or CD36 (87); aminopeptidase-N (88) might also be involved in this process. NPC1L1-/- knockout mice showed significant reduction in cholesterol absorption, but the cholesterol absorption blocker ezetimibe had no effect in NPC1L1-/- mice, implying that this drug works in an NPC1L1-related manner (86). After absorption cholesterol is transcytosed to the apical membrane, effluxed to HDL in the blood and transported back to the liver (RCT) (89). CD36 was suggested to be important in proximal absorption of dietary FA and cholesterol for optimal chylomicron formation. CD36-/- mice have a proximal reduction of 50% in FA uptake as well as a 60% reduction in cholesterol absorption, but the chylomicron secretion was impaired. The distal segments did not show the same reduction in absorption, which implies different mechanisms in these regions of the intestine (90). SR-BI is known to mediate both selective uptake of HDL cholesterol by the liver and the efflux of FC from peripheral tissue. SR-BI is expressed in the enterocytes of the small intestine, but its role in cholesterol absorption is under debate since SR-BI deficient mice did not affect cholesterol absorption (91). Yet, it was shown that SR-BI overexpression in the small intestine resulted in increased cholesterol and TG absorption (92).

The presence of bile salts is essential for cholesterol absorption as shown by diminished or virtually abolished absorption in CYP7A1-deficient mice (93). Yet, cholesterol might be effluxed back into the intestinal lumen via LXR-activated ABCG5/ABCG8. The disposal of cholesterol via the feces is an important step in the RCT, and thus in the prevention of CVD. Intestinal cholesterol secretion contributed up to 36% of total fecal cholesterol loss (94). ABCG5/ABCG8 are good candidate proteins involved in this process, but probably not the only ones (95). Absorbed cholesterol can be packed into chylomicrons together with TG and released into the lymph and further into the blood. TG are rapidly hydrolyzed by LPL and taken up by peripheral tissue, while chylomicron remnants are transported back to the liver. Since the intestine also generates HDL, cholesterol can also be removed via the efflux pump ABCA1 and the HDL-mediated pathway into the plasma and finally transported back to the liver (89) (Figure 8).

5.6 FA metabolism

FA are important energy suppliers and provide more energy than proteins or carbohydrates. They are used for anabolic processes and molecule formation such as PL, TG, and CE. They are derived by cleavage of dietary TG or by lipolysis of TG in adipose tissue during starvation. After cleavage of TG the FA are released into the blood stream in free form (FFA). In order to undergo degradation, the FA have to be activated and transported to the mitochondria, where a stepwise release of acyl-CoA from FA takes place. The carnitine carrier transport system is necessary for the uptake of FA into the mitochondria. Carnitine-palmitoyl transferase I (CPT-I) is believed to be the rate-limiting enzyme in this process called β-oxidation. FA might also be synthesized by the body itself, which is mainly happening in the liver, the adipose tissue and the lactating mammary gland. FA biosynthesis is regulated by acetyl-CoA carboxylase (ACC) and fatty acid synthase (FAS).

Other enzymes add double bonds or additional carbon atoms to the carbon chain. FA can be elongated, unsaturated, β-oxidized, peroxidized and esterified to TG, CE, and PL. They can exist as FFA in the blood after release from the TG and CE or are incorporated into lipoproteins.

5.7 Current and future treatments of atherosclerosis

To date, the specific origin of atherosclerosis is still not defined and the aim of a lot of scientific investigations. Different approaches exist for the interference with atherosclerosis and the aftereffects (e.g. hypertension, stroke or heart attack).

5.7.1 Preventive sanctions

The easiest way to interfere with atherosclerosis or CVD is to avoid the risk factors such as cigarette smoking. Eating healthy and avoiding too much lipid intake helps reducing weight and

the risk for diabetes as well as high blood pressure and consequently CVD. Regular exercise, and avoidance of smoking and stress can help lowering one's risk for a CVD incident.

5.7.2 Mechanical interventions (angioplasty and bypass)

Angioplasty is a method to widen narrowed arteries with tightly folded balloons that are inserted and blown up applying high pressure. This is done in all arteries (coronary, femoral, peripheral or renal). Another possibility is the insertion of a bypass to increase the blood flow by means of artificial tubing. Moreover, arteries or leg veins are removed and inserted.

5.7.3 Statins

Statins block the rate-limiting step in cholesterol biosynthesis by inhibiting HmgCoAr. First discovered in the 1970s (96) statins block the action of HmgCoAr by binding to the same site of HmgCoA as the enzyme. Therefore, statins lower cholesterol levels of patients with elevated cholesterol and high risk of CVD. Inhibition of HmgCoAr in the liver increases synthesis of LDLR, which takes up excessive LDL cholesterol from the blood stream. Statins lower LDL cholesterol concentration by an average of 1.8 mmol/l which reduces the risk of ischaemic heart disease events by about 60% and stroke by 17% (97). Lovastatin (named mevinolin or MK803 by Merck & Co) was the first commercially available statin, isolated from Aspergillus terreus. Four proposed mechanism of how statins prevent CVD are described, namely improvement of endothelial function, modulation of inflammatory responses, maintenance of plaque stability, and prevention of thrombus formation (98). Yet, there are several side effects such as headache, nausea, vomiting, constipation, diarrhea, rash, weakness, and muscle pain. The most serious (but fortunately rare) side effects are liver failure and rhabdomyolysis. Rhabdomyolysis often begins as muscle pain, but can progress to loss of muscle cells, kidney failure, and death (99).

5.7.4 Fibrates

Fibric acids (fibrates) are amphipatic carboxylic acids, which activate peroxisome proliferater activated receptor alpha (PPARα). They lower blood TG levels by inhibiting VLDL production in the liver and speeding up the removal of TG from the blood. They are effective in inducing β-oxidation in the liver and increasing HDL levels, but do not significantly reduce LDL concentrations (100). They are often used in combination with statins.

5.7.5 BA sequestrants

BA sequestrants bind certain components of bile in the gastrointestinal tract. They disrupt the enterohepatic circulation of BA by sequestering them and preventing their reabsorption from the gut. Since BA are synthesized from cholesterol, their sequestrants lower cholesterol, in particular LDL cholesterol levels (101). They are often also combined with a statin treatments.

5.7.6 Niacin

Niacin (vitamin B3 or nicotinic acid) is a precursor to NADH, NAD+, NADP+ and NADPH, which play essential metabolic roles in living cells. Niacin is involved in both DNA repair and the production of steroid hormones in the adrenal gland. Niacin inhibits hepatic diacylglycerol acyltransferase 2 and therefore TG synthesis and decreases the amount of ApoB-containing lipoproteins (102). Consequently less VLDL are secreted into the blood and the level of HDL cholesterol in blood rises, being important for people who are at high risk for cardiovascular events. It is modestly effective in lowering LDL cholesterol and TG and a combination with statins is often recommended (103).

5.7.7 Ezetimibe

Ezetimibe inhibits the absorption of cholesterol from the diet at the brush border of the small intestine. It was suggested to bind to the NPC1L1 protein on the gastrointestinal tract epithelial cells (104) and in hepatocytes (105). It may have beneficial effects on atherosclerosis progression and plaque stability, but its effects are more pronounced if combined with statins (106).

5.7.8 Angiotensin converting enzyme (ACE) inhibitors

Renal failure and CKD are connected with an increase in CVD risks. ACE converts angiotensin I to angiotensin II thereby inducing hypertension, which is also a risk factor for a CVD event. By blocking ACE hypertension is reduced (25).

5.7.9 LXR

Activation of LXR has been shown to reduce atherosclerosis in atherosclerotic mouse models by removing excessive cholesterol from macrophages and/or preventing cholesterol absorption from the intestine (94, 107, 108). Yet, LXR agonist activation involves the negative side effect of inducing liver steatosis, because target genes of the lipid metabolism in the liver and other tissues are also activated.

5.8 Nuclear receptors

Nuclear receptors (NR) differ from membrane-bound receptors, which are activated by growth factors, neurotransmitters, and peptide hormones. NR are activated by small molecules, which enter the nucleus of target cells or are generated on demand. If the ligand is a hormone, the receptor is called nuclear hormone receptor (NHR). Others, of which the ligand is currently unknown, are called orphan NR. Depending on the type of NR and the presence of coactivators or corepressors, the NR can reside in the cytoplasm until activation of a suitable ligand and then

enter the nucleus or they are constantly present in the nucleus, independent of the activation state. Once activated by a specific ligand, NR act as transcription factors (TF) (109).

Several hundred putative NR have been identified, ranking from nematodes to man, of which 49 are expressed in the mouse (110). Twenty-eight of the 49 NR are expressed in the macrophage, including endocrine receptors, adopted orphan receptors, and orphan receptors (111). It has been proposed that NR have one common ancenstral orphan "receptor", which showed early diversification and acquired ligand binding (112). They constitute a family of TF, which share a modular structure of 5-6 conserved domains encoding specific functions (Figure 9). The classification of NR is made according to the DNA binding domain (DBD) and the ligand binding domain (LBD), which both have the highest evolutionary conservation (113). The first ancestral NR appeared in the metazoans and subsequently diversified into the six receptor sub-families, which were already recognizable at the time of the Arthropoda-Chordata split over 700 million years ago (114). All different classes of NR have a set of functional domains.

The receptors contain variable N-terminal and C-terminal domains, as well as a hinge region of variable length between the DBD and LBD. The LBD, located in the C-terminal half of the receptor, recognizes specific hormonal and nonhormonal ligands and thus directs specificity to the biologic response. The LBD domain is a multifunctional domain, which in addition to binding the ligand, is responsible for homo- or heterodimerization, ligand dependent transcriptional activity, interaction with heat shock proteins, and sometimes mediates hormone reversible transcriptional repression.

The crystal structure of NR LBD shows a common fold comprising 12-α helices (H) and a short β-turn (s1-s2). They are arranged in three layers as an antiparallel α-helical sandwich, where the top part corresponds to a rather invariable region and the lower part contains a variable region with the ligand-binding pocket (LBP) (Figure 10). The DBD contains cysteines and other conserved residues that are required for the high affinity DNA binding. It is also a target for post-translational modifications and is involved in nuclear localization and interactions with TF and coactivators. The hinge region, which is poorly conserved, allows rotation of the DBD. NR have two transcriptional activation sites, the N-terminal AF-1 and the C-terminal AF-2. Whereas AF-1 is a ligand independent autonomous transactivation site, AF-2 is strictly ligand-dependent. AF-2 is also highly conserved among the different NR (Figure 9).

NR can exist as homo- or heterodimers with retinoic X receptor (RXR) (115, 116). Each partner binds to specific response element (RE) sequences that exist as half-sites separated by variable length nucleotide spacers between direct or inverted half-site repeats. The overall structure of heterdimeric arrangements do not differ much from a homodimer. Nevertheless, it has been

suggested that there is an energetic link between the LBP and the dimerization interface when NR build heterodimers with RXR (117).

Several years ago Mangelsdorf et al. proposed 4 different classes of NR. Class 1 receptors including the known steroid hormone receptors, which function as homodimers binding to half-site RE inverted repeats. Class 2 receptors exist as heterodimers with RXR receptor partners and function in a ligand-dependent manner. The last two classes include orphan receptors, which function as homodimers binding to direct RE repeats (Class 3) or monomers binding to single site RE (Class 4) (118).

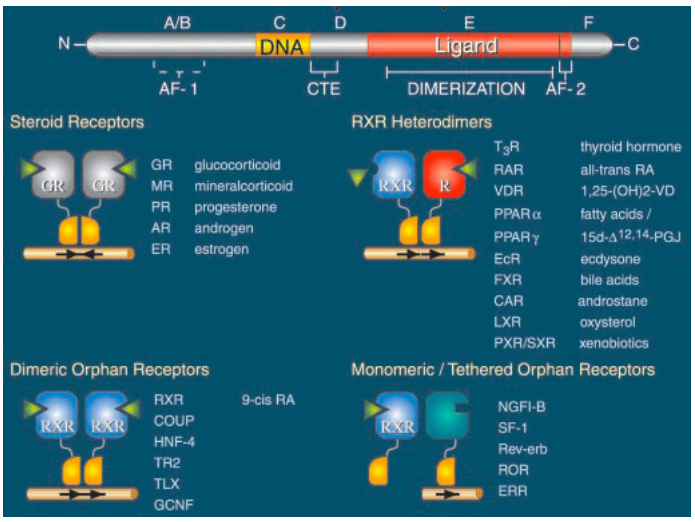

Figure 9. Structure and functional organization of NR (115)
The six domains (*A–F*) of NR comprise regions of conserved function and sequence. All NR contain a central DBD (*region C*), which includes two zinc finger modules. A LBD (*region E*) is contained in the C-terminal half of the receptor. Situated between the DBD and LBD is a hinge domain of variable length (*region D*), and a variable N-terminal region (*A/B*) contains the activation site AF-2. Most receptors also contain a C-terminal *region F* of variable length. Many members of the NR family form homo- or heterodimers. Moreover, amino acid sequences important for dimerization are contained within the DBD and LBD (115, 116)

Sequence alignment and phylogenetic tree construction led to the classification of the big family of human NR into six evolutionary groups by the Nuclear Receptor Nomenclature Committee in 1999. According to this classification, each NR has a trivial name and a formal nomenclature, which should be always mentioned when working with NR (119-121). In Table 1 all human NR are listed with both trivial and formal nomenclature.

Group 1 contains thyroid hormone receptors (TR), retinoic acid receptors (RAR), vitamin D receptor (VDR), and peroxisome proliferator activated receptors (PPAR), as well as orphan receptors such as retinoid-related orphan receptors (ROR), REV-ERB, constitutive androstante receptor (CAR), pregnane X receptor (PXR), LXR and others.

Group 2 includes RXR, chicken ovalbumin upstream promoter transcription factor (COUP-TF), and hepatocyte nuclear factor 4 (HNF-4).

Group 3 includes the steroid receptors with estrogen receptors (ER), glucuronide receptors (GR), progesterone receptors (PR), and androgen receptors (AR) as well as the estrogen receptor-related receptors (ERR).

Group 4 is a small group, which contains the nerve growth factor induced clone B group of orphan receptors (NGFI-B), nuclear receptor-related 1 (NURR1), and neuron-derived orphan receptor 1 (NOR1).

Group 5 is another small group that includes the steroidogenic factor 1 and the receptors related to the *Drosophila* Fushi Tarazu Factor-1 (FTZ-F1).

Group 6 contains only the germ cell nuclear factor (GCNF1) receptor, which does not fit well into other subfamilies (116).

Table 1 Trivial names and formal nomenclature of human NR

All nuclear receptors have a trivial and a formal nomenclature. This table shows the shortenings of the trivial names as well as the formal nomenclature and ligands for each receptor mentioned (116). $^{\alpha}$FXRβ is a pseudogene in humans but it is a functional lanosterol receptor in mice (122, 123).

Names	Nomenclature	Ligand
TRα	NR1A1	Thyroid hormones
TRβ	NR1A2	Thyroid hormones
RARα	NR1B1	Retinoic acid
RARβ	NR1B2	Retinoic acid
RARγ	NR1B3	Retinoic acid
PPARα	NR1C1	Fatty acids, leukotriene B_4, fibrates
PPARβ	NR1C2	Fatty acids
PPARγ	NR1C3	Fatty acids, prostaglandin J_2, thiazolidinediones
Rev-erbα	NR1D1	Orphan
Rev-erbβ	NR1D2	Orphan
RORα	NR1F1	Cholesterol, cholesteryl sulfate
RORβ	NR1F2	Retinoic acid
RORγ	NR1F3	Orphan
LXRα	NR1H3	Oxysterols, T0901317, GW3965
LXRβ	NR1H2	Oxysterols, T0901317, GW3965
FXRα	NR1H4	Bile acids, fexaramine
FXRβ$^{\alpha}$	NR1H5	Lanosterol
VDR	NR1I1	Vitamin D, 1,25-dihydroxyvitamin D_3
PXR	NR1I2	Xenobiotics, 16α-cyanopregnenolone
CAR	NR1I3	Xenobiotics, phenobarbital
HNF4α	NR2A1	Orphan
HNF4γ	NR2A2	Orphan
RXRα	NR2B1	Retinoic acid
RXRβ	NR2B2	Retinoic acid
RXRγ	NR2B3	Retinoic acid
TR2	NR2C1	Orphan
TR4	NR2C2	Orphan
TLL	NR2E2	Orphan
PNR	NR2E3	Orphan
COUP-TFI	NR2F1	Orphan
COUP-TFII	NR2F2	Orphan
EAR2	NR2F6	Orphan
ERα	NR3A1	Estradiol-17β, tamoxifen, raloxifene
ERβ	NR3A2	Estradiol-17β, various synthetic compounds
ERR α	NR3B1	Orphan
ERRβ	NR3B2	DES, 4-OH tamoxifen
ERRγ	NR3B3	DES, 4-OH tamoxifen
GR	NR3C1	Cortisol, dexamethasone, RU486
MR	NR3C2	Aldosterone, spirolactone
PR	NR3C3	Progesterone, medroxyprogesterone acetate, RU486
AR	NR3C4	Testosterone, flutamide
NGFI-B	NR4A1	Orphan
NURR1	NR4A2	Orphan
NOR1	NR4A3	Orphan
SF1	NR5A1	Orphan
LRH-1	NR5A2	Orphan
GCNF	NR6A1	Orphan
DAX-1	NR0B1	Orphan
SHP	NR0B2	Orphan

After all, the structure of NR ligand binding, dimerization and DNA binding is much more complex than shown in Figure 9. Applying *in silico* molecular modeling in combination with crystallography allows a better understanding and characterization of NR. Figure 10 shows the crystal structure of the LXRα/RXRβ heterodimer, where each NR is bound to an agonist and a coactivator, respectively. The LXR agonist T0901317 is a synthetic, non-steroidal LXR agonist that occupies the center of the LXRα LBP. Its hydroxyl head group interacts with two residues (H421 and W443) in a similar way as the oxysterols with their 22-, 24- or 27-hydroxyl group, implying the importance of these hydrogen acceptors for efficient LXR agonism (124). As far as solved crystal structures are concerned, the LXR structure resembles to VDR and PXR, to which it is also most closely related in a phylogenetic context (124).

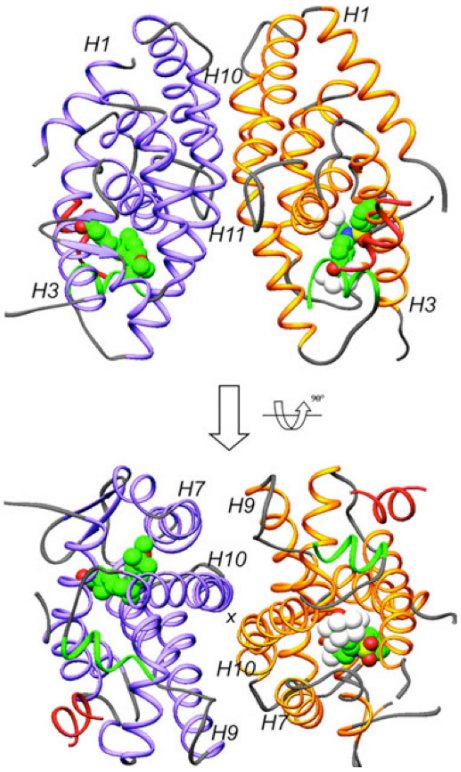

Figure 10. Structural overview of the LXRα/RXRβ LBD-heterodimer (124)
Two views separated by 90° give a better insight in the structure of the LXRα/RXRβ heterodimer. The LXRα LBD is shown in yellow and the RXRβ LBD in purple, except for the activation domain, AF-2 helices, which are green. GRIP-1 peptides, bound coactivators, are colored red. T0901317 was used as a LXR agonist and the pesticide metabolite methoprene acid (MPA) as a selective RXR agonist. They are shown in space-filling representation, with carbon, oxygen, nitrogen, sulfur and fluoride atoms colored in green, red, blue, yellow and white, respectively (124).
The LBP is generally located behind helix 3 and in the front of helices 7 and 10 and is surrounded with mostly hydrophobic amino acids. A few polar parts at the end of the LBP, close to the β-turn are responsible for the correct ligand binding and selectivity of the pocket (116).

5.8.1 Coactivators and corepressors

Coactivators and corepressors are crucial for transmitting the signal to the transcriptional machinery to switch between activation and repression (26). Many coactivator and corepressor proteins are components of multisubunit coregulator complexes with a diversity of enzymatic activities. Coactivators interact with ligand-activated NR with at least one LXXLL motif, where L=leucine and X=any amino acid (125). Similarly, corepressors are recruited in absence of ligands. They also have a certain motif, an N-terminally elongated helix, the LXX I/H IXXX I/L motif or Cornr-box (H=histidine, I=isoleucine) (126).

Both types of proteins are divided into two generic classes: The first class consists of enzymes that are capable of covalently modifying histones with acetylating and deacetylating activities (histone acetyltransferases=HAT, histone deactetylases=HDAC), methylating and demethylating enzymes (e.g. histone methyltransferse=HMT and lysine-specific demethylase 1=LSD1, Jamongie domain factors) (127-131), proteinkinases, protein phosphatases, poly(ADP)ribosylases, ubiquitin, and small ubiquitin-related modifier (SUMO) ligases. The second class includes components of a family of ATP-dependent remodeling complexes. Chromatin remodeling machinery, such as the SWI/SNF complex, alters the structure of the nucleosome in an ATP-dependent manner, presumably by modifying the histone–DNA interface, and it often causes nucleosome sliding (132).

NR bind to *cis*-active elements in promoters and enhancers of target genes and activate transcription in a signal (ligand)-dependent manner. Transcriptional activation requires the actions of many coactivator complexes that are recruited in a parallel and/or sequential manner. Enzymatic activities related to certain components of coactivator complexes result in nucleosome remodeling and covalent modifications of histones, such as methylation, acetylation, and phosphorylation (133).

The corepressor matrix is defined by sequence-specific repressors, which are bound to unliganded or antagonist-bound NR. They actively repress transcription by binding to *cis*-active elements in promoters and enhancers of target genes. These factors antagonize actions of coactivator complexes (for example through histone deacetylase activity, phosphatase activity, and corepressor-associated nucleosome remodeling activities (NRM)), and mediate covalent modifications (e.g. methylation of histones) that serve as initiators for the recruitment of additional factors involved in transcriptional repression (133). The action of corepressors and coactivators is illustrated in Figure 11.

Very well known coactivators for many NR are the p160 family and CBP/p300. They act both as molecular scaffolds as well as acetylases of different substrates (134, 135). Silencing mediator for retinoic and thyroid hormone receptors (SMRT) and nuclear corepressor (NCoR) represent some of the most common corepressors. They contain at least three independent repressor domains that are capable of active repression (136, 137).

Several different coactivators and corepressors are shown and partly described in the supplemental data (Table A) (113).

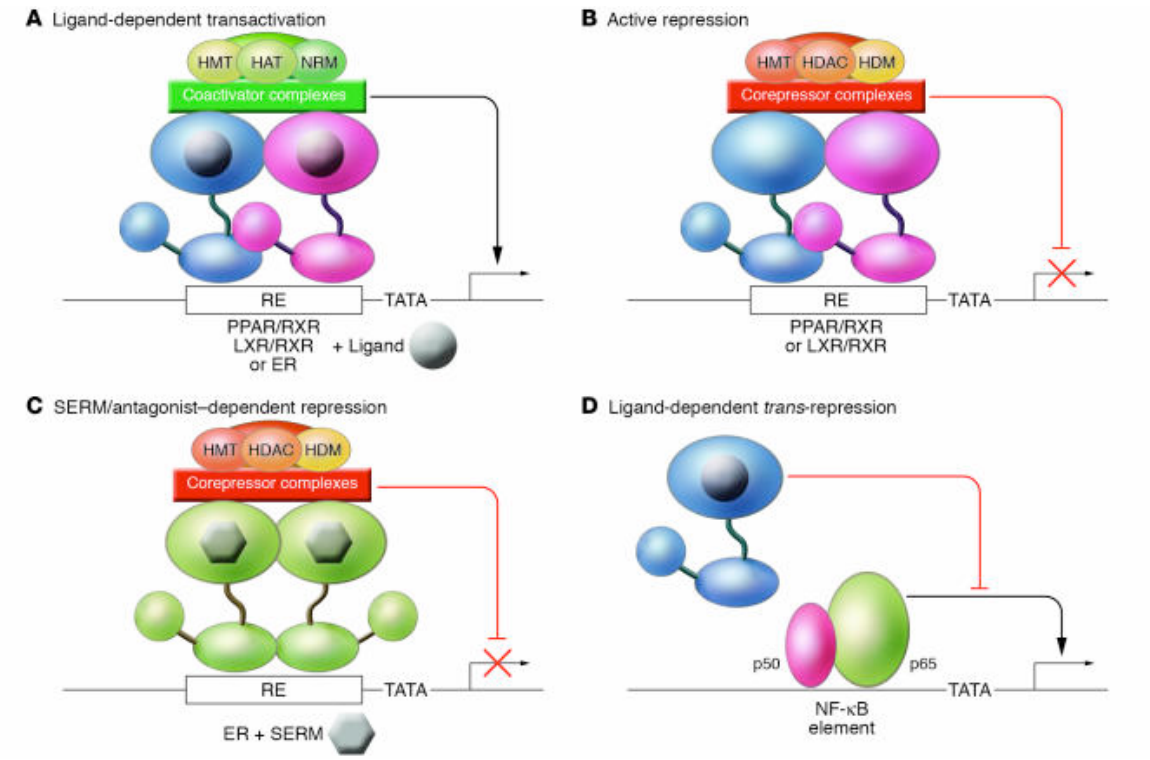

Figure 11. Mechanisms of transcriptional activation and repression by steroid hormone and heterodimeric NR (26)

(A) Ligand-dependent transactivation: The binding of hormones or synthetic agonists causes the recruitment of coactivator complexes to the LBD. The illustration shows a simplified form of coactivation. In general, ligand-dependent transcription of NR target genes is associated with the recruitment of coactivator complexes that act in a combinatorial or sequential manner. These complexes are associated with a number of enzymatic activities, including HAT, HMT, and NRM activities. Structurally distinct ligands show different recruitment of these factors, resulting in altered patterns of gene activation. (B) Active repression: A subset of heterodimeric NR, including PPAR/RXR and LXR/RXR heterodimers, are capable of binding to RE in the absence of ligand and recruiting corepressor complexes that actively repress transcription. A number of corepressor complexes are associated with HDAC, HMT and NMR activities that are generally different from those associated with coactivator complexes. Histone demethylase (HDM) activity is also involved. (C) SERM/antagonist–dependent repression: Some selective ER modulators (SERM), such as tamoxifen, and PPAR antagonists promote corepressor interactions with the LBD, resulting in active repression. (D) Ligand-dependent trans-repression: Many NR, including GR, ER, PPAR, and LXR are capable of antagonizing signal-dependent activation of inflammatory response genes by transcription factors such as NF-κB (26).

5.8.2 Posttranslational modification

NR and their coregulators can be posttranslationally modified themselves, including phosphorylation, acetylation, activation of small ubiquitin-related modifier (SUMOylation), ubiquitination, and methylation (138). The phosphorylation sites of NR are located in the N-terminal A7B region but also in the DBD and the LBD (139). Most of these sites are serines surrounded by prolines and therefore interact with proline-dependent kinases such as mitogen-activated protein kinases (MAPK). Together with other kinases such as Akt (also called protein kinase B) or protein kinase C they support the transcriptional activation. Yet, phosphorylation can also lead to termination of transcription through decreasing ligand affinity or DNA dissociation. Deregulation of NR phosphorylation with ligand-independent activities takes place

in certain diseases. Phosphorylation of coactivatiors may enhance the interaction with NR and induce redistribution of corepressors from the nucleus to the cytoplasm (116).

5.8.3 RXR

RXR can form homodimers as well as heterodimers with a number of different NR, which is a unique ability. Controversies exist whether there is a separate RXR-mediated signaling pathway or whether RXR only serves as a partner for other NR thereby modulating their actions. Rexinoids selectively activate RXR whereas 9-cis retinoic acid (9-*cis* RA) activates both RXR and retinoic acid receptors (RAR). Retinoids are derivatives of vitamin A and show similar effects as their precursor in development, differentiation, homeostasis and many more. *In vivo* experiments in type 2 diabetic rodents demonstrated that rexinoids show similar effects as thiazolidinediones that activate PPARγ and are insulin sensitizers. They decreased cardiovascular risk and displayed tissue-specific gene expression (140-142). Yet, retinoids have unwanted side effects such as teratogenic potential. Therefore, the complexes of RXR, which are responsible for the side effects, need to be identified in order to develop modified rexinoids. Since RXR build heterodimers with other NR such as PPAR and LXR, these NR might be responsible for the antidiabetic action of rexinoids. Vice versa, since agonists of both partners activate the heterodimers, RXR might also have a regulatory part in lipid homeostasis.

RXR exists in three isoforms, namely α, β, and γ. The β isoform is widely expressed, whereas RXRα is predominantly found in liver, kidney, spleen, placenta, and epidermis. RXRγ is present in muscle and brain.

5.8.4 LXR

LXR are a family of TF, which were identified as orphan members of the NR superfamily in 1995 (143). The identification of a specific class of oxidized derivatives of cholesterol as ligands for LXR has been crucial to understand the function of these receptors *in vivo* and first suggested their role in the regulation of lipid metabolism (144). This role was confirmed by the analysis of LXR-deficient mice, demonstrating the essential function of one of the two LXR isoforms in the liver as a major sensor of dietary cholesterol (57).

The two isoforms, LXRα (Nr1h3) and LXRβ (Nr1h2), are distinctively expressed within different tissues. While LXRα is most abundantly expressed in macrophages, liver, kidney, intestine and adipose tissue, LXRβ is ubiquitously distributed (www.nursa.org/10.1621/datasets.02001) (Figure 12). Therefore, it is likely that both isoforms exert distinct functions in different tissues. As already described before, the NR of group III build heterodimers with RXR (5.8.3) and these heterodimers can be activated by ligands for both LXR and RXR.

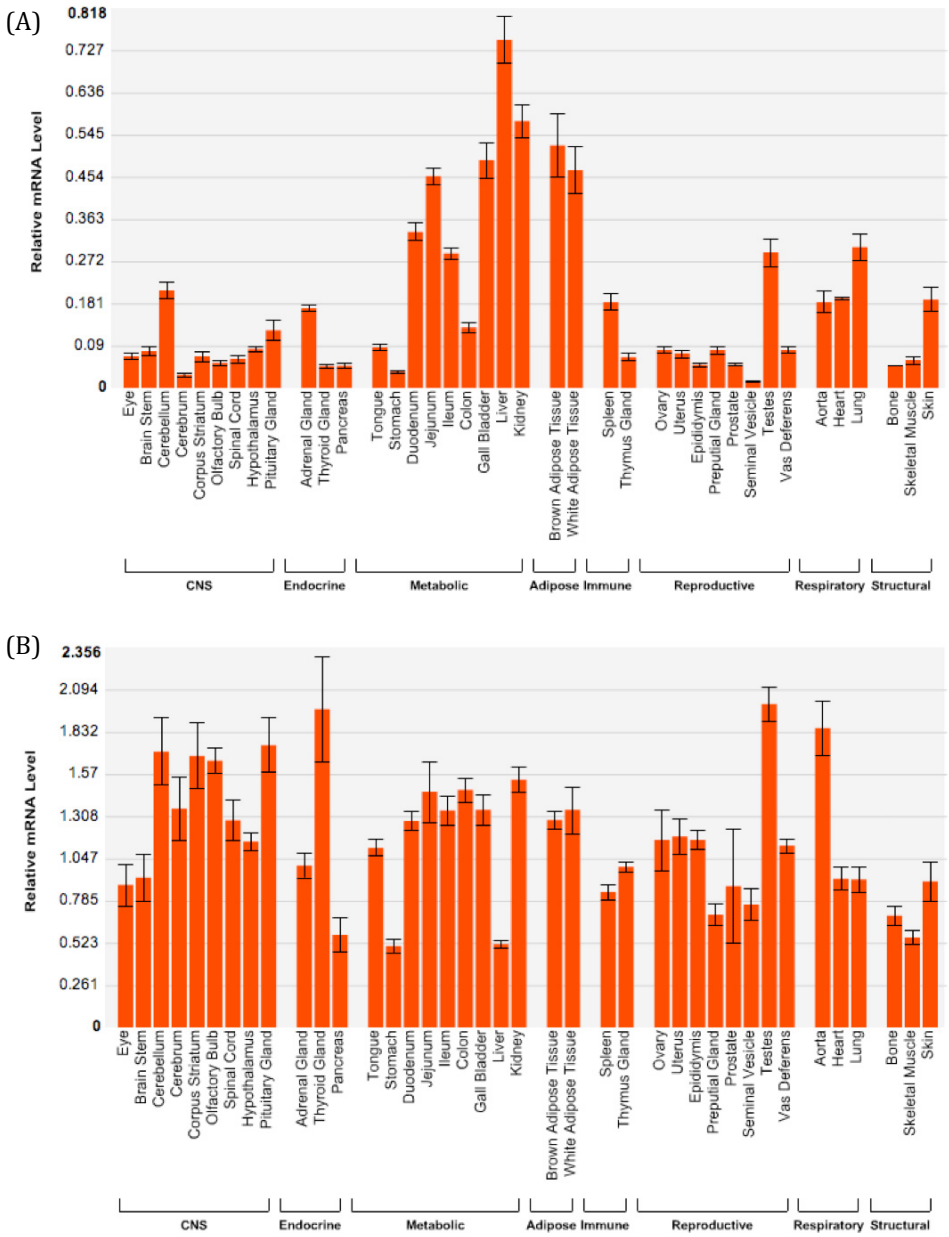

Figure 12. Tissue distribution of LXRα and LXRβ

Tissue distribution for (A) LXRα demonstrates its highest abundance in liver, kidney, intestine and adipose tissue. It is also expressed in macrophages, which are not shown in this figure. (B) In contrast, LXRβ is ubiquitously expressed (www.nursa.org/10.1621/datasets.02001, D. J. Mangelsdorf).

In peripheral cells such as macrophages, LXR are likely to coordinate a physiological response to cholesterol loading by regulating the transcription of several genes involved in cholesterol efflux and catabolism, including ABCA1 and ABCG1 (Figure 13) (145-149). The activation of LXR leads to induction of the RCT, which is responsible for the transport of excessive cholesterol from peripheral tissue back to the liver.

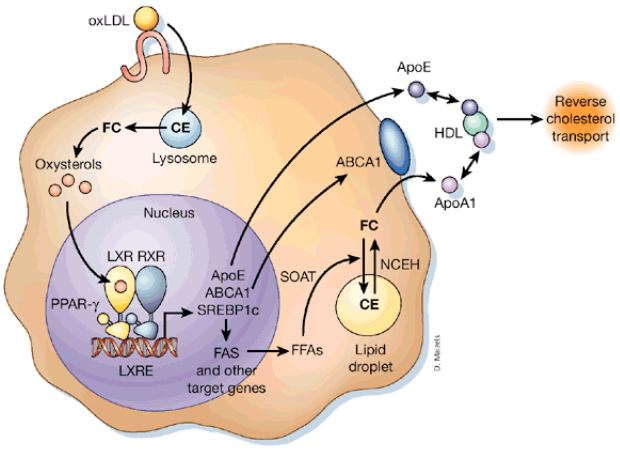

Figure 13. Mechanisms in the macrophage for protection from toxic effects of FC (150) Oxysterols, generated from FC, activate LXR. LXR/RXR heterodimers increase the transcription of target genes including ApoE and ABCA1, which are linked to efflux of cholesterol to extracellular acceptors, and FAS, which leads to the synthesis of free fatty acids (FFA) used for cholesterol esterification by acyl-CoA: cholesterol acyltransferase (ACAT), also called sterol O-acyltransferase (SOAT). PPAR may promote cholesterol efflux by inducing LXR expression. CE, cholesterol ester; LXRE, LXR response element; NCEH, neutral cholesterol ester hydrolase (150).

In the liver, LXR apparently regulate cholesterol, FA, and TG metabolism. This latter effect is partly mediated by SREBP1c activation (151, 152) and the upregulation of its downstream target genes e.g. LPL (153), FAS (154), and stearoyl-CoA desaturase 1 (SCD-1) (155). Additionally, carbohydrate response element-binding protein (ChREBP) is activated by LXR (156) and enhances hepatic FA synthesis. In the intestine, LXR ligands were shown to reduce dietary cholesterol absorption by ABCA1, ABCG1, and ABCG5/G8 activation (146, 157, 158). In rodents but not in humans, LXR enable BA synthesis by activation of CYP7A1 (159). Recent publications in atherosclerotic mouse models have shown that LXR activation by GW3965 and T0901317, two synthetic non-steroidal LXR ligands, resulted in decreased atherosclerosis (160, 161). Unfortunately, concomitant induction of lipogenic genes led to hypertriglyceridemia and liver steatosis, which is an undesirable effect of most LXR agonists.

Phosphorylation of LXRα in macrophages affects gene transcription. While some genes are insensitive to phosphorylation (ABCA1, ABCG1) others get modulated upon phosphorylation. LXRα is phosphorylated in cholesterol-loaded macrophages *in vitro* and in atherosclerotic lesions *in vivo* (162). Another modification of LXR is carried out by the protein sirtuin 1 (SIRT1), which is a NAD^+ dependent deacetylase in mammals regulating physiological processes such as apoptosis, fat metabolism, and neurodegeneration. It has been reported that SIRT1 positively regulates LXR by promoting deacetylation and subsequent ubiquitination. Therefore, it is an activator of LXR turnover and SIRT1 deficiency leads to a reduced induction of LXR target genes. Most interestingly, RCT is impaired in SIRT1-/- mice (163).

The controversy of LXR activation supports the constantly ongoing search for novel LXR agonists that show only partial activation, are selective for specific tissues or selective for LXRβ since it is assumed that LXRα is responsible for the induction of lipogenic genes. Such agonists are also called small molecule NR modulators (SNuRMs) and are selective with partial function-, cell-, and/or promoter specific action.

5.8.5 LXR and its influences on metabolism and disease

LXR have been shown to reduce atherosclerotic plaque development (107, 108) and influence in carbohydrate metabolism, fat metabolism, inflammation, immune response and angiogenesis (164). Two LXR agonists, T0901317 and GW3965, showed reduced plasma glucose in leptin-deficient diabetic ob/ob mice. Both reduced the expression of key enzymes involved in hepatic gluconeogenesis and glucose output (165, 166). It was also demonstrated that LXR stimulated glucose-induced insulin secretion by isolated pancreatic β-cells (167, 168). In fact, LXRβ seemed to be mandatory for the maintenance of β-cell structure and function in mice. Nonetheless, chronic LXR activation by T0901317 led to apoptosis of pancreatic β-cells by inducing lipogenesis (169). Kalaany et al. showed that LXRα/LXRβ double knockout (DKO) mice were resistant to western type diet (WTD) induced obesity (170). Overexpression of LXRα in adipose tissue, however, reduced adipogenesis and LXR agonists stimulated release of FFA from 3T3-L1 adipocytes, suggesting enhanced lipolysis (171).

LXR exert anti-inflammatory effects in macrophages after different stimuli such as LPS by downregulating tumor necrosis factor (TNF-α) or IL-1β (172). Moreover, LXR show anti-inflammatory effects in hepatic Kupffer cells (173) or human airway smooth muscle cells (174). They are also suggested to be an important drug target concerning Alzheimer's disease because of their ability to regulate genes involved in inflammation and lipid metabolism in the brain (175).

LXR agonists increase the renin expression in kidney as well as the plasma renin activity. Renin synthesis induced by β-adrenergic stimulation is abolished in LXRα as well as LXRα/LXRβ DKO mice (176). Recently, it has also been assumed that LXR might have important implications in cancer (164).

An overview of possible sites of LXR involvement in different diseases is shown in Table 2.

Table 2. Therapeutic implications of LXR ligands

LXR activation was already shown to have an impact in a lot of different diseases and its impact in many more will be studied in the future. This table gives an insight in known and future implications of LXR (164).

Diseases in which LXR agonists may be helpful	Metabolic disorders • Low plasma HDL level • Diabetes mellitus* • Niemann-Pick type C disease Cardiovascular diseases • Atherosclerosis* • Restenosis after angioplasty Inflammatory and autoimmune disorders • Rheumatoid arthritis* • Asthma, COPD • Multiple sclerosis* • Sepsis* Skin diseases • Allergic dermatitis* • Epidermopathy of prematurity* • Psoriasis Other conditions • Infertility • Impaired uterine contractility • Alzheimer's disease* • Cancer* • Hepatoprotection in severe cholestasis*
Potential side effects of LXR agonists	• Hypertriglyceridemia and elevation of LDL • Liver steatosis and damage • ↑ Fat storage in adipose tissue ? • Lipotoxicity • Pancreatic β-cell damage • Increased renin synthesis • Reduced invasiveness of cytotrophoblast cells (? impaired conceptus implantation, reduced placental perfusion, preeclampsia) • Reduced hCG production (? ↑ risk of abortion)
Diseases in which LXR antagonists may be helpful	• Hypertriglyceridemia • Liver steatosis • Adrenoleukodystrophy

* Diseases, in which the beneficial effect was demonstrated *in vivo* in experimental animals.

5.8.6 Agonists for LXR and their structural requirements

Cholesterol itself and metabolites of its biosynthesis such as oxysterols or desmosterol are known to be natural LXR activators. An important factor for LXR binding and activation with high affinity is the position-specific monooxidation of the sterol side chain. Enhanced binding is also achieved through 24-oxo ligands that act as hydrogen bond acceptors in the side chain. Moreover, introduction of an oxygen molecule on the sterol B-ring results in LXRα selectivity (177).

Being active as a ligand is often only dependent on the stereoselectivity of a compound. 22(R)-hydroxycholesterol is a natural agonist for LXR, whereas 22(S)-hydroxycholesterol is an antagonist for LXR.

To date, there are several steroidal and non-steroidal synthetic agonists for LXR known. An agonist binds to the LBD via hydrogen bonding and thereafter the NR turns into its active formation. This active formation then recruits the binding of coactivators to the LBD, which leads to the transcriptional start of target genes (178). It is obvious that distinctive agonists show different binding efficiency for the LBD. Consequently, this leads to different conformational changes, hetero- or homodimerization, and diverse recruitment of coactivators or corepressors.

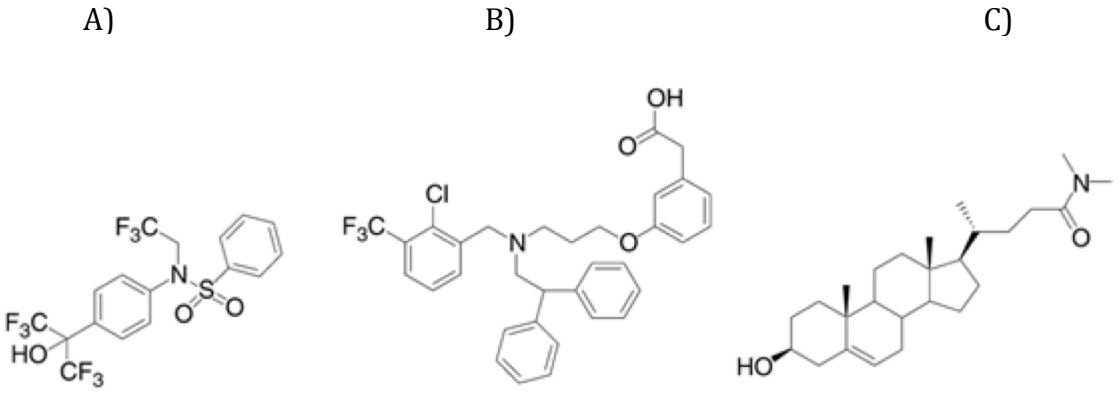

Figure 14. Chemical structures of 3 different LXR agonists
The structures of (A) T0901317, (B) the Glaxo Smith Kline compound GW3965, and (C) DMHCA.

N-(2,2,2-Trifluoroethyl)-N-[4-[2,2,2-trifluoro-1-hydroxy-1-(trifluoromethyl)ethyl]phenyl]-benzene-sulfonamide (T0901317, Tularik compound), (Figure 14A), is a potent non-steroidal synthetic activator of LXR with an EC_{50} value of 85nM for both LXR isoforms and a K_i value of 60nM for LXRα and 50nM for LXRβ (177). The EC_{50} value is the expression for the half maximal effective concentration and describes the concentration of a drug or antibody, which induces a response halfway between the baseline and maximum. It is commonly used as a measure of drug potency. K_i value is the equilibrium dissociation constant and describes the binding affinity of drugs, receptors or transporters. Moreover, it has been published that T0901317 inhibits the development of atherosclerosis in LDLR-/- mice (107). It has been demonstrated that this synthetic compound is also a potent pregnane X receptor (PXR) agonist. The compound shows the same binding efficiency and activation potency for both LXR and PXR. Therefore, studies with this compound showing LXR effects might not be only related to LXR but also to PXR (179). In fact, T0901317 also activates farnesoid X receptor (FXR) (180).

3-[3-[N-(2-chloro-3-trifluoromethylbenzyl)-(2,2-diphenylethyl)amino]propyloxy]phenyl-acetic acid hydrochloride (GW3965), (Figure 14B), is another non-steroidal synthetic LXR agonist, that is more specific for LXR than the Tularik compound. The EC_{50} values for LXRα and LXRβ are 190nM and 30nM, respectively. It has already been shown that GW3965 inhibits development of

atherosclerosis in ApoE-/- mice (108). Yet, GW3965 also induced liver steatosis, though to a milder extent than T0901317.

N,N-dimethyl-3β-hydroxy-cholenamide (DMHCA), (Figure 14C), has been identified as a potent synthetic steroidal LXR activator *in vitro* and *in vivo* (181). It induces ABCA1 expression in macrophages and liver, but has only negligible effects on hepatic SREBP1c activation (approximately one tenth of that observed for either T0901317 or GW3965) (181). The EC_{50} value for DMHCA both for LXRα and LXRβ is 2μM whereas the K_i values are 130nM for LXRα and 100nM for LXRβ (177).

5.9 Atherosclerotic mouse models

Finding and defining novel drugs and therapeutic treatments require animal models, although there is often a big difference in the metabolic regulations and gene expressions between species, namely humans and animals, especially rodents. Most mouse models are highly resistant to atherosclerosis, even when fed a high fat/high cholesterol western type diet (WTD). In fact, the inclination to develop atherosclerosis also depends on the genetic background of different mouse strains.

The **C3H/HeJ**-strain is one of these prototypical atherosclerosis-resistant models. Another atherosclerosis-resistant strain is the **FVB** model. In contrast, **C57Bl/6J** (BL/6) mice have been studied as a model, being highly susceptible to atherosclerosis upon treatment with WTD. The BL/6 strain showed reduced HDL cholesterol (182), but also a different response to inflammatory gene regulation than non-susceptible models (183). Moreover, endothelial cells (EC) from these 2 strains respond differently to mmLDL. The EC of the BL/6 strain displayed a much higher induction of MCP-1, M-CSF, and heme oxygenase 1 than EC from C3H/HeJ mice. These data suggest that the higher susceptibility for atherosclerosis in the BL/6 model is in part due to genetic differences in the response of EC to mmLDL (184). **BALB/c** mice are known for the production of plasmacytoma on injection with mineral oil, forming the basis for the production of monoclonal antibodies and develop cancers in mammary glands upon stimulation and reticular neoplasm, primary lung tumors, and renal tumors.

Inducing mutations, it was possible to develop mouse strains that are more susceptible to atherogenesis than wild type C57Bl/6J mice (185). The most common and widely used atherosclerotic mouse model is the apolipoprotein E deficient mouse (**ApoE-/-**), which was first created in 1992 (36). ApoE is an important mediator in lipoprotein clearance from peripheral tissues back to the liver via the HDL-mediated RCT (84). ApoE-/- mice develop atherosclerotic lesions resembling those observed in humans with regular chow diet, which are exacerbated when the mice are fed a WTD (186). Yet, it is very important to maintain the C57Bl/6J

background. A comparison of ApoE-/- on C57Bl/6J background with ApoE-/- on CH3/HeJ showed no differences in plasma lipid parameters but the C57Bl/6 background resulted in a significant increase of lesion formation (185). ApoE-/- mice on a FVB background had higher total cholesterol and HDL levels and less plaque formation than ApoE-/- on a BL/6 background (187). ApoE-deficient mice on a BALB/c background develop atherosclerotic lesions in a similar manner as on the C57Bl/6J background. Total serum cholesterol concentrations in BALB/c ApoE-deficient mice fed regular chow or a high-fat diet, respectively, were similar with those for C57BL/6J ApoE-deficient mice. The advantage of this background allows studying atherosclerosis in a mouse strain that can concomitantly develop other pathological traits that are not readily inducible in mice with the C57BL/6J background (188).

The creation of ApoE-/- double knockout mice (e.g. together with LDLR-/-, SR-BI-/-, or P-selectin-/-) (189) allows studying the influence of further genetic regulatory mechanisms in a complex disease. Moreover, the development of bone marrow transplantation gives the possibility to selectively study effects of gene knockout in macrophages on the development of atherosclerosis (190). The ApoE-/- model also proves to be useful in fields unrelated to atherosclerosis such as Azheimer's dementia and gene therapy. Moreover, it is a proper model for the application of noninvasive microscopy in atherosclerosis (36).

ApoE-/- mice with partial kidney ablation constitute the best model for studying the effects of chronic renal failure on plaque development and composition (44).

Other promising models are the **LDLR-/-** mice and transgenic mice that express human apolipoprotein B or mutant forms of APOE, such as the **ApoE*3Leiden (E3L)** mouse. These models are now being used to study the pathogenesis of atherosclerotic lesions, as well as the influence of genetics, environment, hormones, and drugs on lesion development (186).

E3L mice develop hyperlipidemia and are highly susceptible to diet-induced atherosclerosis (191). In fact, the expression of the mutated human APOE3 gene results in a slightly attenuated clearance of ApoB-containing particles via the LDLR pathway. As a result, cholesterol and TG levels are only moderately increased when mice are fed a chow diet. Yet, on a WTD these mice show a more humanized lipoprotein cholesterol distribution. VLDL cholesterol levels are dependent on cholesterol levels in the diet, whereas VLDL–TG levels reach a normotriglyceridemic human profile.

CETP.E3L is a model of the E3L model, crossbred with human CETP transgenic mice. CETP expression in E3L mice shifts the distribution of cholesterol from HDL to VLDL/LDL, reduces

plasma-mediated SR-BI-dependent cholesterol efflux, and represents a pro-atherogenic factor in E3L mice (192).

Unfortunately, there is also a sex-specific difference since female mice are more prone to get atherosclerosis and develop more severe plaques than male mice. This difference is only pronounced in younger mice, but disappears in older animals. This is controversial to humans, where males are more inclined to develop atherosclerosis than females (193).

5.10 Novel non-invasive microscopy techniques

Novel microscopy techniques have the advantage of being non-invasive, because they allow the detection and control of atherosclerotic plaque development without killing the animals. They give a better possibility to observe the development of certain diseases such as CVD. They allow detection and quantification of the plaque composition (lipids, calcium, collagen, elastin, and different cell types). Detection of lipid or calcium deposits in any tissue apart from the vasculature is possible as well as the identification of fibrosis in form of collagen deposits in different tissues.

Atherosclerotic lesions consist of macrophages, T cells, VSMC, collagen, and elastin. The latter two build up the necrotic core of a mature plaque and the fibrous collagen is necessary for the stability of atherosclerotic plaques. Promising non-invasive techniques are magnetic resonance imaging, x-ray angiography, intravascular ultrasound, optical, and coherence tomography. The disadvantage of these methods is the lack in resolution and specificity, which is necessary for analyzing the plaque composition and structure. The major challenges are physical restrictions of the microscope objectives, the accessibility of the major blood vessel, and the movements associated with the heart beat, breathing and other animal motion (194). Nonlinear optical (NLO) microscopy gives the possibility for three-dimensional imaging of tissues and live animals. The three major types of NLO techniques include two-photon excitation (TPE) fluorescence, second-harmonic generation (SHG), and coherent anti-Stokes Raman scattering (CARS) microscopy (195).

TPE is defined by the simultaneous absorption of two photons, each having half of the energy needed for excitation of a specific fluorophore. The probability of simultaneous absorption of two photons is very low. The most commonly used fluorophores have excitation spectra in the 400–500nm range, whereas the laser in TPE excites the fluorophores between ~700 and 1000nm range. If the fluorophore absorbs two infrared photons simultaneously, it absorbs enough energy to be raised into the excited state. If the density of photons is very high (as may be achieved by high peak power laser pulses) in conjuction with focusing to a small spot, then the rate of TPE is high and generates a fluorescence signal comparable to single photon

excitation levels. This technique results in a confocal sectioning effect in which the excitation is confined to the plane of focus. Consequently, out of plane photo-bleaching and phototoxicity are reduced which allows longer observation times for live cell imaging. TPE gives autofluorescence signal at around 500nm (Figure 15) and is a superior microscopy technique compared to conventional confocal microscopy (CFM), because it allows deeper penetration into scattering tissue as a consequence of the longer excitation wavelengths and thinner laser sectioning of thick tissues. A major disadvantage is the higher cost of the pulsed lasers compared to the constant wave lasers used in CFM (196).

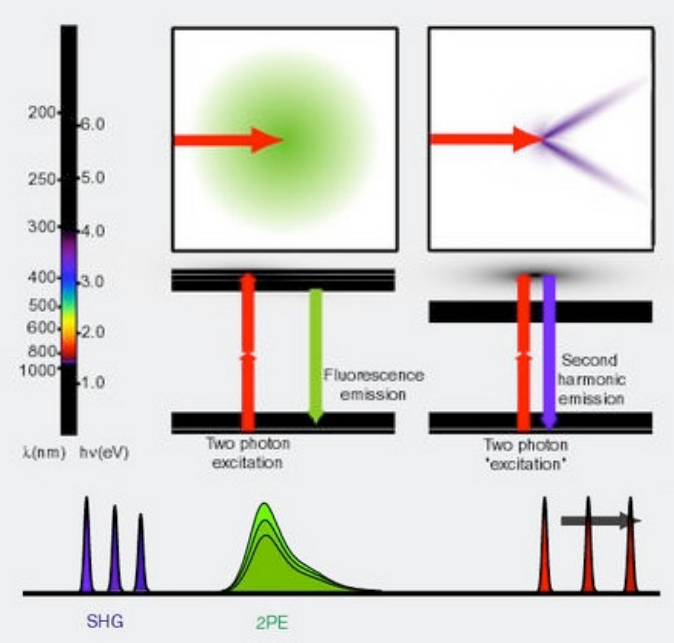

Figure 15. Exitation and emission scheme for SHG and TPE
Autofluorescence from TPE and SHG signals are different in their emission wavelength. After excitation in the NIRF (800-1000nm) the SHG signal is detectable at 388 to 409nm (blue-shifted signal) and the autofluorescence signal of TPE at 500 to 550nm (green-shifted signal).

SHG is a nonlinear optical process, in which photons interacting with a nonlinear material are effectively "combined" to form new photons with twice the energy, and therefore twice the frequency and half the wavelength of the initial photons. Excitation wavelength is in the near infrared fluorescence (NIRF) at about λ=800nm, which allows deeper tissue penetration (Figure 15). Instead of being absorbed by a molecule, photons emanating from the excitation beam are scattered via a process of harmonic up-conversion. As SHG does not involve excitation of molecules, the tissues or cells do not suffer from photobleaching or phototoxicity effects. For SHG essentially all the harmonic light may be detected with a wide aperture objective in the forward direction (direction of the excitation laser beam), and a small part travelling in the backward direction. The exact ratio between forward and backward signal depends on the sample characteristics: for thin structures, the major signal is measured in the forward direction, whereas in more turbid media, a greater part of it is scattered backwards. There is no need for special objective lenses but two different filter sets for the detection of the signals for TPE and SHG are necessary. Collagen fibers as well as muscle myosin and microtubules produce strong

second-order nonlinear effects (detected by SHG) under high photon flux illumination and can be visualized in the microscope with proper filters (197, 198). The use of SHG systems, together with TPE, is beneficial for imaging blood vessels *in vivo*. Elastin, a major structural protein of the vessel wall, produces a bright autofluorescent signal after TPE and elastin fibres have already been successfully imaged (199, 200). While TPE loses some energy during relaxation of the excited state, SHG is energy conserving. Moreover, the increased penetration depth by the NIRF excitation light is especially beneficial for imaging through the vessel wall from outside to study the structural features of the atherosclerotic lesions at the luminal side of a vessel, which is important for visualizing plaques *in vivo* (194).

In the traditional Raman spectroscopy, part of the laser light is shifted in frequency when it scatters from a sample of interest. This frequency shift is equal to the vibrational frequency of the atomic bond, so samples are chemically characterized by measuring these frequencies. Elastic or Raleigh scattering (the photon has the same energy as the initial photon) as well as inelastic scattering occur, which shifts the frequency of the original photon to the energy of the vibrational state of the molecule. The frequency of the emitted light might be lower than the excitation photon (the molecule absorbs energy) giving a red signal (stokes-shift) or higher (the molecule loses energy) giving a blue signal (anti-stokes shift) (Figure 16).

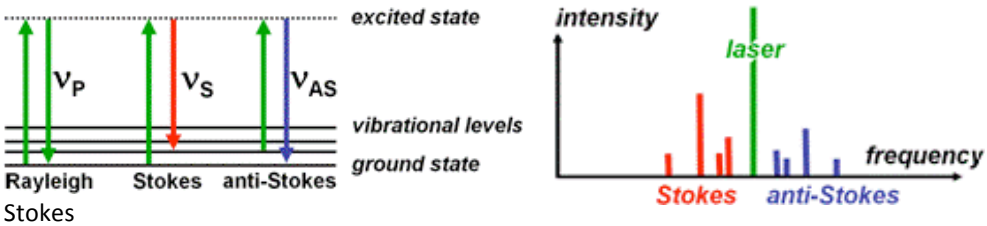

Figure 16. Raman spectroscopy Possibilities of light scattering: Rayleigh scattering (no Raman effect), Stokes scattering (molecule absorbs energy), shifting the energy to red light, and anti-Stokes scattering (molecule loses energy), shifting the energy to blue light. The Stokes signal is easier detectable because it produces a stronger signal.

Each atomic bond can have many vibrational modes, including stretching and bending. The benefits of Raman spectroscopy are that any type of material can be investigated with this technique. Yet, only 1 in approximately 10^{10} photons is Raman-scattered. Biological samples have low Raman scattering, so it takes a whole day to acquire an image. The laser used for Raman spectroscopy is a continuous wave (CW) laser similar as used in CFM. The coherent anti-Stokes Raman scattering (CARS) is a third-order nonlinear optical process that, unlike Raman spectroscopy, employs multiple photons to address the molecular vibrations. It produces a signal in which the emitted waves are coherent with one another. It involves a pump beam at a frequency of ω_p, and a Stokes beam at a lower frequency, namely ω_s. These two nonlinear beams are converted to a coherent anti-Stokes beam with frequency of $2\omega_p$-ω_s. The anti-Stokes beam is generated in the phase matching direction giving a blue signal and travelling antiparallel to the Stokes beam. The image contrast in CARS microscopy is created when the frequency difference

(ω_p-ω_s) between pump and Stokes beam is tuned to be resonant with a Raman-active molecular vibration of the sample (ω_{vib}). The wavelengths for the laser pulses are chosen in the NIRF, which reduces the background from two-photon processes. The Stokes pulse (1064nm) is emitted from a narrow-band Nd:YAG laser and the pump pulse from a mid-band optical parametric oscillator (OPO) (Figure 17). The system is different to normal Raman spectroscopy because the CARS approach produces a large and directional signal. Therefore it allows much faster imaging of samples (201). Some examples for vibration energies are 2850cm^{-1} for a CH_2-streching or 3015cm^{-1} for a HC=C vibration. Lipid droplets have already been successfully imaged with the CARS system (202). Here the vibrational frequency of the CH_2 bonds is used since these chemical bonds are very frequent within lipid droplets and give a strong Raman response. Molecules with lower concentration or a weaker Raman response are still difficult to image (203). One tricky part is given by the fact that there is a lot of background signal generated from other organic molecules. Therefore it is tricky to image optimal cooling temperature (OCT) medium-embedded sections of tissues. Recently, wide-field CARS was applied to image both the strong –CH as well as the weak =CH signal which implicated the identification of saturated as well as unsaturated FA (201). A new challenge is the detection of calcium deposits by using the vibrational modes of calcium-hydroxyapatite as a signature of calcification, since calcium itself has no vibrational change and thus cannot be detected. The combination with SHG/TPE suggests perfect imaging of lipid and calcium deposits in the plaque of an atherosclerotic vessel with parallel imaging of collagen-containing fibrous caps.

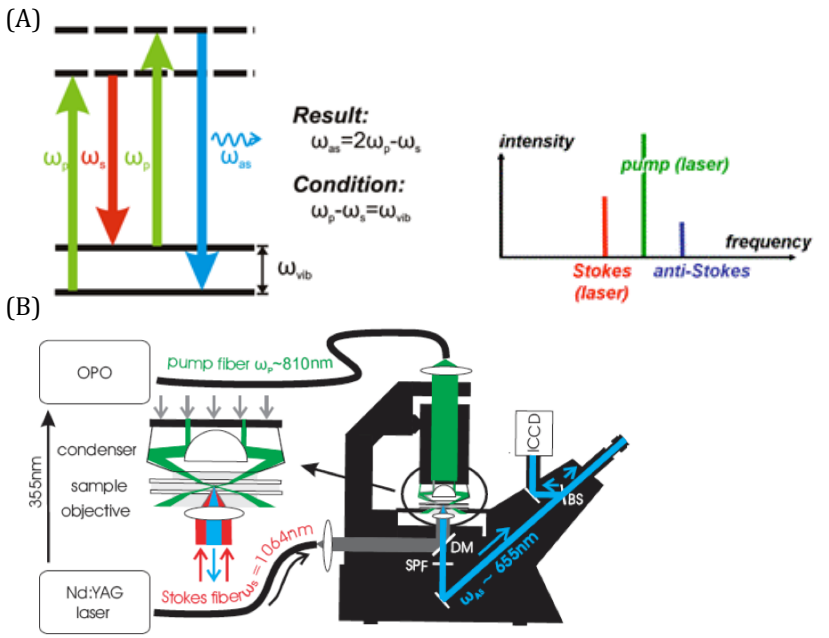

Figure 17. The non-linear optical process of CARS (201)
(A) Energy level scheme of CARS shows that it is a 4-photon process. A CARS signal (blue) results if the wavelength difference between pump and Stokes beam is equivalent to the vibrational wavelength of the molecule (ω_p-ω_s=ω_{vib}). (B) The excitation for CARS is in the NIRF, using 1064nm as the Stokes pulse emitted by a Nd:YAG laser and about 800nm for the pump puls by an optical parametric oscillator (OPO) (201, 203).

Stimulated Raman scattering (SRS) has a higher sensitivity than spontaneous Raman microscopy by implementing high-frequency (megahertz) phase-sensitive detection. It has a major advantage over previous coherent Raman techniques because it allows background-free and readily interpretable chemical contrast (204).

6 Aims of this doctoral thesis

This thesis was focussed at a novel agonist for the nuclear liver X receptor (LXR). This agonist is N,N-dimethyl-3β-hydroxy-Δ^5-cholenamide (DMHCA) and is a synthetic, steroidal activator of LXR. LXR plays a role in a lot of different pathways, such as cholesterol and lipid metabolism, inflammation and carbohydrate metabolism. It has been shown the LXR activation by different agonists reduced atherosclerotic plaque formation but still have the drawback of inducing liver steatosis (107, 108). Since DMHCA has been shown to have a favorable potential in LXR activation (181), my aims were to synthesize this compound and study:

- gene regulation upon DMHCA treatment in mouse peritoneal macrophages (MPM) and other cell lines in comparison with T0901317 and GW3965 applying microarrays and real-time PCR
- regulatory effects of DMHCA in *in vivo* experiments using wild type and ApoE-/- mice
- protein and gene regulation in MPM and liver as well as liver pathology after i.p. injection of DMHCA
- effects of DMHCA in different mouse models and its impact on atherosclerosis

In fact, this part of my thesis resulted in the manuscript "*Synthetic LXR agonist attenuates plaque formation in apoE-/- mice without inducing liver steatosis and hypertriglyceridemia*" by Kratzer et al., which was published in The Journal of Lipid Research in 2009 Feb;50(2):312-26. Epub 2008 Sep 23.

Moreover, I worked with non-invasive microscopy techniques in atherosclerosis and calcification of chronic kidney disease and atherosclerosis. They provide an alternative to conventional staining techniques and give more flexibility in studying impacts of drugs independently of concentration and time period. Two photon excitation (TPE) and second harmonic generation (SHG) were applied for the detection of elastin and collagen in combination with coherent anti-Stokes Raman scattering (CARS) for the identification of lipids and calcium deposits within the aorta of ApoE-/- mice with partial kidney ablation. The data achieved were compared with oil red O staining for lipids and von Kossa staining for calcification. This project was performed in the laboratory of Dr. Moshe Levi at the Institute of Renal Disease and Hypertension at the University of Colorado at Denver, USA in cooperation with the Beckman Laser Institute, Irvine, California, USA under the supervision of Dr. Bruce Tromberg and Dr. Eric Potma. The studies are not complete and are still ongoing in the Levi and Tromberg laboratories.

7 Materials and Methods

7.1 List of chemicals

Table 3. Chemicals and solutions used for cell culture experiments

chemical/solution	company
Dulbecco´s modified Eagle´s (DMEM) medium	Gibco
fetal bovine serum (FCS)	PAA
RPMI1640	Gibco
L-glutamin	PAA
penicillin/streptomycin	Cambrex
fungizone	Gibco
trypsin	PAA
LPDS	self made
acLDL	self made
aggLDL	self made
PBS	Self made
ethanol	Merck
DMSO	Merck
GW3965	Glaxo Smith Kline
22-(R)-hydroxycholesterol	Sigma-Aldrich
T0901317	Cayman Chemical, Ann Arbor, MI, USA
DMHCA	Self made and Wyeth Pharmaceuticals, PA, USA
9-cis-retinoic acid	Sigma-Aldrich
^{14}C-acetate	Amersham
^{14}C-mevalonate	Amersham
3% thioglycollate medium	Self made
peptone 140	Gibco
peptone 110	Gerbu Biochemicals
L-cystein	Serva
glucose	Sigma
sodium chloride	Roth
sodium thioglycollate	Sigma
Sodium sulfite	Merck
formaldehyde	Sigma-Aldrich
glycine	Roth/Lactan
phorbol myristate acetate (PMA)	Merck
LPS	Fisher Scientific
HBBS	Invitrogen
serum replacement 3 50x	Sigma
Collagenase XI	Sigma
histopaque	Sigma

Table 4. Chemicals and solutions used for RNA techniques

chemical/solution	company
nuclease-free H_2O	Fresenius, Ambion
diethylpyrocarbonate (DEPC)	Sigma-Aldrich
M-MLV Reverse Transkriptase	Invitrogen, Lofer, Austria
oligo-dT-anchored-primer	Sigma-Aldrich
RNAsin	Promega GmbH, Germany
iScript RT kit	BioRad
LightCycler FastStart DNA Master SYBR Green I	Roche Applied Bioscience, Austria
QuantiFast SYBR Green PCR Kit (2000)	Qiagen
Fast SYBR Green Master Mix	Applied Biosystems
Morpholinopropansulfonic acid (MOPS)	Roth
SDS	Serva
glycerin	Merck
1M phosphate buffer	Self made
EDTA	Gibco
ethidium bromide	Sigma-Aldrich
agarose	Gibco
dNTP-set	Invitrogen, Lofer, Austria
tri-reagent	Invitrogen, Lofer, Austria
trizol	Gibco
Rneasy kit	Quiagen
formamide, re-distilled	Invitrogen, Lofer, Austria
NaOAc	Roth
glycerol	Sigma

Table 5. Chemicals and solutions used for other biochemical methods

chemical/solution	company
acrylamid/bisacrylamid	Sigma Aldrich
TEMED	Sigma Aldrich
ammonium persulfate	BioRad
Tris	Roth
glycine	Roth

glycerin	Merck
β-Mercaptoethanol	Merck
Tween20	Sigma Aldrich
milkpowder	Interspar
T4-DNA ligase	New England Biolabs
dNTPs	Invitrogen, Lofer, Austria
HotFire polymerase	Solis Biodyne
Advantage^{R} cDNA Polymerase Mix	BD Biosciences
NaOAc	Roth
primer	Invitrogen, Lofer, Austria
TAE buffer	Self made
DNA 100 bp ladder	New England Biolabs
NH_4Oac	Merck
Na-Acetate	Roth
polyclonal rabbit anti-goat immunoglobuline-HRP	DakoCytomation
polyclonal goat anti-rabbit immunoglobuline-HRP	DakoCytomation
polyclonal rabbit anti-rat immunoglobuline-HRP	DakoCytomation
chromogen AEC	DakoCytomation
mLXRα	Santa Cruz
mLXRβ	Santa Cruz
LXRα/β	Santa Cruz
hLXRα	Perseus Proteomics
hLXRβ	Perseus Proteomics
mouse anti-rabbit NDRG1	Santa Cruz
mouse anti-goat Trb3	CallBiochem
MOMA-2	Acris
Alexa Fluor 568 phalloidin	Invitrogen
ECL^{TM} western-blotting detection reagents	Amersham
prestained protein ladder	Fermentas
VECTASHIELD mounting medium plus DAPI	Szabo Scandic
Bradford reagent	BioRad
10x SDS-running buffer	self made
separating gel buffer	self made
stacking gel buffer	self made
SDS sample buffer	self made
10x blot washing buffer	self made
10x blot washing buffer	self made
NaCl	Merck
HCl	Merck
Na_2HPO_4	Merck
KH_2PO_4	Merck
Tween 80	Sigma
Carboxymethylcellulose (CMC)	Merck
Nembutal (pentobarbital sodium)	Merck
Optimal cooling temperature (OCT) medium	Sanova Pharma GesmbH Diagnostik
Oil red O powder	Sigma
silver nitrate	Sigma, Merck
sodium thiosulfate	Sigma
phenol	Lactan/Roth
hematoxylin	Dako
Proteinase K	Lactan/Roth
Protease inhibitor cocktail PIC	Sigma
A/B sepharose beads	Santa Cruz
sucrose	merck
dithiothreitol	Sigma
leupeptin	Sigma
antipain	Sigma
pepstatin	Sigma
NH_4HCO_3	Sigma
$CaCl_2.2\ H_2O$	Merck
Acetonitrile HPLC grade	Merck
DDT	Sigma
IAA	Sigma
Modified trypsin sequencing grade	Promega
3 β-Hydroxy-Δ5-cholenic acid	Sigma
N,N-Dimethylamine,anhydrous	Sigma
Szintilation cocktail	Perkin Elmer
2-propanol	Roth
n-hexan	Roth
diethylether	Roth
Acetic acid	Roth

7.2 Buffer and solution preparation

7.2.1 Isolation medium for MPM

3% thioglycollate solution: Seventeen g peptone 140, 3g peptone 110, 0.25g L-cysteine, 6g glucose, 2.5g sodium chloride, 0.5g sodium thioglycollate, 0.1g sodium sulfite, and 0.7g agar were dissolved in 1L ddH_2O and the solution is sterile filtrated.

7.2.2 Phosphate buffered saline (PBS)

10X PBS: 80g NaCl, 2.0g KCl, 14.4g Na_2HPO_4, and 2.4g KH_2PO_4 were dissolved in 1L ddH_2O. The pH was adjusted to 7.4 with HCl and the volume brought to 1L with additional distilled H_2O. The solution is sterilized by autoclaving and is used in a 1:10 dilution for cell culture.

7.2.3 Solutions for Western blotting

10x SDS running buffer: 30.3g Tris, 150.1g glycine and 10g SDS were dissolved in 1L ddH_2O.

separating gel buffer (buffer 1): 18.2g Tris and 4mL 10% SDS were dissolved in 80mL ddH_2O. After setting the pH to 8.8 with HCl, the volume was filled up to 100ml with ddH_2O.

stacking gel buffer (buffer 2): 6g Tris were dissolved in 90ml ddH_2O, the pH was adjusted to 6.8 with HCl and the volume was filled up to 100ml with ddH_2O.

SDS sample buffer: 2.15g SDS and 0.76g Tris were dissolved in 45mL ddH_2O. The pH was set to 6.8 with HCl and 10ml glycerol (80%) and some granules of bromphenol blue were added.

10x blot buffer: 12.1g Tris, 30g glycine and 1mg/mL EDTA were dissolved in 1L ddH_2O.

10x blot washing buffer: Five g Tween20, 90g NaCl and 1M TrisHCl (pH 7.4) were dissolved in 1L ddH_2O.

5% milk powder: Five g milk powder were dissolved in 1X blot washing buffer.

Cell lysis buffer: 0.25 M sucrose, 1 mM EDTA, 1 mM dithiothreitol, 20 g/ml leupeptin, 2 g/ml antipain and 1 g/ml pepstatin were dissolved in ddH_2O and the pH adjusted to 7.0 with HCl.

7.2.4 Gel electrophoresis

40x TAE buffer: 193.6g Tris, 65.5g Na-acetate and 14.9g EDTA were dissolved in 800mL ddH_2O. After the pH was set to 7.2 with acetic acid the volume was adjusted to 1L with ddH_20.

DNA sample buffer: 5mL glycine, 250µL 40X TAE buffer and 1 granule of bromophenol blue were added to 4.75mL ddH_20 to give a total volume of 10mL.

7.3 Primer list

Real-time PCR primers were designed with primer designer version 2.0.

Table 6. Primer sequences of mouse genes for real-time PCR

Gene	Forward primer	Reverse primer
ABCA1	CTCTTCATGACTCTA GCCTGGA	ACACAGACAGGAAG ACGAACAC
ABCG1	GGTATCAAGGAAGA	TGTGACTGTCAGTAG
	GTCAGTGC	CTGCTGG
ABCG5	CAAGACTGCTTCTCC TACGTCCTGC	CCAGCTCAGCCAAGA GAAGGACAAT

Gene	Forward primer	Reverse primer
ABCG8	AGTGGTCAGTCCAACACTCTG	GAGACCTCCAGGGTATCTTGAA
ChREBP	GCATCGATCCGACACTCACC	GATGCGCCGCTTCCAGTAAT
CYP7A1	AGACCTCCGGGCCTTCTT	ATCACTCGGTAGCAGAAGGCAT
FAS	GAAGCCGAACACCTCTGTGCAGT	GCTCCTTGCTGCCATCTGTATTG
ACC	GGACTTGGAGCAGAGAACCTTCG	CAAGCTGGTTGTTGGAGGTGTA
LDLR	CTCCTGCATTCACGGTAGCC	CCCACTGTGACACTTGAACTTG
HmgCoAr	CTATTGCACCGACAAGAAGCCT	GCCATCACAGTGCCACATACAA
SREBP1c	ACTGTCTTGGTTGTTGATGAGCTGGAGCAT	ATCGGCGCGGAAGCTGTCGGGGTAGCGTC
Cyclophilin A	TTCCAGGATTCATGTGCCAG	CCATCCAGCCATTCAGTCTT
HPRT	GCCTGTATCCAACACTTCG	GCTGACCTGCTGGATTACA
CAR6	AGTGGTCTGAGCAGTATCC	TGTCCGTTGTTAGTCATAGTG
AQP9	TTGTATCCGTGCCAGGTG	CCAGAGTTGAGTCCGAGAG
TRB3	TGTCTGATCCGCTGTCTC	CTGGTCCATCTCCCTTCG
IDI1	AATAGTTGCTGTAGTCATCC	TGTTAGATAATCCATTTCATTTAG
NDRG1	GAGCAACCTACACTTATTCATC	CATTCCACCACAGCATCC

Gene	Forward primer	Reverse primer
ERO1L	TGGAGCCGTGGATGAGTC	CCTTGTAGCCTGTGTAGCG
HMGCS	TTGGCAGGGAAGAGGGTTGGAGTG	GGCCGAGGTTGCAGGGAGTCTTG
STARD4	CGAAGAAGATGAGTGGCGAG	CCAGCAGTGGTGTAACGCAT
CYP51	CATCGCCTGCGCCTTCACTCTC	TTTCTCCGCTTTCTCCCCAACTTT
SCD1	ACTACCACCACACCTTCC	CGTCTCCAGTTCTCTTAATCC
SREBP2	TTGAGGATGAGGCTAAGAG	ATCAGTGTGCTTGGTAGG
REV-ERB	CATACTTCCCACCATCACCTAC	ACTCGGCTGCTGTCTTCC
NPC1	AATGCCTGCCGTGATGTG	CGCTTGTCCGTTGTCTTTATTG
SIRT1	GCTGACGACTTCGACGACG	TCGGTCAACAGGAGGTTGTCT
DHCR24	CAACCTGATGGACATCCTGG	ACGATGACTCGATGCCTGTG
LXRα	CCTGATTCTGCAACGGAGTTGTG	CACGTTGTAATGGAAGCCAGAGG
LXRβ	CTCTGCCTACATCGTGGTCATCT	ATGAAGGCATCCATCTGGCAGGT
API6/CDL5/SPα	ACCTGTAAGTTCCAGCCTGC	ACTGCAACGGAACGGAAGAC
SR-BI	GAGCACGTTCTACACGCAG	GGTCTGACCAAGCTATCAGGTT
APOE	ACGCTGTCTGACCAGGTCCA	GCTCACGGATGGCACTCACA

Table 7. Primer sequences of human genes for real-time PCR

Gene	Forward	Reverse
NDRG1	CCTACCGCCAGCACATTG	GTCGCTCAATCTCCAGGTC
TRB3	AGGGAAGAGGAGGGAGAC	TCTGGAAGGCACTGAAGG
SIRT1	GCCTTGCTGTAGACTTCC	TGTTCTGGGTATAGTTGCG
ERO1L	GTTAGTGGTTACTTGGATGATTG	ACAGCACAGTCCCTTCTTC
ABCA1	AAGGCTACCAGTTACATTTGAC	TTCTCAGGATTGGCTTCAGG
ABCG1	GAGCCCAAGTCGGTGTGTG	TCAGATGTCCATTCAGCAGGTC
NPC1	GCAGCCACATAACCAGAG	AATGCCTGCCGTGATGTG
FAS	GCCGCCATCTACAACATC	CTTCCACACTATGCTCAGG
REV-ERB	AGTTTGAATGACCGCTCTC	GGGATGGTGGGAAGTAGG
SREBP1c	TCAGCGAGGCGGCTTTGGAGCAG	CATGTCTTCGATGTCGGTCAG

CYP51a1	GGTAGGCAAGACATTTACTTAC	AACTGGATTAGGCACATCG
Cyclophilin A	TGACTTCACACGCCATAATG	TGCCATCCAACCACTCAG
LXRα	CCTGTGCCTGACATTCCTCCTG	CACACGCTGCATAGCTCGTTCC
LXRβ	ATGTCCTCTCCTACCACGAGTTC	GTAGTGGAAGCCGGAGGCCTTGT

7.4 Synthesis of N, N-dimethyl-3β-hydroxycholenamide (DMHCA)

The molecular weight (MW) of DMHCA=401.64g/mol. The synthesis was performed according to Louw et al (205). Starting with 1g of 3 β-Hydroxy-Δ^5-cholenic acid, the 3-step synthesis of DMHCA gave an output of 30% for the first time and 50% the second time. The summary of the synthesis is shown in the Results part and the detailed procedure and purity control is described there.

7.5 Cell culture

All cells were grown in a humidified incubator with 5% CO2 at 37°C. All media used in cell culture were supplemented with 1% L-glutamine and 1% streptomycin/penicillin and either 10% FCS, 10%LPDS or serum-replacement. Before use, media were pre-warmed to 37°C in a water bath.

7.5.1 RAW264.7 (ATCC Number: TIB-71)

RAW264.7 is a male *mus musculus* macrophage cell line established from a tumor induced by Abelson murine leukemia virus. These cells are negative for surface immunoglobulin, Ia, and Thy-1.2. Routinely the cells were maintained in DMEM medium (4.5g/L glucose) with 10% FCS and medium was replaced every 2 to 3 days. For subcultivation cells were split in a ratio of 1:4.

7.5.2 HepG2 (ATCC Number: HB-8065)

HepG2 cells are male human hepatocytes, expressing HmgCoAr and hepatic TG lipase activities. HepG2 cells demonstrate decreased expression of apoA-I mRNA. Cells were maintained in DMEM medium with 10% FCS, 1% P/S and 1% glutamine. Medium renewal was twice a week. For subcultivation cells were trypsinated and split in a ratio of 1:4 to 1:6.

7.5.3 Caco-2 (ATCC Number: HTB-37)

Caco-2 cells are derived from human colorectal adenocarcinoma. Upon reaching confluence, the cells express characteristics of enterocytic differentiation. Caco-2 cells express retinoic acid binding protein I and retinol binding protein II. They are cultivated in EMEM plus 20%FBS.

7.5.4 Mouse peritoneal macrophages (MPM)

MPM were obtained from 6-8 week old male or female C57BL/6, ApoE-/- or LXR-/- mice. Mice were injected intraperitoneally (i.p) with 3ml of sterile 3% thioglycollate medium. After 3 days mice were killed by cervical dislocation and MPM were washed from the peritoneal cavity with 10ml of sterile PBS. Cells were centrifuged at 150xg for 5 minutes and the pellet was washed once with PBS. Macrophages were resuspended in DMEM supplemented with 10% FCS or LPDS and seeded out into a T-75 flask. After 2-4 hours cells were washed with 1XPBS to remove cells except macrophages and fresh medium was added.

7.5.5 THP-1 monocytes (ATCC Number: TIB-202TM)

THP-1 cells are human monocytes that synthesize and secrete M-CSF and apolipoprotein E (apoE). Cells were grown in suspension in bicarbonate buffered RPMI 1640 medium containing 10% FCS or LPDS. Cultures were maintained by the addition of fresh medium. For macrophage differentiation cells were grown in cell culture medium supplemented with PMA to give a final concentration of 160nM for 3 days whereby the medium was refreshed every 24 hours. For subcultivation part of the culture was transferred into a new T-75 flask and fresh medium was added.

7.5.6 Human peritoneal macrophages (hPM)

2L human peritoneal fluid (male patient with peridonitis, received 2g vancomycin, 3 days later the PD fluid was clear and used to harvest macrophages) was centrifuged at 2000 rpm for 15min.Then washed once with HBBS (Hank's buffer) and centrifuged for 10min at 1500 rpm, then twice with RPMI1640 and centrifuged 10min at 1500 rpm. The cells were resuspended in RPMI1640 (+ 2mmol Glutamine) + 10% FCS and 1% P/S(100U/mL) and plated in 2 six-well plates overnight. The next day, the cells were washed once with HBBS and treated with RPMI1640 + 2%FCS plus 2 different LXR agonists.

7.5.7 Perinuclear blood mononuclear cells (PBMC)

Twenty units heparin were put in 60cc (60mL) syringe. Two 50mL Falcon tubes were filled with 15mL Histopaque (SIGMA) and the blood was added slowly, so it does not mix with the histopaque. About 30mL of blood was put in each tube and filled up to 50mL with 1XPBS. Then, the tubes were centrifuged for 20min at 1500rpm at 4°C. The middle layer (white layer), containing the cells, was put into new 50mL tube, which was filled up to 50mL with 1XPBS again. It was centrifuged at 1000rpm at 4C for 10min. The supernatant was taken off and the tube was filled up to 30mL with 1X PBS. An aliquot was taken and the cells were counted in a Neubauer chamber. The counted 1.9 million cells/mL (which gave a total number of $5.7x10^{10}$ cells) were washed again, taken up in 24mL RPMI1640 and plated into 2 six-well plates. Cells were left to attach about 3 hours and treated with LXR agonists and LPS for different time points.

7.5.8 Treatment of cells with agonists

Depending on the cell type, cells were plated in 10% or 2% FCS containing RPMI1640 medium, serum-free RPMI1640, 5% or 10% LPDS, or DMEM containing serum-replacement. Agonists were dissolved in either ethanol or DMSO.

7.6 RNA isolation, reverse transcription and quantitative real-time PCR

Total RNA from mouse tissues was isolated using the Trizol procedure according to the manufacturer´s protocol (Invitrogen, Lofer, Austria). Total RNA from cells was isolated using

RNeasy Mini Kit (Qiagen, Hilden, Germany). Quantitative gene expression analysis was performed on a LightCycler 480 (Roche Diagnostics, Mannheim, Germany) using the Quantifast™ SYBR®GREEN PCR Kit (Qiagen, Austria). Other machines used were Applied Biosystems StepOne Plus Real-Time system Singleplex PCR and an icycler from BioRad, both working with SYBR®GREEN. For RNA quantification 150ng -2 µg of total RNA was reverse transcribed according to the manufacturer's instructions using random hexamer primers (Finnzymes, Espoo, Finland). In general, 6 ng template cDNA was used for each real-time PCR. PCR primers used for real-time PCR were designed with primer designer version 2.0.

Melting curve analysis was performed to ensure that a single PCR product was amplified and no primer dimers were generated. PCR efficiency of each transcript was determined using 4 dilutions (1:5, 1:25, 1:125, 1:625) in triplicate of a pool of all available cDNA of one experiment. To confirm accuracy and reproducibility a minimum of 3 samples per condition were measured in triplicate. Crossing points were determined by Second Derivate Maximum Method and PCR efficiencies were calculated from the slope, according to the established equation $E=10^{[-1/slope]}$. Data calculations and determination of statistical parameters were performed with the public domain program relative expression software tool REST (http://www.gene-quantification.com/download.html) using a pair-wise fixed reallocation randomization test (206). Data are displayed as expression ratios normalized to a reference gene. Initially, amplifications of murine cyclophilin A were performed as internal controls for variations in mRNA amounts. In the liver, cyclophilin A expression varied between mouse genotypes and therefore hypoxanthine guanine phosphoribosyl transferase (HPRT) was used as reference gene. In macrophages, aorta, and ileum data are displayed as expression ratios normalized to cyclophilin A or 36b4 as reference gene.

7.7 Quantification of nucleic acid concentrations

Concentrations of nucleic acids were determined photometrically using a NanoDrop spectrophotometer at wavelengths of 260nm and 280nm. An optical density (OD) of 1 corresponds to approximately 50 µg/ml double-stranded DNA or 40 µg/ml single-stranded DNA and RNA. The ratio between the readings at 260 nm and 280 nm (OD260/OD280) provides an estimation of the purity of the nucleic acid preparation. Highly pure DNA or RNA is characterized by ratios between 1.8 and 2.0. Concentrations were calculated according to the following equation:

$$c\ [\mu g/ml] = OD_{260} \times D \times F$$

D = dilution factor F = multiplication factor
(dsDNA = 50; RNA = 40)

7.8 Western blot

Nuclear extraction (207) and protein quantitation were performed as described (208). Aliquots (100 µg of protein) were separated by SDS-PAGE and blotted onto nitrocellulose membranes. For immunoblot analysis, SREBP1 antibody (Santa Cruz Biotechnology, Heidelberg, Germany) (1:1000) was visualized with horseradish peroxidase-conjugated goat anti-rabbit IgG (1:2000, Dako Österreich GmbH, Vienna, Austria) using the Enhanced Chemiluminescence (ECL) Western Blotting Detection System Kit (Amersham Biosciences, GE Healthcare Europe GmbH, Vienna, Austria). Gels were calibrated with the Sigma marker wide range (Sigma, Vienna, Austria). Membranes were exposed to ECL Hyperfilm (Amersham Biosciences). The same procedure was performed for any other antibody used in this thesis.

7.9 Immunofluorescence

Cells were plated onto chamber slides (4-well), treated with different LXR agonists for 24 hours in LPDS medium. Then, cells were kept on ice, once washed with medium and fixed with 4% PFA for 10-15min. Thereafter the cells were washed twice with 1xPBS, the fixation was stopped by incubating with 20mM glycine in medium for 10-15min. After the fixation stop cells were washed twice with 1xPBS again and kept in the fridge until antibody incubation. Without blocking: Cells were washed three times with 1xPBS (without Calcium) on ice and then permeated with 0.1% triton X-100 in 1xPBS for 30min in the cold room (4˚C). Next, the cells were washed again once with the 0.1% Triton X-100 1xPBS solution and the antibody was added in fresh solution (with triton) in dilution (1:50 for NDRG1 and 1:200 for TRB3) and kept overnight in the cold room. The next day, the samples were washed three times with 1xPBS (+0.1% Triton X-100) and incubated for about 1 hour with the 2˚ antibody (Alexa 488 anti-rabbit for both 1˚antibodies, diluted 1:200 in 0.1% Triton X-100) as well as with Phalloidin (Alexa 568) for f-actin staining (cytoskeleton of the cells). Then, cells were washed twice with 0.1% Triton X-100 (in 1xPBS) and then once with 1xPBS. Then, after removing the chambers, a drop of the mounting medium with DAPI (Vectashield) was added, the slides were covered with a coverslip and the edges were sealed with nail polish and imaged with the Zeiss LSM 510 META on Axionvert 200M.

7.10 Microarrays

Microarrays were performed with cDNA of mouse peritoneal macrophages treated with different LXR agonists.

7.10.1 ABI Mouse Genome Survey Arrays hybridizations

Mouse Genome Survey Arrays V1.0 (Applied Biosystems) were used to determine the transcriptional profiles of MPM treated with T0901317 and ethanol (control). DIG-labeled cDNA

probes were generated by reverse transcription of 20µg total RNA using the Chemiluminescent RT-Labeling kit (Applied Biosystems, Foster City, CA, US) according to the manufacturer's protocol. Array hybridization, chemiluminescence detection, image acquisition and analysis were performed using Chemiluminescence Detection Kit and 1700 Chemiluminescence Microarray Analyzer (Applied Biosystems) following the manufacturer's instructions.

Each microarray was first pre-hybridized at 55°C for 1 hour in hybridization buffer containing blocking reagent. Oligo-dT-primed, DIG-labeled cDNA targets were fragmented, mixed with internal control target, and hybridized to the equilibrated microarrays in a volume of 1.5ml at 55°C for 16 hours. After hybridization, the arrays were washed with hybridization wash buffer and chemiluminescence rinse buffer. Enhanced chemiluminescent signals were generated by incubating arrays with alkaline phosphatase conjugated anti-digoxigenin antibody followed by incubation with Chemiluminescence Enhancing Solution and a final addition of Chemiluminescence Substrate. Four images were collected for each microarray using the ABI 1700 Chemiluminescent Microarray Analyzer. Images were auto-gridded and the chemiluminescent signals were quantified, corrected for background and spot and spatially normalized.

7.10.2 Data analysis of microarrays

Normalization, statistical analysis and visualization of microarray data was performed using GeneSpring 7.3.1 software (Agilent Technologies, Palo Alto, CA, USA). The following data calculation was applied to identify significantly up- and downregulated genes.

Data transformation: Measurements with values below 10 were adjusted to 10. Normalization was done to the 50th percentile per chip. Additionally, normalization was done to specific samples (control samples) per gene. The Cross Error Model was applied to identify probes with valid expression signals (control signal values between 96 and 2151545).

All probes with normalized signal values between 0.667 and 1.334 in both groups were subtracted. From the resulting probe list (4980 genes) statistically significantly up- and downregulated genes were identified applying Welch t-test (parametric test, variances not assumed equal) and a p-value cut-off < 0.05.

7.11 Detection of LXRE

Potential liver X response elements (LXRE or direct repeats 4 (DR4)) were studied using the in silico program "Rephex" from Phenex Pharmaceuticals AG, Ludwigshafen, Germany. Rephex is a web-based database interface based on a genome-wide dataset of putative promoter regions comprising the area from 10kB before to 20kB after the start codon of a gene. The algorithm scans sequences of interest for

specific motifs (e.g. the direct repeat 4 (DR4) for LXRE (AG[GT]TCA-NNN-AG[GT]TCA). A maximum of two mismatches (MM) are allowed within a sequence. The received dataset is saved in a database and can be searched for different information such as motif, gene name, gene ID, and gene description. Furthermore, the algorithm allows a restriction for the MM rate and minimum of hits by changing the sequence length of the putative promoter region. To date, Rephex is restricted for the species mouse, human, and rat, but also allows also combined data retrieval between the species. Datasets are received from the Ensembl database (http://www.ensembl.org/index.html). Additional information such as annotation is gained from BioMart tool (http://www.ensembl.org/biomart/martview). Further formatting is performed with the EMBOSS package (http://emboss.sourceforge.net/). Hereby, the program "fuzznuc" is important, which allows pattern search including MM on DNA sequences. The automation of data processing and of the database itself (http://www.mysql.de/) is realized with phyton scripts (http://www.python.org/). Sequences with perfect match and one MM were supposed to be potential DR4. We examined human and mouse promoters of potential novel LXR target genes.

7.12 Animals and diets

Animal experiments were performed in accordance with the standards established by the Austrian Federal Ministry of Education, Science and Culture, Division of Genetic Engineering and Animal Experiments (Vienna, Austria). C57Bl/6 (Himberg, Austria) and apoE-deficient mice on a C57Bl/6 background (Charles River WIGA GesmbH, Sulzfeld, Germany) were maintained in a clean environment on a regular light-dark cycle (14h light, 10h dark). Before the initiation of the corresponding diets mice were kept on a standard laboratory chow diet. Male C57Bl/6 mice were fed chow diet or western type diet (WTD; TD88137 mod. containing 21% fat and 0.2% cholesterol, ssniff, Soest, Germany and Harlan Teklad, USA) ± DMHCA or T0901317 (80 mg/kg body weight/day) (Cayman Chemical Company, Ann Arbort, USA) for 4 or 15 days. To study atherosclerotic lesion formation, male and female apoE-deficient mice were fed ad libitum the WTD ± DMHCA (8 mg/kg body weight/day) for 11 weeks. To elucidate gene regulation by DMHCA in apoE-null mice in short time experiments, male mice were fed chow diet ± DMHCA (80 mg/kg body weight/day) for 4 days or WTD ± DMHCA (8 mg/kg body weight/day) for 15 days. Diets were supplemented with the respective LXR ligand at a level sufficient to provide the appropriate mg/kg food dose on consumption of a 5 g diet by a 25 g mouse per day. Body weight and food intake were monitored regularly. DMHCA was synthesized as described (205) and/or was obtained from Dr. E. M. Quinet (181) from Wyeth pharmaceuticals, Collegeville, PA, USA. Purity was checked by thin layer chromatography and ^{1}H-NMR.

Furthermore, 10-12 week old male mice were intraperitoneally (i.p.) injected with vehicle alone (1.3% Tween80 and 0.25% carboxymethylcellulose) or with vehicle plus 50 mg T0901317

(Cayman Chemical, Ann Arbor, MI, USA) per kg body weight as well as 50mg DMHCA per kg body weight for 6 days. At the end of the experiment, mice were fasted for 4h and then sacrificed.

7.12.1 Mice for non-invasive microscopy

Mice were grouped between WTD and chow diet, which were both adjusted in calcium and magnesium content (Harlan Teklad, USA). These two groups were divided into three subgroubs according to sham-operated, uninephrectomized and 5/6 nephrectomized. Surgery was performed in male ApoE-/- mice at Jackson laboratory according to Gagnon et al. For 5/6 nephrectomy the right renal cortex is sequentially electrocoagulated and the left kidney is totally nephrectomized (209).

From these different groups there were also 4 different time points. Group one was killed after a time period of 6-11 weeks, group 2 after 19-20 weeks, group 3 and 4 were fed for the same time period as group 2 (late stage of plaque development). Mice were anaesthetized with phenobarbital (100uL per mouse), the whole animal was perfused with 10mL 1X PBS by applying heart puncture with a butterfly needle (23 gauge ¾). After the animal was freed from all blood, the tissues were fixed by perfusing with 2% 10-20mL freshly prepared PFA (in 1X PBS) or postfixed in fresh 2% PFA when the rest of the tissue was used for RNA isolation. Then, some of the aortas were imaged directly with the ZEISS system for SHG/TPE signal (group I). The 2nd and 3rd group were cut open (en face) on the descending aorta and stained with oil red O (comparative method). The brachiocephalic artery (BCA) was cut apart from the aortic root and both were frozen in OCT for cryosectioning and traditional staining. Group IV was mainly used for measuring gene regulation via real-time PCR and the BCA were post-fixed and cut into 2 parts (one for SHG, one for CARS, supposedly the samples will be exchanged within the UCHSC and UC Irvine).

7.13 Dissections, cryosections and stainings

ApoE -/- mice were anesthetized with 100µL Phentobarbital (Nembutal), respectively. Then, the mice were cut open with surgical instruments and blood was taken from the vena cava. Next, the sternum was cut open and a butterfly needle was used to perfuse the heart on the left ventriculum. First, the blood is removed from the body by perfusing with 1xPBS/1mM EDTA for 10min and then the tissues are fixed by perfusing the whole animal with 4% PFA (optionally 10% sucrose and 1mM ETDA were added). After removing all the organs, the aorta was dissected out using micro surgical instruments.

7.13.1 Cryosectioning

The hearts were embedded in OCT medium and frozen at -20˚C and 5-10µm cryosections were taken on a HM560 Microm microtome. The sections were used for the different staining such as Oil red O, MOMA-2 or von Kossa.

7.13.2 Preparation of histological sections and lesion analysis

For analyses of atherosclerotic lesions at the aortic root the upper two thirds of the heart were fixed in 4% formaldehyde, embedded in tissue medium (Tissue-Tek O.C.T, Sanova Pharma GesmbH Diagnostik, Vienna, Austria) and frozen at -20°C. After approximately 600 µm, 8 µm cryosections of the aortic root were cut and lipid-rich regions were stained with Oil Red O (Sigma, Vienna, Austria) and counterstained with hemotoxylin (Richard-Allen Scientific, Kalamazoo, MI, USA). Macrophages were detected with monoclonal rat anti-mouse antibody MOMA-2 (Acris, Hiddenhausen, Germany). Tissue specimens were fixed with acetone for 10 min at room temperature (RT). The slides were UV blocked and the sections were incubated with MOMA-2 diluted 1:600 for 30 min at RT. Subsequently, the sections were incubated with a biotinylated polyclonal rabbit anti-rat IgG (1:75, Dako Österreich GmbH, Vienna, Austria) for another 30 min at RT. The substrate chromogen AEC (Dako) was applied for 10min at RT. The sections were counterstained with hemotoxylin. Images were taken with ScanScope T3 whole slide scanner (Aperio Technologies, Bristol, UK). Mean lesion area at the tricuspid valves was analyzed using Adobe Photoshop.

7.13.3 En face analysis of aortas

For *en face* analysis, apoE-deficient mice were euthanized using 300 µl of Nembutal (diluted 1:5) and the heart was perfused for 10 min with PBS and for 15 min with 4% formaldehyde. Then the aorta was dissected, opened longitudinally from the heart to the iliac arteries and stained with Oil Red O. Images were analyzed with Adobe Photoshop and a software algorithm which had been programmed with Interactive Data Language (IDL, ITT Visual Information Solutions, Boulder, USA). Briefly, the amount of plaques was calculated by the ratio A_{plaque}/A_{total} after segmentation steps of the images with background and needle separation. The extent of lesion area is expressed as the percentage of the total area of aorta section covered by the lesion. Statistical analysis of the plaque area was performed using the statistic program SPSS 14.0, applying a student's *t*-test.

7.13.4 Oil red O staining

First a stock solution is prepared: 0.75g Oil Red O powder in 150mL Isopropanol (0.25-0.5% solution). After mixing well and sitting for a while (about 15-30min), the stock keeps for up to a year. Next the working solution is prepared: 90mL of stock are mixed with 60mL of dH_2O (3:2), vortexed well and leaved to stand for 10min and then filtered through a Whatman-filter (takes quite long) or a 0.22um filter (faster). For the staining procedure samples are dipped shortly (a few

seconds) into 60% isopropanol and stained for 10-15min in working solution. Next, samples are shortly dipped into 60% isopropanol (might be repeated a few times to get rid of excess oil red O stain). It is usually recommendable to perform counterstaining with hematoxylin. Therefore samples are shortly washed in dH_2O, a few drops of hematoxylin were added onto the samples and incubated for 1min to 3min. After thoroughly washing with tap H_2O and the samples are fixed with glycerin (1:3 with 1xPBS, self-made) under a coverslide.

7.13.5 Nile red staining

For staining of lipid droplets, cells were fixed with 4% PFA in PBS, pH 7.4, for 20min and incubated with a 1:1000 dilution of a Nile red (SIGMA) stock solution (100µg/mL in acetone which is stored at -20˚C) for 5min (210). Excessive dye was removed by washing in PBS. For life cells and fixed tissues the dye was applied either directly to the culture medium or directly onto the humid tissue (tissue should never dry out) for 2-3 minutes. The fluorescence is photographed in the FITC channel and appears yellow/orange when excitation is at 488nm (450-490) and emission is recorded at 515±40nm.

7.13.6 Von Kossa staining

Cryosections of the bracheocephalic artery (BCA) are rinsed with deionized water for a few minutes and the water is blotted off with filter paper. Then, the cryosection is surrounded with a hydrophobic pen and stained with 3% silver nitrate (in water) for at least 30min under UV light. The staining is finished once the sample turns black because of the calcium nitrate and the excessive silver nitrate can be removed by dumping it onto paper towels. Then, 5% sodium thiosulfate is added again to fix the calcium complex and the slides are repeatedly dumped into deionized water to rinse off excessive thiosulfate. Thereafter, the samples are counterstained with Nuclear Fast Red for 5min and rinsed off with tap water. Samples are finally dehydrated, cleared and mounting media is added before applying the coverslip.

7.14 Lipid quantification and measurement of enzymes related to liver injury

Blood was collected by retro orbital bleeding and EDTA-plasma was prepared within 20 minutes. Plasma triglyceride (TG) (DiaSys, Holzheim, Germany), total cholesterol (TC) (Greiner Diagnostics AG, Langenthal, Switzerland), HDL cholesterol (Technoclone GmbH, Vienna, Austria), alanine aminotransferase (ALT) (Roche Diagnostics, Mannheim, Germany) and aspartate aminotransferase (AST) (Thermo Electron Corporation, Louisville, CO) concentrations were measured enzymatically. To determine hepatic lipid contents total lipids were extracted from livers and lipid parameters were determined using above mentioned kits. For analysis of hepatic TG-associated fatty acids lipids from livers were extracted and separated by TLC. The TG band was scraped, methylated, and analyzed by gas-liquid chromatography using heptadecanoic acid as internal standard.

7.14.1 Lipoprotein profile

Plasma samples of 7 overnight fasted female apoE-deficient mice fed WTD + DMHCA for 11 weeks were pooled and compared with those of 7 apoE-deficient mice fed WTD alone as a control. Lipoproteins were isolated by fast protein liquid chromatography on a Pharmacia FPLC system (Pfizer Pharma, Karlsruhe, Germany) equipped with a Superose 6 column (Amersham Biosciences, Piscataway, NJ). 200 µl pooled plasma samples were diluted, subjected to FPLC analysis and lipoproteins were eluted with 10 mM Tris-HCl, 1 mM EDTA, 0.9% NaCl, and 0.02% NaN3 (pH 7.4). Fractions of 0.5 ml each were collected and TG and TC concentrations were assayed enzymatically using above mentioned kit. To enhance sensitivity, reaction buffers were supplemented by the addition of sodium 3,5-dichloro-2-hydroxy-benzenesulfonate (Sigma-Aldrich, Vienna, Austria).

7.14.2 Neutral lipid extraction from tissues

For measuring triglycerides 50mg of a certain tissue was put into a glass vial (Purex) with a screw cap, 4mL of Folch solution (chloroform:methanol; 2:1) were added and the sample was homogenized in an Ultratorrax tissue homogenizer. Next, the samples were centrifuged at around 2500rpm for 20min and 3mL of the supernatant was put into a new glass tube. Then, 0.8mL of 50mM NaCl was added, vortexed well and centrifuged at 3500rpm for 10min. Now, the lower (lipid phase) was isolated (about 2.5mL). 100µL of this extract were put into a new vial and 100µL of 75mg/mL Triton X-100 (in Folch solution) was added, then the liquid was evaporated under nitrogen gas and redissolved in 100µL water. An aliquot of this (depending on the concentration about 30µL) are used for measurement with the TG kit. The standards and blank were treated in the same way (Triton X-100 in water was used here). For TC and FC measurements we followed the same procedure without adding Triton X-100.

7.14.3 Fecal bile acid determination

Male C57Bl/6 mice were fed chow diet ± T0901317 or DMHCA (80 mg/kg body weight/day) for 4 days. Every day feces were collected from each animal. 500 µl distilled water was added to a mixture of 100 mg of freeze-dried feces supplemented with 100 µl internal standard solution (deuterated deoxycholic acid, lithocholic acid, glyco-conjugated cholic acid, and glyco-conjugated chenodeoxycholic acid; 4 ng of each) and bile acids were extracted twice with 2ml chloroform:methanol (2:1, v:v). Extracts were centrifuged, the organic layer was isolated and evaporated under nitrogen. Bile acids were determined as published recently (211).

7.14.4 Quantification of cholesterol and triglycerides by gas chromatography

First approximately 60 mg frozen tissue is weighed into numbered glass tubes (Fisher, 12x75mm) and 100 ul Coprostanol (200ug /ml isooctane) and 100ul 17:0 Triglycerides (1 mg /ml). Next, 2 ml of chloroform/methanol (2:1) (BHT 10 mg/100ml) is added to the tube and the tissue is

homogenized for one minute. Thereafter, 1ml PBS is added, vortexed, and centrifuged at 1500rpm for 5 minutes. Next, the upper phase (water phase), aspirated off and the lower phase (Chloroform phase) is transferred into new numbered tubes (Fisher, 12x75mm). Then, the solution is evaporated by nitrogen gas and 1ml of chloroform/methanol is added to dissolve the lipids. From these solutions, 500ul are transferred to new numbered capped tubes and are used for the cholesterol assay. The leftover is evaporated for the triglyceride assay.

For triglyceride determination thin layer chromatogram (TLC) plates and the solvent were prepared (60 mL of heptane + 40 ml isopropyl ether + 3 ml acetic acid). After scoring the TLC (divide into 6) 100 uL of the chloroform/methanol solution of the lipids were spotted to the TLC plate and the TLC plate was put into the glass case for 40 minutes. Next, 0.2% dichlorofluoresein was sprayed and the TG area was marked under UV light. Thereafter, the silica was scraped using a razor blade and collected into numbered capped tube. Next, 6ml of chloroform/methanol (4:1) was added overnight. The next day, 1 mL was put into numbered capped tube and 15:0 R/20 was added as internal standard and all liquid was evaporated under nitrogen gas. After adding 500µL bortrifluorid (BF3) the samples were incubated in boiling water for 30 minutes. Next, 500 µL water was added as well as 1 mL of hexane and the samples were vortexed, and centrifuged at 1500 rpm for 5 minutes. Now, the upper phase (hexane phase) was transferred into new numbered tubes (Fisher, 12x75mm) and the samples were evaporated under nitrogen gas (N_2). Finally, 100uL of hexane was added and the samples were put into vials for analysis in the gas chromatograph (GC).

For the cholesterol determination the samples were evaporated under N_2, next 100 µL of 10M KOH and 900 µL of ethanol were added. The samples were vortexed and incubated at 70 C for 2 hours. Then, 500 µL of water were added as well as 500µL of acetic acid and 1mL of hexane. The samples were mixed well, centrifuged at 1500 rpm for 5 minutes and the upper phase (hexane phase) was transferred into numbered capped tubes. Thereafter, all liquid was evaporated under gaseous N_2 and 100µL pyridine and 50µL BSTFA was added and the samples were incubated at 60˚C for 15 minutes and then kept overnight at 4˚C. The next day, 1mL water and 1mL hexane were added to the samples. After mixing well and centrifuging at 1500 rpm for 5 minutes, the upper phases (hexane phase) of all samples were transferred into new numbered capped tubes. Then, the samples were evaporated under N_2, 100µl hexane was added and the samples were put in GC vials and analyzed with GC. GC protocol was adapted from Miyazaki et al. (212).

7.15 Cholesterol biosynthesis

Mouse peritoneal macrophages were treated with LXR agonists for 12h in serum-replacement containing medium for 12h. Then medium was changed and LXR agonists were freshly added together with either ^{13}C acetate or ^{13}C mevalonate and cells were treated for another 12h.

Therafter, medium was removed in the cold room (4°C) and washed twice with BSA containing 1XPBS, then lipids were extracted with 2mL hexan/2-propanol by shaking for 1h in the cold. The extracted lipids were separated on a TLC and put into scintillation cocktail and radioactivity was measured after overnight incubation on a β-counter. Proteins were isolated with 0.1M NaOH and determined with Bradford.

7.16 Microscopy techniques

The Zeiss 510 NLO META is a confocal fluorescence microscopy, which in conjunction with the Coherent Chameleon laser allows excitation wavelengths in the Near Infrared Fluorescence (NIRF). It allows the detection of certain structural proteins such as collagen -mainly collagen I- and elastin in the aortic tissue applying stwo photon excitation and second harmonic generation. The excitation wavelength is at 800nm**.**

7.16.1 Two photon excitation

Two-photon excitation (TPE) is defined by the simultaneous absorption of two photons, that each has half of the energy needed for excitation of a specific fluorophore. The efficiency of TPE is given by the presence of high concentrations of photons. The probability of the near-simultaneous absorption of two photons is very low. This technique results in a confocal effect where the excitation is confined to the plane of focus. Consequently, photobleaching and photo-toxicity are reduced which allows longer observation times for live cell imaging. Moreover, this method allows deeper penetration into scattering tissue as a result of the longer wavelengths and thinner laser sectioning of thick tissues.

7.16.2 Second harmonic generation

The second harmonic generation (SHG) signal was measured through a 10X or 25X water objective at half of the wavelength of the excitation ($\lambda/2$ = 400 nm). A band-pass filter enabled to select the detection spectral range (400 ± 25 nm), and to reject the infrared excitation beam. In the set-up we used there were three different filters to detect the collagen with the second harmonics which is blue-shifted (388 to 409nm), the elastin autofluorescence which is green-shifted (500-550nm) in the aortic tissue, and one filter for Nile red staining (560-650 nm). The Nile red staining was used to detect the lipids within the plaque area in comparison to the CARS signal. Yet, we had to apply spectral unmixing since there was an overlap in the signal.

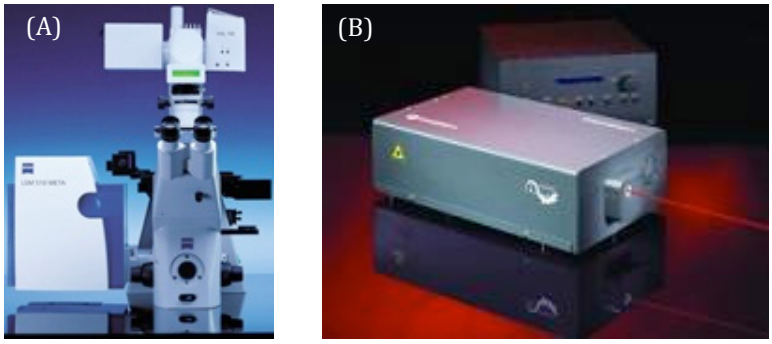

Figure 18. Set-up description for SHG/TPE
(A) Zeiss LSM 510 META on Axionvert 200M microscope is used for confocal and two-photon imaging employing (B) the coherent chameleon laser ultra II as laser source. This laser gives femtosecond pulsed light programmatically tunable from 680–1080nm and is used together with Zeiss LSM 510 META system. This laser allows excitation light in the near infrared (NIRF), which is necessary to get SHG/TPE signal.

In our setting we used the excitation in the NIRF for the detection of emission of certain molecules that give autofluorescence signal (elastin which is the structural component in the arterial walls), and also a specific SHG signal (collagen which gives the arterial wall it's stiffness and also builds up the fibrous caps of the arterial plaques).

7.16.3 Description of the system for the nonlinear multimodal imaging

CARS allows detection of any molecule with vibrational changes, so to say any organic molecule. We used CARS for the detection of lipids and calcium in the form of calcium hydroxyapatite. The combination with SHG/TPE provides a proper alternative to classical staining techniques with the advantage of non-invasiveness.

The pump and Stokes beams required for the CARS process were derived from a synchronously pumped optical parametric oscillator (OPO) system. The 1064 nm, 7-ps pulses of a 76 MHz mode-locked Nd:Vanadate laser source (High-Q, Hohenems, Austria) provided the Stokes radiation. A portion of the same 1064 nm source was used to pump an OPO (Levante, Berlin, Germany), tunable in the 760 – 960 nm range, which delivered the pump beam for the CARS process. The frequency difference between the pump and the Stokes radiation was set to 2852 cm^{-1}, corresponding to the symmetric CH_2 vibration of lipids. The pump beam was set to 816.3 nm, resulting in the generation of a CARS signal at 658 nm. In addition, the 816.3 nm radiation also served as the driving beam for the SHG process. The collinearly overlapped pump and Stokes beams were passed through a laser scanner (Fluoview 300, Olympus, Center Valley, PA) and focused with a 20x UPLAPO objective (Olympus) with 0.75 NA into the tissue sample. Average power at the sample was 15 mW for each beam.

The inverted microscope (IX 71, Olympus) was equipped with three photomultiplier tubes (PMT). In the forward direction, the SHG and CARS light were captured by a condenser lens (0.55 NA) and directed to a 760 nm longwave pass dichroic mirror (Chroma, NH). The reflected light was passed on to a 600 nm shortwave pass dichroic mirror (Thor Labs, Newton, NJ) for separate detection of the SHG and forward (F-) CARS signals. The CARS detector consisted of two 650 ± 40 nm bandpass filters (Chroma) and a red-sensitive PMT, while the SHG detector included a set of two 400 ± 40 nm bandpass filters and a PMT photodetector. In the backward direction, TPEF signal was directed by a 760 nm longpass dichroic mirror through a 550 ± 20 nm bandpass filter set onto a PMT. All nonlinear signals were detected by red-sensitive PMTs (R3896, Hamamatsu, Hamamatsu City, Japan).

7.17 Bioavailability analysis of DMHCA by liquid chromatography and tandem mass spectrometry (LC-MS/MS)

DMHCA content in mouse plasma was measured by means of electrospray ionization MS/MS analysis after separation by HPLC. An API-3000 triple quadrupole mass spectrometry (Applied Biosystems, Foster City, CA, USA) coupled with a Perkin Elmer liquid chromatography system was used for the study. Analytes were separated on Sunfire C18, 2.1 x 50 mm, 5 µm using acetonitrile and 5 mM ammonium acetate in water (90:10; v/v) as mobile phase. DMHCA and triamcinolone acetonide (internal standard) were analyzed in positive ionization mode. DMHCA was extracted from mouse plasma (20 µl) and tissues (200 mg) by liquid extraction with dichloromethane (1 ml). Triamcinolone acetonide (12.5 ng) was added to each sample as internal standard before vortexing. After phase separation by centrifugation at 10000 g for 5 min, dichloromethane was collected and evaporated under nitrogen stream. The residue was dissolved in 250 µl of water:methanol (25:75; v/v) and subjected to LC-MS/MS analysis.

7.18 2-D-Gel electrophoresis

The first step was the isoelectric focusing. Samples were filled up with reswelling solution to 600µL total volume and vortexed well. After writing down the number of the strips, the samples were distributed into the strip holder. Thereafter, the strips were put into the strip holder and 2.5mL dry strip cover fluid was quickly added onto the gel strip. The equilibration was started after adding the number of strips (30V, 3-4µA) and ran for 13h and 35min.

After the equilibration was stopped, the gels were put in a new strip holder, respectively. The 1cm pieces of the filter pads were wet and put on both ends of the gel strip. Then, the electrodes were put at the end of the filter pads, 4-5mL cover fluid was added quickly and isoelectric focusing (IEF) could take place. Adding the number of strips protocol 1 was used (50V 3h, 300V 3h, 600V 3h, 8000V Gradient). Important enough, the filter pads were changed every 2 hours in order to get rid

of excessive salt. After 16h 14min the IEF was stopped (50000 Vh were reached) The gel strips were frozen at -70˚C for the further procedure. The next day, the gel strips were thawed and put into the covers of the strip holders, 15mL equilibration buffer (plus DTT) were added onto the el strips and shook for 15min. was used for rough molecular weight determination. Equilibration buffer was discarded and new equilibration buffer was added (plus Jod-Acetamide) and shook again for 15min. After cutting off a little bit at both ends of the gel strip, it was put onto the gel. Half of a filter pad was wet with 10µl low molecular weight standard (Cy3-labeled) standard and put in front of the cathode end. The strips were fixed with 1% low-melting agarose and the gel plates were put into the running buffer and the agarose was left to dry for 5min. Anode buffer was filled into the chamber and cathode buffer was added up to the maximum line. Finally, also anode buffer was added up to the same level as the cathode buffer. Thereafter, program 2 was started and the gels were run overnight. Next, the gels were scanned within the glass plates after washing and carefully drying. After scanning the Image Quant software was used for setting the spot saturation and the region of interest. Next, the gels were taken out of the glass plates and put in H_2O and after removing the water 500mL of fixing solution was applied and gels were shook for at least 1 hour. Thereafter, the fixing solution was discarded, fresh water added again and the gel kept in the cold room. The evaluation and analysis was done with Mascot gel imaging software and spots with target proteins were picked and analyzed with LC-MS/MS.

7.18.1 LC-MS/MS-analysis

Protein spots were excised from gels and tryptically digested according to the method by Shevchenko et al. (213). Peptide extracts were dissolved in 0.1% formic acid and separated on a nano-HPLC system (Ultimate 3000™, LC Packings, Amsterdam, Netherlands). 70µl samples were injected and concentrated on the loading column (LC Packings C18 Pep- Map™, 5 µm, 100 Å, 300µm inner diameter x 1mm) for 5 min using 0.1% formic acid as isocratic solvent at a flow rate of 20 µl/min. The column was then switched into the nanoflow circuit, and the sample was loaded on the nanocolumn (LC-Packings C18 PepMap™, 75 µm inner diameter x 150 mm) at a flow rate of 300 nl/min and separated using the following gradient: solvent A: water, 0.3% formic acid, solvent B: acetonitrile/water 80/20 (v/v), 0.3% formic acid; 0 to 5 minutes: 4% B, after 40 minutes 55% B, then for 5 minutes 90% B and 47 minutes reequilibration at 4% B. The sample was ionized in a Finnigan nano-ESI source equipped with NanoSpray tips (PicoTip™ Emitter, New Objective, Woburn, MA, USA) and analysed in a Thermo-Finnigan LTQ linear iontrap mass-spectrometer (Thermo, San Jose, CA, USA). The MS/MS data were analyzed by searching the NCBI non-redundant public database with SpectrumMill Rev. 03.03.078 (Agilent, Darmstadt, GERM) software. Acceptance parameters were three or more identified distinct peptides according to Carr et al (214).

7.19 Statistics

Statistical analyses in experiments except real-time PCR analyses (see above) were performed using the Student's *t*-test. Data are expressed as mean ± S.D. $^{*}P < 0.05$; $^{**}P \leq 0.01$; $^{***}P \leq 0.001$

8 Results

LXR agonists have the positive effect of reducing atherosclerosis by mediating the RCT via an induction of cholesterol efflux and reduction of intestinal cholesterol absorption (107, 108). Unfortunately, the common LXR agonists have a deleterious side effect, which is the initiation of lipogenesis, leading to accumulation of lipids in the liver and consequently to liver steatosis and hypertriglyceridemia.

Therefore, we were looking for an LXR agonist that retains the positive effect of cholesterol clearance without exhibiting the negative side effects of lipid accumulation. When we searched the literature, we found two compounds, the non-steroidal DMHCA and YT-32, which did not stimulate lipid accumulation in the plasma and liver of WT mice (181, 215). Both, however, have not been investigated for their antiatherosclerotic properties and I decided to synthesize and work with N,N-dimethyl-3β-hydroxy-Δ^5-cholenamide (DMHCA).

8.1 Synthesis of N,N-dimethyl-3-β-hydroxy-Δ5-cholenamide (DMHCA)

One part of DMHCA we used for our experiments was received from Wyeth pharmaceuticals, Collegeville, PA, USA, but the main part was synthesized inhouse. The synthesis of DMHCA was performed on the basis reported by Louw et al. (216). Starting with 1g of 3 β-hydroxy-Δ^5-cholenic acid, the 3-step synthesis of DMHCA resulted in 30% and 50% endproducts in my fist and second syntheses. The summary of the synthesis is shown in Figure 19 and all intermediate steps are described as follows.

The first step is necessary to protect the hydroxyl group at carbon 3 from the starting material. Here the use of formic acid leads to the formation of formic ester of 5-cholenic acid-3-ß-ol (**1**). 1g (2.6 mmol) of 3 β-hydroxy-Δ^5-cholenic acid + 7g concentrated formic acid (p.a.) were heated under argon atmosphere under reflux for 30 min. The hydroxy compound was dissolved quickly and after a few minutes a white precipitate was formed. After 30 minutes the mixture was cooled to room temperature (RT) and filtered by suction. The precipitate was washed two times with 2 mL formic acid. Washing with cyclohexane should be avoided since this procedure resulted in a sticky mass. Therefore, the isolated substance was dried under vacuum at RT and then at 70°C over KOH pellets. We got a yield of 0.9g (84%; MW=402.58) cholenic formiate ($C_{25}H_{38}O_4$) with a melting point (Mp) of 156-158°C.

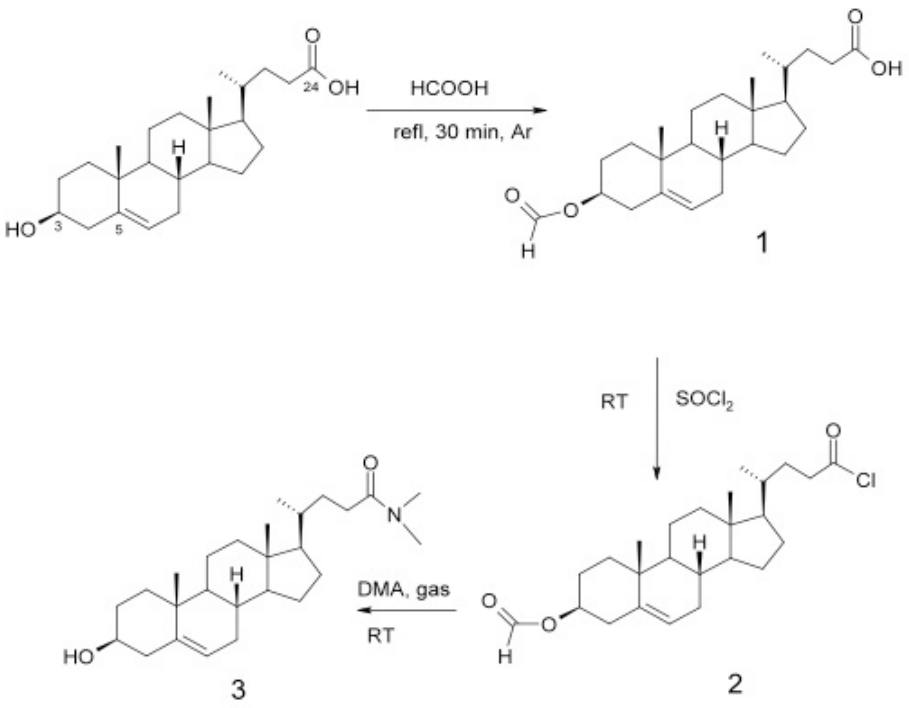

Figure 19. Synthesis of DMHCA
The synthesis of DMHCA is performed in three steps.
Purity of intermediate products and end product was verified with thin layer chromatography (TLC) and nuclear magnetic resonance (NMR) spectroscopy.

For verification by TLC (Figure 20C) the samples were dissolved in dichlormethane and separated by chloroform/acetone/glacial acetic acid in a volume to volume ratio of 100:50:0.4 (v/v/v). The retention factor (R*f*) for cholenic acid and its ester (**1**) was 0.7 and 0.8, respectively. Spots were visualized using an aqueous solution of kalium permanganate ($KMnO_4$). Moreover, infrared spectra (IR see Figure 20A) and nuclear magnetic resonance (NMR see Figure 20B) spectra were taken.

The next step in the synthesis was the preparation of the acid chloride (**2**). In a light protected, magnetically stirred round-bottomed flask equipped with a $CaCl_2$ drying tube 0.9g (9 mMol) **1** was treated with 3mL freshly distilled thionyl chloride ($SOCl_2$). The mixture was kept for about 3h until most of the gas production had ceased. The dark brown solution was diluted with 10 mL dry toluene, evaporated to dryness, dissolved again in 10 mL toluene and evaporated again. The second intermediate was an acid chloride ($C_{25}H_{37}ClO_3$) with a MW of 421.02 g/Mol (**2** in Figure 19).

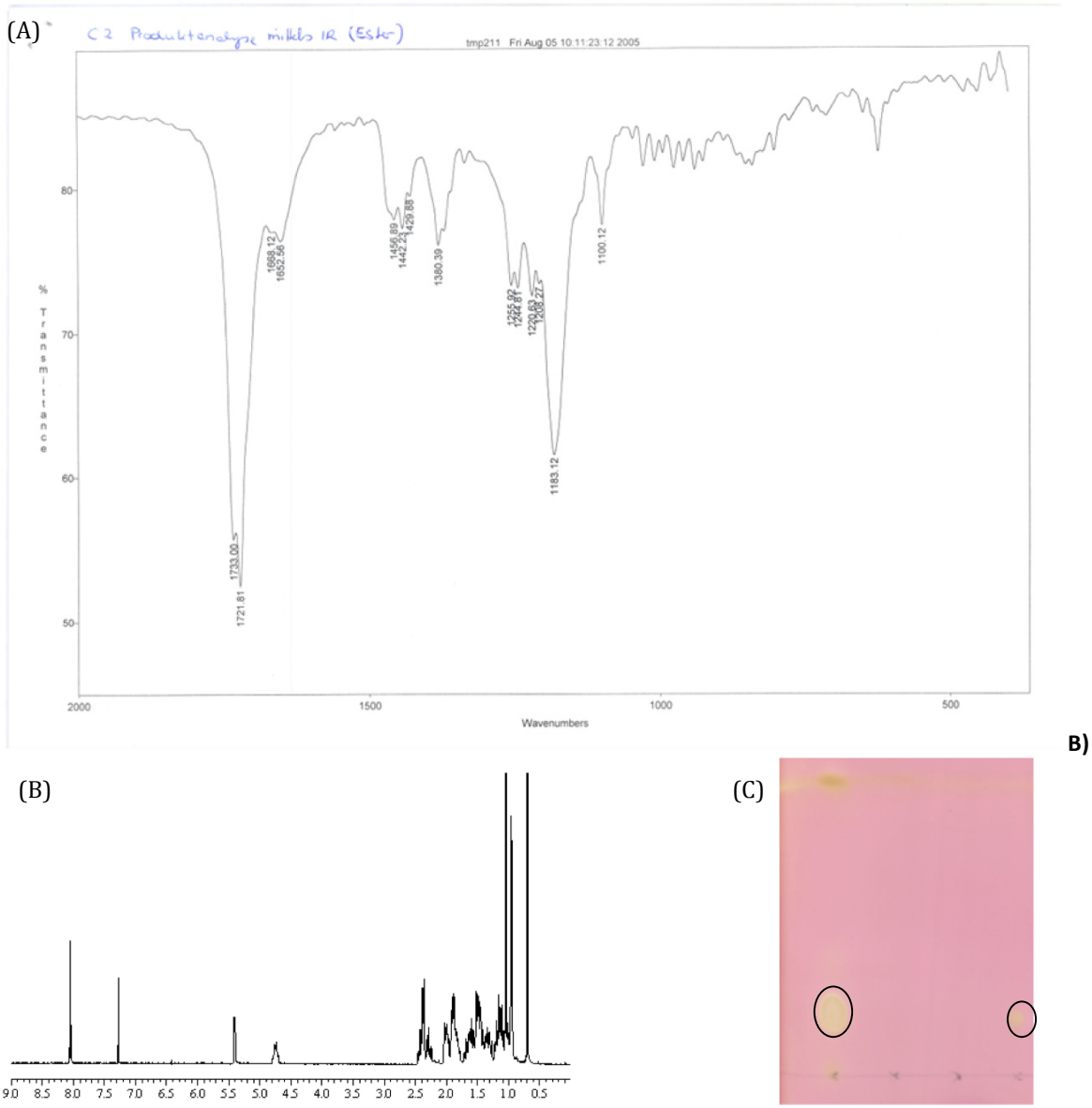

Figure 20.IR,NMR, and TLC of the first intermediate in DMHCA synthesis
(A) represents the IR spectrum of the first intermediate, the formiate. The peak at 1700cm^{-1} represents the ester bond of the formiate. (B) ^{1}H-NMR spectrum of cholenic formiate (**1** in Figure 19) in deuterated chloroform ($CDCl_3$). The smaller peak at 8 ppm represents a trace of HCOOH. (C) The first spot in the TLC represents the first intermediate, the formiate of the hydroxycholenic acid. The second and third spot represent the solvent and supernatant of the reaction, giving no visible spots. The last spot represents the starting material, which has nearly the same R_f as the intermediate.

The third step was the preparation of the dimethylamide and deprotection. The raw acid chloride (**2**) was dissolved again with dry toluene (20mL) in the magnetically stirred round-bottomed flask, a septum was attached and the solution was cooled in an ice bath. Dimethylamine gas was bubbled slowly through a needle (Figure 21). Excessive dimethylamine and the generated hydrochloride were removed via separated tubing and after the exothermic reaction had ceased (30 min) the product (DMHCA) was removed by suction (Figure 22A). The precipitate was washed with 3mL toluene and the combined filtrate was rotary evaporated to dryness. TLC was performed using toluene/acetone (3:1) and showed complete amidation and deprotection.

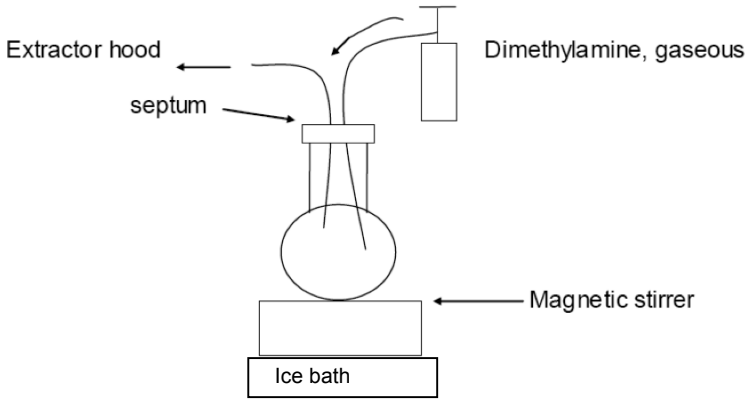

Figure 21. Setup for the final step in DMHCA synthesis
The third step in the DMHCA synthesis is highly exothermic and therefore needs a cooling bath with ice. Dimethylamine is inserted with a needle and the gaseous hydrochloride, which is produced as a byproduct, is removed via extra tubing in the septum. Thus, the procedure has to be performed in the hood.

The acid chloride (**2**) had an R*f* of 0.5 whereas DMHCA (**3**) held an R*f* of 0.25. After addition of 10 mL toluene/acetone (3:1; v/v) in order to dry flash the raw material a white precipitate was formed (320mg) and vacuum dried over paraffin pellets. The filtrate was dry-flashed using a glass-sintered funnel with a diameter of 5 cm (silica 15-30 µ). Total used toluene/acetone mixture was 200 mL. The collected pure fractions were evaporated to dryness resulting in 300mg slightly brown crystals. ^{1}H-NMR analysis ($CDCl_3$) showed that the dry flashed product had higher purity for since the directly isolated precipitate contained about 30% free carboxylic acid (Figure 22B). Therefore, it was dissolved in CH_2Cl_2 and dry flashed using a mixture of CH_2Cl_2/acetone first 9:1 and then 8:2.

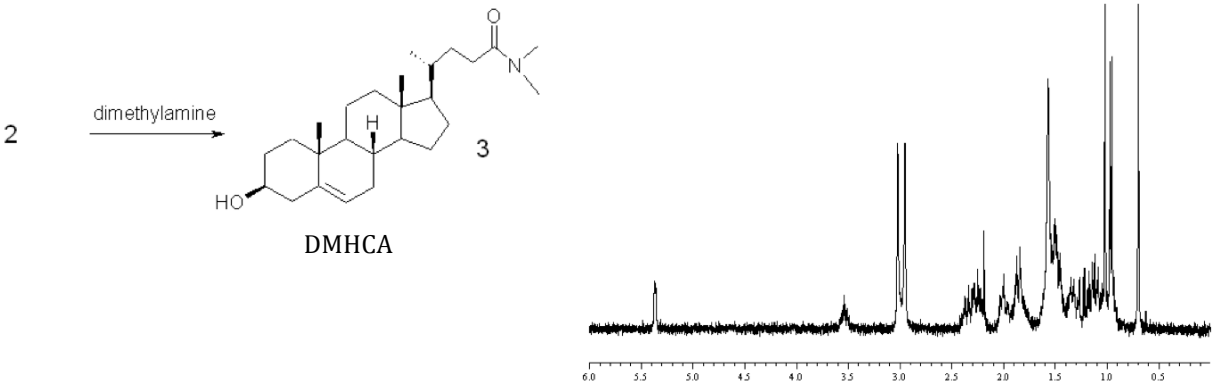

Figure 22. Final synthesis step and ^{1}H NMR of DMHCA
The final step in the synthesis of DMHCA comprises the amidation of the acide chloride as well as the deprotection at C3 as seen on the left image. The purification was verified with ^{1}H NMR of the product in $CDCl_3$, showing the amidbonding of DMHCA at 3.0 ppm.

The isolated pure fractions were evaporated and dried, having an Mp of 183-185 °C. The total yield was 520mg (50 % overall) of $C_{26}H_{43}NO_2$ and are defined as N,N-dimethyl-3-β-hydroxy-Δ^5-cholenamide (DMHCA) with a MW of 401.64g/Mol.

8.2 Gene regulation by DMHCA in comparison with other LXR agonists in different cell lines

The LXR agonists were either dissolved in ethanol or dimethylsulfoxide (DMSO), which both are good organic solvents, whereas different agonists were preferably dissolved in the same solvent.

8.2.1 Influence of time and concentration

Differences in gene regulation of DMHCA were studied with different concentration and incubation times in order to figure out which is the best and most efficient treatment in different cell lines.

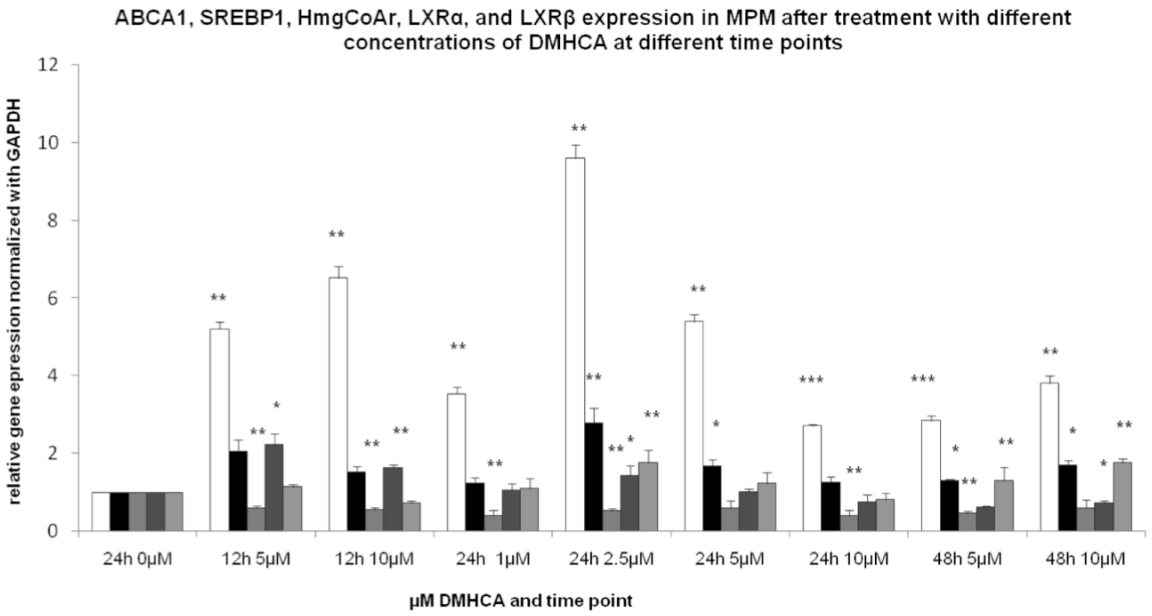

Figure 23. Concentration and time dependent gene regulation upon DMHCA treatment in MPM
Concentration and time dependent regulation of ABCA1, SREBP1, HmgCoAr, LXRα, and LXRβ in the mouse peritoneal macrophages (MPM). Expression values were calculated by pairwise fixed reallocation test with mGAPDH normalization relative to control (arbitrarily set to 1). Data are expressed as mean ± SD. $^{*}P < 0.05$, $^{**}P \leq 0.01$, $^{***}P \leq 0.001$.

The treatment with 2.5µM DMHCA and 24h incubation gave the most efficient induction of gene regulation as the ABC transporter A1 was highest induced (Figure 23). Yet, SREBP1c was also induced, but the difference between the 2 genes was also more pronounced. Both LXRα and LXRβ were also induced by 2.5µM DMHCA. HmgCoAr, the key enzyme in cholesterol biosynthesis, was significantly downregulated in almost all combinations of time and concentration. Furthermore, the effect of different concentrations of DMHCA on ABCA1 and SREBP1c mRNA expression was checked in cell lines such as RAW264.7 macrophages (Figure 24A), human HepG2 liver cells (Figure 24B), and human Caco-2 colon carcinoma cells (Figure 24C).

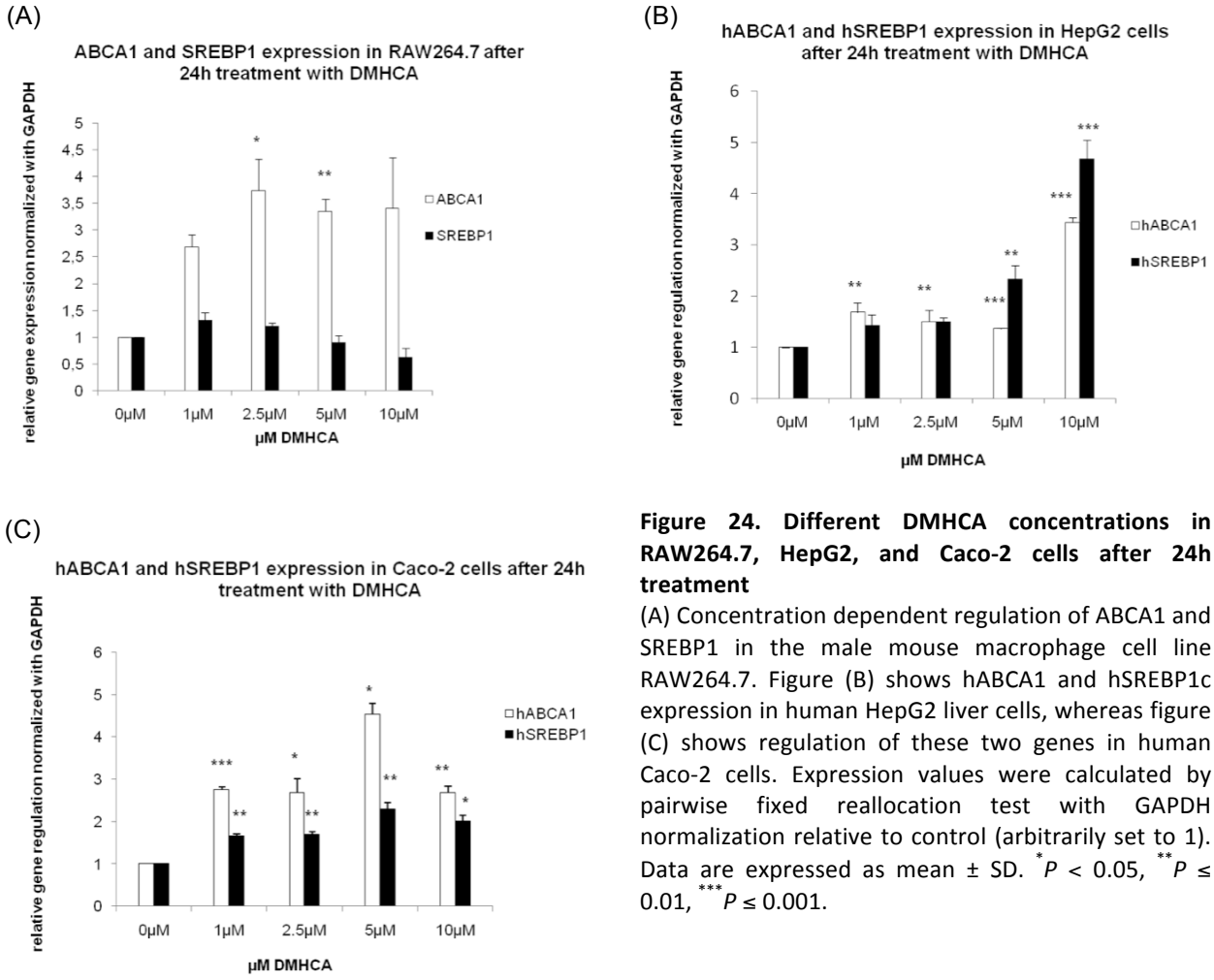

Figure 24. Different DMHCA concentrations in RAW264.7, HepG2, and Caco-2 cells after 24h treatment

(A) Concentration dependent regulation of ABCA1 and SREBP1 in the male mouse macrophage cell line RAW264.7. Figure (B) shows hABCA1 and hSREBP1c expression in human HepG2 liver cells, whereas figure (C) shows regulation of these two genes in human Caco-2 cells. Expression values were calculated by pairwise fixed reallocation test with GAPDH normalization relative to control (arbitrarily set to 1). Data are expressed as mean ± SD. $^{*}P < 0.05$, $^{**}P \leq 0.01$, $^{***}P \leq 0.001$.

Similar to MPM, in RAW264.7 cells 2.5µM and 5µM DMHCA markedly increased ABCA1 mRNA expression, but did not increase SREBP1c (Figure 24A). In HepG2 (Figure 24B) Concentrations higher than 2.5µM DMHCA led to a significant increase in SREBP1c gene expression whereas 1µM did not show any difference compared with 2.5µM, thus we decided to use 2.5µM in this cell line as well. Similar to the other cell lines, 2.5µM increased ABCA1 gene expression, whereas SREBP1c was induced to a lesser extent than with higher concentrations. DMHCA also activated ABCA1 in human Caco-2 colon carcinoma cells with all different concentrations, but also induced SREBP1c expression (Figure 24C). For our comparison studies of DMHCA with other LXR agonists we used 1µM of T0901317 and GW3965, respectively (217, 218).

8.2.2 Gene regulation in different cell lines

Then, mRNA expression of several genes were checked in macrophages and acetylated (ac) LDL loaded foam cells with and without DMHCA treatment (Figure 25). These experiments showed that DMHCA induced LXR target genes in both macrophages and macrophage-derived foam cells. ABCA1

was highly induced in both cell types whereas SREBP1c gene regulation was slightly induced. LXRβ was slightly induced upon DMHCA stimulation in MPM and foam cells, which was significant in foam cells.

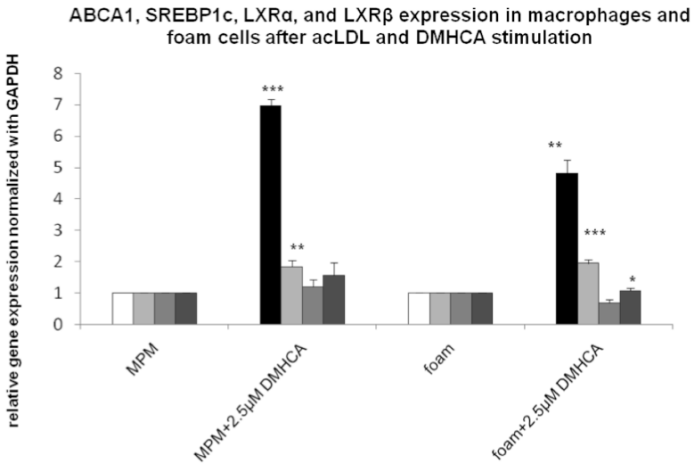

Figure 25. Comparison of gene expression in macrophages and foam
Gene expression on mRNA level of ABCA1, SREBP1c, LXRα, and LXRβ after 2.5μM DMHCA treatment for 24h in MPM and macrophage-derived foam cells. Expression values were calculated by pairwise fixed reallocation test with GAPDH normalization relative to control (controls were arbitrarily set to 1, individually for each cell line). Data are expressed as mean ± SD. $^{*}P < 0.05$, $^{**}P \leq 0.01$, $^{***}P \leq 0.001$.

8.2.3 Microarrays and verifications

Since it has already been shown that DMHCA does not induce SREBP1c to the same extent as T0901317 (181), microarrays from Applied Biosystems were used to compare the gene regulation between T0901317 and DMHCA. Female C57Bl/6 mice, aged 8-10 weeks were used in two independent experiments to get biological replicates (5 and 6 mice, respectively). After isolation of MPM the cells were treated for 24h with either 1μM T0901317, 2.5 μM DMHCA, or ethanol (control). Twenty μg of RNA was used per chip (see Materials and Methods) for each array. Two arrays per treatment group (control, DMHCA and T0901317) were hybridized, which gave a total of 6 arrays. We evaluated the two LXR-treated groups versus the control group separately as well as compared them to each other and combined them as the treatment group versus the control group. The microarray experiments were performed in collaboration with Dr. Christian Guelly, Core Facility Molecular Biology, Center for Medical Research, Medical University Graz.

8.2.3.1 DMHCA versus control

First, the pathway distribution of genes that were differently regulated in DMHCA compared to control treatment was examined (Figure 26). The list of all regulated genes can be found in the supplemental data of this thesis.

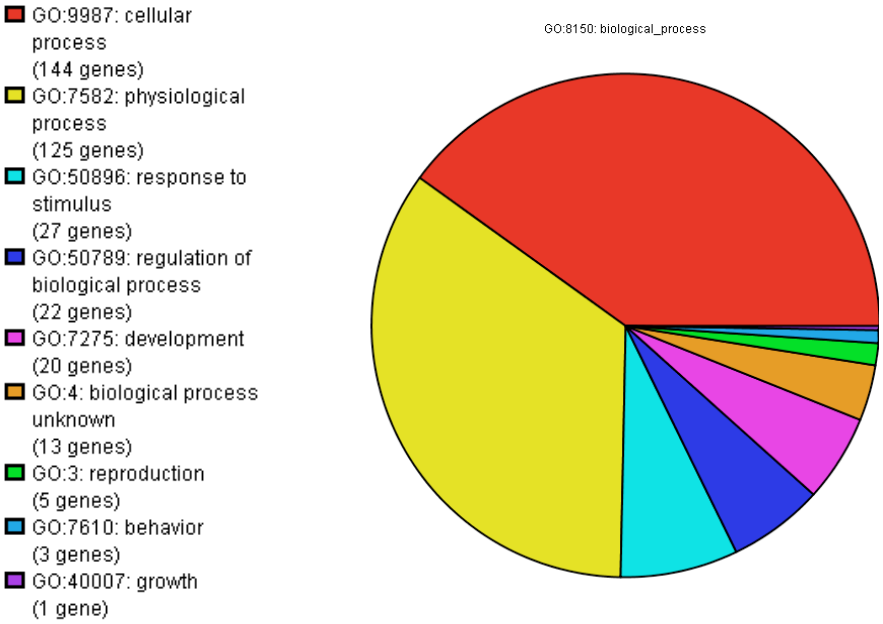

Figure 26. Pathway analysis in MPM DMHCA-treated versus control-treated, down in upon DMHCA treatment
The pie chart shows that most genes downregulated with DMHCA play a role in cellular and physiological processes.
The highest significantly downregulated pathway upon DMHCA treatment was the lipid pathway.

The list of the different pathways is shown in more detail in Table 8. Apparently, the lipid metabolism is highly regulated upon DMHCA treatment. The lower the p-value is, the higher is the significance for the importance of the pathway.

Table 8. Pathway analysis of downregulated genes in DMCHA treated MPM versus control treated MPM
Most abundant pathways regulated by DMHCA in comparison to control treated cells are shown including the percentage of genes in category and of genes in list in category as well as the p-value.

Category	Genes in Category	% of Genes in Category	Genes in List in Category	% of Genes in List in Category	p-Value
GO:16126: sterol biosynthesis	25	0,183	16	9,816	1,48E-25
GO:16125: sterol metabolism	58	0,425	20	12,27	1,30E-24
GO:6695: cholesterol biosynthesis	22	0,161	13	7,975	2,77E-20
GO:8203: cholesterol metabolism	54	0,395	17	10,43	2,77E-20
GO:6694: steroid biosynthesis	62	0,454	17	10,43	4,01E-19
GO:8202: steroid metabolism	123	0,9	21	12,88	9,59E-19
GO:8610: lipid biosynthesis	182	1,332	20	12,27	4,45E-14
GO:6629: lipid metabolism	481	3,521	28	17,18	2,77E-12
GO:44255: cellular lipid metabolism	387	2,833	25	15,34	4,89E-12
GO:8299: isoprenoid biosynthesis	12	0,0878	6	3,681	2,29E-09
GO:6720: isoprenoid metabolism	22	0,161	6	3,681	1,68E-07
GO:9241: polyisoprenoid biosynthesis	2	0,0146	2	1,227	0,000141
GO:16114: terpenoid biosynthesis	2	0,0146	2	1,227	0,000141
GO:16109: tetraterpenoid biosynthesis	2	0,0146	2	1,227	0,000141
GO:16117: carotenoid biosynthesis	2	0,0146	2	1,227	0,000141
GO:16108: tetraterpenoid metabolism	2	0,0146	2	1,227	0,000141
GO:16116: carotenoid metabolism	2	0,0146	2	1,227	0,000141
GO:16096: polyisoprenoid metabolism	6	0,0439	2	1,227	0,00206
GO:6721: terpenoid metabolism	6	0,0439	2	1,227	0,00206

Category	Genes in Category	% of Genes in Category	Genes in List in Category	% of Genes in List in Category	p-Value
GO:10025: wax biosynthesis	3	0,022	1	0,613	0,0354
GO:10166: wax metabolism	3	0,022	1	0,613	0,0354

Setting the p-value ≤ 0.1 and the fold change (*FC*) ≤ 0.5 I found 406 genes that were downregulated by DMHCA in comparison to control treated cells. Utilizing higher stringency (p≤0.05, *FC*≤0.5) we still got a list of 194 genes that are differently regulated (Table C in supplemental data). At p≤0.01 and *FC*≤0.5) 33 genes were left that were downregulated with DMHCA versus control. Genes from the lipid and cholesterol metabolism gave the highest significant values for being regulated (see p-value from Table 8), especially genes from the sterol biosynthesis pathway (Table 9).

Table 9. Downregulated genes from the lipid metabolism in MPM treated with DMHCA versus control treated cells

Genes that were downregulated upon DMHCA treatment compared to control treated and play a role in lipid metabolism are listed in this table *FC*≤0.5, p≤0.1.

	gene name
596934	StAR-related lipid transfer (START) domain containing 4
435645	hydroxysteroid (17-beta) dehydrogenase 7
402854	monoglyceride lipase
332108	cholesterol 25-hydroxylase
542220	sterol-C4-methyl oxidase-like
795835	RIKEN cDNA 0610007P14 gene
552647	phosphomevalonate kinase
550613	sortilin-related receptor, LDLR class A repeats-containing
633117	mevalonate kinase
931530	sterol regulatory element binding factor 2
826570	isopentenyl-diphosphate delta isomerase
503224	sterol-C5-desaturase (fungal ERG3, delta-5-desaturase) homolog (S. cerevisae)
371384	male sterility domain containing 1
851403	7-dehydrocholesterol reductase

	gene name
430706	low density lipoprotein receptor
656522	acetoacetyl-CoA synthetase
729339	NAD(P) dependent steroid dehydrogenase-like
453584	acyl-CoA synthetase long-chain family member 3
634387	cytochrome P450, family 51
559603	mevalonate (diphospho) decarboxylase
909892	3-hydroxy-3-methylglutaryl-Coenzyme A synthase 1
640447	24-dehydrocholesterol reductase
893502	farnesyl diphosphate farnesyl transferase 1
603979	apolipoprotein C-III
565056	isopentenyl-diphosphate delta isomerase
898783	fatty acid binding protein 3, muscle and heart
730299	transmembrane 7 superfamily member 2
833590	laminin, beta 2

Concerning the upregulated genes by DMHCA versus control 121 genes had a p-value ≤ 0.1 or and a *FC* ≥ 2, 61 genes with p-value ≤ 0.05 and *FC* ≥ 2, and 8 genes with p ≤ 0.01 and *FC* ≥ 2. The most interesting genes, next to the common known LXR target genes ABCA1, ABCG1 or PLTP were Interleukin 18 binding protein (IL18BP), carbonic anhydrase 6 (CAR6), Tribbles homolog 3 (TRB3), N-myc downstream regulated gene 1 (NDRG1) and aquaporin 9 (AQP9). TRB3 and NDRG1 were further investigated. Tables and figures are found in supplemental data (Figure A, Table D and Table E).

8.2.3.2 T0901317 versus control

MPM were treated with T0901317 and compared with control cells. Looking at upregulated genes upon T0901317 treatment, the lipid transport and cellular lipid metabolism were the most highly affected pathways. In Table 10 genes from those pathways are listed.

Table 10. Upregulated genes from the lipid metabolism in MPM after T0901317 treatment versus control treatment

Genes involved in lipid metabolism in T0901317-treated MPM compared with control treated cells. *FC*≥2, p≤0.1.

GO:6869: lipid transport		GO:44255: cellular lipid metabolism	
532780	ATP-binding cassette transporter G1	596044	fatty acid synthase
403608	ATP-binding cassette transporter A1	453584	acyl-CoA synthetase long-chain family member 3
598999	phospholipid transfer protein	646071	stearoyl-Coenzyme A desaturase 2
603303	apolipoprotein C-I	575019	stearoyl-Coenzyme A desaturase 1
909582	sterol regulatory element binding factor 1		

Setting the p-value to p≤0.1 and *FC*≥2 66 genes were upregulated by T0901317 compared to control (Table F and Table G in supplemental data). At p≤0.05 and *FC*≥2 only 33 genes were left. At p ≤0.01 and *FC*≥2 only 5 genes were differently regulated. These genes are SCD2, NDRG1, growth differentiation factor 15 (GDF15) and two genes with no Accession number, where only part of the sequence was provided.

Genes that were downregulated upon T0901317 treatment, showed no significant pathway to be involved (Table H in supplemental data). Yet, at low stringency (p≤0.1 and FC≤0.5) 274 were downregulated, increasing the stringency to p≤0.05 the amount of genes reduced to 131 (Table I in supplemental data) and with the highest stringency at p≤0.01 and the same FC≤0.5 there were only 26 genes left.

8.2.3.3 Treatment (DMHCA and T0901317 combined) versus control

By comparing the treatment group (DMHCA and T0901317 put together) versus the control group a lot of known LXR target genes were upregulated. The known cholesterol efflux transporters ABCA1 and ABCG1 as well as the phospholipid transfer protein (PLTP) were upregulated in the treatment group. Setting the p-value ≤0.1, 85 genes were found to be upregulated in the treament group (Table J and Table K in supplemental data), at p-value ≤0.05 56 genes and at p-value ≤0.01 15 genes were left (Table 11). These data showed that both ligands activate common LXR target genes but also differentially activate a lot of genes. An interesting gene is the interleukin 18 binding protein (Il18bp), which is supposed to have anti-atherosclerotic activity (219). It has not been investigated so far, but might be a potential candidate for further investigations.

Table 11. Upregulated genes in treatment group versus control
DMHCA and T0901317 regulated genes were put together as the treatment group and compared versus genes regulated in the control group. (*FC*≥2, p≤0.01)

P-value	Common	Fold change	Genbank	Genbank
0,00666	Abca1	4,98	NM_013454.2	ATP-binding cassette, sub-family A (ABC1), member 1
0,000241	Ndrg1	3,75	NM_010884.1	N-myc downstream regulated gene 1
0,00258	Ero1l	3,40	NM_015774.2	ERO1-like (S. cerevisiae)
0,00253	Abcg1	3,38	NM_009593.1	ATP-binding cassette, sub-family G (WHITE), member 1
0,00663	C1ql1	3,19	null	complement component 1, q subcomponent-like 1
0,00249	Faah	2,81	NM_010173.2	fatty acid amide hydrolase
0,0036	Dusp6	2,72	NM_026268.1	dual specificity phosphatase 6
0,00624	Pltp	2,70	NM_011125.1	phospholipid transfer protein
0,00533	3110018I06Rik	2,46	null	RIKEN cDNA 3110018I06 gene
0,00576	null	2,27	null	null
0,00572	Gadd45a	2,27	NM_007836.1	growth arrest and DNA-damage-inducible 45 alpha
0,00635	2310005P05Rik	2,26	NM_026189.2	RIKEN cDNA 2310005P05 gene
0,00178	Gramd1b	2,07	null	GRAM domain containing 1B
0,00219	Cxcl1	2,02	NM_008176.1	chemokine (C-X-C motif) ligand 1
0,00928	null	2,00	null	null

Two genes that were upregulated by the treatment (both LXR agonist data combined) were further investigated. They are not yet known to be LXR regulated: N-myc downstream regulated gene 1 (NDRG1) and endoplasmic oxidoreductin-1-like protein (ERO1L).

Looking at the genes downregulated in treated versus control, a lot of genes have been found that do not even have an accession number but only a sequence in the original data file. At *FC* ≤0.5 and p-value ≤0.1 we found 454 genes downregulated in the treatment group compared to the control group (Table L in supplemental data). Some interesting genes to mention here were the macrophage receptor with collagenous structure (MARCO), the LDLR related protein 8 (LRP8) and the estrogen-related receptor gamma (ESRRG). Increasing the stringency (FC ≤0.5 and p-value ≤0.01) a total amount of 99 genes were downregulated (Table M in supplemental data). Interesting to mention were triggering receptor expressed on myeloid cells 1 (TREM1), the apolipoprotein CIII (APOCIII), glycoprotein Ib, beta polypeptide (GP1BB), and the activation-induced cytidine deaminase (AICDA). APOCIII links hyperlipidemia with vascular endothelial cell dysfunction (220). GP1BB is supposed to have antithrombotic properties (221).

8.2.3.4 DMHCA versus T0901317

Next, the differences between DMHCA and T0901317 treatment were investigated, which was supposed to give insight into the different regulation properties of the two LXR agonists. Checking the differences between DMHCA and T0901317, similar results were found as by comparing DMHCA with control, including genes of the cholesterol biosynthetic pathway and the lipid

biosynthetic pathway. Investigating the differences between DMHCA and T0901317, 298 genes were found to be downregulated between with DMCHA treatment compared to T0901317 treatment with $FC \geq 2$ and p-value ≤0.1 (Table N in supplemental data). The genes built a group of 265 mapped genes and 33 unmapped (evaluated with http://www.pantherdb.org). Thereof 29 genes were involved in lipid metabolism (Table 8). Increasing the stringency (p ≤0.05), 163 genes were differentially regulated (Table O in supplemental data), which was reduced to 30 genes when the p-value was set ≤0.01.

Table 12. Genes involved in lipid and cholesterol metabolisms from DMHCA treated versus T0901317 treated MPM

Genes in this table are downregulated in the DMHCA treated group versus the T0901317 treated group with FC≥2 and p-value ≤0.1. All these genes play a role in lipid and cholesterol metabolisms.

Common	Genbank	Description
Stard4	NM_133774.2	StAR-related lipid transfer (START) domain containing 4
Fads1	NM_146094.1	fatty acid desaturase 1
Acot2	NM_134188.2	acyl-CoA thioesterase 2
Hsd17b7	NM_010476.2	hydroxysteroid (17-beta) dehydrogenase 7
Mgll	NM_011844.3	monoglyceride lipase
Sc4mol	NM_025436.1	sterol-C4-methyl oxidase-like
Fasn	NM_007988.1	fatty acid synthase
0610007P14Rik	null	RIKEN cDNA 0610007P14 gene
Pmvk	NM_026784.1	phosphomevalonate kinase
Sorl1	NM_011436.1	sortilin-related receptor, LDLR class A repeats-containing
Cds1	NM_173370.3	CDP-diacylglycerol synthase 1
Idi1	NM_145360.1	isopentenyl-diphosphate delta isomerase
Sc5d	NM_172769.1	sterol-C5-desaturase (fungal ERG3, delta-5-desaturase) homolog (S. cerevisae)
Dhcr7	NM_007856.2	7-dehydrocholesterol reductase
Ldlr	null	low density lipoprotein receptor
Aacs	null	acetoacetyl-CoA synthetase
Acsl3	NM_028817.1	acyl-CoA synthetase long-chain family member 3
Cyp51	NM_020010.1	cytochrome P450, family 51
Mvd	NM_138656.1	mevalonate (diphospho) decarboxylase
Scd2	NM_009128.1	stearoyl-Coenzyme A desaturase 2
Hmgcs1	NM_145942.2	3-hydroxy-3-methylglutaryl-Coenzyme A synthase 1
Srebf1	NM_011480.1	sterol regulatory element binding factor 1
Scd1	NM_009127.2	stearoyl-Coenzyme A desaturase 1
Dhcr24	NM_053272.1	24-dehydrocholesterol reductase
Fdft1|LOC627717	NM_010191.2	farnesyl diphosphate farnesyl transferase 1
Idi1	NM_145360.1	isopentenyl-diphosphate delta isomerase
Fabp3	NM_010174.1	fatty acid binding protein 3, muscle and heart
Tm7sf2	NM_028454.1	transmembrane 7 superfamily member 2
Lamb2	NM_008483.2	laminin, beta 2

Comparison of DMHCA treatment with T0901317 treatment led to 128 mapped and 13 unmapped genes (http://www.pantherdb.org) that were upregulated upon DMHCA treatment. For the upregulated genes in DMHCA treated versus T0901317 treated cells I did not find any gene

involved in the lipid metabolism that was differentially regulated between DMHCA and T0901317. The highest number of differently regulated genes was found for biological process unclassified (51), immunity and defense (12), signal transduction (22), and protein modification (19), nucleoside, nucleotide and nucleic acid metabolism (18) (Table P in supplemental data). Applying the lowest stringency 140 genes were upregulated by DMHCA compared T0901317 treatment. Setting the p-value ≤0.05 73 genes were left (Table Q in supplemental data), which were reduced to 10 genes when the p-value was set ≤0.01. Genes that were upregulated in DMHCA versus T0901317 with the highest stringency are not related to the lipid metabolism (Table R in supplemental data).

8.2.3.5 Verification of differentially regulated genes by real-time PCR

Male and female WT mice were i.p. injected with thioglycollate and isolated MPM were treated thereafter with either DMHCA or T0901317 for 24h, respectively.

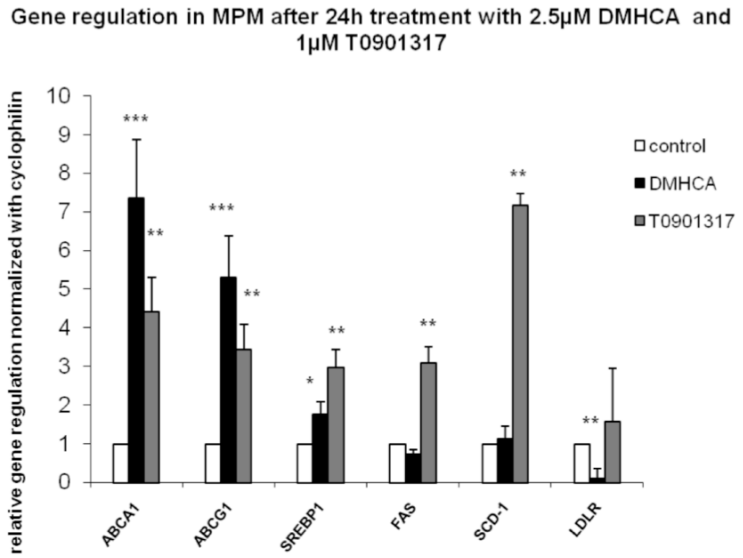

Figure 27. Verification of LXR target genes by real-time PCR
The same mRNA (MPM from female C57Bl/6 mice) that was used for the microarrays was taken for real-time PCR. Real-time PCR expression ratios in MPM including cyclophilin A normalization were calculated by pairwise fixed reallocation test. Controls without DMHCA were arbitrarily set to 1. Data are expressed as mean values from 3 samples performed in triplicate ± SD. $^{*}P < 0.05$; $^{**}P \leq 0.01$; $^{***}P \leq 0.001$.

The verification by real-time PCR using the same cDNA as in the microarray experiments proved the results of the microarrays (Figure 27). DMHCA did not regulate genes from the FA biosynthesis, such as FAS, stearoyl-CoA desaturase 1 (SCD-1) and even downregulates the LDLR. The cholesterol efflux transporters ABCA1 and ABCG1 were significantly induced with both agonists, but with DMHCA even to a higher extent whereas SREBP1c was more upregulated with T0901317.

Since I spent one year in Denver, verification of further target genes was performed in macrophages isolated from male C57Bl/6 mice on an icycler real-time machine from BioRad. Some of those genes have already been verified by real-time PCR in Graz proving the regulation using the same cDNA as for the microarray experiments. Using MPM from male mice treated with either DMHCA or T0901317, pairwise fixed reallocation test with the REST program was performed as

well as the comparative C_T (ΔΔCP) method. In fact, we had the possibility to compare DMHCA and T0901317 treated MPM with GW3965 treated MPM. GW3965 is another synthetic, non-steroidal LXR agonist, which shows no binding affinity to any other nuclear receptor. We used 1μM concentration of this compound as reported in the literature (217, 218).

ABC transporters were upregulated with each agonist (ABCA1 (Figure 28A) and ABCG1 (Figure 28B)), whereas DMHCA did not induce SPREB1c (Figure 28C) or SCD-1 (Figure 28D) mRNA expression. FAS (Figure 28E) was slightly but not significantly increased and LDLR (Figure 28F) was repressed upon DMHCA treatment, as was SREBP2 (Figure 28G) which was repressed upon treatment with each of the three agonists.

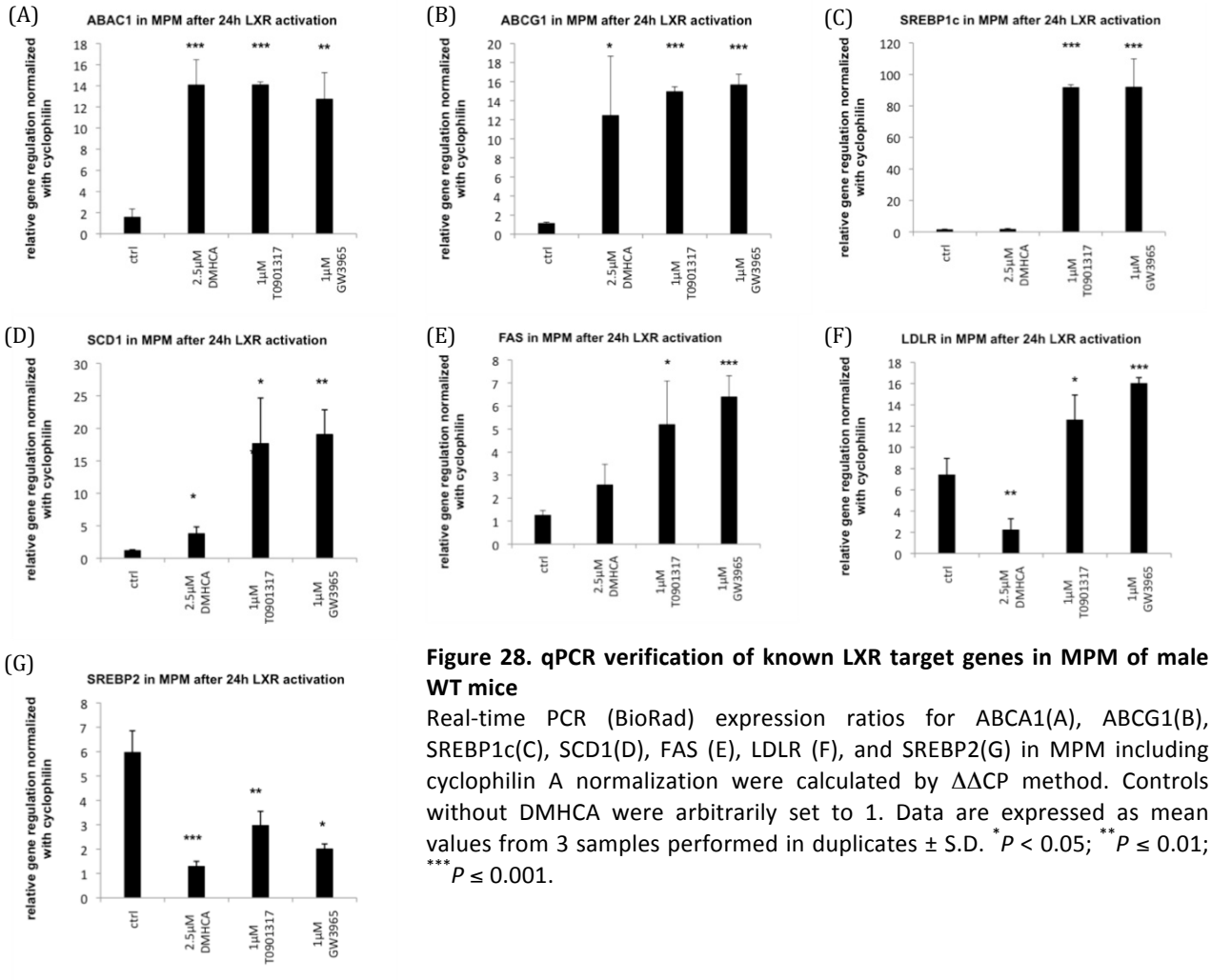

Figure 28. qPCR verification of known LXR target genes in MPM of male WT mice

Real-time PCR (BioRad) expression ratios for ABCA1(A), ABCG1(B), SREBP1c(C), SCD1(D), FAS (E), LDLR (F), and SREBP2(G) in MPM including cyclophilin A normalization were calculated by ΔΔCP method. Controls without DMHCA were arbitrarily set to 1. Data are expressed as mean values from 3 samples performed in duplicates ± S.D. $^{*}P < 0.05$; $^{**}P \leq 0.01$; $^{***}P \leq 0.001$.

Genes that were not known to be LXR agonists, but have been regulated in the microarray experiments, were additionally analyzed by real-time PCR. Hereby, CAR6, TRB3, AQP9, ERO1L, NDRG1, SIRT1 DUSP1, BMP2, and CD36 (Figure 29A-E, G, M, N, and Q) were highly upregulated upon DMHCA treatment and were not or only slightly regulated upon treatment with the other

agonists. In contrast, INSIG1, CYP51, STARD4, HMGCS, HmgCoAr, ALDOC, SORL1, FABP3, and FSP1 (Figure 29F, H-L, O, P, and R) were downregulated upon DMHCA treatment whereas the other agonists led to no or a slight regulation of these genes.

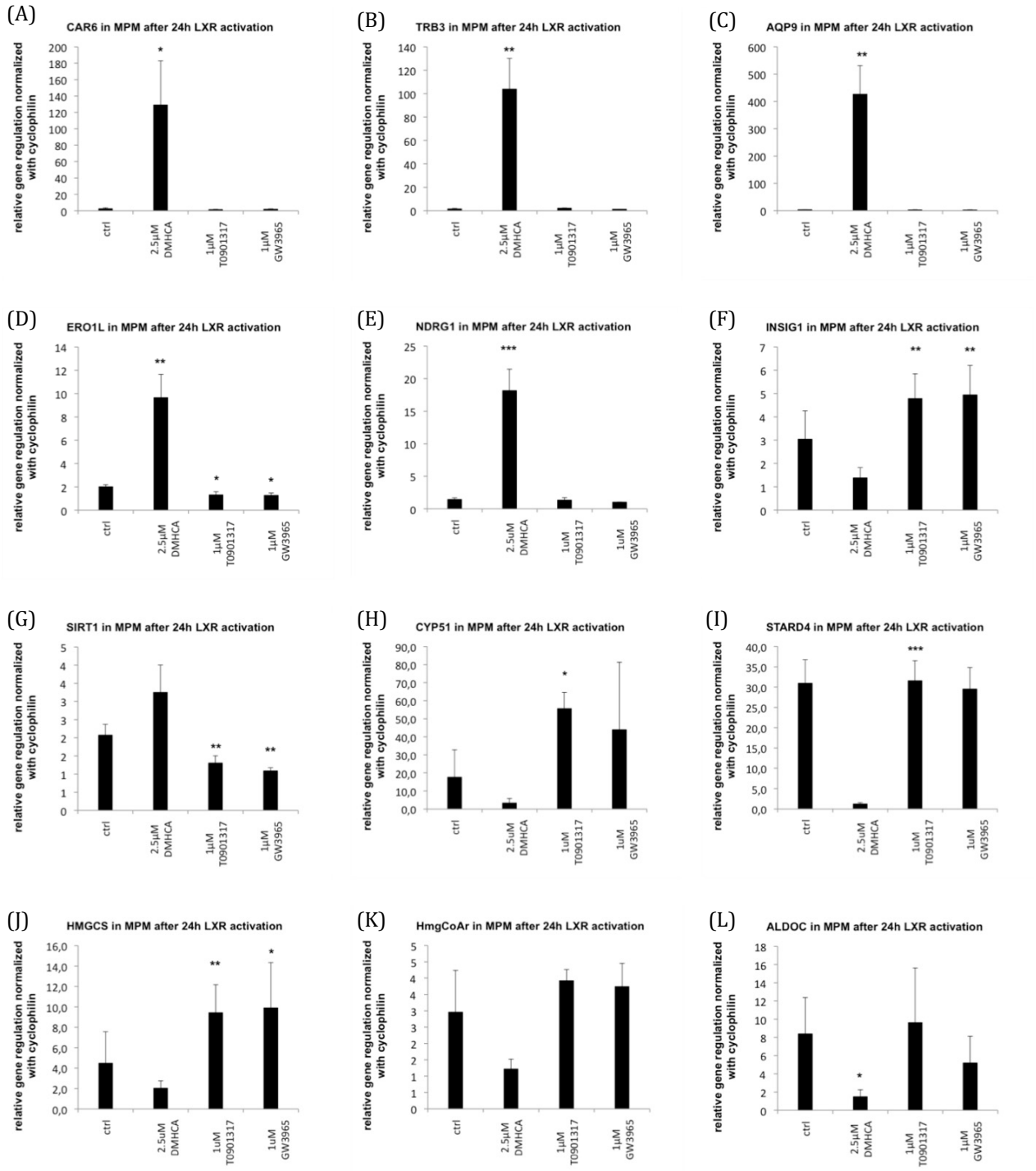

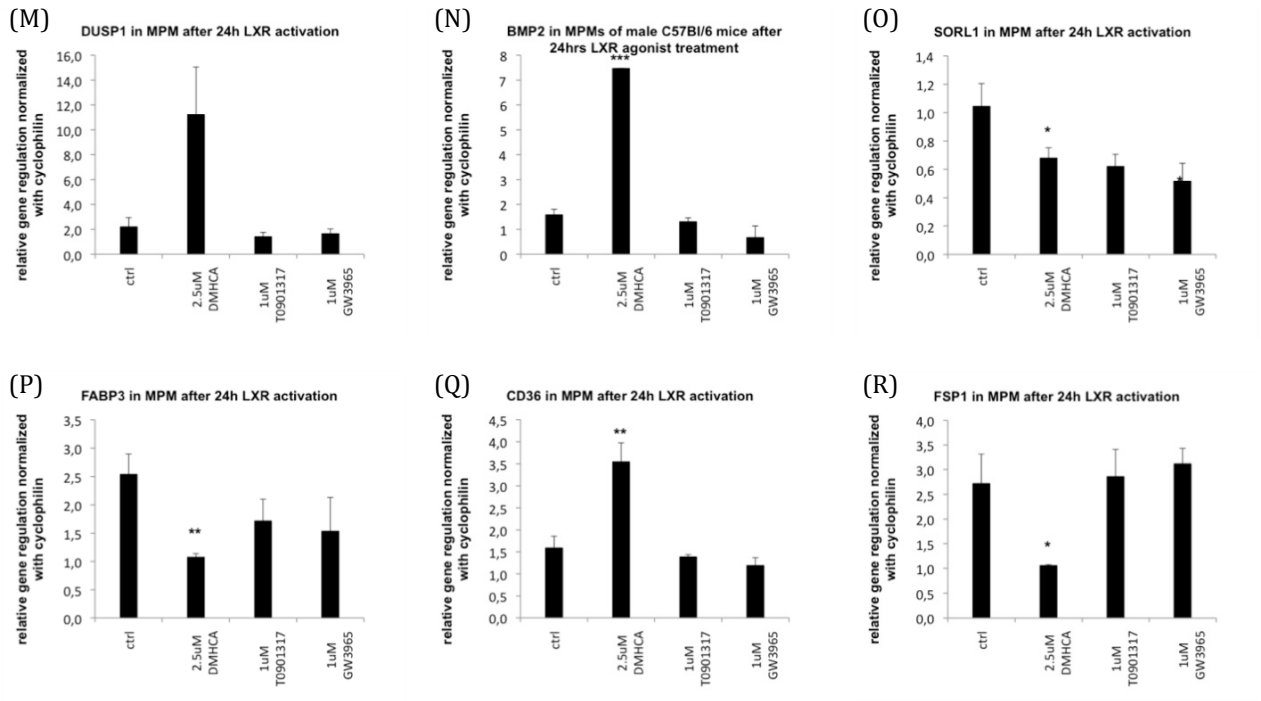

Figure 29. Real-time PCR verification of potential LXR target genes in MPM of male WT mice
Real-time PCR was performed on an icycler from BioRad and expression ratios for CAR6, TRB3, AQP9, NDRG1, ERO1L, INSIG1, SIRT1, CYP51, STARD4, HMGCS, HmgCoAr, ALDOC, DUSP1, BMP2, SORL1,,FABP3, CD36, and FSP1 in MPM including cyclophilin A normalization were calculated by ΔΔCP method. Data are expressed as mean values from 3 samples performed in duplicates ± S.D. $^{*}P < 0.05$; $^{**}P \leq 0.01$; $^{***}P \leq 0.001$

Furthermore, part of the microarray data were confirmed by real-time PCR in MPM of female WT mice after either DMHCA or T0901317 treatment.

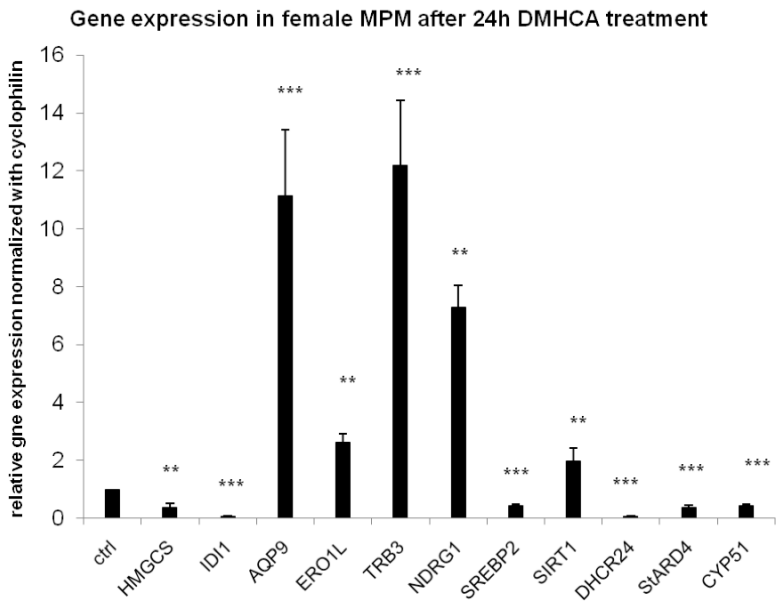

Figure 30. Verification of unknown LXR target genes by qPCR
100ng RNA from MPM of female C57Bl/6 mice was reverse transcribed. This cDNA is independent from the one used for microarrays. Real-time PCR expression ratios in MPM including cyclophilin A normalization were calculated by pairwise fixed reallocation test. Controls without DMHCA were arbitrarily set to 1. Data are expressed as mean values from 3 samples performed in duplicate ± S.D. $^{**}P \leq 0.01$; $^{***}P \leq 0.001$.

Similar to the data achieved by microarray experiments and real-time PCR, I could show in MPM of female mice that DMHCA upregulated AQP9, ERO1L, TRB3, NDRG1 and SIRT1, whereas it

downregulated genes from the cholesterol biosynthesis pathway such as HMGCS, IDI1, DHCR24, STARD4, CYP51 and the cholesterol sensor SREBP2. N-myc downstream regulated gene 1 (NDRG1) interacts with APO A-I and A-II and may have a role in the general mechanisms of HDL-mediated cholesterol transport (222). NDRG1 deficiency leads to Schwann cell dysfunction, suggesting that NDRG1 is essential for maintenance of the myelin sheaths in peripheral nerves. In humans mutations of NDRG1 lead to the so called Charcot-Marie-Tooth disease, which shows demyelination in the brain (223). Tribbles Homolog 3 (Trb3) is a negative regulator of adipogenesis by promoting Acetyl-CoA carboxylase (ACC) ubiquitination and degradation through an association with the E3 ubiquitin ligase COP1 (224). Endoplasmic oxidoreductin-1-like protein (ERO1L) alpha expression together with adiponectin secretion is induced during early phase of adipogenesis but are downregulated at the terminal phase, following an increase of Sirt1 (225). Sirtuin 1 (Sirt1) deacetylates and induces LXR activity and is known to extend the lifespan. Moreover, the RCT is inhibited in Sirt1-deficient mice (226).

The regulation of NDRG1 and TRB3 was further investigated, from which the expression in the male macrophage cell line RAW264.7 (Figure 31) as well as in the human monocyte cell line THP-1 (Figure 33) was checked.

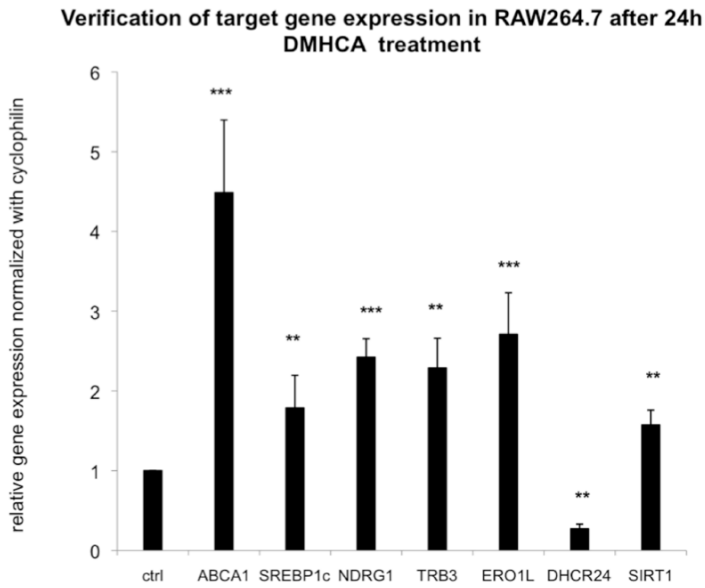

Figure 31. Verification of target gene expression in RAW264.7 after DMHCA treatment by qPCR
RAW264.7 were treated with 2.5µM DMHCA in 10%LPDS medium for 24h. Real-time PCR was performed for ABCA1, SREBP1c, NDRG1, TRB3, ERO1L, DHCR24, and SIRT1. Expression ratios in RAW264.7 including cyclophilinA normalization were calculated by pairwise fixed reallocation test. Controls without DMHCA were arbitrarily set to 1. Data are expressed as mean values from 3 samples performed in triplicate ± SD. $^{*}P < 0.05$; $^{**}P \leq 0.01$; $^{***}P \leq 0.001$.

All target genes except for DHCR24 were upregulated after DMHCA treatment in RAW264.7 cells, which verified the data received from the microarray experiments. SREBP1c was also induced but to the same extent as seen in the real-time verifications with the same cDNA used for microarray experiments. I also measured FC and CE concentrations in RAW264.7 macrophages and foam cell after treatment with DMHCA.

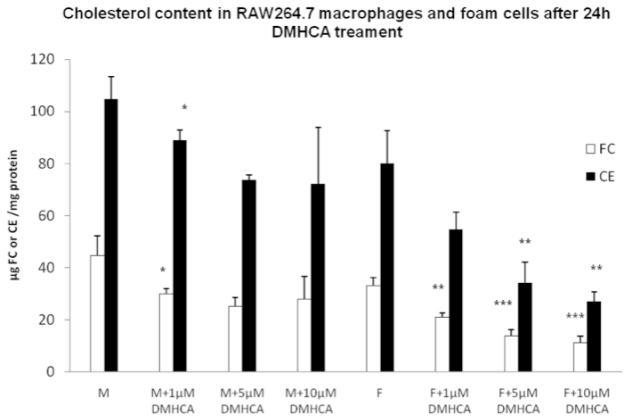

Figure 32. Cholesterol content in macrophages and foam cells after DMHCA treatment

RAW264.7 macrophages and foam cells were treated for 24h with 3 different concentrations of DMHCA and lipids were extracted thereafter. FC and CE content was measured and normalized to the protein content of the cells. M=macrophages, F=macrophage-derived foam cells after treatment with acLDL. SD. $^{*}P < 0.05$; $^{**}P \leq 0.01$; $^{***}P \leq 0.001$.

FC and CE concentrations in RAW264.7 macrophages and foam cells were reduced by DMHCA treatment (Figure 32). These results confirm our observations that DMHCA leads to a reduction in cholesterol biosynthesis as seen in the microarray experiments by downregulation of genes involved in cholesterol biosynthesis.

Furthermore, the mRNA expression of NDRG1, TRB3, and ABCA1 was checked in human THP-1 cells.

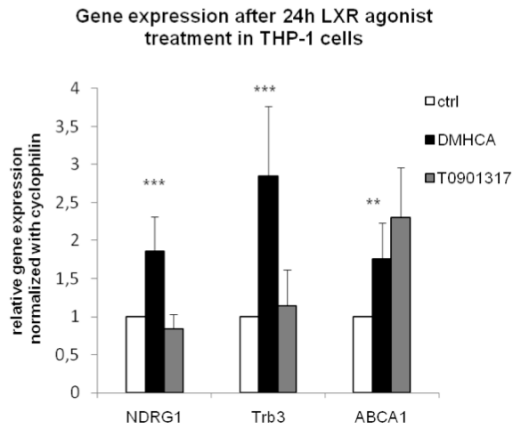

Figure 33. mRNA expression of NDRG1, TRB3, and ABCA1 in THP-1 cells

The human macrophage cell line THP-1 was first differentiated to macrophages and then treated with DMHCA and T090317 for 24hrs. Real-time PCR was performed on an icylcer from BioRad and expression ratios for NDRG1, Trb3 and ABCA1 in THP-1 cells including cyclophilin A normalization were calculated by ΔΔCP method. Data are expressed as mean values from 3 samples performed in duplicates ± SD. $^{*}P < 0.05$; $^{**}P \leq 0.01$; $^{***}P \leq 0.001$

All three genes, NDRG1, TRB3, and ABCA1 were upregulated by DMHCA, but only ABCA1 was also induced by T0901317.

8.2.3.6 LXRE of potential LXR target genes

Having identified several so far unknown LXR target genes by microarray profiling and verifying them by real-time PCR, we checked for potential liver X response elements (LXRE or direct repeats (DR4)) in collaboration with Phenex Pharmaceuticals AG, Ludwigshafen, Germany. Sequences with only one mismatch (MM) are supposed to be potential DR4. We examined human and mouse

NDRG1, ERO1l, TRB3, and SIRT1 for LXRE (Table 13). Further LXRE for more genes can be looked up in the supplemental data (Table S)

Table 13. Potential LXRE for ERO1L, NDRG1, TRB3, and SIRT1
Human and mouse direct repeat 4 (DR4=LXRE): 'AG[GT]TCA-NNNN-AG[GT]TCA' of new target genes such as ERO1L, NDRG1, TRB3, and SIRT1 are shown.

Position	Sequence	MM
ERO1L		
ERO1-like protein alpha precursor (EC 1.8.4.-) (ERO1-Lalpha) (Oxidoreductin-1-Lalpha) (Endoplasmic oxidoreductin-1-like protein) (ERO1-L). [Source:Uniprot/SWISSPROT;Acc:Q96HE7] , Chr: 14, Cyto: q22.1		
-9151	TGGTCAAACTAGTCCA	2
-6919	GGATCATTTGAGGTCA	2
-1624	AGATCACTTAAGGTCA	1
-1288	GGGTCACCTGAGCTCA	2
3335	AGTTCACAGAATGTCC	2
6510	GGATCACCTGAGGTCA	2
-18946	AGATCACCAGAGGTCA	1
-17316	GGATCATCTGAGGTCA	2
-10118	GGATCACTTGAGGTCA	2
-4164	AGATCATTTGAGGTCA	1
-1765	AGTTCAAATGACTTAA	2
-413	AGGGCAGCATATGTCA	2
5175	AGATCACCTGAGGTCA	1
9704	GGATCACTTGAGGTCA	2
ERO1LB		
ERO1-like protein beta precursor (EC 1.8.4.-) (ERO1-Lbeta) (Oxidoreductin-1-Lbeta) (Endoplasmic oxidoreductin-1-like protein B). [Source:Uniprot/SWISSPROT;Acc:Q86YB8] , Chr: 1, Cyto: q42.3		
-15171	AGGTAATGATTGGTCA	2
-14420	AGGCCAAGGCAGATCA	2
-14410	AGATCACCTGAGGTCG	2
-11025	GGATCATTTGAGGTCA	2
-7882	AGGCCAGACAAGTTCT	2
-4559	GGATCACCTGAGGTCA	2
-4216	TATTCAAACAAGTTCA	2
-4163	AGGTCAGAGTAGGCAA	2
2838	AGGTAATTGAAGTTCA	1
2848	AGTTCAAAGAACTTAA	2
-19808	AAGTGAGTGGAGTTCA	2
-13668	AAATCACCTGAGGTCA	2
-13042	GGTTCACTTGAGGTCA	1
-1599	AGATCACCTGAGGTCA	1
2367	GGATCACCTTAGGTCA	2
2845	AGTTCTTTGAACTTCA	2
4389	AGTTCATCAATGGTAA	2
4792	AGATCACTTGAGGTCA	1
8844	AGGTGAGATGAGTTCT	2
9863	AATGCAAATTAGTTCA	2
mouse ERO-1 like beta		
ENSMUSG00000057069		
ERO1-like beta (S. cerevisiae) [Source:MarkerSymbol;Acc:MGI:1914725] , Chr: 13		
-19927	AGGTGACAGGAGTTCG	2
-19238	AGGTCAGAGAACTTAA	2
-6866	AGCTCATGTCAGATCA	2
-4371	AGTTCACCCATGCTCA	2
1885	GGTTAAGTGAAGTTCA	2
5560	AGGTCAGAGGAGTTCT	1
8743	AGGTGACTGGAGTTCT	2
-17397	AGGACATGGGAGGGCA	2
-10910	AGTTGAGGAGAGGGCA	2
-10614	AGGTTAGGTTAGTTCT	2
-10580	AGGTTAGGTTAGTTCT	2
-6649	TGGTCAAGTGTGTTCA	2
5924	ATGTCATTTCAGTTCA	1
NDRG1		
protein NDRG1 (N-myc downstream-regulated gene 1 protein) (Differentiation-related gene 1 protein) (DRG-1) (Reducing agents and tunicamycin-responsive protein) (RTP) (Nickel-specific induction protein Cap43) (Rit42). [Source:Uniprot/SWISSPROT;Acc:Q92597] , Chr: 8, Cyto: q24.22		
-16192	GGATCACCTGAGTTCA	2
-14775	TGGTCAACAGAGGCCA	2

Position	Sequence	MM
-14737	AGTTCAGTTAGTTTCA	2
-14186	AGTTAATTTTAGGTCA	1
-10790	AGCTTAAATGAGTTCA	2
-5932	TGTCCATTTTAGGTCA	2
-5638	AAGTCACCATAGGTGA	2
-453	GAGTCATGAAAGTTCA	2
-18871	AGGTTCAAAGAGTTCA	2
-16485	GGATCACCTGAGGTCA	2
-15169	AGGCCAAGGTAGGCCA	2
-12723	AGATCTGCACAGGTCA	2
-7571	AGGCCAGCCAACTTCA	2
-7320	AGGTTGTATTAGGTCA	2
-6825	AGGTCACTTGAGGTCA	0
2965	AGGCCAGCGGATTTCA	2
5463	AGTCCAAAGGAGGACA	2

mouse

N-myc downstream regulated gene 1 [Source:MarkerSymbol;Acc:MGI:1341799] , Chr: 15

-14298	AGGTCAGACAGGGTCA	1
-7752	AGGTCAGCTTATTTGA	2
-5256	AGGTCTAACTAGTTCT	2
2824	AGTCCAGTTAAATTCA	2
2912	GCTTCATCTCAGGTCA	2
-14957	AGGTGATTTAAAGTCA	2
-4546	AGTCCAAAGAAGGACA	2
-3516	AGTGCACTGAGGGTCA	2
-2502	TGGTCAAGTCAAGTCA	2
2518	AGGACATCCAAGGACA	2
3516	AGGTCACAGGGAGTCA	2
5181	AGATCAATGTAGTACA	2

SIRT1

NAD-dependent deacetylase sirtuin-1 (EC 3.5.1.-) (hSIRT1) (hSIR2) (SIR2-like protein 1). [Source:Uniprot/SWISSPROT;Acc:Q96EB6] , Chr: 10, Cyto: q21.3

-17920	GGATCACCTGAGGTCA	2
-12893	TGGTCACCATAGTTAA	2
-11034	AGATCACCTGAGGTCA	1
-9238	AGTAGAGTTAAGTTCA	2
-8301	GGGTCACCAGAGCTCA	2
-3183	AGTACAAAAGAGTTGA	2
-18993	GGGTCACTTGAGGTCA	1
-15416	GGATCATCTGAGGTCA	2
-12270	GGATCACTTGAGGTCA	2
-9524	AAATCACTTGAGGTCA	2
-5166	CGATCACTTGAGGTCA	2
-4437	AGATCACTTGACGTCA	2
5152	AGGTCAATTTAAGTTA	2
7571	ATTTCAAAAGAATTCA	2
9914	AGTTGATTTAAGATCA	2

mouse SIRT1

sirtuin 1 ((silent mating type information regulation 2, homolog) 1 (S. cerevisiae) [Source:MarkerSymbol;Acc:MGI:2135607] , Chr: 10

-17765	AGGTCAGGGCGGTTCG	2
-7838	AGGTCAGCTGAGGGCC	2
-3489	AGGTCATACTCAGTCA	2
-18371	AGGCCAGTGAAGGCCA	2
-14162	AGGTTATCAACGTTCA	2
-8818	AGTTAAGGTCTGGTCA	2
-7731	AGTTAATTGGAATTCA	2
-957	AGTTCAAAAAAGGCCT	2

TRIB3

Tribbles homolog 3 (TRB-3) (Neuronal cell death-inducible putative kinase) (p65-interacting inhibitor of NF-kappaB) (SINK). [Source:Uniprot/SWISSPROT;Acc:Q96RU7] , Chr: 20, Cyto: p13

-16092	AGATCACTTGAGGTCA	1
-8028	AGATCACTTGTGGTCA	2
-5469	AGATCACGCCAGTGCA	2
-4829	GGATCATTTAAGGTCA	2
6875	GGTTCACTTGAGGCCA	2
9474	AGATCACCTGAAGTCA	2
-19993	GGATCACCTGAGGTCA	2
-15186	AGGCCACCCGAGTTCC	2
-10850	AGGTAAAGGGGGTTCA	2
-6362	GGATCACCTGAGGTCA	2
-4912	AGTTCTGATGAGTTCC	2
4712	AGGTCACCTGAGGTCA	0
5136	GGGTCAAGAGAGGTCT	2

Position	Sequence	MM
mouse TRIB3		
tribbles homolog 3 (Drosophila) [Source:MarkerSymbol;Acc:MGI:1345675] , Chr: 2		
-14288	AGTTCAAGGCAGGCCA	1
-13642	AGGTCAAACCATGGCA	2
-5823	AGTTGTTGGTAGTTCA	2

Position	Sequence	MM
-5797	AAGTCAGACAAGGTCA	1
6814	GTTTCAGGGCAGGTCA	2
-6879	AGTGCAGGCCAGCTCA	2
-5233	AGGCCATGGCAGGACA	2
-4954	AGTTGCGCACAGTTCA	2
-2999	AGCTCAATCCAGTTCT	2
8090	AGTTCAGTTAACCTCA	2

8.2.3.7 Immunofluorescence of NDRG1 and TRB3

Immunofluorescence with antibodies for two potential candidates for LXR activation in MPM was performed.

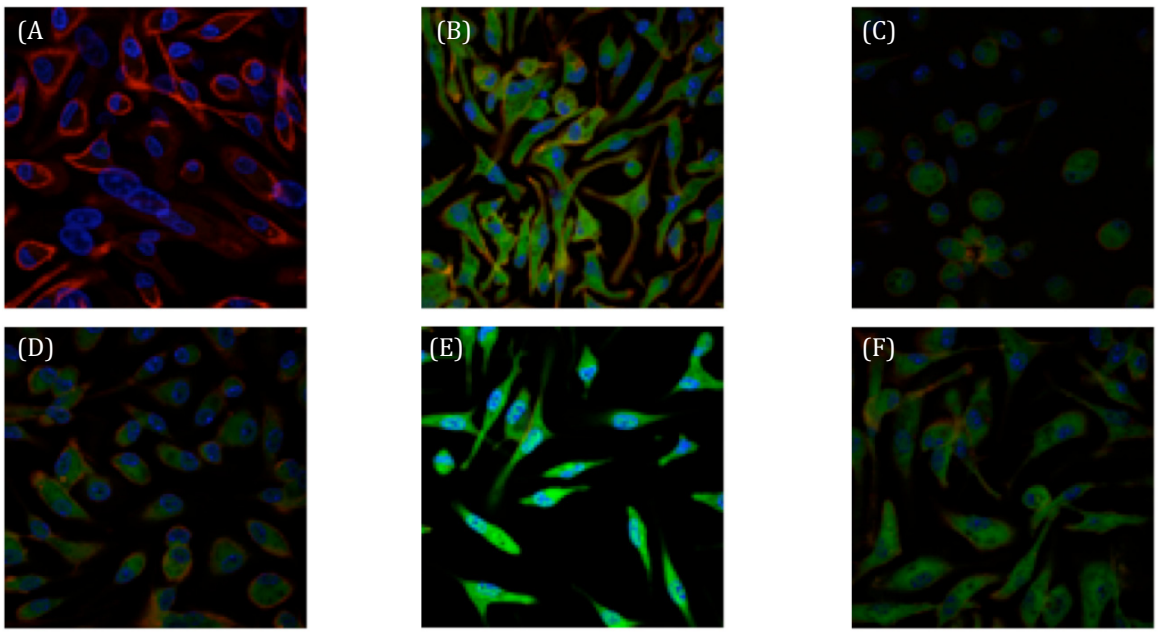

Figure 34. Immunofluorescene images of NDRG1 in MPM after 24h DMCHA and T0901317 treatment
MPM were treated for 24h with 2.5µM DMHCA, 1µM T0901317 and ethanol for the control. Thereafter, cells were incubated with a NDRG1 or TRB3 antibody overnight and 1h with an anti-rabbit secondary antibody. green=NDRG1/TRB3, red=f-actin from a phalloidin marker, blue=DAPI stained nuclei. (A) Control, (B) DMHCA and (C) T0901317 treated cells after NDRG1 staining. (D) Control, (E) DMHCA, and (F) T0901317 treated cells after TRB3 staining.

The images show that DMHCA upregulated NDRG1 and TRB3 in MPM whereas T0901317 does it only to a lower extend. In fact, these genes were very low expressed in control cells. Evaluation of intensity was performed using Image J. Here I could show that DMHCA led to a 7-fold increase in intensity of the NDRG1 whereas T0901317 led only to a 3.5-fold increase, implying an upregulation of NDRG1 with both agonists (Figure 34 A-C). Using a TRB3 antibody I found that TRB3 expression was increased 3.5-fold by with DMHCA, whereas T0901317 increased the signal to 1.2-fold (Figure

34D-F). Further experiments have to be done to prove these results since the antibodies do not work well in Western blotting experiments.

8.2.4 DMHCA reduces mRNA expression of inflammatory genes in mice

Next, verification of our findings was performed in human peritoneal macrophages (hPM), which were received from the peritoneal fluid of a male patient with peridonitis, who received 2g vancomycin. After 3 days the peritoneal fluid was clear and the macrophages were harvested by centrifugation and plated in the DMEM medium until they became adherent. Then they were treated with the LXR agonists in the same manner as MPM or cell lines. Similar gene regulation was found as with the cell lines and MPM. DMHCA induced ABCA1 and ABCG1 even higher than T0901317, which was already shown in MPM. It also induced the potential novel LXR target genes NDRG1, TRB3, ERO1L, and SIRT1, whereas T0901317 failed to induce these genes except ERO1L. Moreover, DMHCA did not induce FAS and repressed induction of INSIG1 and CYP51, whereas T0901317 induced all these genes. SREBP1c was induced upon treatment with both LXR agonists. Some additional genes, that have recently been shown to be LXR targets, were studied and it was found that DMHCA induced NPC1 as well as REV-ERBα. (Figure 35) (227, 228).

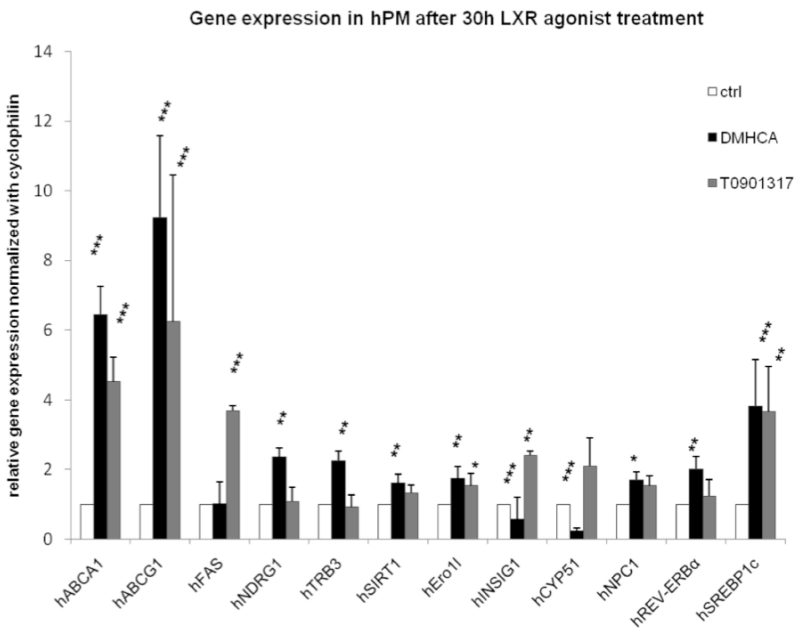

Figure 35. Gene expression of known and unknown LXR target genes in hPM from a male patient after 30hrs incubation with either DMHCA or T0901317
Macrophages were received from a male patient with peridonitis. Real-time PCR was performed on a Applied Biosystems StepOne Plus Real-time system Singleplex PCR with SYBR Green. Expression ratios for target genes in human peritoneal macrophages (hPM) including cyclophilin A normalization were calculated by ΔΔCP method. Data are expressed as mean values from 2 samples performed in triplicates ± SD. $^{*}P < 0.05$; $^{**}P \leq 0.01$; $^{***}P \leq 0.001$

Treatment of human peritoneal macrophages, with DMHCA led to a reduction in TNFα (32.2%) and IL-8 (12.6%) secretion into the medium after stimulation with LPS. We could also show a reduction in IL-6 in the supernatant of blood peripheral mononuclear cells (BPMC) after DMHCA treatment

and 24h LPS stimulation. Cells were treated for 30h to 48h with the LXR agonist and the last 6h to 24h stimulated with LPS (1μg/mL).

Moreover, DMHCA treatment resulted in a repression of IL6 (Figure 36E) and iNOS (Figure 36F) mRNA levels in both LXRα, LXRβ and LXR double knockout mice in comparison to another well-known LXR agonist (GW3965) (performed by Noam Zelcer from P. Tonotonoz laboratory, UCLA, California). These data indicate that this effect is clearly independent of LXR activation. ABCA1 (Figure 36A) and ABCG1 (Figure 36B) were markedly induced by DMHCA and the agonist does not show any selectivity for either isoform of LXR. SREBP1c and FAS were not regulated by DMHCA. Interestingly, DMHCA plus LPS did not induce IL-6 and iNOS, neither in wild type (WT) nor in LXR knockout mice. It has been shown that LXR agonists have anti-inflammatory effects (54) but DMHCA reduces the inflammatory genes independently of LXR.

API6 was not regulated in LXRα-/- mice, but still upregulated in LXRβ-/- mice and not activated in the LXR double knockout mice (Figure 36G). Thus, API6 is only regulated upon LXRα activation, which has already been shown in previous work (229). APOE was not induced by any of the two LXR agonists (Figure 36H).

Pro-inflammatory genes RANTES (Figure 36I) and COX2 (Figure 36J) were downregulated by DMHCA plus LPS both in WT and LXR knockout mice.

(A)

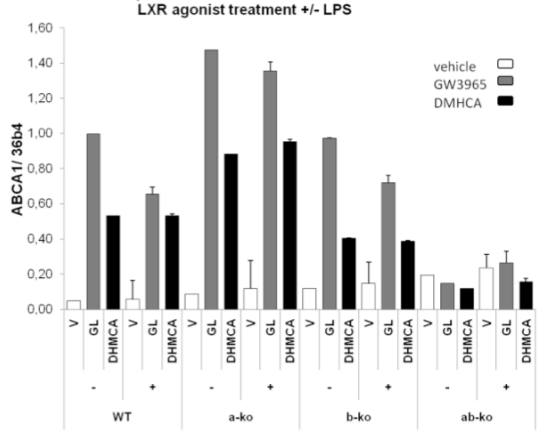

(B)

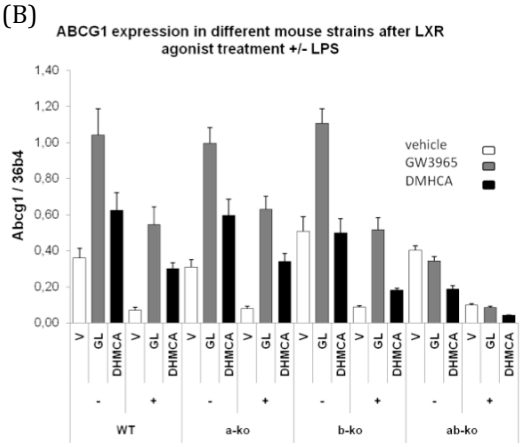

(C)

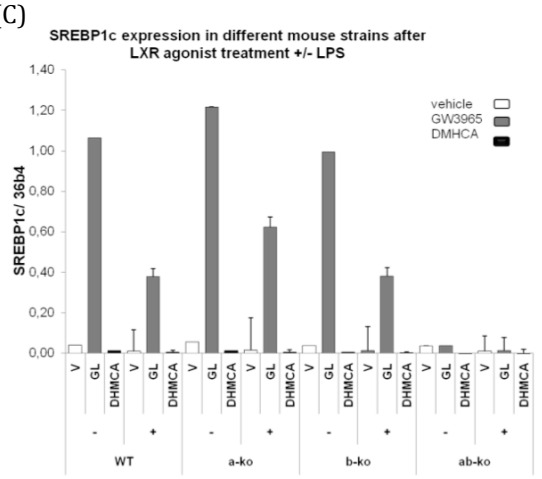
SREBP1c expression in different mouse strains after LXR agonist treatment +/- LPS
SREBP1c/ 36b4
vehicle
GW3965
DMHCA
WT
a-ko
b-ko
ab-ko

(D)

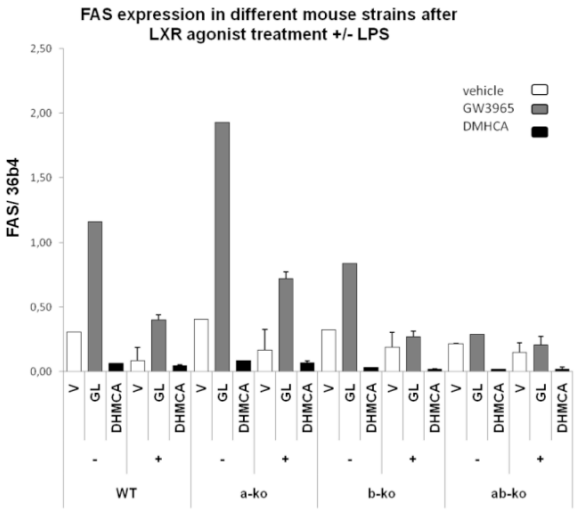
FAS expression in different mouse strains after LXR agonist treatment +/- LPS
FAS/ 36b4
vehicle
GW3965
DMHCA
WT
a-ko
b-ko
ab-ko

(E)

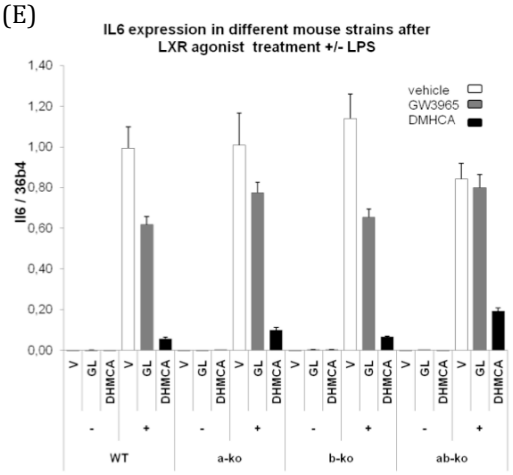
IL6 expression in different mouse strains after LXR agonist treatment +/- LPS
Il6 / 36b4
vehicle
GW3965
DMHCA
WT
a-ko
b-ko
ab-ko

(F)

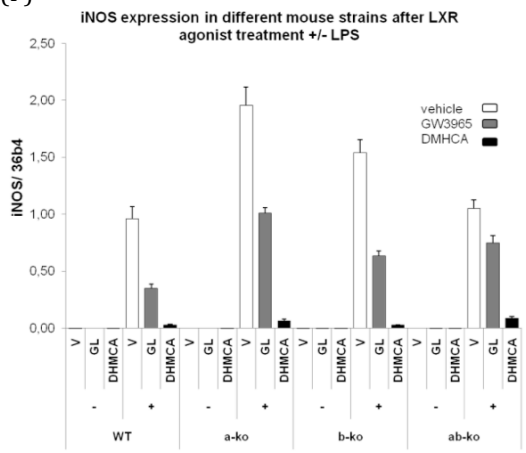
iNOS expression in different mouse strains after LXR agonist treatment +/- LPS
iNOS/ 36b4
vehicle
GW3965
DMHCA
WT
a-ko
b-ko
ab-ko

(G)

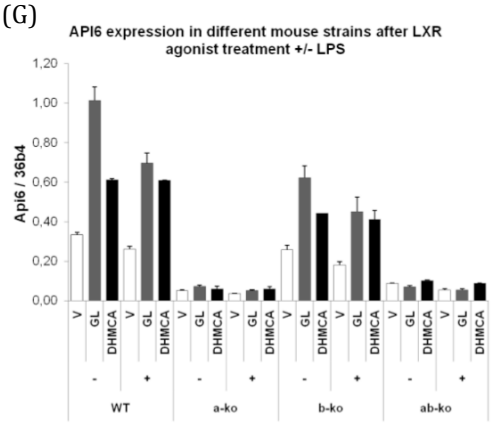
APl6 expression in different mouse strains after LXR agonist treatment +/- LPS
Apl6 / 36b4
WT
a-ko
b-ko
ab-ko

(H)

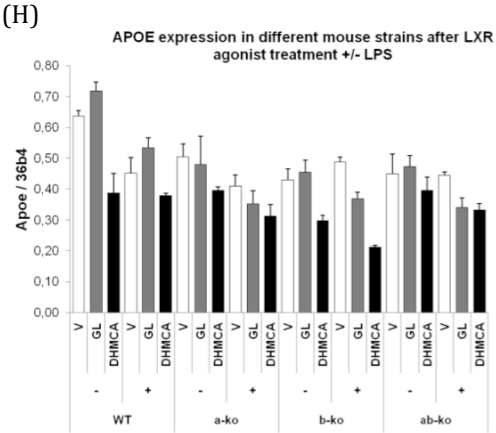
APOE expression in different mouse strains after LXR agonist treatment +/- LPS
Apoe / 36b4
WT
a-ko
b-ko
ab-ko

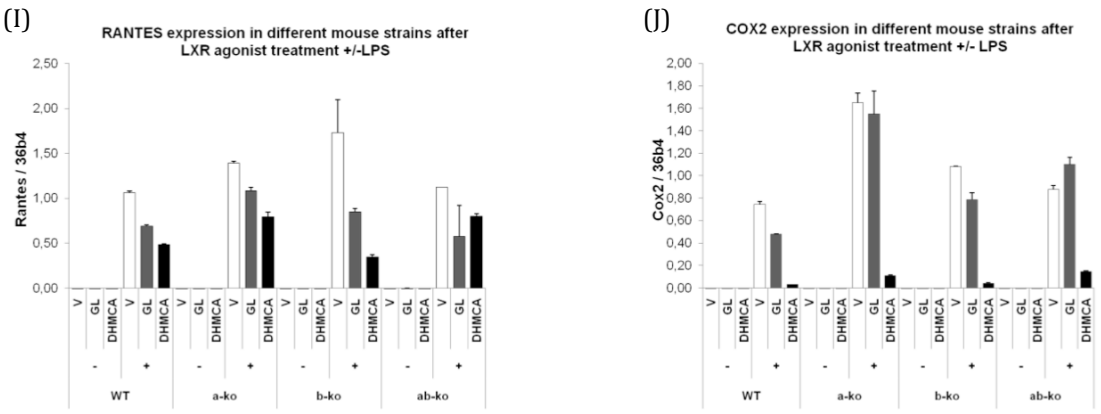

Figure 36. Gene regulation in WT, LXRα-/-, LXRβ-/- and LXRα/β-/- mice after LXR agonist treatment (GW3964 and DMHCA) plus/minus lipopolysaccharide (LPS)

Thioglycolate-elicited macrophages were harvested from LXR deficient mice and WT mice 3 days after injection. Macrophages were treated with the LXR agonists DMHCA and GW3965 for 24h and then 6h more with the inflammation stimulus LPS. Real-time PCR was performed for ABCA1, ABCG1, SREBP1c, FAS, IL6, iNOS, API6, APOE, RANTES and COX2, applying the ΔΔCP method and normalization was done with the house keeping gene 36b4.

8.3 Cholesterol biosynthesis in MPM

MPM from male WT mice were incubated with or without 5µM DMHCA or T0901317 in serum-depleted medium for 12h. Thereafter, fresh medium containing 1µCi/mL medium ^{14}C mevalonate as the substrate for cholesterol biosynthesis together with the LXR agonists was added for another 12h. Lipids were extracted and thin layer chromatography (TLC) was used to separate the lipid extractions. Spots for CE and FC were cut out and measured on a β-counter, resulting in a 96.1% reduction of FC but a 4.8-fold increase in CE. Similar, but not to the same extent, treatment with T0901317 led to a 65.7% reduction in FC and a 1.7-fold increase in CE.

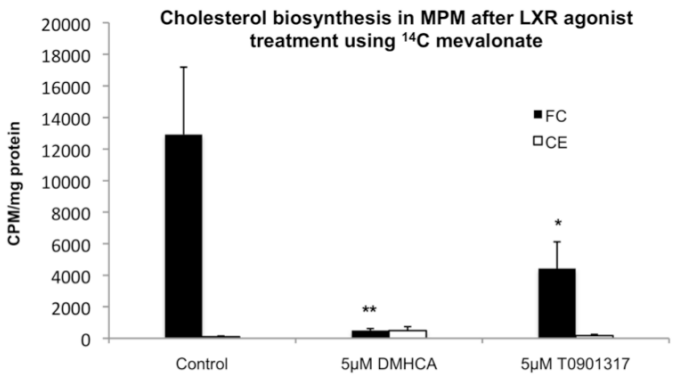

Figure 37 Cholesterol biosynthesis in MPM after LXR agonist treatment using ^{14}C mevalonate

MPMs were incubated with LXR agonists in serum-depleted medium for 12h. Then, fresh medium was prepared with 1µCi ^{14}C mevalonate plus the agonists. Cells were incubated for another 12h. Lipid extraction was performed and separated by TLC. Spots for FC and CE were cut out and radioactivity was measured in a β-counter.

Moreover, MPM were treated with 10µCi ^{14}C acetate/mL medium plus the agonists for 12h after 12h incubation solely with LXR agonists. Lipid extraction was performed and extracts were separated by TLC. Spots for phospholipids (PL), FC, TG, FFA and CE were cut out and radioactivity was measured in a β-counter.

DMHCA reduced FC synthesis also by using acetate as a substrate by 92% (2,5µM) and 93% (10µM), respectively. T0901317 also reduced FC synthesis by 27.8% (1 µM) and 26.6% (10 µM), respectively (Figure 38B). CE synthesis was significantly increased with DMHCA treatment, which was not observed upon T0901317 treatment (Figure 38C). Further investigations are necessary to figure out why DMHCA leads to a CE accumulation and T0901317 does not. PL (Figure 38A) were increased upon T0901317treatment but not upon DMHCA treatment, whereas TG (Figure 38D) were increased by treatment with both agonists.

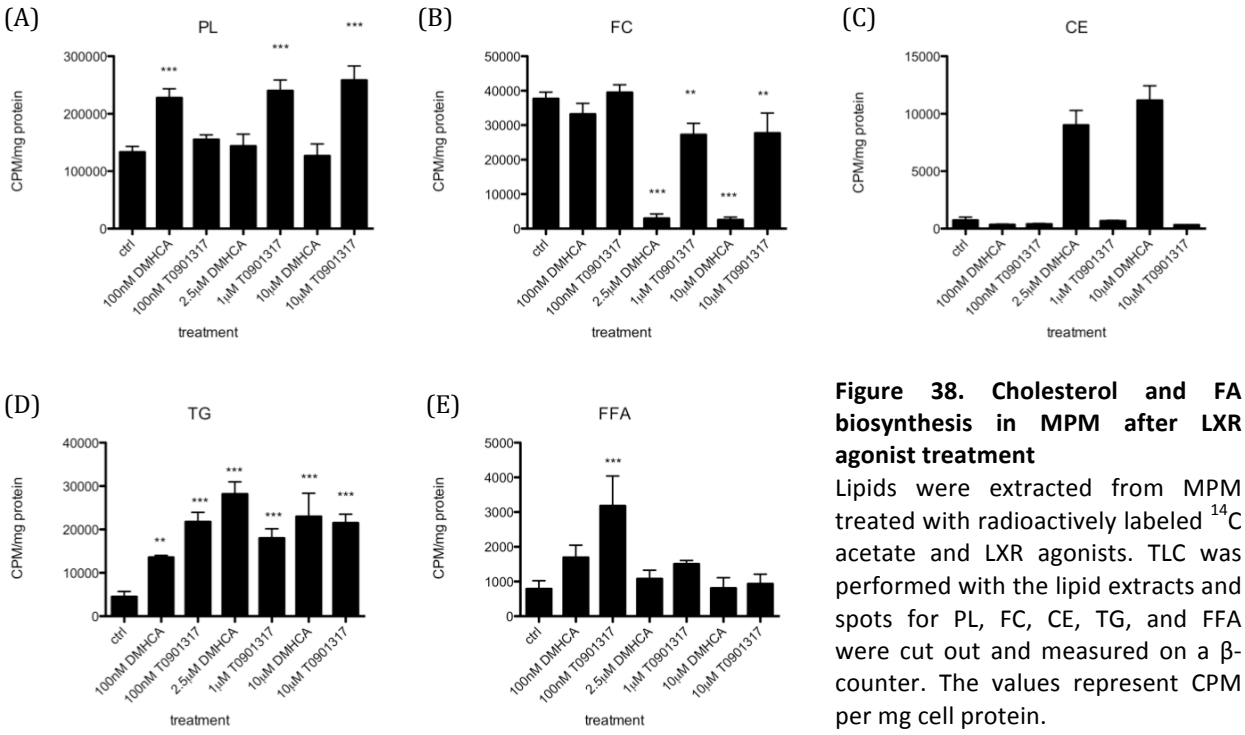

Figure 38. Cholesterol and FA biosynthesis in MPM after LXR agonist treatment
Lipids were extracted from MPM treated with radioactively labeled ^{14}C acetate and LXR agonists. TLC was performed with the lipid extracts and spots for PL, FC, CE, TG, and FFA were cut out and measured on a β-counter. The values represent CPM per mg cell protein.

8.4 Regulation of proteins in livers and macrophages by DMHCA treatment

Proteins of MPM and livers from female WT mice, which were i.p. injected with DMHCA, were separated by 2-D-gel electrophoresis. After evaluating the intensities (fold change≥2), spots were picked and evaluated by LC-MS/MS.

(A) (B) (C)

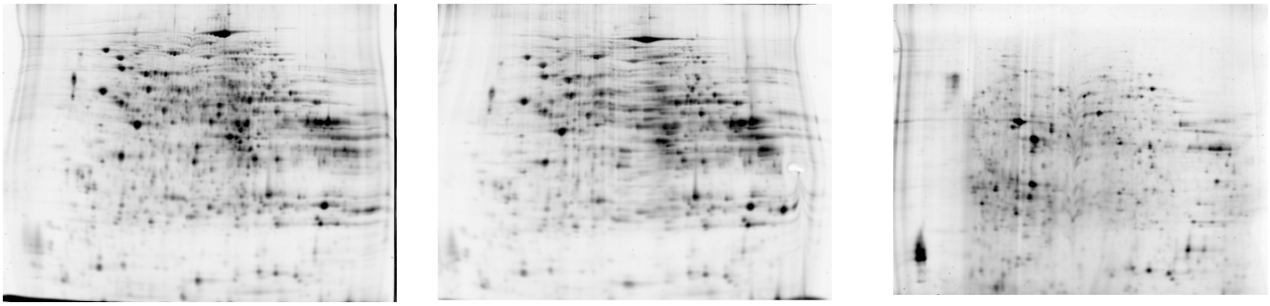

Figure 39. Images of two dimensional gel electrophoresis from liver and macrophage proteins
Female C57Bl/6 mice were i.p. injected with DMHCA (50mg/kg BW in 1.3% Tween80 + 0,25% CMC) for 6 days. 50µg of livers were labeled with either Cy3 or Cy5 and 950µg were added for a total of 1mg for each color. In A) livers from controls were labeled with Cy3 and from DMHCA-treated mice with Cy5 whereas in B) the labeling was done conversely. For the macrophages 50µg were labeled with either Cy3 or Cy5 and 320µg were added which gives a total of 370µg for each color. The two dimensional gel for MPM can be seen in C) where controls were labeled Cy5 and DMHCA-treated cells with Cy3.

The two dimensional gel electrophoresis of MPM from DMHCA i.p. injected mice led to 119 annotated DAVID ID, where the pathways being most highly involved are the glycolysis/gluconeogenesis and pyruvate pathways (http://david.abcc.ncifcrf.gov/). The complete list of genes can be found in the supplemental data (Table T). Cathepsin D, which is a lysosomal protease, was upregulated after DMHCA injection. It might play an important role in ABCA1-mediated cholesterol efflux (230). Aldehyde dehydrogenase 2 was also upregulated upon DMHCA injection and is known to play a protective role against oxidative stress. Several more proteins, playing a role in glycolisis/glyconeogenesis, have been found to be regulated in MPM after DMHCA i.p. injection.

In the liver, 33 annotated DAVID ID (http://david.abcc.ncifcrf.gov/) were identidfied, which are mostly involved in glutathione metabolism and metabolism of xenobiotics by cytochrome P450. Most proteins were downregulated, e.g. vinculin, albumin 1, and glutathione s-transferases (Table U in supplemental data).

8.5 Short-term treatment with DMHCA

After we had shown the *in vitro* effects of DMHCA, the impacts of DMCHA were studied in WT and ApoE-/- mice in short-term treatments (4d, 7d and 15d). We investigated low and high concentrations of DMHCA in the food (8 and 80mg/kg body weight (BW), respectively) as well as i.p. injections (50mg/kg BW) and its influence on liver steatosis and gene regulation.

8.5.1 Intraperitoneal injection of DMHCA in comparison with T0901317

Six days after i.p. injection of DMHCA or T0901317 blood and the liver were harvested and the differences in liver and plasma lipid parameters were examined. The treatment with T0901317 led

to severe liver steatosis in all mice, whereas the DMHCA treatment showed no difference compared with the control injected mice (Table 14). There were no significant differences in the plasma lipid parameters, but the liver of the T0901317 treated mice showed an increase in liver TG of 50% (Table 14). Similar studies were already performed by Quinet et al. (181).

Table 14. Plasma and hepatic TG and TC concentrations of male C57Bl/6 (WT) mice on chow diet and i.p. injected with DMHCA or T0901317 for 6 days (50 mg/kg BW/day)

		Plasma		Liver	
	n	TG (mg/dl)	TC (mg/dl)	TG /mg/g)	TC (mg/g)
controls	5	34 ± 2.2	91 ± 6.3	2.69 ± 0.40	5.05 ± 0.48
DMHCA	5	35 ± 13	83 ± 18	2.59 ± 1.49	4.29 ± 0.76
T0901317	5	37 ± 10.0	123 ± 30	4.05 ± 0.91*	4.50 ± 0.42

These results were further confirmed by performing lipid staining of liver cryosections from these mice with oil red O. Unfortunately, we couldn't get proper cryosections from livers of T0901317 injected mice to further confirm our results. The tissue was dried out and damaged from the freezing procedure. Yet, we could show that there is no significant macroscopic difference in the livers of control and DMHCA treated mice (Figure 40).

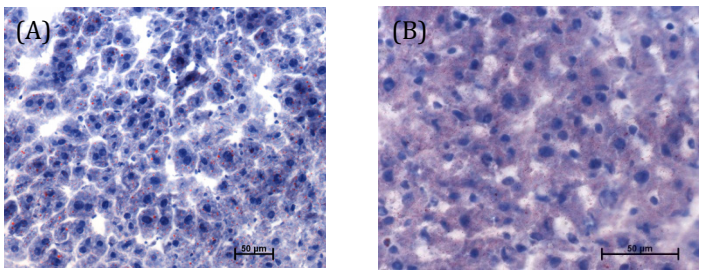

Figure 40. Cryosections of livers from i.p. injected mice
WT mice that have been either injected with (A) 1.3% Tween80 plus 0.25% carboxymethylcellulose (CMC) as control or with (B) 50mg/kg BW DMHCA. Cryosections were performed on a microtome and are 10μm thick, respectively. Then sections were stained with oil red O for lipid accumulation. The scale bar represents a segment of 50μm.

8.5.1.1 Liver pathology

In order further investigate the effects of DMHCA on liver tissue we performed paraffin sections and looked at liver histology.

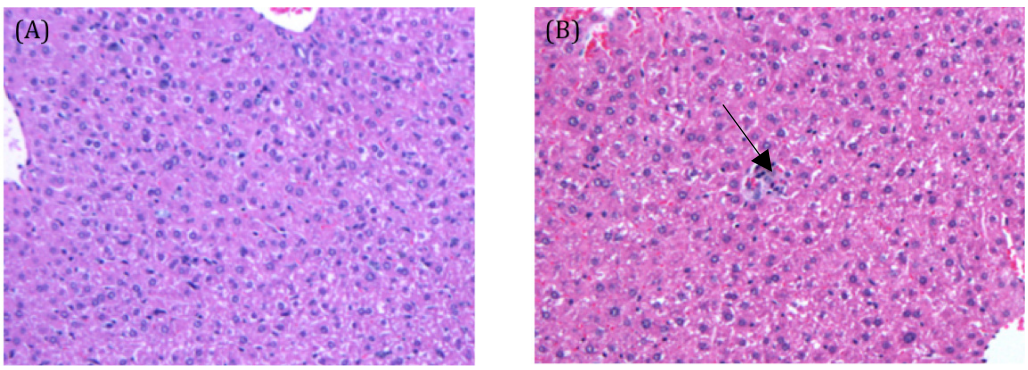

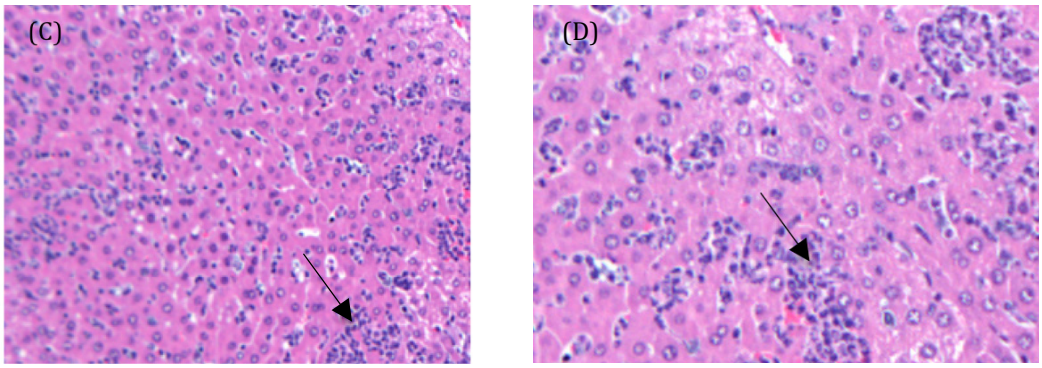

Figure 41. H&E staining of livers from WT mice after i.p. injection of DMHCA
WT mice were divided in the following groups: (A) controls without i.p. injection and perfusion, (B) i.p. injected with vehicle (1.3% Tween80 + 0.25% CMC) and perfused, (C) i.p. injected with 50mg/kg BW/day DMHCA without perfusion and (D) i.p. injected with DMHCA and perfusion. Livers were embedded into paraffin and sections were stained with hematoxylin and eosin.

Although there were some accumulations of Kupffer cell nodules (marked with arrows in Figure 41B-D) the livers of DMHCA treated mice they did not show any peridonitic changes when compared with the control (Figure 41). Moreover, also the perfusion of the livers did not lead to any significant change in liver structure (Figure 41A,B,D). In fact, there were no severe pathological changes between the groups, from which we deduced no toxic or harmful effects of the vehicle ± DMHCA onto the livers.

8.5.1.2 Gene regulation after 6 days i.p. injection of DMHCA and T0901317

Since we could prove the (visual and chemical) absence of liver steatosis after treatment with DMHCA, we also determined mRNA expression levels of specific target genes in peritoneal macrophages (Figure 42) and livers of these i.p. injected mice (Figure 43).

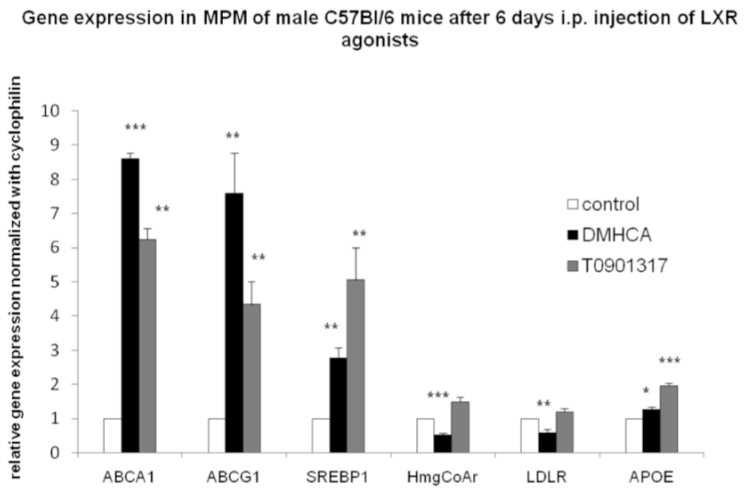

Figure 42. Gene expression profiles in macrophages of male mice, which have been injected i.p. with 50mg DMHCA or T0901317/kg BW/day for 6 days
Five male WT mice were i.p. injected with 1.3%Tween80 and 0.25% CMC solution ± 50mg/kg BW DMHCA or T0901317, respectively. Total RNA was isolated and reverse transcribed into cDNA. Real-time PCR was performed and expression values were calculated by pairwise fixed reallocation test with cyclophilin A normalization relative to control (controls were arbitrarily set to 1). Data are expressed as mean ± SD. $^{*}P < 0.05$, $^{**}P \leq 0.01$, $^{***}P \leq 0.001$.

ABCA1 and ABCG1 mRNA expressions were found to be highly induced after i.p. injection of both LXR agonists, even to a higher extent after DMHCA injection. SREBP1c was upregulated much higher after T0901317 treatment than DMHCA treatment. I could also show that mRNA expression of HmgCoAr and the LDLR, were significantly downregulted in DMHCA treated macrophages whereas APOE was only slightly induced with both agonists and more pronounced after T0901317 treatment (Figure 43).

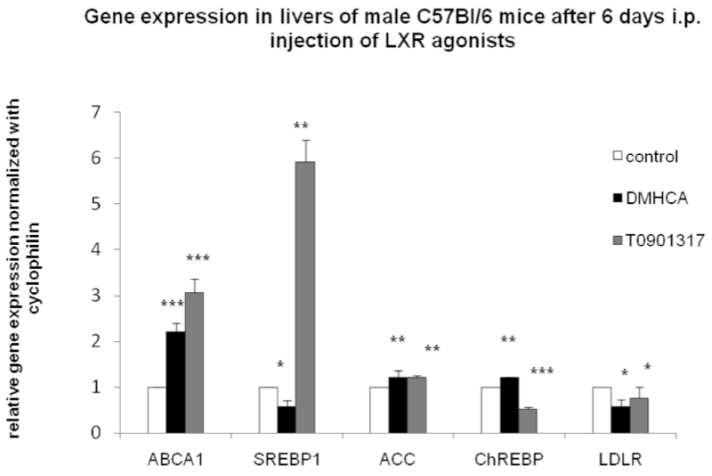

Figure 43. Gene expression profiles in livers of male mice, which have been injected i.p. with 50mg DMHCA or T0901317 /kg BW/day for 6 days
Five male WT mice were i.p. injected with 1.3%Tween80 and 0.25% CMC solution ± 50mg/kg BW DMHCA or T0901317, respectively. Total RNA was isolated and reverse transcribed into cDNA. Real-time PCR was performed and expression values were calculated by pairwise fixed reallocation test with cyclophilin A normalization relative to control (controls were arbitrarily set to 1). Data are expressed as mean ± SD. $^{*}P < 0.05$, $^{**}P \leq 0.01$, $^{***}P \leq 0.001$.

In the liver ABCA1 was induced upon DMHCA and T0901317 treatment (Figure 43). SREBP1c was repressed upon DMHCA treatment in comparison with control and T0901317 treated (6-fold increase of SREBP1c) groups. LDLR was repressed upon the treatment with both agonists, but more pronounced upon DMHCA treatment. Acetyl-CoA carboxylase (ACC) was slightly, but significantly, increased whereas carbohydrate response element-binding protein (ChREBP) is downregulated upon T0901317 treatment and slightly increased upon DMHCA treatment.

8.5.2 High and low doses of DMHCA and T0901317 within the diet

8.5.2.1 Lipid parameters and gene regulation in WT mice after 7 days feeding WTD and DMHCA

Female C57Bl/6 mice were fed with a WTD containing 8 mg DMHCA/kg body weight (BW)/day for 7 days. I checked plasma and liver lipid parameters (Table 15) and gene regulation (Figure 44).

Table 15. Plasma and hepatic TG and TC concentrations of male and female C57Bl/6 mice on WTD with or without 8mg DMHCA/kg BW/day for 7 days after a 4h fasting period.

		n	Plasma		Liver	
			TG (mg/dl)	TC (mg/dl)	TG (mg/g tissue)	TC (mg/g tissue)
male	WTD	4	36.0 ± 10.1	128.6 ± 9.68	13.4 ± 3.63	4.86 ± 1.54
	WTD+DMHCA	5	39.4 ± 2.51	125.6 ± 51.1	10.2 ± 0.91	5.75 ± 2.26
female	WTD	4	37.0 ± 9.69	105.9 ± 7.31	11.0 ± 2.90	4.88 ± 1.05
	WTD+DMHCA	4	29.9 ± 9.85	97.8 ± 10.1	11.3 ± 1.33	5.58 ± 1.76

No significant differences in lipid parameters were observed between WTD and WTD + DMHCA. In the liver, mRNA expression of CYP7A1, ABCG1, ABCG5, ABCG8, and SREBP1c were significantly upregulated whereas ABCA1 was not regulated and FAS was significantly downregulated. Additionally, the mRNA expression level for SHP, which is a target gene of the farnesoid X receptor (FXR), was checked, but no regulation was observed. Moreover, the regulation of API6/SPα/ CDL5 was examined, which plays a role in macrophage apoptosis within atherosclerotic lesions (231), but no regulation within the liver could be detected (Figure 44).

Figure 44. Gene expression in liver from male C57Bl/6 mice.
Mice were fed WTD ± DMHCA for 7 days. RNA was isolated, reverse transcribed and real-time PCR was performed.
Expression values were calculated by pairwise fixed reallocation test using hypoxanthine phospho-ribosyltransferase (HPRT) normalization relative to control (controls were arbitrarily set to 1). Data are expressed as mean ± SD. $^{*}P < 0.05$, $^{**}P \leq 0.01$, $^{***}P \leq 0.001$, n=2 per group.

Furthermore, gene regulation in the intestine was examined. LXR play an important role in the intestinal tract as regulators of cholesterol absorption and we could already show that DMHCA regulated the LXR target genes ABCA1 and SREBP1c in human Caco-2 colon carcinoma cells.

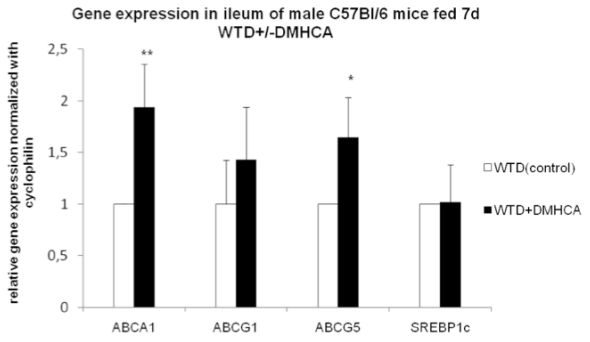

Figure 45. Gene expression in ileum from male C57Bl/6 mice.
Mice were fed a WTD ± DMHCA for 7 days. RNA was isolated, reverse transcribed and real-time PCR was performed with the listed genes. Expression values were calculated by pairwise fixed reallocation test using Cyclophilin A normalization relative to control (controls were arbitrarily set to 1). Data are expressed as mean ± SD. $^{*}P < 0.05$, $^{**}P \leq 0.01$, n=2 per group.

DMHCA significantly induced the LXR target genes ABCA1 and ABCG5 in ileum, whereas ABCG1 was not significantly induced. SREBP1c regulation was not different to the control, WTD fed mice (Figure 45).

8.5.2.2 Lipid parameters, liver pathology, gene and protein expression after 4d feeding chow diet containing DMHCA or T0901317

Male wild type (C57Bl/6) mice were fed with chow diet containing T0901317 or DMHCA (80 mg/kg BW/day) for 4 days in order to see the response of higher concentrations of the LXR agonists on lipid levels, gene and protein regulation. Although all mice ate comparable amounts of food and showed similar body weights, liver weights were significantly increased in T0901317-fed animals, which was the result of severe steatosis compared to controls. In contrast, liver weight remained unchanged and the liver color appeared normal in DMHCA-fed mice. Oil red O staining of liver specimens from DMHCA-treated animals revealed minimal steatosis (Figure 46).

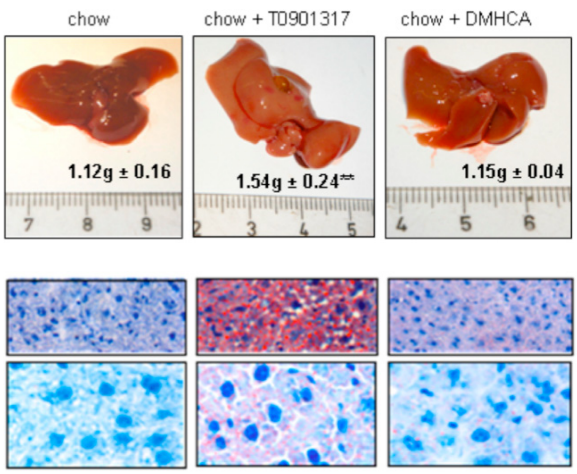

Figure 46. Livers and stainings of liver cryosections after treatment with DMHCA or T0901317 after DMHCA and T0901317 treatment for 4 days
Liver analyses of C57Bl/6 mice fed chow diet ± T0901317 or DMHCA (80 mg/kg BW/day) for 4 days. Livers were weighed and cryo-sections were stained with oil red O and hematoxylin. Original magnification: 100x (top row), 600x (bottom row).

Moreover, SREBP1c protein (Figure 47A) and mRNA expression (Figure 47B) in the liver revealed less SREBP1c upregulation upon DMHCA than T0901317 treatment. T0901317 feeding significantly enhanced SREBP1c mRNA levels by 4.4-fold compared to control. There were no differences in the content of the precursor SREBP1 protein (pSREBP1) between the different diets. However, T0901317 markedly increased mature, transcriptionally active hepatic nuclear SREBP1 (nSREBP1) protein by 2.9-fold. On the contrary, DMHCA treatment resulted in 1.6-fold increased SREBP1c mRNA expression, whereas it did not change nSREBP1 protein levels (Figure 47A) Thus, DMHCA induces neither hypertriglyceridemia nor liver steatosis whereas T0901317 induces severe liver steatosis.

(A) (B)

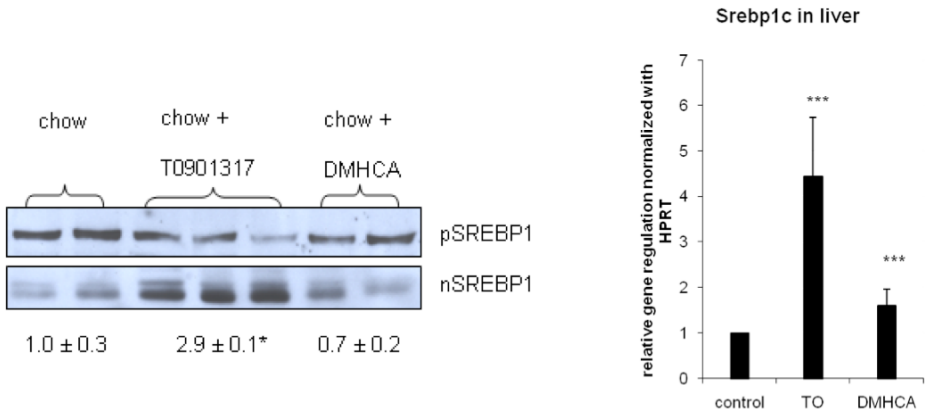

Figure 47. SREBP1c protein and mRNA expression after DMHCA and T0901317 treatment for 4 days
Liver analyses of C57Bl/6 mice fed chow diet ± T0901317 or DMHCA (80 mg/kg BW/day) for 4 days. (A) Western blot analysis of precursor (p) and mature (n) SREBP1 expression and (B) Real-time PCR analysis of SREBP1c mRNA expression normalized with HPRT. $^{*}P < 0.05$, $^{***}P \leq 0.001$.

The different effects of T0901317 and DMHCA were also confirmed by measuring the TG concentrations, which were significantly 2.4-fold increased upon T0901317 treatment when compared to controls (Table 16). In contrast DMHCA showed only a slight increase in TG levels. In addition, plasma ALT concentration was increased in T0901317 fed mice indicating liver damage, but was not significantly altered upon DMHCA treatment.

Table 16. WT mice 4days treatment DMHCA or T0901317 liver and plasma lipid parameters
C57Bl/6 mice fed chow diet ± T0901317 or DMHCA (80 mg/kg BW/day) for 4 days and blood was taken by retroorbital bleeding. $^{*}P < 0.05$; $^{**}P \leq 0.01$; $^{***}P \leq 0.001$

		Liver		Plasma
	n	TG (mg/g)	TC (mg/g)	ALT (U/l)
chow	8	19.7 ± 1.6	2.4 ± 0.1	38 ± 7.8
chow+T0901317	8	47.6 ± 8.9***	2.0 ± 0.2	241 ± 95 **
chow+DMHCA	8	24.5 ± 4.8*	2.6 ± 0.1	49 ± 15

These data clearly demonstrate that T0901317 had a profound effect on hepatic fat content with a drastic increase in plasma ALT levels after 4 days of feeding, whereas DMHCA only mildly increased hepatic TG concentrations with no detectable liver damage.

8.5.2.3 Gene regulation in different tissues after 4d treatment with DMHCA and T0901317

Next, mRNA expression levels of various LXR target genes were determined in ileum, duodenum, and liver (Figure 48 to Figure 50) after feeding the animals chow diet ± T0901317 or DMHCA (80mg/kg BW/day).

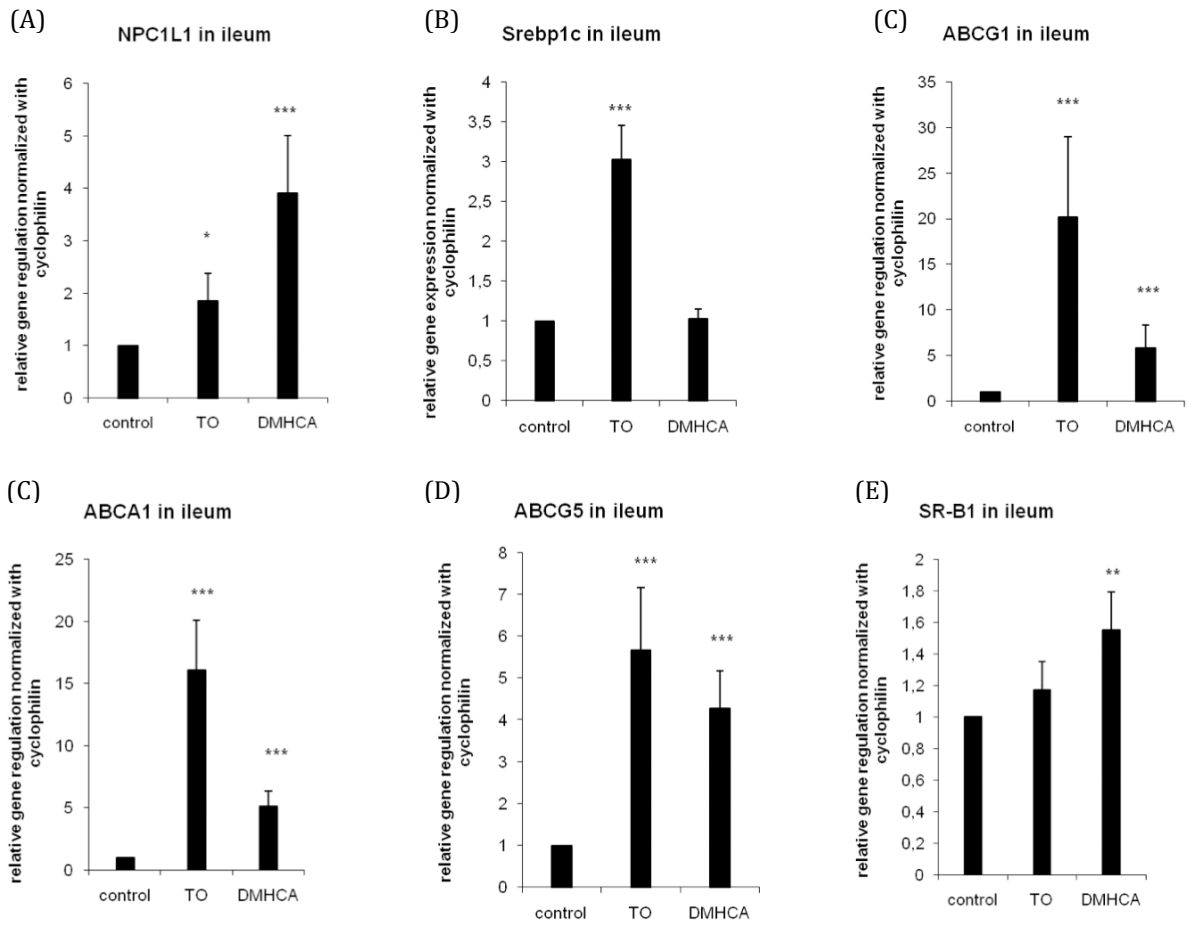

Figure 48. Gene regulation in ileum after 4d feeding of chow ± DMHCA or T0901317 (80mg/kg BW)
Real-time PCR expression ratios in ileum upon LXR agonist treatment in chow fed mice including cyclophilin A normalization were calculated by pairwise fixed reallocation test. Controls fed chow without LXR ligand were arbitrarily set to 1. Data are expressed as mean values ± SD; n = 3 performed in duplicate. $^{*}P < 0.05$; $^{**}P \leq 0.01$; $^{***}P \leq 0.001$.

It was found that 4d treatment with either LXR agonists led to an increased expression of ABCA1, ABCG1, ABCG5, and NPC1L1 in ileum (Figure 48). Whereas T0901317 highly increased SREBP1c in ileum, DMHCA did not regulate this gene (Figure 48B). Moreover, DMHCA treatment resulted in a slight but significant upregulation of SR-BI (Figure 48E).

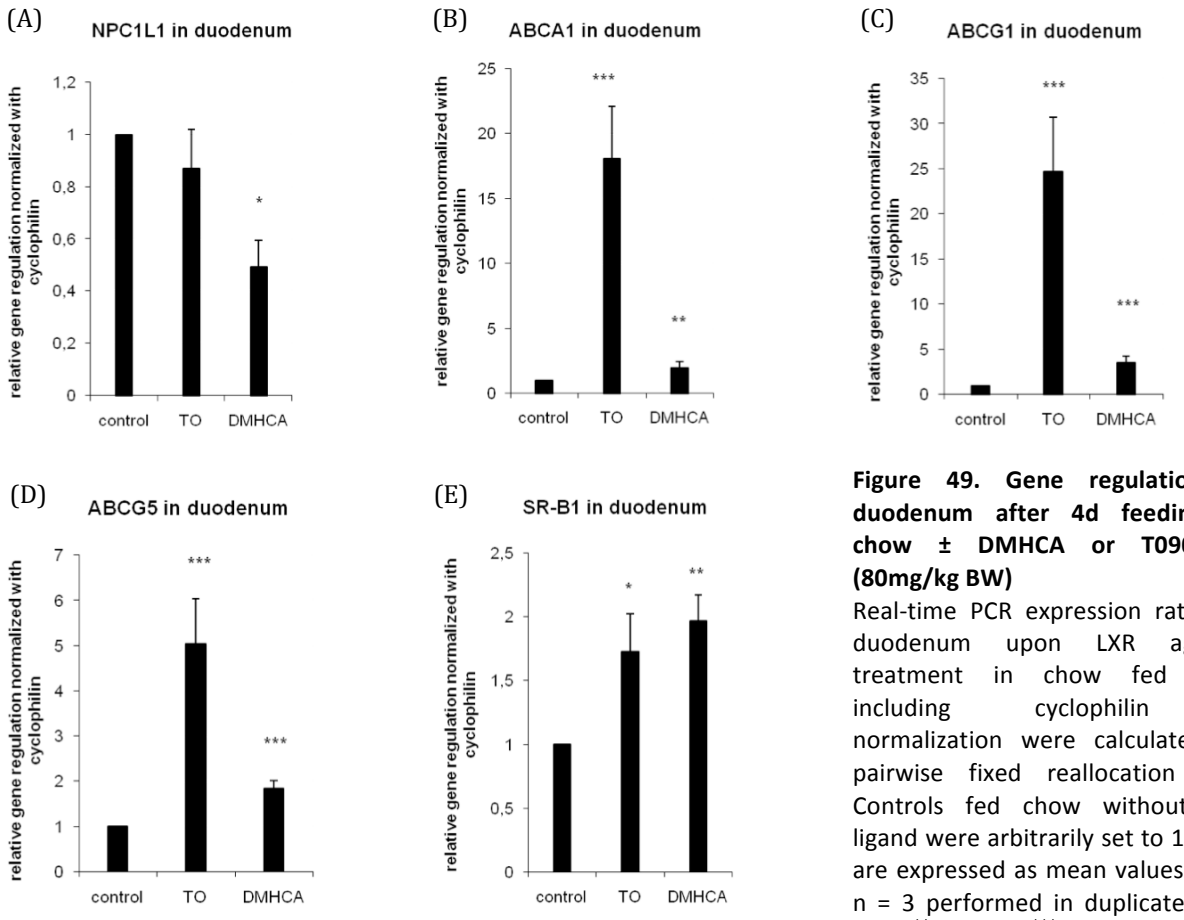

Figure 49. Gene regulation in duodenum after 4d feeding of chow ± DMHCA or T0901317 (80mg/kg BW)

Real-time PCR expression ratios in duodenum upon LXR agonist treatment in chow fed mice including cyclophilin A normalization were calculated by pairwise fixed reallocation test. Controls fed chow without LXR ligand were arbitrarily set to 1. Data are expressed as mean values ± SD; n = 3 performed in duplicate. $^{*}P < 0.05$; $^{**}P \leq 0.01$; $^{***}P \leq 0.001$.

In duodenum the ABC transporters A1, G1 and G5 were likewise upregulated with each agonist (Figure 49B-D), whereas NPC1L1 (Figure 49A) was significantly reduced upon DMHCA treatment, implying reduced cholesterol absorption. SR-BI was significantly increased with T0901317 and DMHCA compared to untreated controls (Figure 49E). Unfortunately, we do not have data for SREBP1c regulation in duodenum.

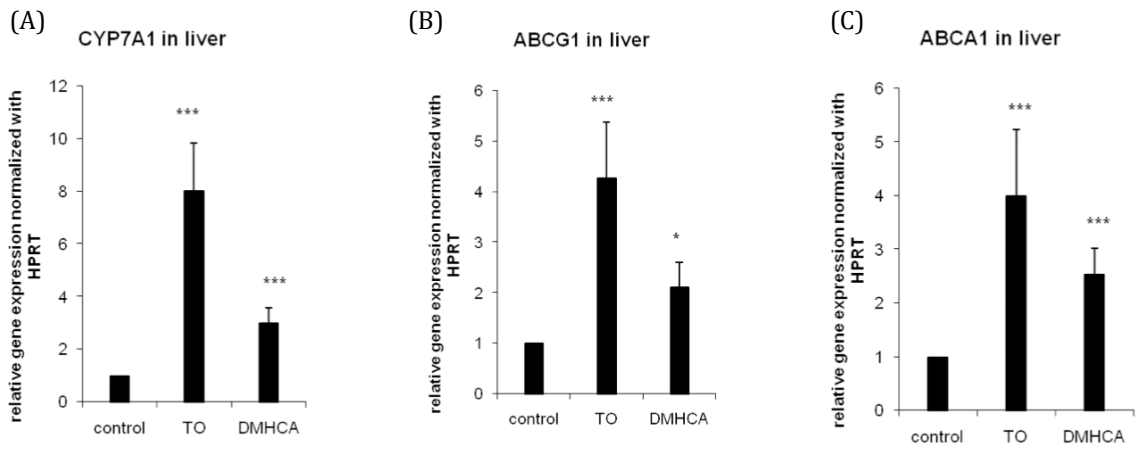

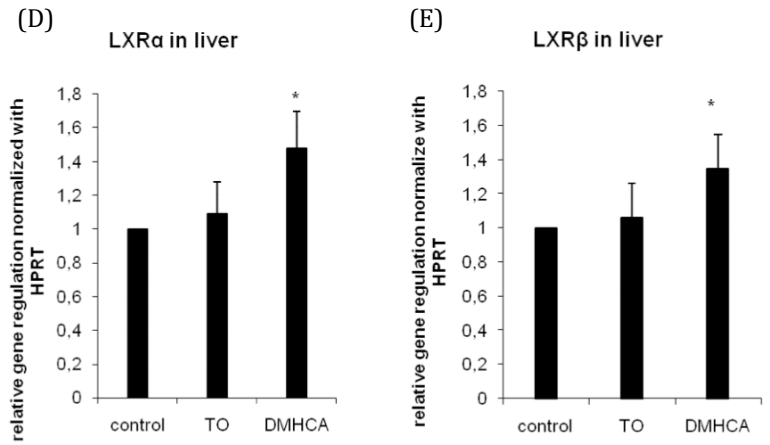

Figure 50. Gene regulation in liver after 4d acute feeding of chow ± DMHCA or T0901317 (80mg/kg BW)
Real-time PCR expression ratios in liver upon LXR agonist treatment in chow fed mice including cyclophilin A normalization were calculated by pairwise fixed reallocation test. Controls fed chow without LXR ligand were arbitrarily set to 1. Data are expressed as mean values ± SD; n = 3 performed in duplicate. $^{*}P < 0.05$; $^{***}P \leq 0.001$.

In the liver, we have already shown that T0901317 led to a marked induction of SREBP1c, whereas DMHCA only slightly induced this gene (Figure 47). CYP7A1, ABCA1, and ABCG1 were highly induced with each LXR agonist. Interestingly, DMHCA led to a slight but significant induction of both LXR isoforms (Figure 50). Furthermore, we investigated cholesterol loss by bile acid (BA) production and BA excretion into the feces. We measured total BA concentration and concentration of two different BA, deoxycholic and lithocholic acid (Figure 51) (in collaboration with G. Fauler, Clinical Institute of Medical and Laboratory Diagnostics, Medical University of Graz).

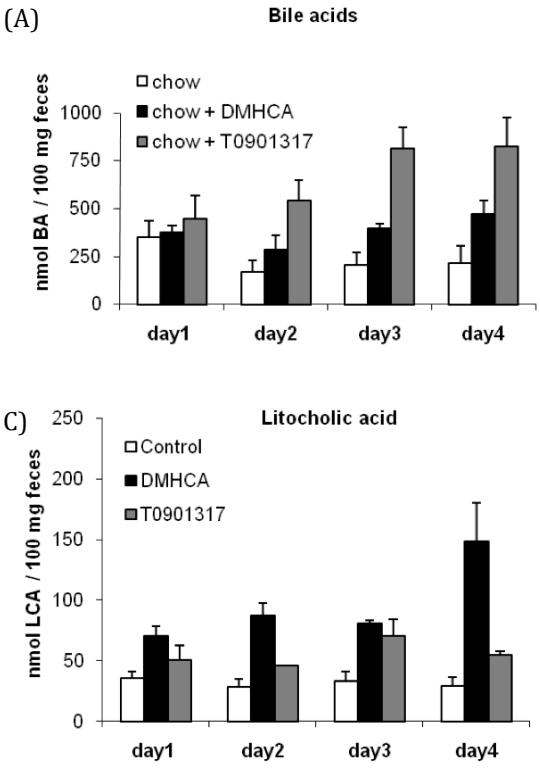

Figure 51. BA excretion during feeding of WT mice DMHCA and T0901317 for 4d
WT mice were fed 80mg DMHCA or T0901317/kg BW/day in chow diet for 4 days. Feces were collected and (A) BA content and distribution of (B) deoxycholic and (C) lithocholic acid were measured on each day.

Both LXR agonists increased BA excretion, but, starting from the second day, T0901317 did so to a greater extent than DMHCA (Figure 51A). This implies that both compounds successfully induce enzymes that are responsible for the cholesterol conversion to BA. The composition of the BA in the feces was different after the two treatments. T0901317 treated mice had a much higher content of deoxycholic acid during all four days (Figure 51B), whereas DMHCA treated mice showed higher lithocholic content, most distinctive on the fourth day (Figure 51C).

8.5.2.4 Lipid parameters, lipid composition and liver pathology 15d after DMHCA treatment of WT mice

To check whether a treatment longer than 4 days of WTD with 80mg DMHCA/kg BW/day affects lipid parameters, we fed male C57Bl/6 mice for 15 days with the same diet. Plasma TG concentrations were not significantly altered by DMHCA in both diets suggesting that a high dose of DMHCA fed for more than two weeks does not induce hypertriglyceridemia in wild type animals. Plasma TC levels were significantly reduced by 32% in mice fed chow diet + DMHCA but remained unchanged in mice fed WTD + DMHCA when compared to controls. Hepatic TC concentrations were markedly decreased on both diets by DMHCA (54% and 56%, respectively). In contrast, hepatic TG levels were not changed by DMHCA in WTD, but were significantly increased 2.4-fold by DMHCA in chow diet. Plasma aspartate aminotransferase (AST) levels were slightly but not significantly increased on chow diet + DMHCA and unaltered by DMHCA in WTD-fed animals (Table 17).

Table 17. Plasma and hepatic TG and TC concentrations of male C57Bl/6 mice fed chow or WTD ± DMHCA for 15 days.

WT mice were fed different diets containing no or 80mg/kg BW DMHCA. Data are expressed as mean ± SD values of 6-8 mice aged 8 - 12 weeks. *, $P < 0.05$; ***, $P \leq 0.001$.

	Plasma			Liver	
	TG (mg/dl)	TC (mg/dl)	AST (IU/l)	TG (mg/g tissue)	TC (mg/g tissue)
chow	62.3 ± 10.3	127 ± 16.4	30.1 ± 13.0	14.0 ± 6.4	2.16 ± 0.40
chow + DMHCA	52.6 ± 8.2	86.8 ± 15.5***	47.7 ± 13.2*	33.8 ± 14.9*	1.00 ± 0.45***
Chow + T0901317	45.8 ± 4.3**	309.3 ± 80.3***	53.7 ± 19.1*	111.2 ± 43.2***	0.49 ± 0.18***
WTD	45.6 ± 8.1	208 ± 65.9	26.7 ± 8.7	32.1 ± 12.8	4.28 ± 0.55
WTD + DMHCA	54.9 ± 10.8	217 ± 50.6	21.4 ± 7.3	35.1 ± 11.1	1.88 ± 0.44***
WTD + T0901317	39.4 ± 15.6	419.4 ± 80.7***	35.8 ± 11.9	111.1 ± 24.0***	0.5 ± 0.14***

Since we found slightly increased TG levels in DMHCA-treated livers on chow diet (2.8-fold increase), we checked the hepatic fatty acid composition in the TG fraction. Palmitate (C16:0), palmitoleate (C16:1), stearate (C18:0), oleate (C18:1), and linoleate (C18:2) were significantly increased (Figure 52A). T0901317 treatment led to a much more pronounced increase in these fatty acids. No alterations were observed in mice fed WTD plus DMHCA compared to WTD alone, whereas T0901317 led to a more significant increase in myristate (14:0), palmitate (C16:0),

spalmitoleate (C16:1), stearate (C18:0), oleate (C18:1), and arachidate (C20:0) as seen in Figure 52B.

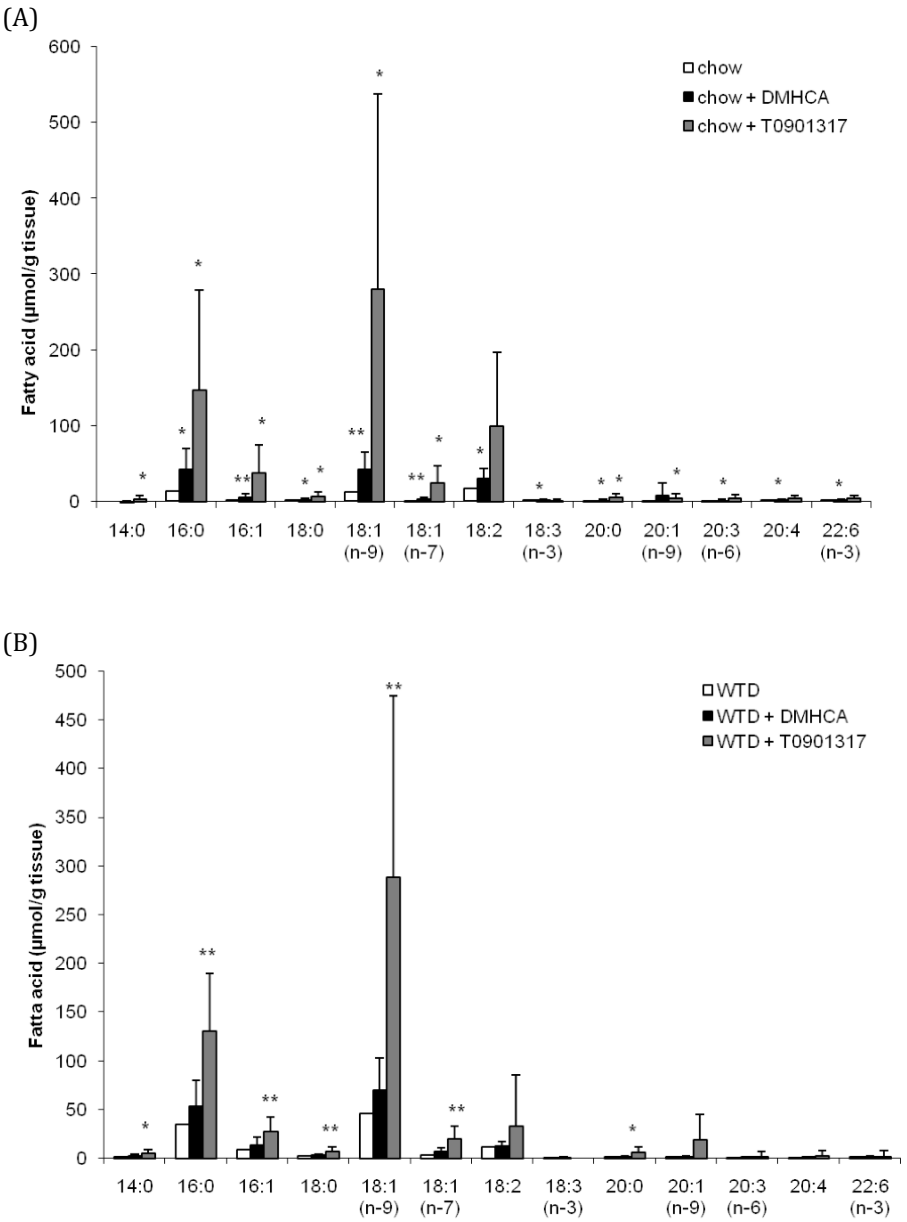

Figure 52. FA distribution in WT mice fed 15d with chow plus/minus DMHCA
C57Bl/6 mice were fed (A) chow diet or (B) WTD (containing 80 mg DMHCA/kg BW/day) for 15 days. Fatty acid (FA) composition in the livers was determined by gas chromatography after methylation using heptadecanoic acid as internal standard. Data represent mean values ± SD; n = 8. $^{*}P < 0.05$; $^{**}P \leq 0.01$

In order to prove the absence of liver steatosis on DMHCA treated mice, oil red O staining of liver sections after the treatments were performed. The lipid staining from DMHCA-treated mice revealed macroscopically no differences in lipid accumulation upon the absence or presence of DMHCA in both diets. T0901317 treatment resulted in severe steatosis with enlarged lipid droplets on both diets (Figure 53).

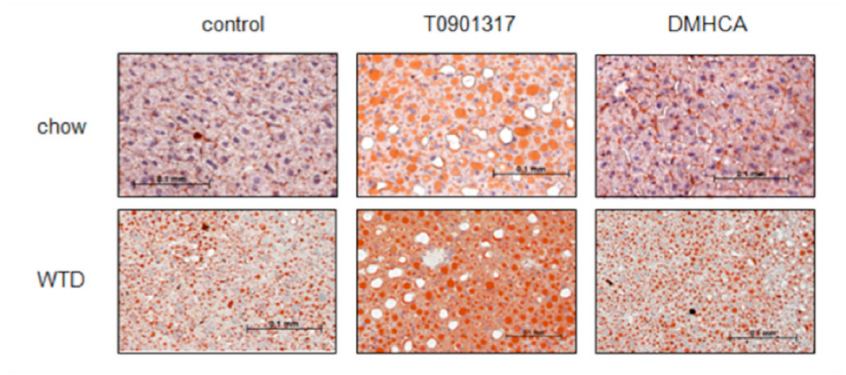

Figure 53. Oil red O staining of 8µm cryosections from the livers of male C57Bl/6 mice
This figure shows representative cryosections from livers of C57Bl/6 mice fed chow diet or WTD ± T0901317 or DMHCA (80 mg/kg BW/day) for 15 days. Liver sections were stained with oil red O and hematoxylin. The length of the bar in the images represents 100µm.

8.5.2.5 Effect of DMHCA on mRNA expression of LXR target genes in WT mice after 15d of feeding

Target mRNA expression levels in livers of C57Bl/6 mice fed chow or WTD ± T0901317 or DMHCA (80 mg/kg body weight/day) for 15 days were analyzed by real-time PCR. In chow diet, treatment with DMHCA led to a significant 2.5-fold increase of CYP7A1 mRNA expression (Figure 54A). Additionally, the expression levels of ABCA1, ABCG1, ABCG5, and ABCG8 were significantly increased by 1.9-, 2.1-, 3.5- and 2.8-fold, respectively. Hepatic SREBP1c, FAS and ChREBP mRNA quantities were unaltered upon DMHCA treatment. T0901317 in chow diet resulted in more pronounced increase of CYP7A1, ABCA1, ABCG1, and ABCG5/G8 mRNA expression compared to controls, but also enhanced SREBP1c, FAS, and ChREBP mRNA by 4.7-, 3.4-, and 1.3-fold, respectively (Figure 54A). Similar real-time PCR results were obtained when mRNA levels were determined from livers of mice fed WTD plus the LXR agonists. Both ligands significantly increased CYP7A1 and ABCG8 mRNA expression; only T0901317 resulted in an increase in ABCG1 and ABCG5 expression, whereas ABCA1 mRNA was unaltered by T0901317 and DMHCA treatment. T0901317 significantly increased SREBP1c and FAS by 3.4- and 47.3-fold, respectively, DMHCA did not alter SREBP1c mRNA expression. While FAS mRNA was significantly increased by 2.7-fold, ChREBP was even significantly decreased upon DMHCA treatment by 47% (Figure 54B).

(A)

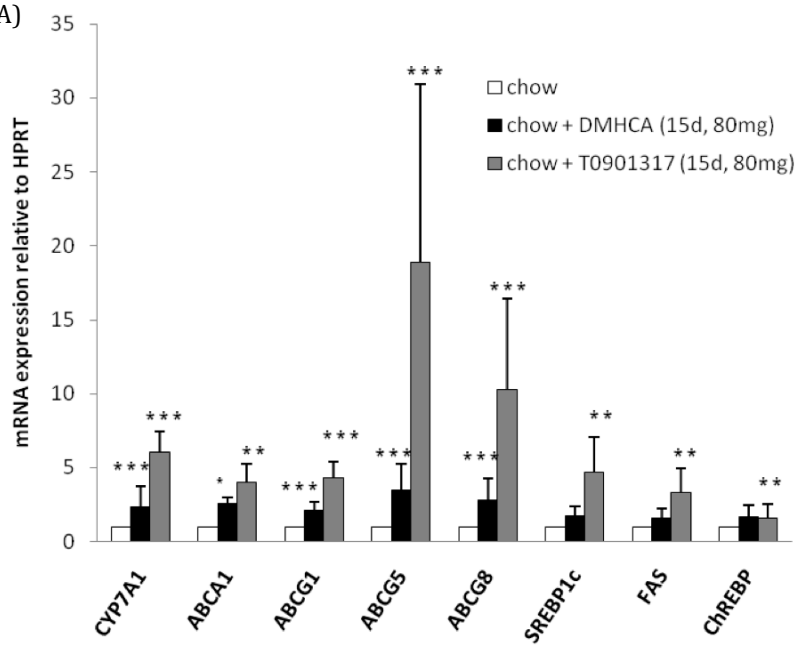

(B)

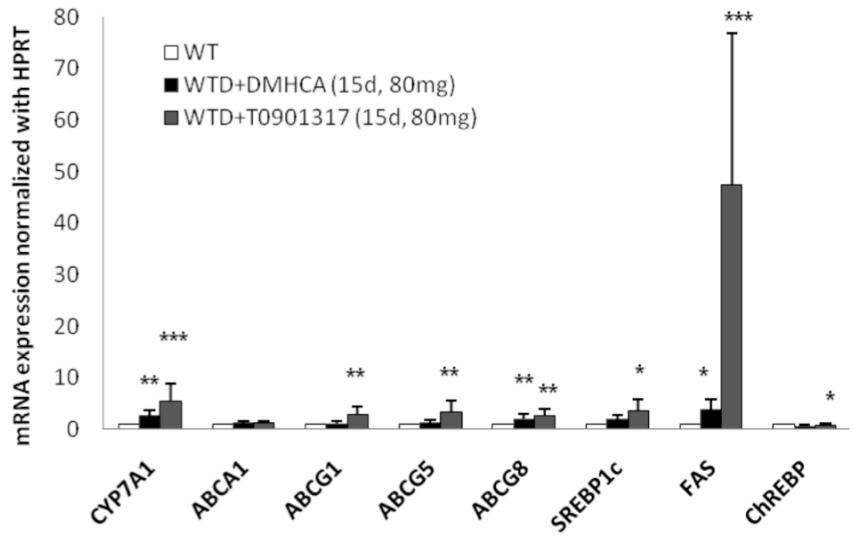

Figure 54. Liver gene analyses of C57Bl/6 mice fed chow diet or WTD ± T0901317 or DMHCA (80 mg/kg BW/day) for 15 days.
Real-time PCR expression ratios upon LXR agonist treatment in chow fed mice including HPRT normalization were calculated by pairwise fixed reallocation test. Controls fed chow or WTD without LXR ligand were arbitrarily set to 1. Data are expressed as mean values ± SD; n = 8 performed in duplicate. $^{*}P < 0.05$; $^{**}P \leq 0.01$; $^{***}P \leq 0.001$.

We also analyzed ABCA1, ABCG1, ABCG5, ABCG8, and SREBP1c mRNA levels in ileum of T0901317 and DMHCA in chow diet. All these ABC transporters and SREBP1c were significantly increased by both ligands, again the upregulation was higher by T0901317 treatment, except for ABCG8, which was similarly activated by both ligands (Figure 55).

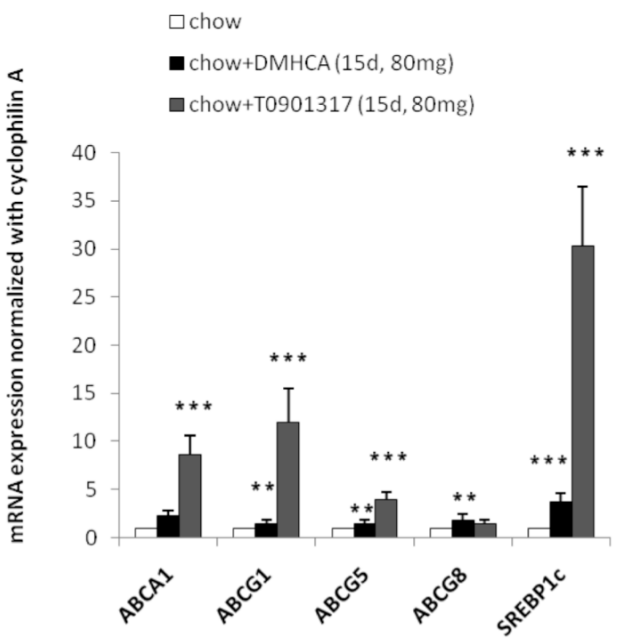

Figure 55. Effect of LXR activation on mRNA expression levels in ileum of C57Bl/6 mice.
C57Bl/6 mice were fed chow diet ± T0901317 or DMHCA (80 mg/kg BW/day) for 15 days. Real-time PCR expression ratios upon LXR agonist treatment in ileum including cyclophilin A normalization were calculated by pairwise fixed reallocation test. Controls fed chow without LXR ligand were arbitrarily set to 1. Data are expressed as mean values ± SD; n = 3. $^{*}P < 0.05$; $^{**}P \leq 0.01$ $^{***}P \leq 0.001$.

8.5.2.6 Short-term treatment of ApoE-/- mice with low and high doses of DMHCA

Next, the effects of short-term DMHCA administration on target gene expression were determined in ApoE-/- mice. Mice were fed normal chow diet (in the absence or presence of 80 mg DMHCA/kg BW/day) for 4 days or WTD (in the absence or presence of 8 mg DMHCA/kg BW/day) for 15 days. In the liver, treatment with DMHCA resulted in a significant induction of CYP7A1 mRNA expression on both diets, whereas ABCG5 and ABCG8 were significantly increased by DMHCA only in the chow diet (1.4- and 1.3-fold, respectively). ABCA1, LDLR and HMGCR mRNA were not altered upon feeding both diets. SREBP1c was found to be significantly 52% decreased upon DMHCA in the chow diet (Figure 56A and Figure 56E).

In addition, it was examined whether DMHCA had an influence on gene expression in the aortas. Administration of DMHCA to chow and WTD significantly increased ABCA1 mRNA levels in the aortas by 1.4- and 1.7-fold, respectively, whereas ABCG1 was significantly elevated by DMHCA only in chow diet by 1.9-fold (Figure 56B and Figure 56F). Additionally, ABCA1 mRNA expression in MPM was significantly increased by DMHCA upon chow and WTD feeding (1.7- and 3.1-fold, respectively) (Figure 56C and Figure 56G). In the ileum, ABCA1, ABCG1, and ABCG5 were all significantly increased upon DMHCA administration in the chow diet (2.7-, 1.9- and 1.3-fold, respectively) (Figure 56D). Whereas ABCA1 mRNA quantity was significantly 1.7-fold increased in mice fed WTD supplemented with DMHCA, no changes were observed in ABCG1 and ABCG5 mRNA levels (Figure 56H).

To summarize, all effects on mRNA expression levels were similar in ApoE-/- mice after short-term feeding of both diets with the high dose of DMHCA in chow diet resulting in higher and more significant changes.

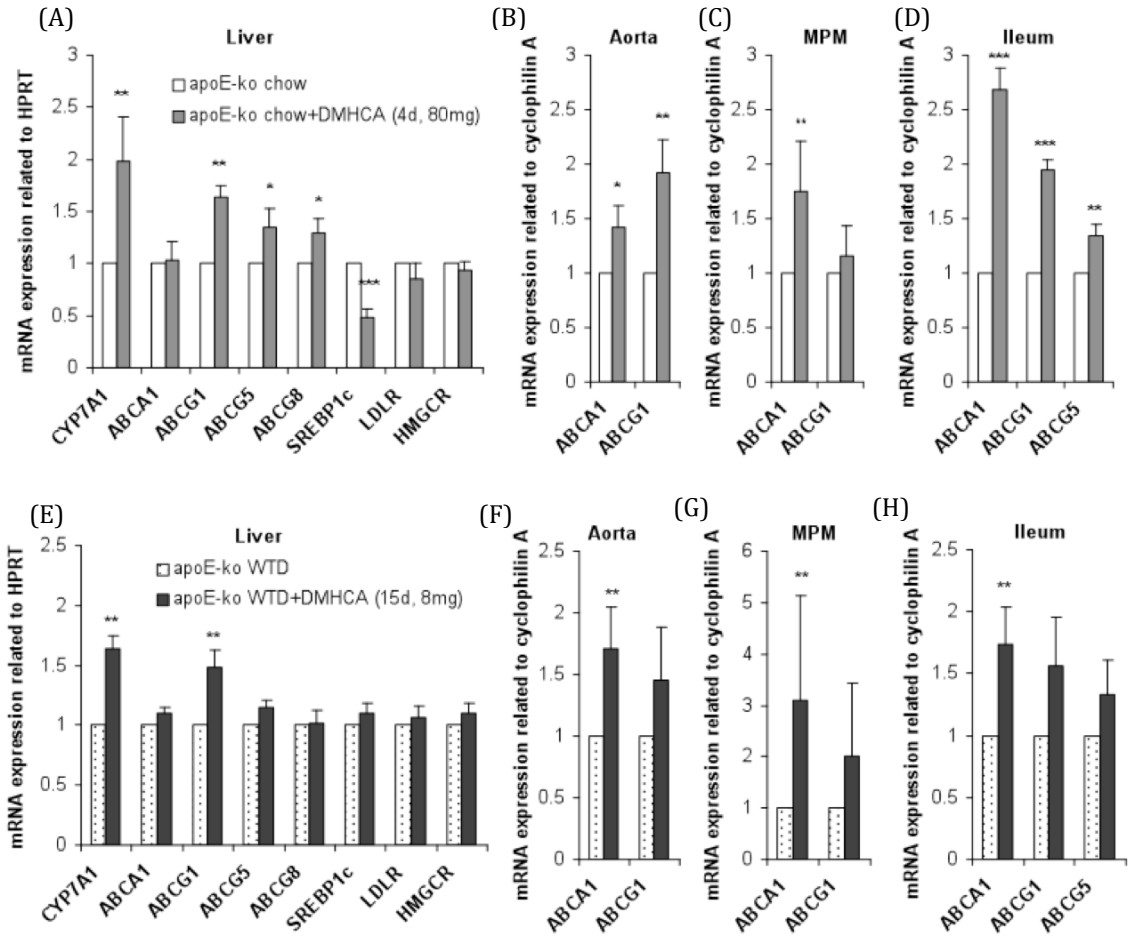

Figure 56. Regulation of LXR target mRNA levels in ApoE-/- mice by short term administration of DMHCA.
(A-D) Male mice were fed chow diet ± DMHCA (80 mg/kg body weight/day) for 4 days or (E-H) WTD ± DMHCA (8 mg/kg body weight/day) for 15 days. Real-time PCR expression ratios in (A, E) liver, (B, F) aorta, (C, G) MPM and (D, H) ileum including HPRT or cyclophilin A normalization were calculated by pairwise fixed reallocation test. Controls fed diets without DMHCA were arbitrarily set to 1. Data are expressed as mean values from 3 samples performed in triplicate ± SD. $^{*}P < 0.05$; $^{**}P \leq 0.01$; $^{***}P \leq 0.001$.

8.5.2.7 Plasma and liver lipid parameters and liver lipid composition after short-term treatment of ApoE-/- mice with DMHCA

To examine whether DMHCA treatment affects plasma and hepatic lipid parameters in ApoE-/- animals in a short-term treatment, male mice were fed chow ± 80 mg DMHCA/kg body weight/day for 4 days. In addition, we wanted to check whether WTD fed for 15 days ± 8 mg DMHCA/kg BW/day has an effect on lipid parameters. We found that plasma TG and TC concentrations were not significantly changed upon DMHCA treatment on both diets. Additionally, plasma AST levels were similar in all animals (Table 18).

Table 18. Plasma and hepatic TG and TC concentrations of overnight fasted male ApoE-/- mice
The mice were fed chow diet ± DMHCA (80 mg/kg body weight/day) for 4 days or WTD ± DMHCA (8 mg/kg body weight/day) for 15 days. Data are expressed as mean ± SD values of 6 animals. ***, $P \leq 0.01$.

	Plasma			Liver	
	TG (mg/dl)	TC (mg/dl)	AST (U/l)	TG (mg/g)	TC (mg/g)
chow	103 ± 35	567 ± 111	30.9 ± 11.1	39.3 ± 8.2	2.5 ± 0.43
chow+DMHCA (4d, 80 mg)	121 ± 21	531 ± 19	29.4 ± 14.3	18.1 ± 6.1***	2.0 ± 0.45
WTD	187 ± 67	1110 ± 285	38.1 ± 20.5	32.6 ± 6.4	7.5 ± 2.2
WTD+DMHCA (15d, 8 mg)	205 ± 61	1038 ± 203	29.2 ± 15.6	34.6 ± 10.1	5.5 ± 0.64

In the liver, TG were significantly decreased by chow diet plus DMHCA, whereas in WTD no difference was observed with DMHCA addition. Furthermore, the hepatic fatty acid composition in the TG fraction especially oleate (C18:1), palmitate (C16:0), linoleate (C18:2), and α-linolenic acid (C18:3) were significantly decreased (Figure 57A). In contrast, no significant alterations in the hepatic fatty acid composition were observed in mice fed WTD plus DMHCA compared to WTD alone (Figure 57B).

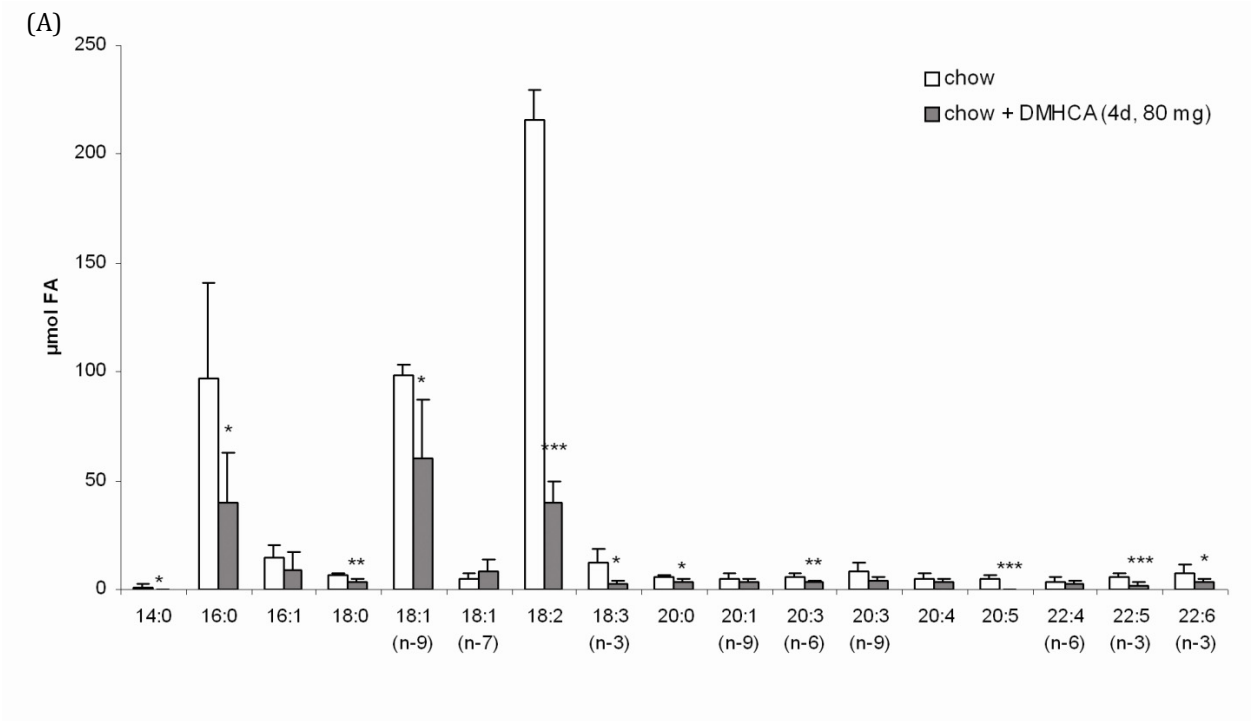

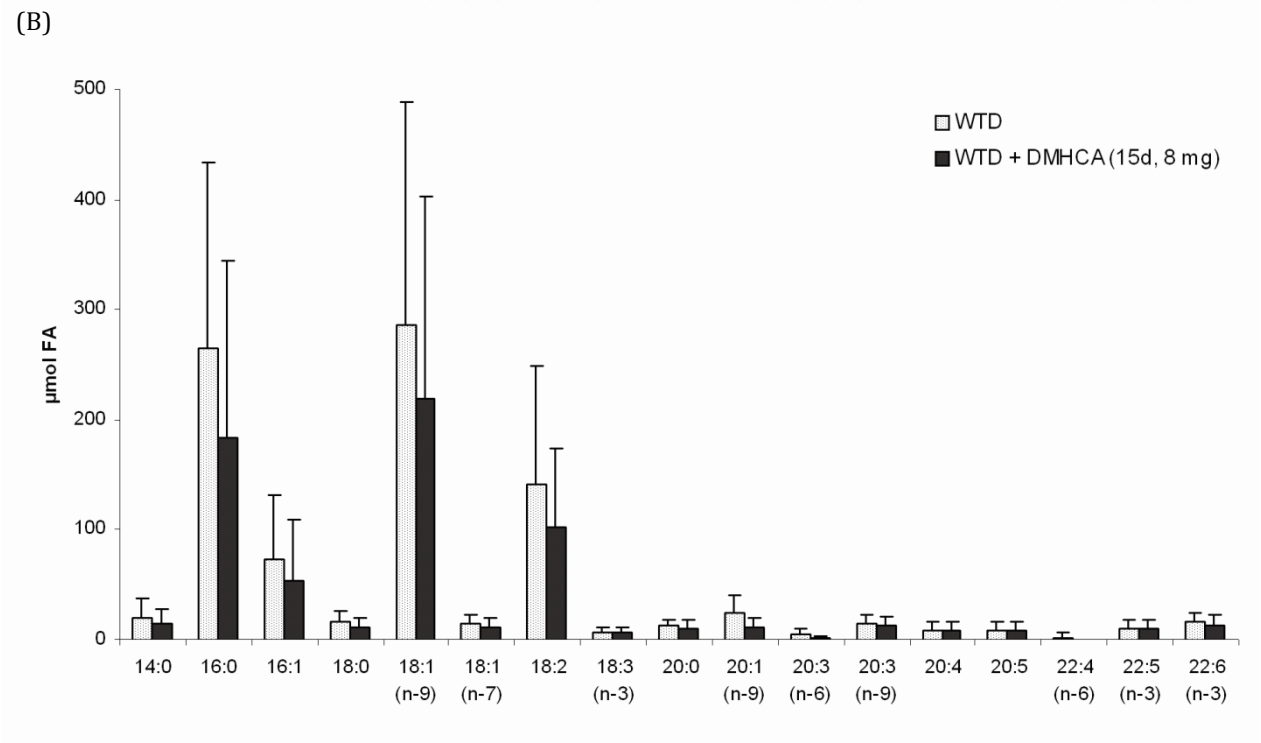

Figure 57. Effect of DMHCA on hepatic FA composition in ApoE-/- mice.
Male ApoE-/- mice were fed (A) chow diet ± DMHCA (80 mg/kg BW/day) for 4 days or (B) WTD ± DMHCA (8 mg/kg BW/day) for 15 days. FA composition in the livers was determined by gas chromatography after methylation using heptadecanoic acid as internal standard. Data represent the mean values ± SD; n = 8. $^{*}P < 0.05$; $^{**}P \leq 0.01$; $^{***}P \leq 0.001$.

8.6 Bioavailability of DMHCA

To determine bioavailability of DMHCA, we measured DMHCA concentrations in the plasma and various tissues (in collaboration with Rajendra S. Kadam and Uday Kompella, University of Colorado, Denver). Yet, only the high concentrations (80mg/kg BW) led to the detection of DMHCA in the plasma, whith values between 1 and 27ng/mL after 15d feeding chow diet plus DMHCA and between 2 and 7ng/mL after 15d feeding WTD plus DMHCA. Furthermore, we evaluated the distribution of DMHCA within the body and tissues after acute feeding of DMHCA. Mice were conditioned to eat their daily intake within one hour by fasting them overnight before feeding. They were given 5mg DMHCA/g food and ate about half gram in one hour. Thus, the average DMHCA intake was 2.5mg DMHCA/mouse. The food was removed after one hour and blood was taken before feeding and 1h, 2h, 4h, and 8h after feeding. After 8h mice were fed again overnight with 2.5mg DMHCA/g food. Thereafter (24h time point) all tissues, urine and plasma samples were taken and DMHCA concentrations were analyzed as µg DMHCA per gram tissue weight. DMHCA is highly lipophilic and therefore this drug is efficiently taken up by many tissues. DMHCA concentrations in plasma were highest 2h and 4h after the food was given to the mice (Figure 58).

Tissue distribution of DMHCA is shown in (Figure 59). Orally administered DMHCA is excreted to a high extent into feces and very little amount is excreted into urine.

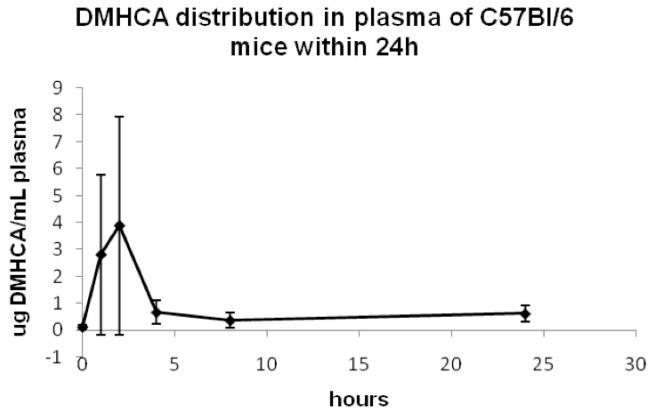

Figure 58. DMHCA distribution in plasma of C57Bl/6 mice within 24h
Mice were given food for 1h, which contained 5mg DMHCA/g food and were fasted thereafter for 8h. Mice ate about half gram in this hour, so the average DMHCA intake was about 2,3mg. After 8hrs fasting food was given back to the mice in a concentration of 2,5mg DMHCA/g food. Blood was taken after 0, 1, 2, 4, 8, and 24h. DMHCA distribution in the plasma was highest after 2 and 4hr. For each time point 3 mice were used for taking blood, except for the 0 and 24h time point, where all 6 mice were used.

As already mentioned above, most DMHCA is excreted with the feces and very little via the urine (Figure 59). We found accumulation of DMHCA in the small intestine, especially in the ileum, but also in the lung, kidney and heart. The abundance in the liver is quite low in the way the distribution is presented here (μg DMHCA/g tissue), but the abundance of liver in the body is much higher as for example the duodenum. A liver weighs about 1g (giving a total amount of DMHCA of 0.5μg) and a duodenum weighs about 0.15g, which is about 1/6th of a liver. A whole duodenum contained about 0.7μg of DMHCA. It is important to state that there was no DMHCA present in the brain, which is important because we found that DMHCA blocks DHCR24, which leads to accumulation of desmosterol, the precursor of cholesterol (T. Pfeifer et al., unpublished).

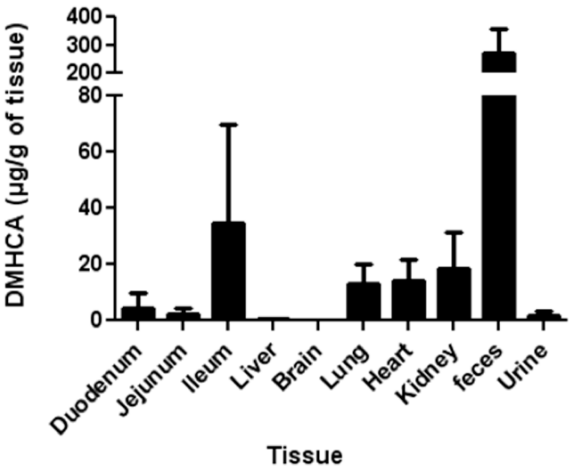

Figure 59. Tissue distribution of DMHCA within 24h
Mice were given food for 1h that contained 5mg DMHCA/g food and were fasted thereafter for 8h. Mice ate about half gram in this hour, so the average total DMHCA intake was about 2.3mg/mouse. After 8hrs fasting food was given back to the mice in a concentration of 2,5mg DMHCA/g food. After 24h mice were euthanized, blood was taken via the vena cava and all relevant tissues isolated from the animals.

With these data we were able to prove that DMHCA is bioavailable in the whole body, since it was detectable in all tissues (except the brain) as well as the plasma.

8.7 Impacts of DMHCA on atherosclerosis and cholesterol metabolism

After investigating the in vitro and in vivo effects of DMHCA we decided to study the impact of this LXR agonist on atherosclerosis. In these studies two atherosclerotic mouse models, the ApoE-/- and LDLR-/- mice, were used.

8.7.1 Chronic treatment with DMHCA

Male and female ApoE-/- and LDLR-/- mice were fed WTD with or without DMHCA (8 mg/kg body weight/day) for 11 weeks. The effect of DMHCA on body weight and lipid parameters was investigated in both mouse models at regular intervals during the long-term treatment.

8.7.1.1 Effect of DMHCA on plasma and liver lipid parameters and body weight

In ApoE-/- the food intake was similar in the different groups. Nevertheless, both male and female mice fed WTD + DMHCA showed slightly decreased body weight gain when compared to mice fed WTD without DMHCA, which reached significance in female mice after 8 weeks of treatment (Figure 60A and B). Plasma TC and TG levels were determined biweekly in the fed state. While no significant differences were observed in plasma TC (Figure 60C) and TG (Figure 60E) concentrations in male mice, female mice showed a significant decrease in both TC (Figure 60D) and TG (Figure 60F) levels.

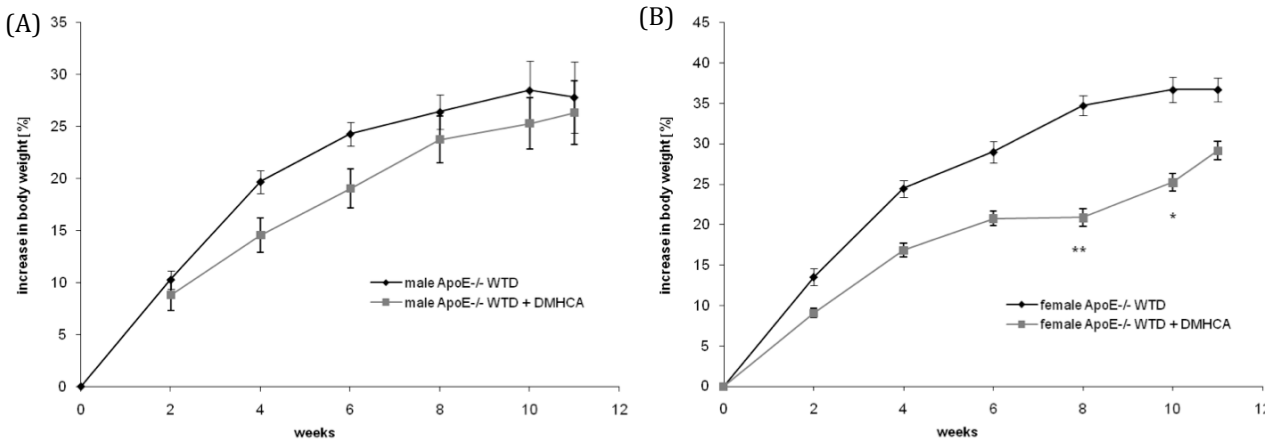

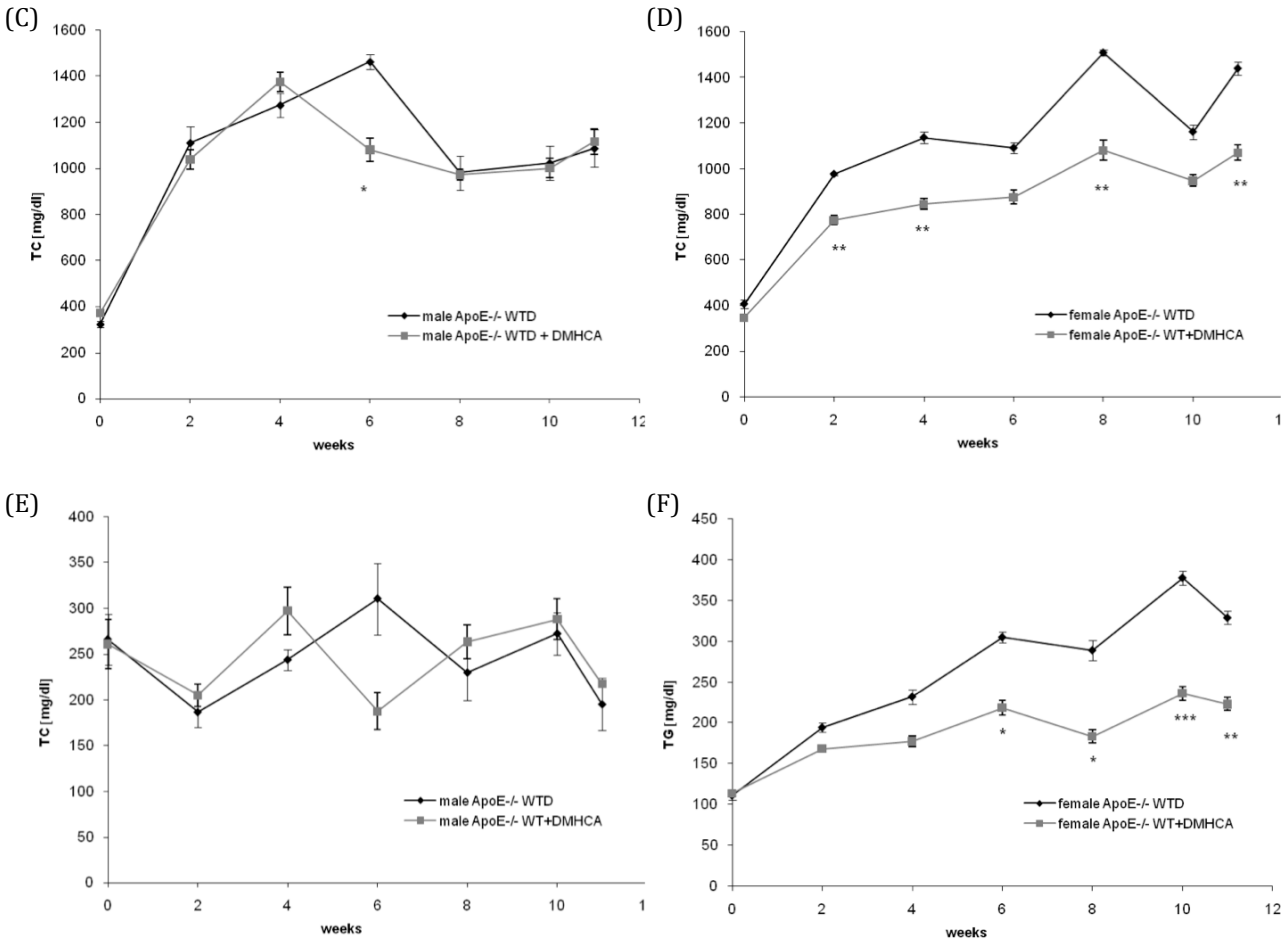

Figure 60. BW increase, TG and TC concentrations in ApoE-/- mice (male and female) during 11 weeks feeding
Body weight and plasma TG and TC concentrations of male and female ApoE-/- mice. Male (n=5) and female (n=7) ApoE-/- mice were fed WTD ± DMHCA (8 mg/kg body weight/day) for 11 weeks. (A, B) Body weight, (C, D) plasma TC and (E, F) TG concentrations in the fed state were determined at 0, 2, 4, 6, 8, 10, and 11 weeks. Data are expressed as mean values ± SEM. $^{*}P < 0.05$; $^{**}P \leq 0.01$; $^{***}P \leq 0.001$.

The changes in plasma lipid levels were similar when mice were fasted for 16h overnight before blood was taken. I found reduced plasma TG levels in male (140 ± 10 mg/dl) and female (163 ± 9 mg/dl) ApoE-/- mice compared to mice fed WTD alone (197 ± 26 and 220 ± 5 mg/dl, respectively), whereas TC concentrations were significantly decreased only in male (799 ± 65 mg/dl versus 1131 ± 52 mg/dl) but not in female animals (587 ± 33 mg/dl versus 638 ± 16 mg/dl, respectively). No significant changes were found in HDL cholesterol levels. Determination of plasma AST or ALT levels did not give reliable results due to lipemic samples. Therefore, I determined bilirubin concentrations and found that they were comparable upon all diets. Therefore, long-term treatment did not lead to liver damage in ApoE-/- mice. Additionally, hepatic TG concentrations were unaltered in both male (15.6 ± 0.1 mg/g) and female (12.7 ± 0.7 mg/g) DMHCA-treated animals compared to control males (16.6 ± 2.8 mg/g) and females (13.2 ± 0.3 mg/g) (Table 19).

Table 19. Lipid parameters of long-term fed ApoE-/- mice

Plasma and hepatic TG and TC concentrations of overnight fasted male and female ApoE-/- mice fed WTD ± DMHCA (8 mg/kg body weight/day) for 11 weeks. Data are expressed as mean values ± SD of 4 animals. *, P < 0.05; **, P ≤ 0.01

	Plasma (mg/dl)				Liver (mg/g)	
Male ApoE-ko	TG	TC	HDL-C	Bilirubin	TG	TC
WTD	197 ± 26	1131 ± 52	13 ± 0.41	2.7 ± 1.4	16.6 ± 2.8	9.5 ± 2.5
WTD+DMHCA	140 ± 10*	799 ± 65*	21 ± 3.0	2.4 ± 1.2	15.6 ± 0.1	7.6 ± 1.5
Female ApoE-ko						
WTD	220 ± 5	638 ± 16	33 ± 0.71	2.6 ± 1.1	13.2 ± 0.3	9.3 ± 1.1
WTD+DMHCA	163 ± 9**	587 ± 33	34 ± 0.78	2.2 ± 1.4	12.7 ± 0.7	8.1 ± 0.4

Since the TG were significantly lower in the DMHCA group of female mice, we performed FPLC separation of plasma lipoproteins from fasted female animals. TG content of the VLDL fraction was 55% decreased after DMHCA treatment (Figure 61A), and the TC content was decreased by 29% (Figure 61B).

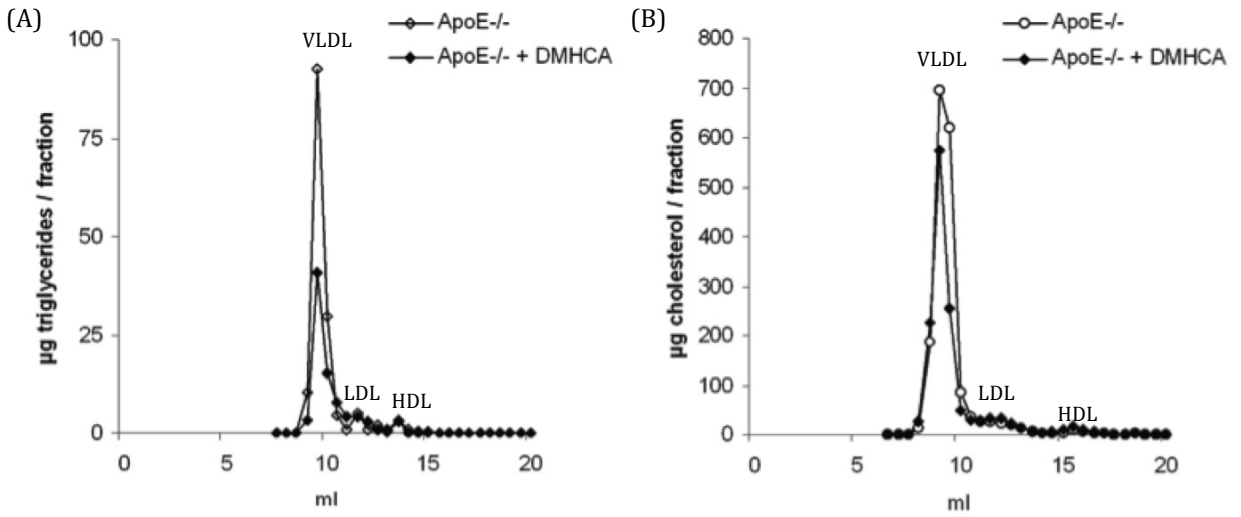

Figure 61. FPLC profile of female ApoE-/- mice

Effect of DMHCA on distribution of triglycerides and total cholesterol in plasma lipoprotein fractions of ApoE-/- mice. Lipoprotein profile of plasma pools of 5 fasted female apoE-deficient mice fed WTD ± DMHCA (8 mg/kg body weight/day) for 11 weeks. Plasma lipoproteins were separated by fast protein liquid chromatography. (A) TG and (B) TC concentrations in each fraction were measured enzymatically.

8.7.1.2 DMHCA reduces plaque formation in ApoE-/- mice

To examine the impact of DMHCA on atherogenesis in ApoE-/- mice, atherosclerotic lesions were evaluated by aortic valve section and *en face* analyses after 11 weeks on WTD in the absence or presence of DMHCA (Figure 62). Mice receiving 8 mg DMHCA/kg body weight/day showed a decrease in average lesion area compared to controls by both *en face* and aortic valve section analysis.

Immunohistochemical staining of macrophages in the aortic valves with a macrophage-specific anti-MOMA-2 antibody and oil red O staining of lipids demonstrated that lipids co-localize with macrophages and are more abundant in control ApoE-/- mice (Figure 62).

Quantification of lipid stained lesions in the *en face* prepared aortas (according to a software algorithm which is described in the materials part) unfolded a significant 20% reduction in lesion formation in the male DMHCA-fed ApoE-/- mice. The number of mice per group taken for the calculation was 3.

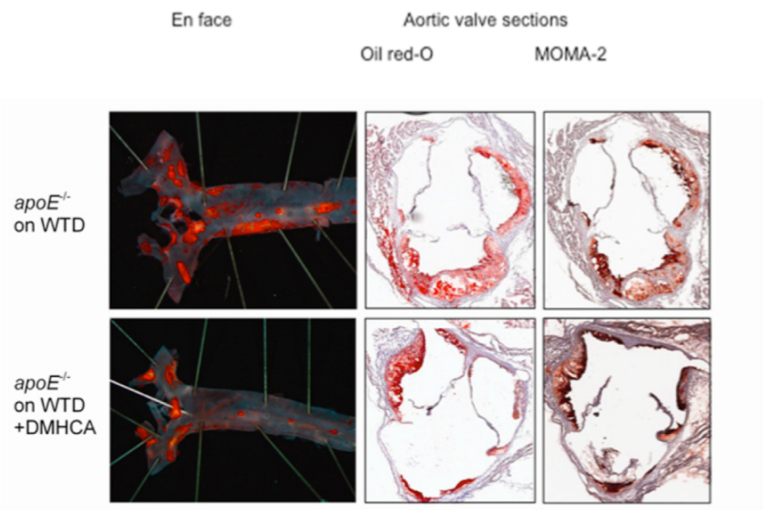

Figure 62. En face preparation and aortic root sections ApoE-/- mice
En face and aortic root section analysis of atherosclerosis in male apoE-/- mice fed WTD ± DMHCA (8 mg/kg body weight/day) for 11 weeks. Representative staining of aorta and aortic valves with Oil Red O and MOMA-2 antibody.

We also saw nearly the same percentage in plaque reduction in the female study groups (22%, number of mice per group was 4), but the variability was too high, thus giving no significance. Thus, we evaluated the plaque zones with a different method (Photoshop) and combined the two methods. The combination of the received values showed a significant reduction in lesion area of both male and female ApoE-/- mice of the DMHCA treatment groups compared to controls (27.7% and 29.5%, respectively) (Figure 63).

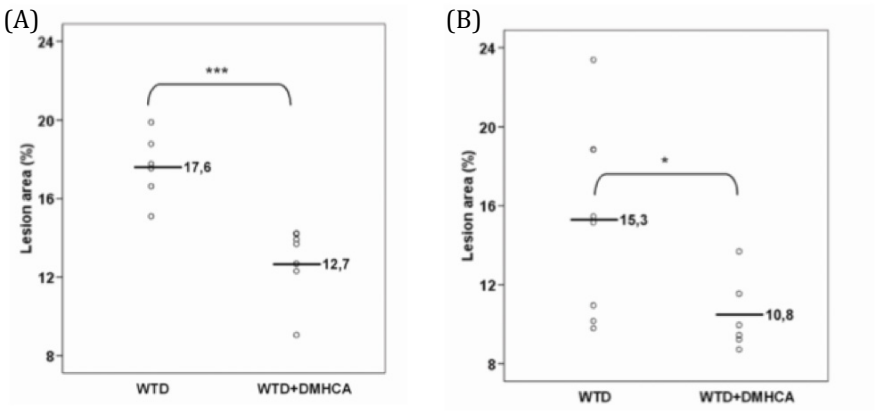

Figure 63. Box blot evaluation of en face staining
Box plot graphics of en face analysis of (A) male (n=6) and (B) female (n=7) ApoE-deficient mice. Both evaluations (Photoshop and specific software algorithm) were combined in this graphics. *, P < 0.05; ***, P ≤0.001

We also quantified the aortic valve sections of those animals. They showed a significant 48% and 54% decrease in lesion area in female and male ApoE-/- mice of the DMHCA treated groups (n=3, respectively) compared to controls. The decrease in lesion area became highly significantly (52%) when both sexes were analyzed together (n=6). Taking more mice for the evaluation of the valve sections the treatment with DMHCA resulted in a significant 45.9% and 48.4% decrease in lesion area in male (n=6) and female (n=7) apoE-deficient mice when compared to controls.

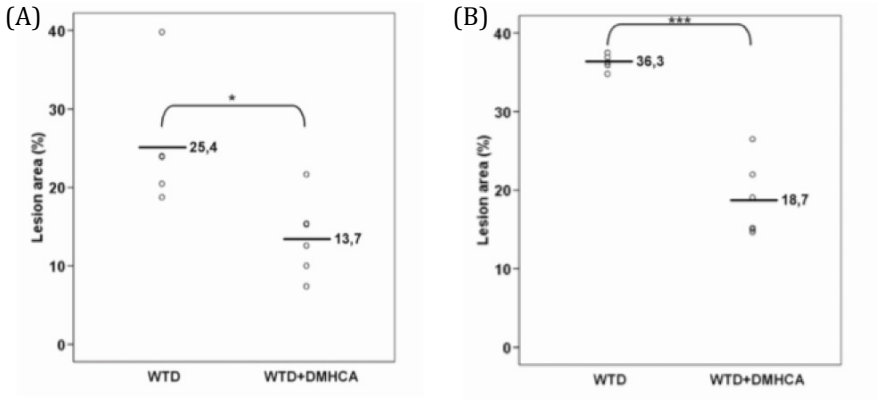

Figure 64. Box blot evaluation of aortic root sections
Box plot graphics of aortic valves analysis of (A) male (n=6) and (B) female (n=6) ApoE-/- mice using Photoshop. *, P < 0.05; ***, P ≤0.001

8.7.1.3 DMHCA and its impacts on LDLR-/- mice

We also studied the influence of DMHCA on LDLR-/- mice. Both male (Figure 65A) and female (Figure 65B) mice showed slightly less body weight gain when DMHCA was added to the WTD compared with the controls. Plasma TC (Figure 65C, D) and TG (Figure 65E, F) concentrations were also lower in the DMHCA groups of both sexes. The female group (Figure 65D, F) showed significant differences at some time points.

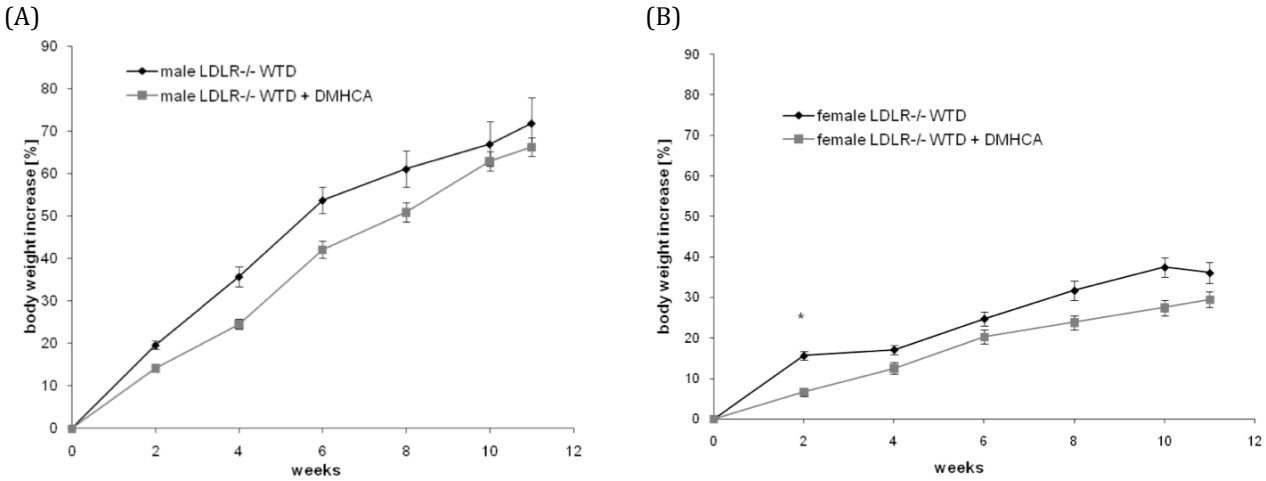

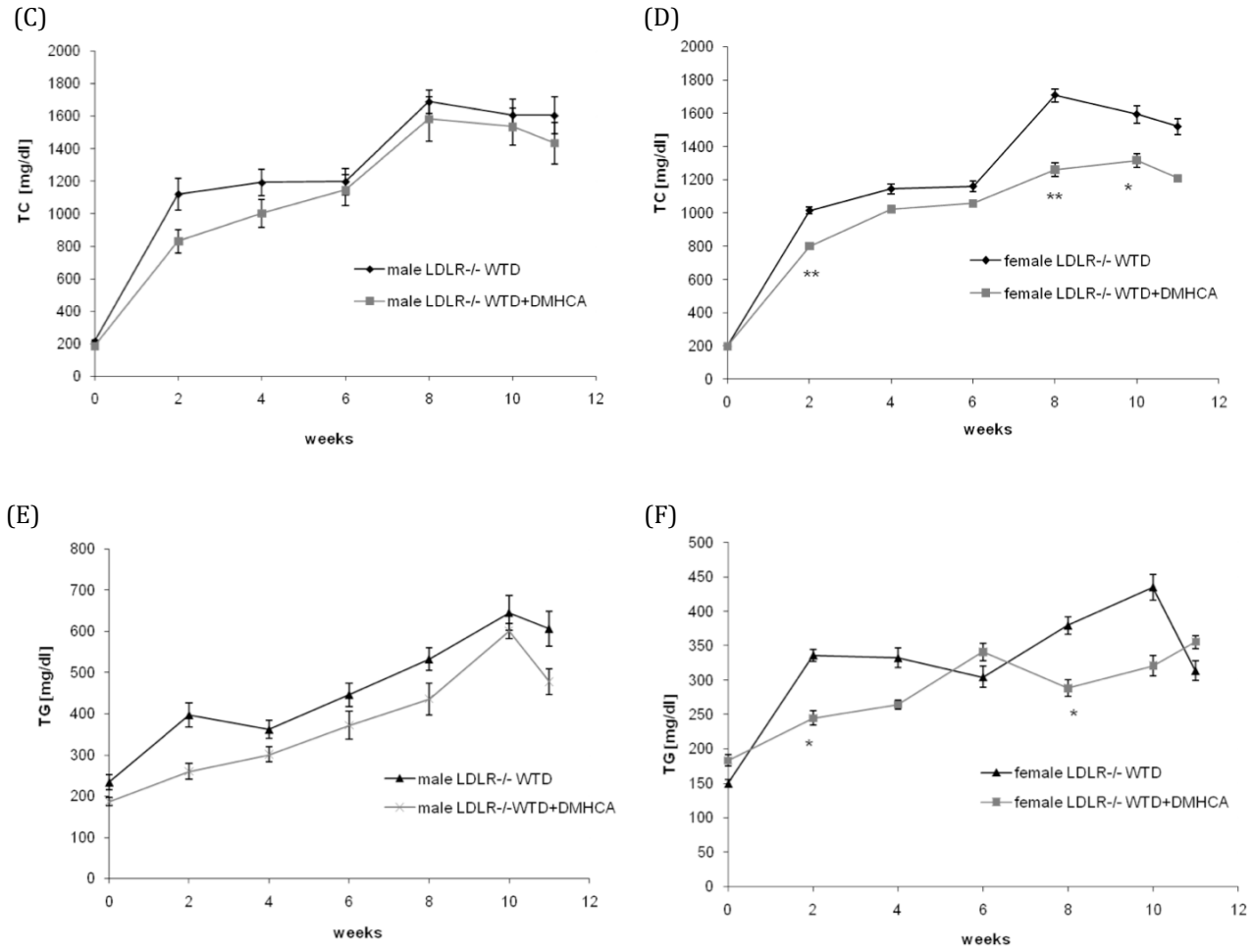

Figure 65. Body weight increase, TC and TG concentrations in male and female LDLR-/- mice during 11 weeks feeding

Male (n=5) and female (n=5) LDLR-/- mice were fed WTD ± DMHCA (8 mg/kg body weight/day) for 11 weeks. (A, B) Body weight, (C, D) plasma TC and (E, F) TG concentrations in the fed state were determined at 0, 2, 4, 6, 8, 10, and 11 weeks. Data are expressed as mean values ± SD. $^{*}P < 0.05$; $^{**}P \leq 0.01$.

After fasting the animals overnight for 16h the trend was the same. Both male and female mice had less plasma TG and TC levels although they did not reach significance. Yet, in the male mice the HDL-C was significantly higher in the DMHCA treated mice compared with the control. In the liver there was no significant difference neither in TG nor TC levels (Table 20).

Table 20 Lipid parameters of long-term fed LDLR-/- mice

Plasma and hepatic TG and TC concentrations of overnight fasted male and female LDLR-/- mice fed WTD ± DMHCA (8mg/kg body weight/day) for 11 weeks. Data are expressed as mean ± SD values of 3 animals. *, P < 0.05

	Plasma (mg/dl)			Liver (mg/g)	
Male ApoE-/-	TG	TC	HDL-C	TG	TC
WTD	345 ± 68	1350 ± 97	82 ± 4	387 ± 37	507 ± 130
WTD+DMHCA	285 ± 85	1247 ± 156	98 ± 1*	431 ± 4	397 ± 90
Female ApoE-/-					
WTD	218 ± 19	1181 ± 301	59 ± 7	470 ± 175	472 ± 46
WTD+DMHCA	135 ± 77	1010 ± 114	61 ± 5	369 ± 104	508 ± 63

Evaluating the aortas of the LDLR-/- mice showed no significant differences in plaque development. Applying a software algorithm (programmed with Interactive Data language) showed a plaque reduction of 3% in the male mice after DMHCA addition into the food, but did not reach significance. However, measuring the difference in female LDLR-/- mice we could not detect a decrease, but even an increase of 15%. If we evaluate the aortas with the Photoshop method we get contradictory results. DMHCA showed no decrease in plaque formation in the male mice here, but even led to an increase of 9% (yet not significantly) and the female mice showed a decrease of 5%, but also not significantly. One of the reasons for these contradictory results might be the low amount of animals (3 per group) and the high variability within the animals. Another reason might be that the feeding period for those mice was too long and the differences in plaques diminished after the long-term feeding. Unfortunately, the aortic valve evaluations are not useful either since we had too little usable valve sections of these mice. Therefore, further experiments were focussed on the ApoE-/- mice.

8.7.1.4 Effect of DMHCA administration on LXR target gene expression in ApoE-/- mice

To elucidate the long-term effect of DMHCA administration on gene expression levels in ApoE-/- mice after 11 weeks on WTD ± DMHCA, gene expression levels in liver, peritoneal macrophages (MPM) and small intestine were analyzed by real-time PCR. In the liver, ABCG1 and CYP7A1 mRNA expression levels were significantly increased by 2.3- and 2.8-fold, respectively, whereas ABCA1, ABCG5, and ABCG8 mRNA expression remained unchanged (Figure 66A). Importantly, hepatic SREBP1c, FAS, and ChREBP mRNA expressions were not upregulated upon DMHCA treatment. These results together with unchanged hepatic TG concentrations corroborate our data that chronic DMHCA administration does not induce liver steatosis.

In MPM, mRNA expression of SREBP1c was slightly but significantly reduced by 13%, whereas LDLR and ACC were markedly decreased by 34% and 24%, respectively. No significant differences were observed in ABCA1 and ABCG1 mRNA levels (Figure 66 B). In the ileum, ABCA1, ABCG1 and ABCG5 mRNAs remained unchanged upon DMHCA administration (Figure 66 C), whereas SREBP1c was significantly decreased by 53%.

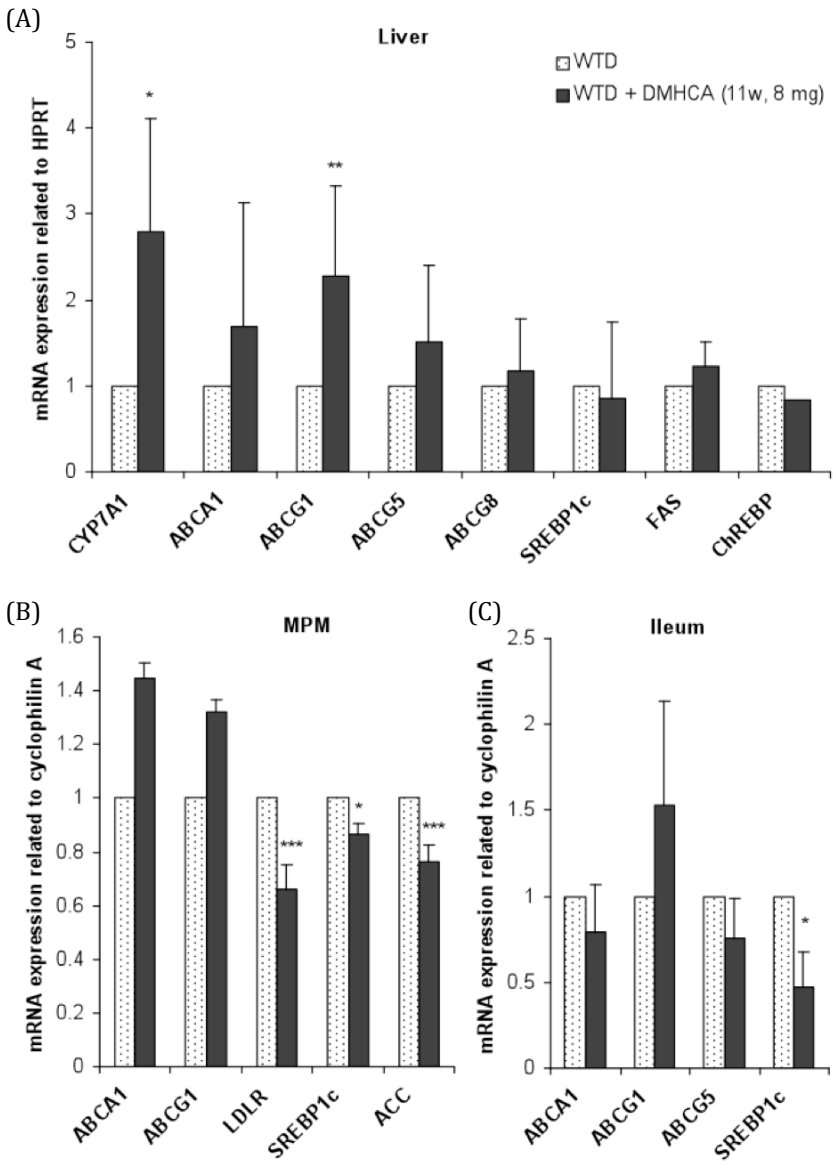

Figure 66. Regulation of LXR target genes on mRNA level after chronic administration of DMHCA to ApoE-/- mice. ApoE-/- mice were fed WTD ± DMHCA (8 mg/kg body weight/day) for 11 weeks. Real-time PCR expression ratios in (A) liver, (B) MPM and (C) ileum including HPRT or cyclophilin A normalization were calculated by pairwise fixed reallocation test. Controls fed WTD were arbitrarily set to 1. Data are expressed as mean values ± SD; n=3 performed in triplicate. $^{*}P < 0.05$; $^{**}P \leq 0.01$; $^{***}P \leq 0.001$.

8.8 Non-invasive microscopy techniques: alternative to conventional staining techniques?

Chronic kidney disease (CKD) is a fatal disease that is related to cardiovascular events. Patients suffering from CKD die more often from cardiovascular events than from renal failure, but the cause for excessive cardivasular mortality in CKD is not known so far (42). Hyperphosphatemia is known to increase vascular calcification and has been determined to be a cardiovascular risk factor in CKD. Kidney injury imbalances a normal phosphor (Pi) pool in the body because Pi excretion is restricted leading to hyperphosphatemia. The skeleton has a reservoir function for excess Pi, which is lost in CKD and results in Pi accumulation in soft tissues such as the vasculature, leading to vascular calcification (40).

We worked with ApoE-/- mice after whole and partly kidney ablation to simulate CKD. Either one kidney was removed (uninephrectomized) or one kidney and 2/3 of the second kidney were eliminated (5/6 nephrectomized). This was performed at Jackson laboratory according to Gagnon et al (209). In this project, we compared traditional staining for lipid accumulation and vascular calcification with non-invasive microscopy techniques. A summary of the so far gained results is described in this part of the thesis

We divided male ApoE-/- mice in 3 different groups: 1) sham-operated control mice, having 2 kidneys, 2) uninephrectomized mice, one kidney removed, and 3) 5/6 nephrectomized, one kidney and 2/3 of the other kidney removed. These groups were fed with either Ca^{2+} and Mg^{2+} adjusted WTD or control diet for 12-30 weeks. Ca^{2+} and Mg^{2+} adjustment was performed to increase the induction of vascular calcification. The mice were divided into four groups for the preparations at different time points and evaluated for the progression of atherosclerosis and vascular calcification. Thus, about 132 mice were fed in different time intervals for a certain time period. Group 1 was killed in a time period of 6-11 weeks, group 2, 3, and 4 after 19-20 weeks (late stage of plaque development).

Figure 67. ApoE-/- mice treatment groups with different diets and surgical interventions

Control diet (1% Ca, 0.2% Mg)	Western diet (1% Ca, 0.2% Mg)
2 kidneys (2K)	2 kidneys
1 kidney (1K)	1 kidney
5/6 nephrectomy (5/6 NX)	5/6 nephrectomy

Mice were perfused with paraformaldehyde applying cardiac puncture. Then, some of the aortas were imaged directly with the ZEISS microscopy system for non-invasive imaging of collagen and elastin (group I). Groups 2 and 3 were cut open (*en face*) on the descending aorta and stained with oil red O (Figure 68) for atherosclerotic plaque development. The brachiocephalic arteries (BCA) were cut apart from the aortic arches and frozen in OCT for cryosectioning and traditional calcium and lipid staining. Group 4 was mainly used for measuring gene regulation by real-time PCR apart from the BCA, which were post-fixed and cut into 2 parts. One half was used for non-invasive imaging of collagen and elastin at the department of Renal Disease and Hypertension, UCHSC, Denver, Colorado, USA. The other half was utilized for alternative imaging of lipid and calcium deposits at the Beckman Laser Institute, UC Irvine, California, USA. Additionally, we used 5/6 nephrecomized LDLR-/- mice for conventional staining techniques of lipid and calcium deposits with atherosclerotic plaques.

8.8.1 Traditional staining of aortas and heart valves from ApoE-/- and LDLR-/- mice

The descending aortas were cut open in the *en face* manner for oil red O staining (Figure 68). The aortic roots and BCA were frozen in OCT medium for staining of cryosections with oil red O for lipids and von Kossa for calcification.

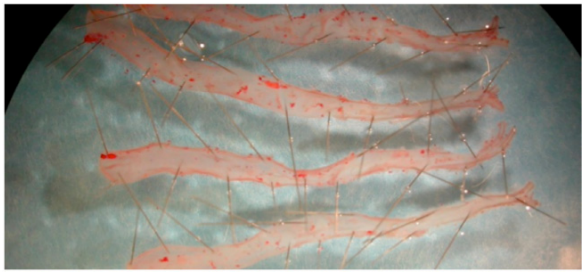

Figure 68. Traditional quantification of plaque area.
The descending aortas were cut open and pinned out. Then, the aortas were stained with oil red O. The samples were illuminated from above with white light and the picture was taken through a low magnification dissecting microscope. The aortas were about 25mm long.

For evaluation of the plaque area we manually drew around the aorta and each lesion and the ratio between these two was taken (Figure 69).

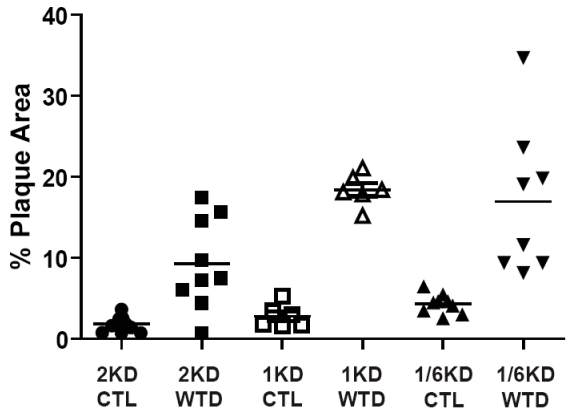

Figure 69. Evaluation of plaque deposits in male ApoE-/- mice with partial kidney ablation
Evaluation of the plaque areas of all 6 treatment groups from 5-8 animals of the 2nd set of animals after 19-20 weeks. The plaques in the descending aortas were stained with oil red O. Evaluation of lesion area was performed by drawing around the total and plaque area and calculating the ratio between total area and plaque area.

The evaluation of the plaque area revealed that 5/6 nephrectomized ApoE-/- mice on WTD resulted in the highest plaque formation compared to all other mouse models, although there was a big variability in the percentage of plaque area.

Cryosections of the aortic root and staining for calcification by applying von Kossa staining were performed. Hearts were frozen in OCT and after sectioning the heart for about 600µm we saw the aortic root with the three aortic valves. Von Kossa staining gave a black staining in presence of calcium within the plaque area (Figure 70). We also stained the BCA sections of group 4 with von Kossa for calcification (Figure 71). Moreover, we stained the aortas of male LDLR KO mice, which were fed with Ca^{2+} and Mg^{2+} adjusted control or WTD for 24 weeks, with oil red O and von Kossa (Figure 72).

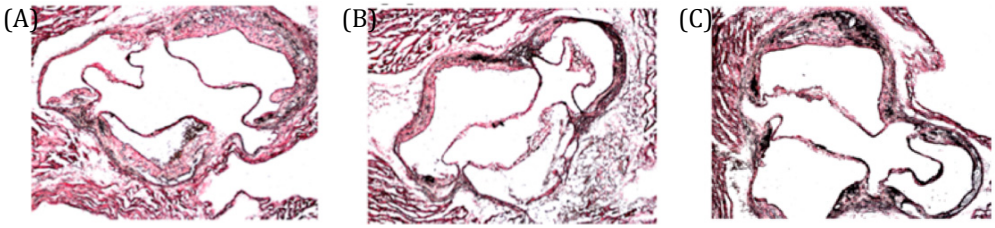

Figure 70. van Kossa staining of the valves on the aortic root
Hearts were fixed in OCT and after cutting about 600µm into the heart, cryosections of 10µm were performed and stained with von Kossa for calcification (black) and counterstained with nuclear fast red (nuclei: red, cytoplasm: pink). (A) control of 2K, (B) control of 5/6 NX and (C) 5/6 NX of WTD

Von Kossa staining in Figure 70 showed calcification in aortic root sections of controls from 2K and 5/6 NX mice and enhanced calcification in 5/6 NX mice on WTD. The calcifications were also enhanced in BCA of 5/6 NX mice on WTD in comparison with controls on WTD (Figure 71).

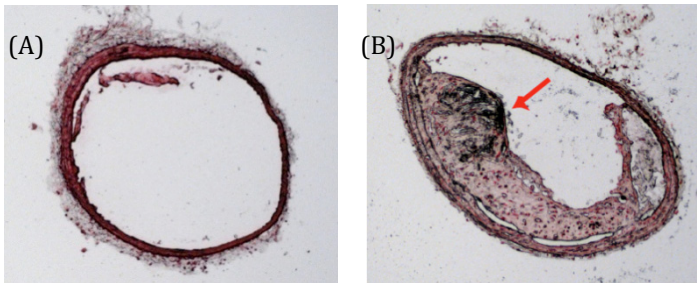

Figure 71. Calcification in the brachiocephalic artery
Five µm cryosections of BCA from 5/6 nephrectomized animals fed (A) control and (B) WTD were performed. Von Kossa staining showed calcification within the atherosclerotic plaque area (black). Counterstaining with nuclear fast red defined the nuclei (red) and the cytoplasm (pink).

Von Kossa staining in the BCA of 5/6 nephrectomized mice showed enhance calcified areas within the atherosclerotic plaque of mice on WTD compared to mice on control diet, where neither calcification nor plaque areas were detectable (Figure 71).

LDLR-/- mice with 5/6 nephrectomy showed both enhanced plaque formation and calcification in the aortic arch after feeding WTD in comparison with control diet (Figure 72).

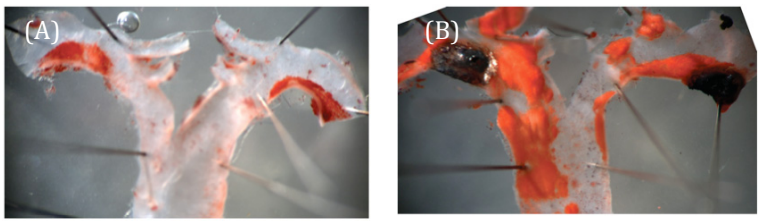

Figure 72. Staining of lipids and calcium in the *en face* aortas of male 5/6 nephrectomized LDLR-/- mice
En face staining of aortic arches from 5/6 nephrectomized LDLR-/- mice on (A) control and (B) WTD. Oil red O for lipids (red) and von Kossa for calcification (shiny silver-gray).

Calcification areas were quantified as described above. The evaluation revealed that LDLR-/- mice fed WTD showed more calcified areas than LDLR-/- mice fed control diet (Figure 73).

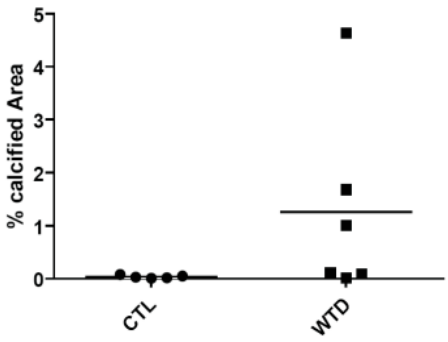

Figure 73. Evaluation of calcification in male 5/6 nephrectomized LDLR-/- mice
Percentage of calcified area relative to total stained area was higher in 5/6 nephrectomized LDLR-/- mice on WTD in comparison with mice on control diet.

8.8.2 Second harmonic generation/two photon excitation and coherent anti-Stokes Raman scattering (SHG/TPE and CARS)

Next to the conventional staining techniques we applied non-invasive microscopy techniques. Using SHG/TPH and CARS techniques the tissues were placed on a small dish with a glass coverslip window, to allow the transmittance of the light. When the aortas were cut open, they were inverted so that the lumen was in contact with the coverslip and a glass cylinder was put on top in order to stabilize the tissue, since the source of the laser light was coming from underneath. The area of detection without tiling was very small. This problem was overcome by using the tiling function without overlap of tiles (Figure 74). Here, using a motorised stage, a grid array of individual images was collected and assembled together to form a single large area image.

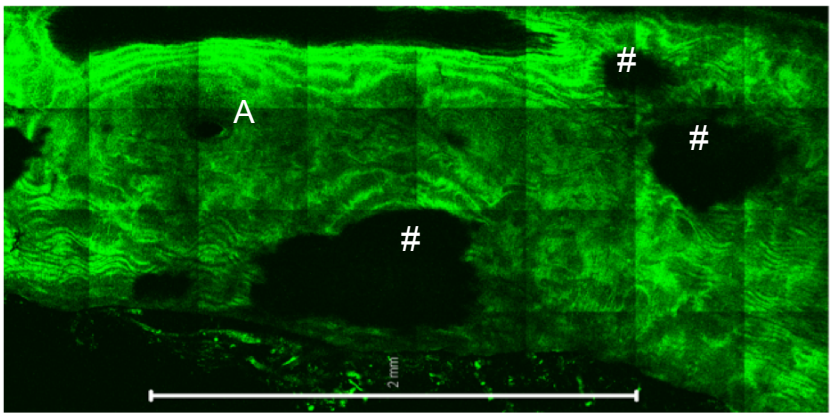

Figure 74. Basic tile imaging without overlap of an aorta piece.
A tiling of 4 x 8 tiles was performed using motorized XY stage on the Zeiss 510 microscope with a 25X water objective. The illumination for the two photon excitation wavelength is 800nm and allows the detection of autofluorescence from elastin. A single Z plane is shown without an overlap of the tiling. The aortic tissue was inversed and the plaques were the first part that touched the surface of the coverslip dish. The regions indicated with # show the areas of atherosclerotic lesions. The region marked as an A designates the exit point of an artery.

The structure of the lamellar aortic tissue was identified by SHG and TPE signals (autofluorescence signal of elastin in Figure 74). To get the 3-dimensional structure of the plaques, serial sectioning in z direction was performed and the tiled z-sections were stitched together. This was performed for all possible tiling compositions, but needed a lot of memory and took a lot of time. We were able to test automated acquisition software from Zeiss called multi time, which performed overlapping of tiles combined with z-sectioning. Thus, smaller pieces of the aortas (applying the automated software) were imaged as seen in Figure 75.

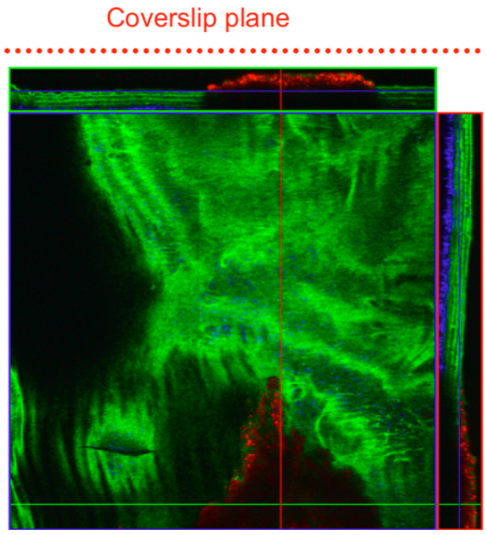

Figure 75. Tiling macro "multitime from Zeiss
A 2 x 2 tiling stack plus image stitching. The laminar wall of the arteries that is made up by elastin layers, which is shown in green. Nile Red staining (red) shows the lipid deposits in the arterial plaques which is mainly seen at the surface of the plaque. Blue=collagen (SHG), Green = elastin (auto-fluorescence TPE)

Using the automated software "Multitime" from Zeiss, a tiling of image stacks was allowed. In comparison to Figure 74 the stacks were acquired with overlap. The software aligned tiles to eliminate grid pattern. In this 2 x 2 array the joins were almost invisible. First, we performed 5 x 10 arrays, which the microscope itself will comfortably collect, however, whilst running the overlay software routine the computer crashed due to lack of memory. (We had 512 x 512 pixels by 80 slices by 9 channels per slice by 50 tiles = 9.5 Gigabytes). With the appropriate software the process would be fully automated. Since we did not have the automated software, we had to manually perform the stacks and acquired a series of tiled images every 5µm for about 100µm through the arterial wall plus plaque and then combine all stacks to a 3D image using another software package (ImageJ). Using the tiling system, we were able to get a larger area of the imaged tissue.

Since SHG/TPE did not detect the plaques themselves (black spot in the images), samples were stained with nile red (1:2000 dilution of a stock solution, 2min incubation) to get a signal from the lipids within the plaque area. Using 800nm excitation we were able to generate the signal at SHG, autofluorescence, and nile red emission. Since there was about 50% overlap between the nile red and autofluorescence emission spectra, we used spectroscopic imaging (META detector) and linear unmixing to separate the signals which required 9 channels per image. We used 30nm wide channels to keep the imaging time under control. Figure 75 shows an overlaid unmixed image (blue = SHG, green = two photon excitation of autofluorescence, red = two photon excitation of nile red). No further smoothing or contrast enhancement was applied to this and any further image.

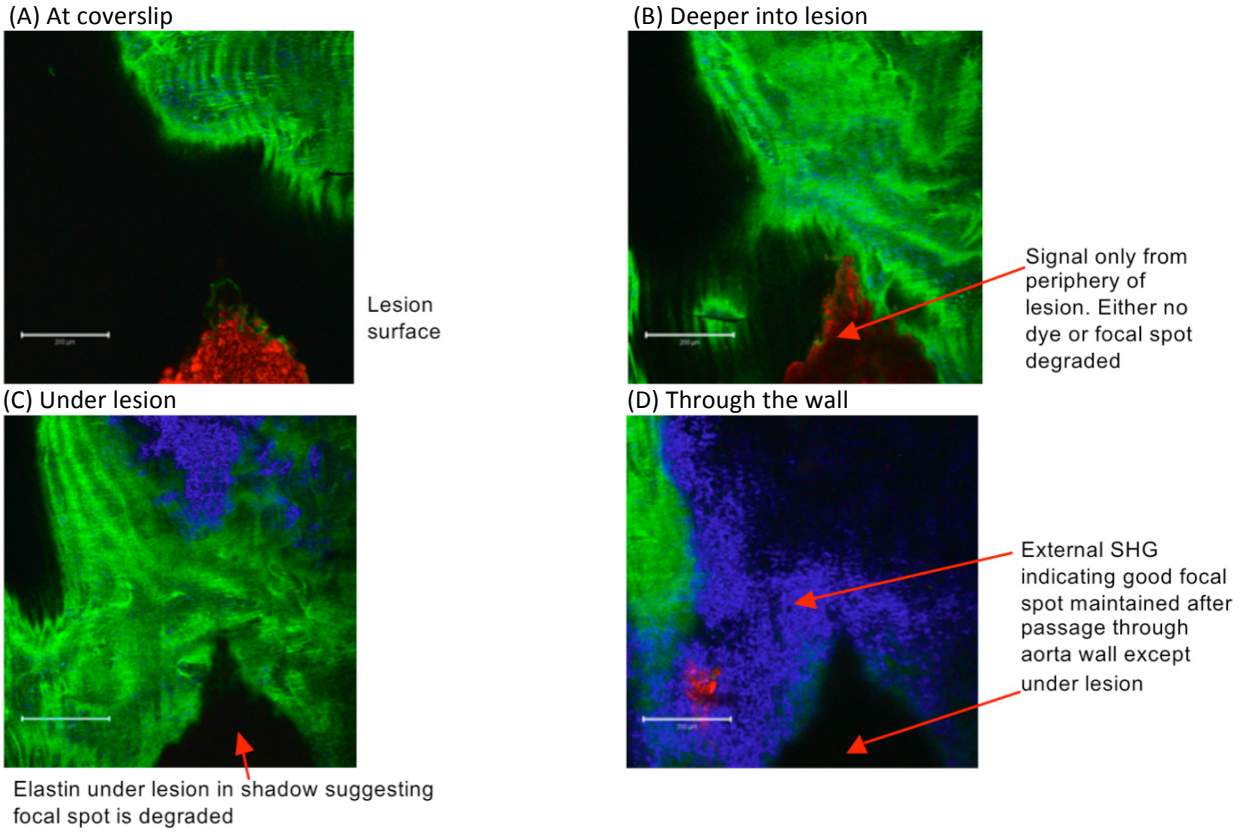

Figure 76. Representative planes from an 80 plane stack.
The aorta was cut into two parts along its axis creating long semicircular sections. The piece was placed lumen side down on a coverslip dish for *en face* imaging. We used a glass weight to flatten the sample onto the coverslip (Edmund optical 1cm diameter 2 cm long rod lens, placed end on). (A) The surface of the lesions appears flat due to contact with the coverslip. The nile red signal was only generated from the surface of the lesion area, because the density of the plaque probably didn't allow the stain to penetrate the whole lesion. (B) Deeper penetration into the lesion showed nile red signal of the lesion only from its periphery together with autofluorescece of the laminar vessel wall. (C, D) Individual elastin layers are well resolved (80 planes at 1 micron intervals). (D) External SHG signal was easily visible even though we had to image through the aorta wall to get to it. No adjustment of laser power or PMT setting was needed. The elastin signal below the lesion was shadowed out. No signals were detected inside the lesion. The scale bar shows 200μm in length.

Figure 76 showed again that we could easily go through the vessel wall with this non-invasive technique. The laminar structure of the vessel wall was detected as the autofluorescence signal from elastin with TPE whereas SHG detected the signal for elastin on the outer surface of the aortic wall. Nile red staining marked the lesion area within the examined aortic tissue. In Figure 76A, the lesion surface stained with nile red is shown together with parts of the vessel wall that touched the coverslip. Since the cut open sample was inverted and the laser light came from underneath the plaque surface was the first imaged area. Figure 76B shows deeper penetration into the lesion, whith either no nile red dye anymore or a degraded focal spot. Figure 76C shows elastin signal below the lesion in shadows, which suggested that the focal spot was degraded. Figure 76D shows that we could image through the vessel wall. External SHG signal from collagen indicated that the focal spot was maintained after passing through the aortic wall except under the lesion area.

For better visualizing of the arterial wall and the plaques inside we preferred to do XZ sections from a tiled stack (Figure 77).

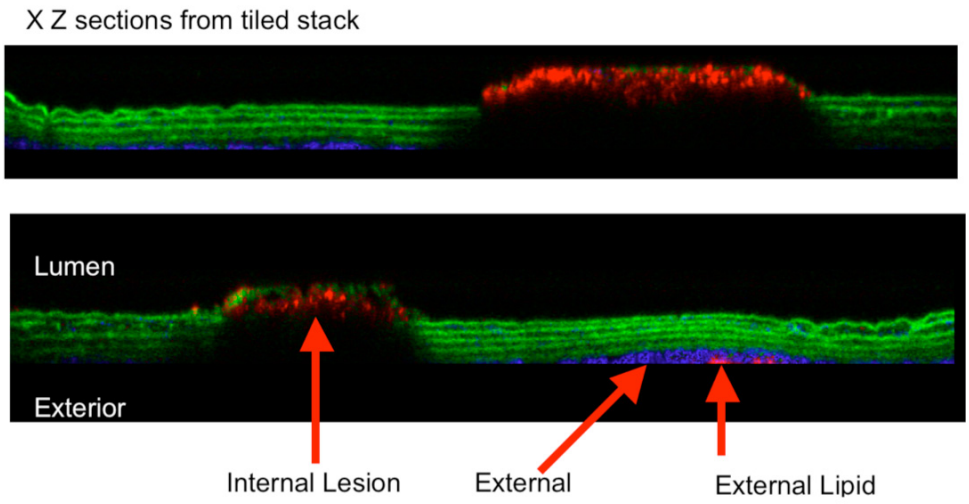

Figure 77. XZ sections of an aorta from a 5/6 NX on WTD with adapted Ca^{2+} and Mg^{2+} content.
The plaque formed from the elastin (green) layers, which means that the typical arterial wall got destroyed upon deposit of macrophages and foam cells in the intima of the arteries. Collagen was detected as external SHG signal (blue) and nile red detected lipids (red) on the surface of the plaque and external of the aortic tissue.

Furthermore, we also tried to image different tissues of the same animals such as liver, kidney, brain, and heart. An image of the aortic sinus within the heart is shown in Figure 78. The lesion area in the aortic root showed a big plaque with green autofluorescence of elastin and the blue SHG signal for collagen. Yet, again only the surface of the lesion showed detectable signal. The plaque composition seems to be too dense to allow the laser light to penetrate the lesion.

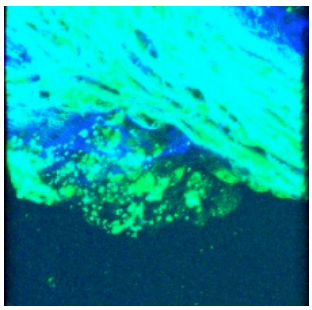

Figure 78. Heart from a 2K ApoE-/- mouse on control diet, looking down into the aortic root.
SHG/TPE signals detected the surface of a plaque within the aortic valve.

Figure 79 shows the image of a BCA with tiling but without automated software. The lack of overlap of tiles led to the grid-like structure of the image since the laser scanned small squares and combined them. The green signal shows the elastin in the laminar wall of the BCA and the blue colour marks the collagen deposit within the plaque.

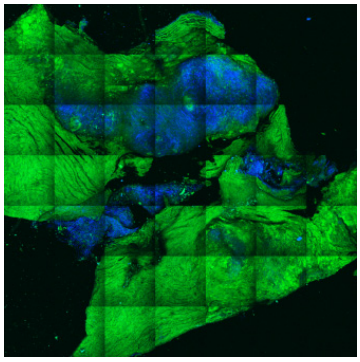

Figure 79. SHG/TPE image of a cut open BCA
Cut open BCA of a 5/6 nephrectomiced ApoE-/- mouse on WTD from group IV. Image shows stacked tiles (7x7). SHG signal of collagen (blue) and autofluorescence signal of elastin (green). The plaque area is defined with the intense SHG signal.

The combined imaging with the CARS system was done in cooperation with the Laser Beckman Institute at UC Irvine, CA. Since SHG/TPE microscopy can only detect collagen and elastin we used CARS for the identification of lipids and calcium within the plaque area. Calcification can be detected as calcium hydroxyapatite, giving a specific Raman spectrum from the inorganic phosphate stretch Raman spectrum was taken with ~1 mW of 532 nm excitation light, integration time was 20 seconds (3 averages). Luminescent background was separately measured and subtracted from the spectrum. Objective lens was 20x, 0.75 NA (air), the same used for taking the nonlinear microscopy images (Figure 80A). The CH_2 streching in lipids gave a specific CARS signal, which was detected together with SHG for collagen and TPE for elastin (Figure 80B). It is noteworthy that the TPE fluorescence from elastin signal overlapped with the CARS signal from elastin.

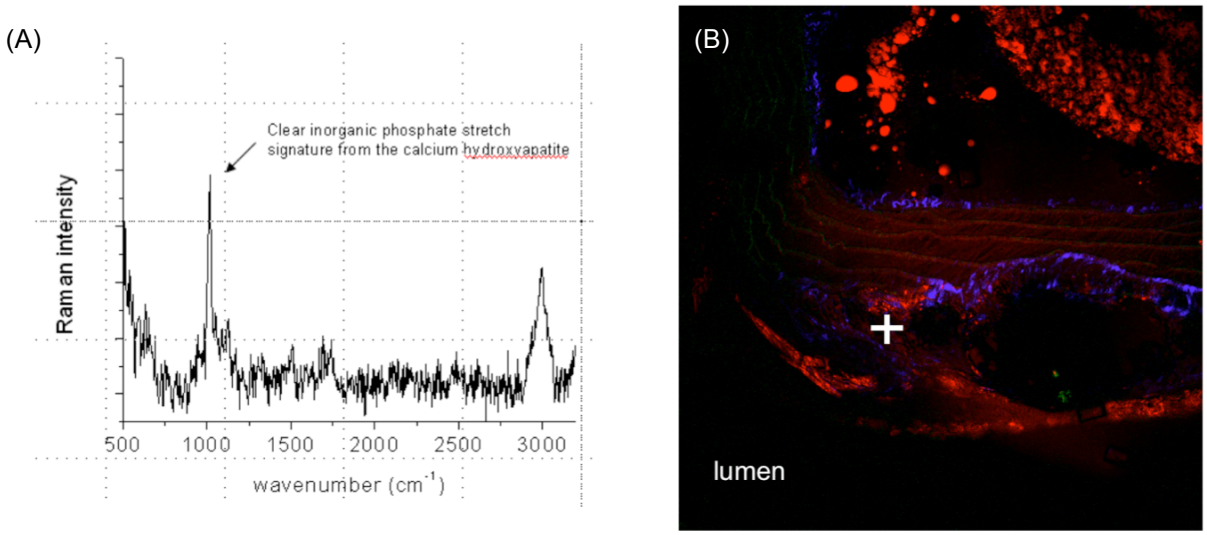

Figure 80. microRaman of calcified region and CARS of lipid areas within sectioned aorta
(A) Detectable signal for the inorganic phosphate stretch from the calcium hydroxyapatite. Raman spectrum was taken at the location of the white cross in the (B) CARS image. This location corresponded to a calcified region according to the images stained with van Kossa. Lipids (CH_2 strechting) were detected with CARS (red), collagen with SHG (blue) and elastin with TPE (green).

Furthermore, we applied the combination of CARS and SHG/TPE on BCA halves. Figure 81A shows lipid detection with CARS in a XZ stack of a BCA combined with collagen and elastin detection. Again the TPE fluorescence of elastin overlaid with CARS signal from elastin. Figure 81B demonstrates the signals of SHG/TPE for collagen and elastin in a XZ sectioning of the BCA half.

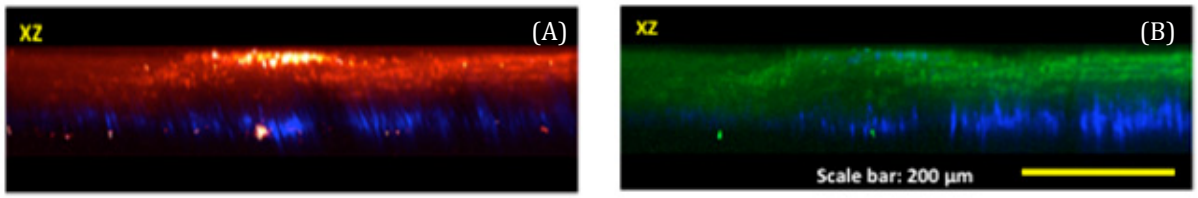

Figure 81. CARS and SHG/TPE image of the bracheosophalic artery (BCA).
(A) CARS signal of lipids (red) together with CARS signal of elastin (red) and SHG signal of collagen (blue) within the plaque area in a XZ stack of the BCA sample. (B) SHG/TPE signal of collagen/elastin (blue/green) of the BCA sample. The scale bar shows a length of 200µm.

Moreover, we detected cellular structures within the plaque areas applying CARS microscopy in a high magnification (Figure 82). These cellular structures can be macrophages or vascular smooth muscle cells and have to be further examined.

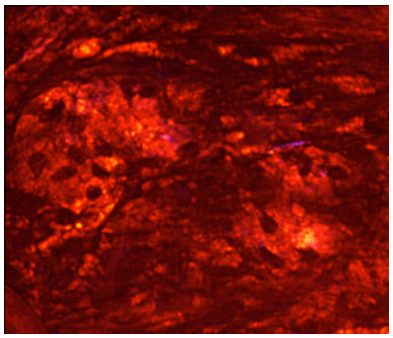

Figure 82. Magnification of a plaque
This image shows a 20-fold magnification (6.5 zoom) of the CARS imaging of lipids within the atherosclerotic plaque. With this magnification cellular structures, which might be macrophages or vascular smooth muscle cells, are detectable.

The combination of SHG/TPE and CARS raises the possibility to image the two main characteristics of atherosclerosis, lipid deposits and calcification. *In vivo* imaging with a combination of these techniques provides a good non-invasive method for observing the developmental stages of atherosclerotic lesions.

9 Discussion

Atherosclerosis is a hallmark for cardiovascular events such as heart attack or stroke. There are several risk factors known to trigger the development of atherosclerotic plaques such as hypercholesterolemia, diabetes, obesity, chronic kidney disease, smoking, stress, alcohol and lack of exercise. Certain possibilities to interfere with these risk factors help reducing the consequences of atherosclerosis. The most prominent of these interventions are statins, which were first identified in the 1970s (96) and block the rate limiting step in cholesterol biosynthesis by inhibiting hydroxymethyl glutaryl Coenzyme A reductase (HmgCoAr) and preventing the formation of mevalonate.

Another approach is related to the liver X receptors (LXR), which have been shown to be important regulators of cholesterol and lipid metabolism (54, 57). LXR are nuclear receptors, which are multifunctional proteins and transfer the signal of their affiliated agonists. They mainly reside in the nucleus where they are bound to the DNA and regulate gene transcription after activation by a selective agonist that is bound to the ligand-binding pocket within the LXR protein. Specific target gene transcription requires certain structural requirements of such agonists (177). The natural LXR agonists are oxysterols but several synthetic steroidal and non-steroidal agonists have been identified with variable specificity, binding affinities and characteristics. The main drawback of most agonists as potential antiatherosclerotic therapeutics is their activation capacity of genes involved in lipid metabolism, which leads to liver steatosis and hypertriglyceridemia. In this thesis, we focussed on a novel synthetic steroidal agonist called N,N-dimethyl-3β-Δ^5-cholenamide (DMHCA), which has been shown to have restricted activation potential for genes from the lipid metabolism whereas it maintained the activation of genes from cholesterol metabolism, relevant for reducing cholesterol accumulation by inducing reverse cholesterol transport (181). In most of the experiments we compared DMHCA with known LXR agonists such as the synthetic non-steroidal T0901317 (217) and GW3965 (218).

The synthesis of DMHCA did not involve any major obstacles, but it was important to work under argon for the first step of the synthesis to get quantitative chemical conversion of the starting substance. Moreover, it was essential to work on ice for the final step in the synthesis since the reaction was generating excessive heat.

First, the regulatory effects of DMHCA in different cell lines were investigated after optimizing concentration and treatment time. In MPM 2.5μM DMHCA for 24h was found to be the most efficient combination. ABCA1, a known LXR target, was highly induced, but SREBP1c was also

upregulated. Compared with the other concentrations and time points the pronounced difference between ABCA1 and SREBP1c activation led to the application of the mentioned combination. Moreover, both LXR isoforms were upregulated only with this treatment and HmgCoAr was significantly downregulated, which was not specific for only this treatment combination. In fact, it is known that LXRα regulates its own transcription via an autoregulatory loop to increase its target gene expression (232). Thus, it can be assumed that activation of LXR with DMHCA activates the autoregulatory loop-mechanism of both LXR isoforms and therefore further increases LXR target gene transcription. Moreover, downregulation of HmgCoAr, the rate-limiting enzyme in cholesterol biosynthesis, raised the question if DMHCA blocks cholesterol biosynthesis. Next to activation of cholesterol efflux transporter ABCA1, this would be an additional mechanism to prevent accumulation of excessive cholesterol within a cell. Similar results were found in the RAW264.7 macrophage cell line.

With respect to the LXR activated induction of liver steatosis, different concentrations of DMCHA were studied in human HepG2 liver cells, where higher concentration than 2.5μM led to an increased induction of SREBP1c. Moreover, studying the activation efficiency of DMHCA on ABCA1 and SREBP1c mRNA expression in human Caco-2 colon carcinoma cells showed that both genes were activated in this cell line, but 2.5 μM led to lowest induction of SREBP1c. Therefore, 2.5μM DMHCA was applied in a 24h treatment in all further cell experiments.

Since macrophages play a significant role in the development of atherosclerotic plaques by formation of lipid laden foam cells (7, 233), gene expression levels in MPM-derived foam cells were examined, where ABCA1, SREBP1c and LXRβ were induced after LXR activation with DMHCA. To further study the properties of DMHCA in LXR target gene activation compared to the well-studied LXR agonist T0901317 cDNA microarray experiments from Applied Biosystems were performed. The aim of this study was to compare gene regulation in DMHCA- or T0901317-activated MPM with control cells and against each other to specifically reveal differences in gene activation by these two LXR agonists. It is important to state that T0901317 has been identified to be no selective LXR activator, but also activates FXR and PXR (179, 180). This had to be taken into account when looking at the results from microarray data.

When microarrays of DMHCA treated MPM were compared with control treated MPM 401 genes were found to be downregulated upon DMHCA activation with $p \leq 0.1$ and fold change (FC) ≤ 0.5. Applying pathway analysis, it was striking that 28 downregulated genes were involved in lipid metabolism including cholesterol and sterol biosynthesis, which implies that DMHCA significantly influences lipid and cholesterol homeostasis. 15-ketosterol was defined as a LXR agonist that suppresses SREBP2 activity and consequently inhibited mRNA expression of HmgCoAr, LDLR and

PCSK9 (234). Moreover, it has been shown that human LDLR is a novel LXRα target gene containing LXRE in its promoter region, which was upregulated by T0901317 in human hepatoblastoma cells (235). Since DMHCA significantly downregulated genes involved in cholesterol biosynthesis and LDLR in MPM when compared to control treated cells, the microarray data suggested that DMHCA leads to reduced uptake of LDL-cholesterol by downregulation of LDLR and downregulation of cholesterol biosynthesis. Related to atherosclerotic plaque formation this could imply less foam cell formation and consequently reduced lesion development.

Moreover, the microarray data revealed 121 genes to be upregulated. Five of them belonged to the lipid transport, among which ABCA1, ABCG1, and PLTP are known LXR target genes. The other two were fatty acid amide hydrolase and fatty acid binding protein 2. The three mentioned LXR target genes were also upregulated upon T0901317 treatment compared with control, which showed that both agonists have common LXR target activation. However, T0901317 activated the upregulation of further genes involved in lipid transport and cellular lipid metabolism, such as apolipoprotein C-I, FAS, SCD1, SCD2, and SREBP1c. These data demonstrated that T0901317 induced lipid metabolism whereas DMHCA did not, supporting a very different activation profile of the two agonists. In total T0901317 upregulated 66 genes with $p \leq 0.1$ and $FC \geq 2$, whereas it downregulated 274 genes with no involvement in lipid metabolism.

Common target gene activation was found when regulated genes from both agonists were put together as the treatment group and were compared to the control group. In the upregulated genes two pathways showed high significance, the lipid transport and the unfolded protein response. Known LXR target genes from the lipid transport were ABCA1, ABCG1 and PLTP. Unknown LXR target genes were lipopolysaccharide binding protein, apolipoprotein C-I from lipid transport and zinc finger DHHC domain containing 3 from lipoprotein metabolism. Another interesting gene that was upregulated within the treatment group is interleukin 18 binding protein (IL18BP), which was supposed to have antiatherosclerotic properties (219). Two further genes, which were significantly upregulated in the treatment group, were N-myc downstream regulated gene 1 (NDRG1) and endoplasmic oxidoreductin 1-like (ERO1L) NDRG1 is ubiquitously expressed and belongs to the α/β hydrolase superfamily without having a hydrolytic catalytic site (236). NDRG1-/- mice showed Schwann cell dysfunction, which suggests its role for maintaining myelin sheats in peripheral nerves. In humans mutations of NDRG1 led to the Charcot-Marie-Tooth disease (223). It was suggested to interact with ApoA-I and A-II and might be involved in HDL-mediated reverse cholesterol transport (222). It has been shown to be regulated by peroxisome proliferator-activated receptor gamma/retinoic X receptor (PPARγ/RXR) but not yet reported to be regulated via LXR activation. Interestingly, the microarray data showed upregulation of this gene with both LXR agonists, which could not be verified by performing qPCR. On the contrary, NDRG1 was highly

upregulated upon DMHCA treatment in male and female MPM, THP-1, male human peritoneal macrophages (hPM) and RAW264.7 cells, whereas T0901317 failed to increase its expression. Furthermore, *in silico* search for potential LXRE sites for this gene revealed one perfect match site at 6.825kb upstream of the start codon in the human promoter as well as another one with 1 mismatch (MM) at 14.186kb upstream of the transcriptional start. Similarly to the 1 MM site in human, one MM site at 14.298kb upstream of the start codon was found in mouse. Moreover, a perfect match site for farnesoid X receptor response element (FXRE) at 18kb upstream of the mouse promoter was detected, which might imply that this gene is also regulated by FXR in mouse but not in human. Immunofluorescence data supported the different activation of NDRG1 in MPM upon LXR activation, but Western blot didn't due to lack in specificity of the antibody.

ERO1L is a thiol protein with two isoforms, ERO1Lα and ERO1Lβ, and mediates secretion of adiponectin, an important antidiabetic and antiatherosclerotic adipokine, in adipocytes. It can be activated by PPARγ as well as sirtuin 1 (SIRT1) blocking (225). In fact, microarray data showed its upregulation in MPM upon stimulation with both LXR agonists, but qPCR verification demonstrated only induction upon DMHCA treatment in MPM, but additional stimulation by T0901317 in hPM. Human promoter regions of both isoforms carry several 1MM LXRE sites. The mouse promoter region of the β isoform also showed 2 potential sites with 1 MM.

Applying the same stringency for downregulated genes in the treatment group in comparison with the control group 454 genes were found with no high significance in any biological pathway and a lot of them not even had an accession number but a sequence in the original data file. Some of them were triggering receptor expressed on myeloid cells 1 (TREM1), apolipoprotein CIII (APOCIII), glycoprotein Ib, beta polypeptide (GP1BB), and the activation-induced cytidine deaminase (AICDA). TREM1 is known to play a role in the inflammatory pathway. It belongs to the TREM family and at least one of its members is expressed in any cell type of the immune response, such as monocytes, neutrophils or macrophages. It is linked to Toll-like receptor 4 signaling and its downregulation might protect against bacterial infection (237). Silencing of TREM1 resulted in attenuation of adaptor and toll-like receptor interacting proteins and downstream target genes such as pro- and anti-inflammatory cytokines (238). Related to macrophages in atherosclerotic plaques this might be involved in the anti-inflammatory properties of LXR activation.

ApoCIII impairs insulin signaling in endothelial cells, linking hyperlipidemia with endothelial dysfunction (220). ApoCIII is a small protein on the surface of VLDL and to a lesser extent on LDL and causes accumulation of atherogenic remnant lipoproteins in plasma. Consequently, plasma levels of ApoCIII containing VLDL and LDL can predict risk of cardiovascular disease (239). So far, nothing is known about LXR regulation of this protein, but the microarray data suggest that LXR

activation directly or indirectly influences the regulation of this gene. In fact, LXR activation might actively repress the transcription of this gene. *In silico* search for possible LXRE gave several 2 MM sites for human and mouse promoters of this gene and one 1 MM site for the mouse promoter. GP1BB is supposed to have antithrombotic properties (221).

Gp1bb has been shown to play a role in thrombus formation. Animal models of the Bernard-Soulier bleeding disorder, such as the GPIb beta -/- mouse, showed decreased thrombus formation (221). Yet, there is nothing known about a regulatory effect of LXR but microarray data suggested that LXR might repress transcription of this gene and thereby contributing to a higher stability in atherosclerotic plaques.

When DMHCA treatment was compared with T0901317 treatment, 298 genes were downregulated upon DMHCA treatment ($FC \leq 0.5$, $p \leq 0.1$), from which some were already found in the comparison of DMHCA with control treatment. Sterol and lipid metabolism showed the highest significance in the pathway matching, which implies that DMHCA posses a different gene activation profile in these metabolic pathways than the well-studied agonist T0901317. In total, 29 genes have been involved in lipid metabolism, more specifically mostly in cholesterol biosynthesis and fatty acid (FA) metabolism. Those genes are e.g. IDI1, DHCR7, DHCR24, CYP51 (cholesterol biosynthesis), LDLR (cholesterol uptake), FAS, SCD1, SCD2, SREBP1c (FA synthesis) and several more. SREBP1c, LDLR, FAS, and SCD1 are known LXR target genes within these pathways and downregulation of these genes proposes a lipid lowering potential of DMHCA. Real-time PCR confirmed downregulation of these genes with DMHCA in comparison with T0901317 treatment in different macrophage cell lines as well as human and mouse primary macrophages. Moreover, radioactive assays after ^{13}C-acetate and ^{13}C-mevalonate incubation of MPM showed a significant reduction in FC and consequently cholesterol biosynthesis upon DMHCA treatment. Interestingly, I detected an increase in CE upon DMHCA treatment, which was not observed with T0901317. The increase was not statistically significant, but obviously present, which would need further investigations. Although, the main site of cholesterol biosynthesis takes place in the liver, every cell itself is capable of synthesizing cholesterol. Therefore, the reduction in macrophage cholesterol biosynthesis as well as blocking receptor-mediated cholesterol uptake by downregulation of LDLR might be important for reduction of atherosclerotic plaque development. However, the mechanistic behind are quite elusive, although T. Pfeifer et al (unpublished) have shown that DMHCA blocks DHCR24 which converts desmosterol to cholesterol and consequently initiating a feedback inhibition of other enzymes in the cholesterol biosynthesis. Additionally, treatment of RAW264.7 macrophages and foam cells with different DMHCA concentrations reduced FC and CE content after lipid extraction in both cell types. In fact, this reduction in cholesterol content was much more pronounced in foam cells, implying a reduction of foam cell formation after DMHCA treatment.

Microarray data showed that DMHCA also downregulated genes from FA biosynthesis when compared with T0901317. There are already several mechanisms shown where lipid and cholesterol metabolism in macrophages can be blocked, giving alternative starting points for treatment of atherosclerosis. One example is 25-hydroxycholesterol-3-sulfate (25HC3S), which is the product of 25-hydroxycholesterol (25HC) sulfation by sterol sulfotransferase SULT2B1b. SULT2B1b inactivated the response of LXR to different oxysterol ligands (240), whereas 25HC3S decreased expression of SREBP1c and its downstream target genes ACC and FAS via the LXR/SREBP signaling pathway and additionally increased cell proliferation. Both 25HC and 25HC3S inhibited HmgCoAr as well as LDLR, but probably through a different mechanism. Thus, sulfation of oxysterols might have a regulatory role in lipid and cholesterol metabolism (241). 15-ketosterol is a weak, but active LXR agonist and shows hypochlesterolemic activity by suppressing SREBP-2, HmgCoAr as well as LDLR (234). *In silico* search revealed several 1 and 2 MM sites for LXRE in human and mouse promoters of HmgCoAr, FAS, ACC, SCD1, SREBP1, SREBP2, CYP51, STARD4 and LDLR (see supplemental data). In fact, LDLR has been identified to be a novel target for LXRα by Ishimoto et al. (235). Deficiency of SCD1 led to LXR-mediated increase of HDL cholesterol and protected against hypertriglyceridemia (155). One perfect match for LXRE was identified in the human promoter and two 1 MM sites in the mouse promoter.

Another interesting gene involved in cholesterol metabolism is INSIG1. It was highly downregulated upon DMHCA treatment versus T0901317 treatment, which was also verified by qPCR. In fact, this might be responsible for the downregulation of genes from the lipid metabolism, because SREBP processing cannot work properly. Checking gene regulation of INSIG2a and INSIG2b showed only upregulation of INSIG2a upon DMHCA treatment.

Moreover acyl-coenzyme A: cholesterol acyltransferase 2 (Acat 2) was downregulated in DMHCA versus T0901317 treatment. This might additionally indicate reduction of atherosclerosis because of a lower number of CE-rich lipid droplets in the macrophages, thus less foam cell formation (242).

Sortilin-related receptor (SORL1) has been shown to be highly induced in atherosclerosis, specifically in the intimal vascular smooth muscle cells (VSMC) of atheromatous lesions (243). Microarray data and qPCR verification revealed downregulation of SORL1 in MPM upon DMHCA treatment compared with T0901317 treatment, implying antiatherosclerotic effects of DMHCA by downregulating SORL1.

Real-time PCR demonstrated a downregulation of the inflammation marker fibroblast specific protein-1 (FSP1), and fatty acid binding protein 3 (FABP3) upon DMHCA treatment, whereas CD36, which is responsible for FA uptake in MPM, was upregulated. CD36 might contribute to

macrophage trapping in the arterial intima and thus promote atherosclerosis (244). The regulation of other antiatherosclerotic genes upon DMHCA mediated LXR activation might compensate for upregulation of CD36.

141 genes were upregulated upon DMHCA treatment compared to T0901317 treatment, but no pathway involved showed high significance. Interestingly, no genes from the lipid metabolism were differentially regulated within this group. The highest number of differently regulated genes was found for biological process unclassified (51), immunity and defense (12), signal transduction (22), and protein modification (19) nucleoside, nucleotide and nucleic acid netabolism (18). Some interesting genes, which were also verified by qPCR, are aquaporin 9 (AQP9), carbonic anhydrase 6 (CAR6), tribbles homolog 3 (TRB3), bone morphogenic protein 2 (BMP2), and dual specificity phosphatase 1 (DUSP1), also called MAPK phosphatase-1 (MKP-1). AQP9 is an aquaglyceroporin membrane channel protein and is important for hepatic glycerol uptake and metabolism. It might be important for glucose and glycerol metabolism in diabetes (245). Moreover, it has been shown that extrahepatic cholestasis leads to downregulation of AQP9 and dysregulated aquaporin channels contribute to bile flow dysfunction of cholestatic hepatocytes (246). Yet, its exact role remains elusive, but microarray data showed high induction upon DMHCA treatment in macrophages in comparison with T0901317 treatment. Verification of these data by qPCR in MPM of male and female WT mice confirmed its regulation. However, it has to be verified if this is a LXR-mediated regulation since *in silico* search for LXRE did only reveal one possible binding site with 1 MM in the human promoter. A potential function of this gene in macrophages is not yet known.

Carbonic anhydrases are zinc-containing metalloenzymes that catalyze the reversible hydration of carbon dioxide and might therefore be responsible for maintaining pH in different tissues and fluids of the body. CAR6 is the only so far known secreted isozyme of the Car family. It is synthesized mainly in the parotid and transported in saliva and milk and suggested to have mucosa-protective role in the gastrointestinal tract as well as respiratory tract (247). In fact, it was also detected in nasal mucosa epithelium and glands, which it might protect against acid surroundings (248). Its role in macrophages is unclear, but qPCR verified its presence in MPM and its regulation upon DMHCA treatment. Human CAR6 promoter region showed several potential 1 MM LXRE whereas the mouse promoter did not carry any site.

TRB3 was highly upregulated upon DMHCA treatment when compared to T0901317 treatment in the microarray experiments, which was verified by qPCR, showing nearly no induction upon T0901317 treatment. TRB3 is a negative regulator of adipogenesis by promoting ACC ubiquitination and degradation and suppressing adipocyte differentiation (249), (224). Upregulation of this gene might be a possible mechanism by which DMHCA leads to

downregulation of target genes from lipid metabolism. Yet, TRB3 knockout mice displayed normal hepatic insulin signaling and glucose homeostasis, thus a redundant role for TRB3 is questionable (250). However, qPCR experiments verified TRB3 mRNA expression and upregulation upon DMHCA treatment in both male and female MPM, hPM, THP-1, and RAW264.7 macrophages. Verification on protein level with Western blot experiments failed due to lack in antibody specificity, but immunofluorescence looked promising. Search for possible LXRE binding sites revealed a highly potential binding site at 4.712 kb downstream of the start codon and two sites with 1 MM at 16kb and 4.829kb upstream of the start codon. The mouse promoter contains 2 promising sites at 5.797kb and 4.288kb upstream of the start codon with one MM, respectively.

BMP2 is an osteogenic gene that plays an important role in bone morphogenesis and vascular calcification (251). However, induction of BMP2 by lovastatin might be responsible for repression of VSMC proliferation and growth, leading to increased stability of atherosclerotic plaques (252). Yet, the function of BMP2 is not well studied in macrophages, where it also might be responsible for vascular calcification, but eventually also for plaque stability as shown for lovastatin. Microarray data showed high induction of BMP2 in MPM after DMHCA treatment in comparison with T0901317, which was verified by qPCR.

DUSP1 is important for regulation of innate immunity. It inhibits the mitogen-activated protein kinase (MAPK) pathway and decreases toll-like receptor (TLR) signaling and possibly gets activated by acetylation. In fact, MKP-1 -/- mice were more susceptible to LPS than their WT littermates. Concerning TLR signaling, macrophages, lacking MPK-1, produce higher levels of proinflammatory cytokines. Thus, this might be an interesting target for intervention in inflammatory diseases (253). In fact, this gene was highly upregulated upon DMHCA treatment versus T0901317 treatment. This was shown both in microarray experiments and qPCR verification, whereas no additional induction was observed with GW3965 or T0901317 treatment. Looking at the promoter region, two sites with 1 MM in the human promoter and 1 region with 1 MM in the mouse promoter were identified.

Another interesting gene is Sirtuin 1 (SIRT1). SIRT1 is an NAD^+-dependent deacetylase, which is known to act positively on aging and a lot of different processes like apoptosis, fat metabolism, glucose homeostasis, and neurodegeneration. It is also known to deacetylate and positively regulate LXR. In fact, deacetylation of LXRα by SIRT1 facilitates its degradation whereas it increases its activity. Moreover, SIRT1 is activated by caloric restriction, which improves atherosclerosis and cholesterol homeostasis in humans and RCT is inhibited in Sirt1-/- mice (163, 226). However, no regulation of SIRT1 by LXR has been reported so far. Examining mRNA expression of SIRT1 in MPM and hPM showed a slight but significant induction in upon DMHCA treatment. No induction could be detected upon treatment with the other LXR agonists. However, no detection of any LXRE in the

mouse promoter region was possible, whereas the human promoter showed several possible LXR binding sites with one or two mismatches. It has to be considered though that those binding sites are very far upstream of the start codon, beginning from 18kb to 12kb. Further studies are necessary to investigate a potential regulatory mechanism of LXR for this gene. One possibility would be to perform luciferase assays with different lengths of the promoter, which would be necessary for all other genes containing possible LXRE sites.

DMHCA is a LXR selective agonist, which was shown by Janoswski et al. applying ligand binding assays (177). We treated MPM from WT, LXRα-/-, LXRβ-/- as well as LXRα/LXRβ double knockout (DKO) with DMHCA and GW3965 before and after LPS stimulation. Regulation of ABCA1 and ABCG1 showed no selectivity for either isoform by DMHCA, indicating that it is a full LXR agonist. Yet, as we and others (181) claimed that DMHCA does not induce genes from FA metabolism, we did not find an induction, even a repression, of SREBP1c and FAS. On the contrary, GW3965 induced these two genes, missing an induction in the LXR DKO mice, which implies that these genes are direct or indirect LXR targets. Looking at API6, which was shown to be a target of LXRα (229), we could prove LXRα selective regulation with both LXR agonists to the same extent. API6/AIM/SPα has been shown to induce survival of macrophages that take up oxLDL, which supports the development of foam cells that accumulate within the intima of arterial walls. Therefore plaque development is increased (231). If this gene is knocked out in macrophages apoptosis is induced, development of foam cells is blocked and fewer plaques are formed in the early state of atherosclerosis. Yet, at a later stage of atherosclerosis the apoptotic effect of lack in API6 leads to less stable plaques and easier plaque rupture. LXR activation upregulated API6 but lack in LXR increases atherosclerosis, which implies that other antiatherosclerotic genes compensate for the atherosclerotic effect of API6 (231).

Microarray data already showed regulation of inflammatory and anti-inflammatory genes upon DMHCA treatment. Thus, the mRNA expression of certain inflammatory genes such as RANTES, COX2, IL6, and iNOS was investigated. RANTES has been shown to have proinflammatory effects in atherosclerotic plaques. Antagonists of RANTES act by inhibiting leukocyte recruitment into the plaques and therefore reducing systemic inflammation (254). All of the investigated inflammatory genes were repressed upon LPS stimulation and DMHCA treatment in the LXR-/- mice, respectively, whereas GW3965 could only decrease their stimulation. This implies that DMHCA shows an anti-inflammatory response in the MPM. In fact, this effect was even seen in the LXR DKO mice, which indicates that this DMHCA effect is LXR-independent. Thus, DMHCA is not only an LXR selective agonist and further investigations are necessary in this field to explore the mechanistic behind the LXR independent anti-inflammatory effects of DMHCA.

LXR activation by T0901317 and GW3965 has been shown to reduce atherosclerotic plaque formation (107, 108), but these agonists also exhibit less favorable effects on lipid metabolism by increasing plasma and hepatic TG concentrations (151). The mechanism for LXR-mediated hepatic lipogenesis is mainly related to increase of SREBP1c expression (255). I have shown with my *in vitro* experiments that DMHCA leads to a diminished and partly repressed induction of SREBP1c while it activates gene transcription of cholesterol efflux transporters and target genes involved in RCT. Thus, I investigated the influence of DMHCA in gene regulation, protein expression and its impact on atherosclerosis in wild type, ApoE-/- and LDLR-/- mice. It is important to state that different drug delivery might give different results. In fact, different drug deliveries led to different bioavailabilities of substances. Quinet et al. (181) claimed low bioavailability of DMHCA, because they showed significant regulation of CYP7A1, ABCA1, and ABCG1 only in mice that were intraperitoneally injected with DMHCA.

We performed both i.p. injections and feeding of DMHCA by mixing it in different concentrations directly into the food. For i.p. injections we used 50mg DMHCA/kg BW/day dispersed in 1.3% Tween80 plus 0.25% carboxymethylcellulose for 6 days. For feeding studies we added DMHCA in a concentration of either 8mg/kg BW (low dose) or 80mg/kg BW/day (high dose) to chow diet or WTD and fed the mice for 4d, 7d, or 15d, respectively. In all, our experiments, independent of the type of drug delivery, we could show distinct regulation of LXR target genes in different tissues upon DMHCA treatment. The fold regulation differed between the treatments but the significance and trend used to be the same. Additionally, in studies where we compared DMHCA with T0901317, the effects in gene regulation were less pronounced for most genes, which underlined the higher LXR activation potency of T0901317. However, the selectivity for LXR is not given for T0901317 since it also activates farnesoid X receptor and pregnane X receptor (179, 180). Furthermore, in all our treatments, in which the two compounds were compared, the lipid parameters differed significantly, which was independent from the type of drug delivery. Both in i.p. injections and feeding of drug-containing food, we could show a significant increase of triglycerides (TG) in livers upon T0901317 treatment, whereas the TG concentrations in livers upon DMHCA treatment did not differ much from the control livers. These data were confirmed by performing oil red O staining of liver cryosections and measuring of alanine aminotransferase/aspartate aminotransferase (ALT/AST) levels in plasma. The levels of these enzymes indicating liver injury were highly increased upon T0901317 treatment but not upon DMHCA treatment. Moreover, we confirmed no liver damage upon i.p. injections with DMHCA by performing pathological stainings, which did not reveal any severe pathological traits. Furthermore, SREBP1c levels were highly increased in livers both on gene and protein level upon T0901317 treatment, but were minimally or not regulated upon DMHCA treatment. One potential explanation

of the difference might be that T0901317 is a ligand of PXR and activates transcription of its target genes such as CD36, leading to increased FA uptake (179). Thus, some effects of T0901317 inducing lipogenesis might be due to activation of PXR. In fact, it is not clear if DMHCA activates or represses other nuclear receptors, which in turn leads to unaltered or repressed expression of SPREBP1c. Experiments in LXRα-, LXRβ-, and LXRα/β-knockout mice indicated that DMHCA shows no selectivity for either isoform. Because DMHCA shows unique gene regulation, which is different from T0901317 and GW3965, different mechanisms are likely to be involved. One similarity is given to 15-ketotsterol, which is a LXR agonist that activates ABCA1, but suppresses SREBP2 processing (234). Interestingly, we showed in our microarray experiments, that LDLR and genes from cholesterol biosynthesis were downregulated in MPM upon DMHCA treatment. These results were also found in MPM and livers after i.p. injection of DMHCA. Furthermore, in the feeding studies LDLR and HmgCoAr were unaltered in the livers of wild type and ApoE-/- mice. SREBP1c mRNA expression in livers of wild type mice was slightly increased but less pronounced than with T0901317 treatment, and interestingly, the mature SPREBP1c protein was unaltered when compared to control, whereas T0901317 highly upregulated the protein expression. In accordance with the microarray data, FAS mRNA expression was usually less elevated upon DMHCA treatment than upon T0901317 feeding, suggesting that downstream genes from SREBP1c are not affected. One possibility for that, might be the activation of genes, such as TRB3, that leads to degradation by ubiquitination of downstream genes such as ACC (224). Similar results were received in ApoE-/- mice, where the high dosage of DMHCA in chow diet showed decreased expression of SREBP1c in livers and unchanged expression of LDLR and HmgCoAr, but high induction of CYP71 and the ABC transporters G1, G5, and G8. Increased expression of ABCA1 and ABCG1 in MPM and aorta confirmed that DMHCA induces cholesterol efflux. Similar results were found in ApoE-/- fed the low dose of DMHCA for 15d. After 15d feeding high dose (80mg/kg BW/day) within chow diet we found a 2.4-fold increase in TG, which was confirmed by measuring the fatty acid composition, showing increase in oleate, palmitate, linoleate, and stearate. However, the treatment with T0901317 led to an 8-fold increase in TG and a more pronounced increase in the mentioned fatty acids. In fact, this difference was more pronounced in the WTD feeding, where DMHCA did not show any significant difference in TG concentration, whereas T0901317 did. Moreover, cholesterol concentrations were reduced both in plasma and liver upon DMHCA feeding in chow diet, whereas they were highly increased in plasma of T0901317 fed animals. Interestingly, both ligands led to a significant reduction of total cholesterol in the livers after feeding both diets. I assume that the high concentrations of both compounds led to an increased LXR response, which led to increased cholesterol efflux and/or cholesterol conversion to bile acids. Feeding of the low dose for 7d in WTD and the high dose for 4d in chow diet and also i.p. injections of both compounds with 50mg/kg BW/day for 6d did not show this pronounced difference in cholesterol levels. In fact, we

could show increased bile acid (BA) concentrations in the feces after 4d feeding chow diet with both compounds of the high dosage, which was more pronounced with T0901317. Interestingly, the composition of BA differed between the two compounds. DMHCA led to a higher concentration of lithocholic acid, whereas T0901317 showed higher deoxycholic acid content, proving again a different mechanism of the two compounds. Similar results were found in ApoE-/- mice after 4d treatment with a high dose of DMHCA in chow diet and 15d treatment with a low dose of DMHCA in WTD. TG concentration was significantly reduced in the liver after 4d feeding of high dose DMHCA containing chow diet, whereas it was unchanged after 15d low dose DMHCA WTD feeding. This was confirmed by measuring fatty acid composition showing reduced fatty acid content in both chow and WTD. TC levels tended to be lower in the livers, but no significance could be reached. Unfortunately, we do not have comparable data from T0901317 treated animals here, but assumed to get the same trend as with the wild type animals.

Apart from lipid parameters and gene expression studies in i.p. injected female mice, we performed protein analysis of MPM and livers, which did not reveal any proteins that were already known to be LXR targets. Therefore, it was questionable if these results were trustworthy. Regulated proteins from the MPM were most highly involved in glycolysis/gluconeogenesis and pyruvate pathways, whereas in the liver most affected pathways were glutathione metabolism and metabolism of xenobiotics by cytochrome P450. One gene that might become interesting is cathepsin D, which was upregulated in MPM upon DMHCA treatment. It might play a role in ABCA1-mediated cholesterol efflux (230). Repeating this experiment together with a T0901317 treatment group would help getting a better insight in protein regulation. Moreover, it might be considerable to rethink the way of drug delivery and treatment time. Furthermore, it is relevant to take the different sexes into account when looking at gene or protein expression. Consistency in picking the same sex when comparing gene expression or other parameters is necessary. As we used female mice in these experiments, it might be possible that male mice give more distinct results.

The bioavailability of DMHCA was checked by measuring its concentrations with high performance liquid chromatography in plasma after 15d feeding wild type mice with low (8mg/kg BW/day) and high dose (80mg/kg/BW) DMHCA in chow diet. The high dose resulted in DMHCA plasma levels of 2-27ng/mL, whereas the lower dose was undetectable (detection limit 0.1ng/mL). After feeding of wild type mice for 1h with 2.5mg total DMHCA in chow diet (equivalent to 80mg/kg BW) plasma and tissue distribution of DMHCA was measured. Two h and 4h after giving the food to the mice the plasma concentrations of DMHCA were highest, showing good bioavailability. Yet, highest DMHCA concentrations were detected within the feces and ileum followed by kidney, heart, lung, duodenum, jejunum, urine, and liver. These data imply that a large amount of DMHCA is directly excreted by the feces and urine, but might be also reabsorbed by all three parts of the small

intestine. Moreover, its presence in all tissues supports bioavailability throughout the body when added to the diet though not in an imbalanced way. Almost no DMHCA was found in the brain, assuming that DMHCA is unable to cross the blood brain barrier. Since it was stated that DMHCA blocks the conversion of desmosterol to cholesterol (T. Pfeifer et al. unpublished), it is a big advantage that DMHCA does not cross the blood brain barrier because accumulation of desmosterol in the brain is avoided, which can lead to desmosterolosis. Desmosterolosis is an autosomal recessive disorder due to mutations in the 3β-hydroxysterol-D24 reductase (DHCR24) gene that encodes an enzyme catalyzing the conversion of desmosterol to cholesterol (63).

After in vitro and in vivo experiments, we examined the effects of DMHCA on the development of atherosclerosis in ApoE-/- and LDLR-/- mice. Despite the lack in traceability of the low dose (8mg/kg BW/day), I decided to feed both male and female mice from each genotype with WTD ± 8 mg/kg BW DMHCA for 11 weeks. Body weight and plasma TC and TG levels were observed biweekly during the whole feeding period. Both sexes in both genotypes showed an increase in body weight. After 11 weeks, animals were fasted overnight and plasma lipid parameters were measured. In ApoE-/-mice reduced plasma TG and TC levels were observed when DMHCA was included in the food, which were more pronounced in overnight fasted animals. Moreover, we observed a significant reduction in atherosclerotic plaque formation in aortas and heart valves of male and female ApoE-/- mice fed DMHCA. We could show a slight increase in HDL and decrease in VLDL of these animals' plasma, which might partly explain the reduced plaque formation. Moreover, similar to GW3965 treated ApoE-/- mice (172), I assume that DMHCA stimulated ABCA1 in macrophage-derived foam cells within the aorta of ApoE-/- mice as was shown in foam cells *in vitro*. Although, DMHCA did not significantly increase ABCA1 and ABCG1 in macrophages or ileum after the 11 weeks feeding, but CYP7A1 and ABCG1 were significantly upregulated in the liver. This finding implies an increased cholesterol efflux and pronounced bile acid conversion similar to our observation in wild type mice fed for shorter time periods. Additionally, LDLR, SREBP1c and ACC were significantly downregulated in the macrophages as was SREBP1c in ileum of 11 weeks-fed mice, suggesting less cholesterol uptake and less fatty acid production. In the liver SREBP1c, FAS, and ChREBP showed no change in regulation upon DMHCA feeding.

Similar to our long-term feeding results, short-term feeding of DMHCA in chow and WTD led to increased ABCA1 mRNA expression in macrophages, aorta, and ileum while its expression remained unchanged in liver. It is known that upregulation of ABC transporters A1 and G1 promotes reverse cholesterol transport of unesterified cholesterol and phospholipids to produce HDL (256-258). HDL cholesterol is delivered to the liver where an LXR-dependent increase of CYP7A1 leads to conversion of cholesterol to bile acids. It has been shown that LXR activation leads to reduced cholesterol absorption (259). We therefore investigated gene regulation upon DMHCA

treatment in the small intestine upon different DMHCA treatments. An increase of the ABC transporters A1, G1, and G5 in ileum of the long-term fed mice was detected. Additionally, an increase of these genes in ilea of short-term fed wild type and ApoE-/- mice was found in ileum and/or duodenum, but T0901317 always led to a more pronounced effect. Niemann Pick like 1 gene (NPC1L1), which is responsible for intestinal cholesterol absorption, was reduced in duodenum upon DMHCA treatment, but increased upon T090317 treatment (104). LXR-mediated conversion of cholesterol to bile acids and further excretion together with decreased intestinal cholesterol uptake are responsible for lower body cholesterol (260, 261). Ezetimibe is a drug that inhibits cholesterol absorption, which results in a reduced delivery of cholesterol back to the liver and thus reduced cholesterol accumulation in the liver. We have shown reduced cholesterol absorption (T. Pfeifer et al. unpublished) and also demonstrated reduced expression of SREBP1c in long-term fed mice. Furthermore, we examined potential liver damage by measuring bilirubin. Bilirubin is a breakdown product of the heme catabolism and it is excreted to the bile. In case of disease its levels are elevated. We therefore measured the bilirubin levels in the plasma of our chronic treatments and found that they were comparable between control and DMCHA treated ApoE-/- mice. Thus, we deduced no liver damage in the DMHCA treated mice. Moreover, FPLC separation of plasma lipoproteins showed a 55% reduction in TG content of the VLDL fraction as well as a 20% of TC, in female ApoE-/- mice fed DMHCA.

Although the same trend for body weight increase and plasma parameters was found in the LDLR-/- mice, plasma parameters did not give a significant difference in the overnight fasted animals and we could not detect significant plaque reduction. These differences might have resulted from too low numbers of animals since we used only 4 and 5 mice, of which only 3 were taken for plaque determination. Additionally, the feeding period might have been too long and the differences between groups got less pronounced.

The second part of this thesis is related to an indirect risk factor of cardiovascular disease. Chronic kidney disease leads to vascular calcification and patients suffering from renal failure most often die from cardiovascular events rather than from renal failure. ApoE-/- and LDLR-/- mice with partial kidney ablation served as a model for chronic kidney disease and were fed a Ca^{2+} and Mg^{2+} adapted chow diet or WTD to induce atherosclerosis and vascular calcification. The aim was to compare traditional staining techniques for lipid and calcium accumulation with non-invasive microscopy techniques. Stainings and imaging were performed in aortas and cryosections of arteries from the aorta and both methods revealed highest plaque development and vascular calcification on WTD-fed mice, where one total kidney and 2/3 of the second kidney were removed.

Second harmonic generation/two photon excitation (SHG/TPE) microscopy has already been used in an aortic mouse model (194) and coherent anti-Stokes Raman scattering (CARS) also showed to be working *ex vivo* and *in vivo*, e.g. for detecting lipid droplets in the intestine (262) as well as for differentiation between saturated and unsaturated lipids in adipocytes (201). Since we lacked the equipment for *in vivo* imaging, we performed all our imaging *ex vivo*, but certainly *in vivo* application is planned. SHG/TPE allows detection of collagen and elastin within the vasculature and partly within atherosclerotic plaque areas. In fact, these techniques could help to detect collagen deposits, a hallmark of late-stage atherosclerosis, within the plaque area. We were able to detect lipids in the atherosclerotic plaques with oil red O staining as well as with CARS combined with SHG/TPE. Moreover, CARS allowed for the first time detection of calcium deposits in form of calcium hydroxyapatite within the atherosclerotic plaque as an alternative to the conventional von Kossa staining. Application of CARS led to identification of certain cell types within the plaque area. These data are currently further investigated, because these cells might be macrophages, foam cells, vascular smooth muscle cells, or a combination of all of them. An important issue is the quantification of plaque areas as well as calcification areas, which should show the same efficiency in both applications. Applying computer software after imaging gives the solution to this issue. In fact, our data suggest that non-invasive imaging will become more important in future applications as it reduces animal and material costs. It allows continuous imaging for both prevention and treatment studies without killing animals at an early stage of intervention or treatment. Additionally, the possibility of three-dimensional videos of an aorta is given, which is not possible to show in this thesis. The only disadvantage is the costs of the set-up itself but this implies the necessity of core facilities for certain equipment.

In conclusion, independent of dosage, treatment time and type of delivery, we could show that DMHCA has a beneficial effect on gene regulation relevant for cholesterol efflux and RCT in macrophages, conversion of cholesterol to bile acids and cholesterol efflux in the liver and cholesterol absorption in the intestine. Interestingly, DMHCA shows a distinct difference in gene regulation of LXR targets involved in lipid metabolism in animals, which was supported by our microarray data. Most known LXR targets related to cholesterol efflux such as the ABC transporters were usually more pronounce upon T0901317 treatment but also significantly increased upon DMHCA treatment. In fact, the microarray data revealed promising new targets, which significantly differ in the regulation when DMHCA and T0901317 treatments were compared. Thereof some were related to inflammatory pathways, which might become more and more important since one has to keep in mind that atherosclerosis is an inflammatory disease. The data received in the *in vitro* experiments sustained the antiatherosclerotic properties of DMHCA. Downregulation of genes from the cholesterol biosynthesis in macrophages together with decreased expression of LDLR

leads to less *in situ* synthesis of cholesterol as well as less uptake of LDL-cholesterol, which diminishes the formation of foam cells, the hallmark of atherosclerosis.

A drawback in the usability of DMHCA is the high degree of direct excretion and thus lack in bioavailability of the drug as well as the fact that it blocks DHCR24 and consequently leads to accumulation of desmosterol. It would be interesting though to perform chromatin immunoprecipitation assays to find out if our potential target genes contain LXRE in their promoter region. Moreover, coactivator and corepressor studies might give a better insight in the regulatory mechanisms of DMHCA.

10 Abbreviations and Acronyms

CVD cardiovascular disease
CKD chronic kidney disease
CRF chronic renal failure
WHO world health organization
LDL low density lipoprotein
LDLR low density lipoprotein receptor
VLDL very low density lipoprotein
HDL high density lipoprotein
acLDL acetylated low density lipoprotein
oxLDL oxidized low density lipoprotein
aggLDL aggregated low density lipoprotein
mmLDL minimally modified LDL
SMC smooth muscle cells
VSMC vascular smooth muscle cells
VCAM vascular cell adhesion molecule
ICAM intracellular adhesion molecule
MCP-1 macrophage chemotactic protein
CCR-2 C-C chemokine receptor 2
MMP matrix metalloproteinase
iNOS inductible nitrix oxide synthase
NADPH nicotinamide adenine dinucleotide phosphate
M-CSF macrophage colony stimulating factor
MSR-A macrophage scavenger receptor A
Th T helper cells
IFN-γ interferon gamma
CD40 member of the TNF-receptor superfamily
IL interleukin
ET-1 endothelin-1
HmgCoAr hydroxymethyl glutary coenzyme A reductase
FC free (unesterified) cholesterol
CE cholesterol ester
DHCR7 7-dehydrocholesterol
RCT reverse cholesterol transport

BBB blood brain barrier

BA bile acids

IHD ischaemic heart disease

PPARα peroxisome proliferator activated receptor alpha

Pi phosphorous

ATP adenosine triphosphate

PMA phorbol 12-myristate 13-acetate

SR-BI Scavenger receptor class B type I

NPC1L1 Niemann Pick C1 like 1

CD36 fatty acid translocase (FAT)

FA fatty acids

FFA free fatty acids

CRF chronic renal failure

ApoE apolipoprotein E

ER endoplasmic reticulum

UPR unfolded protein response

HmgCoAr 3-hydroxymethyl-3-methylglutaryl-CoenzymeA reductase

NSDHL NADH steroid dehydrogenase-like

LBR lamin B receptor

NR nuclear (hormone) receptors

LBD ligand binding domain

DBD DNA binding domain

LBP ligand binding pocket

TF transcription factor

LXR liver X receptor

RXR retinoid X receptor

TF transcription factor

SUMO small ubiquitin-related modifier

MPS mononuclear phagocyte system

TGF transforming growth factor

FGF fibroblast growth factor

SSD sterol sensing domain

INSIG insulin induced gene

SRE sterol response element

bHLH basic-helix-loop-helix

LPL lipoprotein lipase

CETP cholesterol ester transfer protein

LCAT lecithin-cholesterol acyltransferase

FAS fatty acid synthase

SREBP1c sterol regulatory element binding protein

ABCA1 adenosine triphosphate binding cassette transporter A 1

CoA coenzyme A

TG triglyceride

PL phospholipid

BA bile acid

HAT histone acetyltransferase

HMT histone methyltransferase

NMR nuleosome remodeling

HDAC histone deacetylase

HMT histone methyl transferase

HDM histone demethylase

SNuRMs small molecule nuclear receptor modulators

GR glucocorticoid receptor

EC endothelial cells

BL/6 C57BL/6J

M-CSF macrophage colony stimulating factor

MCP-1 macrophage chemoattractant protein 1

HO-1 heme oxygenase 1

ALT alanine transaminase or alanine aminotransferase (ALAT)

AST aspartate transaminase, similar to ALT

MPM mouse peritoneal macrophages

CMC carboxymethylcellulose

DKO double knock-out

Trb3 tribbles homolog 3

BMP2 bone morphogenic protein

MM mismatch

CTSD cathepsin D

TLC thin lazer chromatography

KOH kalium hydroxide

Mp melting point

RT room temperature

R*f* retention factor

BW body weight

FC fold change

11 Bibliography

1. Kwiterovich, P.O., Jr. 2008. Recognition and management of dyslipidemia in children and adolescents. *J Clin Endocrinol Metab* 93:4200-4209.
2. Kannel, W.B. 1998. Overview of atherosclerosis. *Clin Ther* 20 Suppl B:B2-17.
3. Glass, C.K., and Witztum, J.L. 2001. Atherosclerosis. the road ahead. *Cell* 104:503-516.
4. Hume, D. 2006. The mononuclear phagocyte system. *Curr Opin Immunol* 18:49-53.
5. Gordon, S., and Taylor, P.R. 2005. Monocyte and macrophage heterogeneity. *Nat Rev Immunol* 5:953-964.
6. Rock, R.B., and Peterson, P.K. 2006. Microglia as a pharmacological target in infectious and inflammatory diseases of the brain. *J Neuroimmune Pharmacol* 1:117-126.
7. Bobryshev, Y.V. 2006. Monocyte recruitment and foam cell formation in atherosclerosis. *Micron* 37:208-222.
8. Van Ginderachter, J., Movahedi, K., Van den Bossche, J., and De Baetselier, P. 2008. Macrophages, PPARs, and Cancer. *PPAR Res* 2008:169414.
9. Porcheray, F., Viaud, S., Rimaniol, A.C., Leone, C., Samah, B., Dereuddre-Bosquet, N., Dormont, D., and Gras, G. 2005. Macrophage activation switching: an asset for the resolution of inflammation. *Clin Exp Immunol* 142:481-489.
10. Gordon, S. 2003. Alternative activation of macrophages. *Nat Rev Immunol* 3:23-35.
11. Mantovani, A., Muzio, M., Garlanda, C., Sozzani, S., and Allavena, P. 2001. Macrophage control of inflammation: negative pathways of regulation of inflammatory cytokines. *Novartis Found Symp* 234:120-131; discussion 131-125.
12. Bouhlel, M., Derudas, B., Rigamonti, E., Dievart, R., Brozek, J., Haulon, S., Zawadzki, C., Jude, B., Torpier, G., Marx, N., et al. 2007. PPARgamma activation primes human monocytes into alternative M2 macrophages with anti-inflammatory properties. *Cell Metab* 6:137-143.
13. Charo, I. 2007. Macrophage polarization and insulin resistance: PPARgamma in control. *Cell Metab* 6:96-98.
14. Berk, B.C. 2001. Vascular smooth muscle growth: autocrine growth mechanisms. *Physiol Rev* 81:999-1030.
15. Stary, H.C., Blankenhorn, D.H., Chandler, A.B., Glagov, S., Insull, W., Jr., Richardson, M., Rosenfeld, M.E., Schaffer, S.A., Schwartz, C.J., Wagner, W.D., et al. 1992. A definition of the intima of human arteries and of its atherosclerosis-prone regions. A report from the Committee on Vascular Lesions of the Council on Arteriosclerosis, American Heart Association. *Arterioscler Thromb* 12:120-134.
16. Doran, A.C., Meller, N., and McNamara, C.A. 2008. Role of smooth muscle cells in the initiation and early progression of atherosclerosis. *Arterioscler Thromb Vasc Biol* 28:812-819.
17. Clowes, A.W., Reidy, M.A., and Clowes, M.M. 1983. Kinetics of cellular proliferation after arterial injury. I. Smooth muscle growth in the absence of endothelium. *Lab Invest* 49:327-333.
18. Owens, G.K., Kumar, M.S., and Wamhoff, B.R. 2004. Molecular regulation of vascular smooth muscle cell differentiation in development and disease. *Physiol Rev* 84:767-801.

19. Rong, J.X., Shapiro, M., Trogan, E., and Fisher, E.A. 2003. Transdifferentiation of mouse aortic smooth muscle cells to a macrophage-like state after cholesterol loading. *Proc Natl Acad Sci U S A* 100:13531-13536.

20. Nagao, S., Murao, K., Imachi, H., Cao, W.M., Yu, X., Li, J., Matsumoto, K., Nishiuchi, T., Ahmed, R.A., Wong, N.C., et al. 2006. Platelet derived growth factor regulates ABCA1 expression in vascular smooth muscle cells. *FEBS Lett* 580:4371-4376.

21. Collin-Osdoby, P. 2004. Regulation of vascular calcification by osteoclast regulatory factors RANKL and osteoprotegerin. *Circ Res* 95:1046-1057.

22. Trion, A., and van der Laarse, A. 2004. Vascular smooth muscle cells and calcification in atherosclerosis. *Am Heart J* 147:808-814.

23. Trion, A., Schutte-Bart, C., Bax, W.H., Jukema, J.W., and van der Laarse, A. 2008. Modulation of calcification of vascular smooth muscle cells in culture by calcium antagonists, statins, and their combination. *Mol Cell Biochem* 308:25-33.

24. Papaioannou, T.G., Karatzis, E.N., Vavuranakis, M., Lekakis, J.P., and Stefanadis, C. 2006. Assessment of vascular wall shear stress and implications for atherosclerotic disease. *Int J Cardiol* 113:12-18.

25. Saran, A.M., and DuBose, T.D., Jr. 2008. Cardiovascular disease in chronic kidney disease. *Ther Adv Cardiovasc Dis* 2:425-434.

26. Glass, C.K. 2006. Going nuclear in metabolic and cardiovascular disease. *J Clin Invest* 116:556-560.

27. He, Y., Kwan, W.C., and Steinbrecher, U.P. 1996. Effects of oxidized low density lipoprotein on endothelin secretion by cultured endothelial cells and macrophages. *Atherosclerosis* 119:107-118.

28. Brundert, M., Heeren, J., Bahar-Bayansar, M., Ewert, A., Moore, K.J., and Rinninger, F. 2006. Selective uptake of HDL cholesteryl esters and cholesterol efflux from mouse peritoneal macrophages independent of SR-BI. *J Lipid Res* 47:2408-2421.

29. Mahmoudi, M., Curzen, N., and Gallagher, P.J. 2007. Atherogenesis: the role of inflammation and infection. *Histopathology* 50:535-546.

30. Pinderski, L.J., Fischbein, M.P., Subbanagounder, G., Fishbein, M.C., Kubo, N., Cheroutre, H., Curtiss, L.K., Berliner, J.A., and Boisvert, W.A. 2002. Overexpression of interleukin-10 by activated T lymphocytes inhibits atherosclerosis in LDL receptor-deficient Mice by altering lymphocyte and macrophage phenotypes. *Circ Res* 90:1064-1071.

31. Tiwari, R., Singh, V., and Barthwal, M. 2008. Macrophages: an elusive yet emerging therapeutic target of atherosclerosis. *Med Res Rev* 28:483-544.

32. Feng, B., Yao, P., Li, Y., Devlin, C., Zhang, D., Harding, H., Sweeney, M., Rong, J., Kuriakose, G., Fisher, E., et al. 2003. The endoplasmic reticulum is the site of cholesterol-induced cytotoxicity in macrophages. *Nat Cell Biol* 5:781-792.

33. Liang, C., Han, S., Senokuchi, T., and Tall, A. 2007. The macrophage at the crossroads of insulin resistance and atherosclerosis. *Circ Res* 100:1546-1555.

34. Moulton, K.S., Heller, E., Konerding, M.A., Flynn, E., Palinski, W., and Folkman, J. 1999. Angiogenesis inhibitors endostatin or TNP-470 reduce intimal neovascularization and plaque growth in apolipoprotein E-deficient mice. *Circulation* 99:1726-1732.

35. Kockx, M.M., and Herman, A.G. 2000. Apoptosis in atherosclerosis: beneficial or detrimental? *Cardiovasc Res* 45:736-746.

36. Meir, K.S., and Leitersdorf, E. 2004. Atherosclerosis in the apolipoprotein-E-deficient mouse: a decade of progress. *Arterioscler Thromb Vasc Biol* 24:1006-1014.

37. Stary, H.C., Chandler, A.B., Glagov, S., Guyton, J.R., Insull, W., Jr., Rosenfeld, M.E., Schaffer, S.A., Schwartz, C.J., Wagner, W.D., and Wissler, R.W. 1994. A definition of initial, fatty streak, and intermediate lesions of atherosclerosis. A report from the Committee on Vascular Lesions of the Council on Arteriosclerosis, American Heart Association. *Circulation* 89:2462-2478.

38. Stary, H., C, Chandler, A., B, Dinsmore, R., E, Fuster, V., Glagov, S., Insull, W., Rosenfeld, M., E, Schwartz, C., J, Wagner, W., D, and Wissler, R., W. 1995. A definition of advanced types of atherosclerotic lesions and a histological classification of atherosclerosis. A report from the Committee on Vascular Lesions of the Council on Arteriosclerosis, American Heart Association. *Arteriosclerosis, Thrombosis, and Vascular Biology Arterioscler Thromb Vasc Biol* 15:1512-1531.

39. Pepine, C.J. 1998. The effects of angiotensin-converting enzyme inhibition on endothelial dysfunction: potential role in myocardial ischemia. *Am J Cardiol* 82:23S-27S.

40. Hruska, K.A., Mathew, S., Lund, R., Qiu, P., and Pratt, R. 2008. Hyperphosphatemia of chronic kidney disease. *Kidney Int* 74:148-157.

41. Tyson, K.L., Reynolds, J.L., McNair, R., Zhang, Q., Weissberg, P.L., and Shanahan, C.M. 2003. Osteo/chondrocytic transcription factors and their target genes exhibit distinct patterns of expression in human arterial calcification. *Arterioscler Thromb Vasc Biol* 23:489-494.

42. Mathew, S., Tustison, K.S., Sugatani, T., Chaudhary, L.R., Rifas, L., and Hruska, K.A. 2008. The mechanism of phosphorus as a cardiovascular risk factor in CKD. *J Am Soc Nephrol* 19:1092-1105.

43. Reynolds, J.L., Joannides, A.J., Skepper, J.N., McNair, R., Schurgers, L.J., Proudfoot, D., Jahnen-Dechent, W., Weissberg, P.L., and Shanahan, C.M. 2004. Human vascular smooth muscle cells undergo vesicle-mediated calcification in response to changes in extracellular calcium and phosphate concentrations: a potential mechanism for accelerated vascular calcification in ESRD. *J Am Soc Nephrol* 15:2857-2867.

44. Massy, Z.A., Ivanovski, O., Nguyen-Khoa, T., Angulo, J., Szumilak, D., Mothu, N., Phan, O., Daudon, M., Lacour, B., Drueke, T.B., et al. 2005. Uremia accelerates both atherosclerosis and arterial calcification in apolipoprotein E knockout mice. *J Am Soc Nephrol* 16:109-116.

45. Olson, R.E. 1998. Discovery of the lipoproteins, their role in fat transport and their significance as risk factors. *J Nutr* 128:439S-443S.

46. Maxfield, F.R., and Tabas, I. 2005. Role of cholesterol and lipid organization in disease. *Nature* 438:612-621.

47. Dietschy, J.M., and Turley, S.D. 2001. Cholesterol metabolism in the brain. *Curr Opin Lipidol* 12:105-112.

48. Jones, P.J. 1997. Regulation of cholesterol biosynthesis by diet in humans. *Am J Clin Nutr* 66:438-446.

49. Grundy, S.M. 1983. Absorption and metabolism of dietary cholesterol. *Annu Rev Nutr* 3:71-96.

50. Wilson, M.D., and Rudel, L.L. 1994. Review of cholesterol absorption with emphasis on dietary and biliary cholesterol. *J Lipid Res* 35:943-955.

51. Herman, G.E. 2003. Disorders of cholesterol biosynthesis: prototypic metabolic malformation syndromes. *Hum Mol Genet* 12 Spec No 1:R75-88.

52. Koolman, J., Roehm, KH. 1998. *Taschenatlas der Biochemie*.

53. Twiner, M., Rehmann, N., Hess, P., and Doucette, G. 2008. Azaspiracid shellfish poisoning: a review on the chemistry, ecology, and toxicology with an emphasis on human health impacts. *Mar Drugs* 6:39-72.

54. Wojcicka, G., Jamroz-Wisniewska, A., Horoszewicz, K., and Beltowski, J. 2007. Liver X receptors (LXRs). Part I: structure, function, regulation of activity, and role in lipid metabolism. *Postepy Hig Med Dosw (Online)* 61:736-759.

55. Kelley, R.I., and Herman, G.E. 2001. Inborn errors of sterol biosynthesis. *Annu Rev Genomics Hum Genet* 2:299-341.

56. Byskov, A.G., Andersen, C.Y., and Leonardsen, L. 2002. Role of meiosis activating sterols, MAS, in induced oocyte maturation. *Mol Cell Endocrinol* 187:189-196.

57. Peet, D., Janowski, B., and Mangelsdorf, D. 1998. The LXRs: a new class of oxysterol receptors. *Curr Opin Genet Dev* 8:571-575.

58. Jeong, J., and McMahon, A.P. 2002. Cholesterol modification of Hedgehog family proteins. *J Clin Invest* 110:591-596.

59. Haas, D., and Hoffmann, G.F. 2006. Mevalonate kinase deficiencies: from mevalonic aciduria to hyperimmunoglobulinemia D syndrome. *Orphanet J Rare Dis* 1:13.

60. Opitz, J.M. 1994. RSH/SLO ("Smith-Lemli-Opitz") syndrome: historical, genetic, and developmental considerations. *Am J Med Genet* 50:344-346.

61. Yu, H., Li, M., Tint, G.S., Chen, J., Xu, G., and Patel, S.B. 2007. Selective reconstitution of liver cholesterol biosynthesis promotes lung maturation but does not prevent neonatal lethality in Dhcr7 null mice. *BMC Dev Biol* 7:27.

62. Fernandes, J., J., S., Van den Berghe, G., and Walter, J.H. 2006. Inborn metabolic diseases: diagnosis and treatment. *Springer*:561.

63. Mirza, R., Hayasaka, S., Takagishi, Y., Kambe, F., Ohmori, S., Maki, K., Yamamoto, M., Murakami, K., Kaji, T., Zadworny, D., et al. 2006. DHCR24 gene knockout mice demonstrate lethal dermopathy with differentiation and maturation defects in the epidermis. *J Invest Dermatol* 126:638-647.

64. Heverin, M., Meaney, S., Brafman, A., Shafir, M., Olin, M., Shafaati, M., von Bahr, S., Larsson, L., Lovgren-Sandblom, A., Diczfalusy, U., et al. 2007. Studies on the cholesterol-free mouse: strong activation of LXR-regulated hepatic genes when replacing cholesterol with desmosterol. *Arterioscler Thromb Vasc Biol* 27:2191-2197.

65. Kuehnle, K., Ledesma, M.D., Kalvodova, L., Smith, A.E., Crameri, A., Skaanes-Brunner, F., Thelen, K.M., Kulic, L., Lutjohann, D., Heppner, F.L., et al. 2009. Age-dependent increase in desmosterol restores DRM formation and membrane-related functions in cholesterol-free DHCR24-/- mice. *Neurochem Res* 34:1167-1182.

66. Yang, C., McDonald, J.G., Patel, A., Zhang, Y., Umetani, M., Xu, F., Westover, E.J., Covey, D.F., Mangelsdorf, D.J., Cohen, J.C., et al. 2006. Sterol intermediates from cholesterol biosynthetic pathway as liver X receptor ligands. *J Biol Chem* 281:27816-27826.

67. Peri, A., and Serio, M. 2008. Neuroprotective effects of the Alzheimer's disease-related gene seladin-1. *J Mol Endocrinol* 41:251-261.

68. Krakowiak, P.A., Wassif, C.A., Kratz, L., Cozma, D., Kovarova, M., Harris, G., Grinberg, A., Yang, Y., Hunter, A.G., Tsokos, M., et al. 2003. Lathosterolosis: an inborn error of human and murine cholesterol synthesis due to lathosterol 5-desaturase deficiency. *Hum Mol Genet* 12:1631-1641.

69. Brown, M., and Goldstein, J. 1999. A proteolytic pathway that controls the cholesterol content of membranes, cells, and blood. *Proc Natl Acad Sci U S A* 96:11041-11048.

70. Brown, M.S., and Goldstein, J.L. 1997. The SREBP pathway: regulation of cholesterol metabolism by proteolysis of a membrane-bound transcription factor. *Cell* 89:331-340.

71. Horton, J., Goldstein, J., and Brown, M. 2002. SREBPs: activators of the complete program of cholesterol and fatty acid synthesis in the liver. *J Clin Invest* 109:1125-1131.

72. Goldstein, J.L., DeBose-Boyd, R.A., and Brown, M.S. 2006. Protein sensors for membrane sterols. *Cell* 124:35-46.

73. Espenshade, P.J., and Hughes, A.L. 2007. Regulation of sterol synthesis in eukaryotes. *Annu Rev Genet* 41:401-427.

74. Bengoechea-Alonso, M.T., and Ericsson, J. 2007. SREBP in signal transduction: cholesterol metabolism and beyond. *Curr Opin Cell Biol* 19:215-222.

75. Feramisco, J.D., Radhakrishnan, A., Ikeda, Y., Reitz, J., Brown, M.S., and Goldstein, J.L. 2005. Intramembrane aspartic acid in SCAP protein governs cholesterol-induced conformational change. *Proc Natl Acad Sci U S A* 102:3242-3247.

76. Sun, L.P., Li, L., Goldstein, J.L., and Brown, M.S. 2005. Insig required for sterol-mediated inhibition of Scap/SREBP binding to COPII proteins in vitro. *J Biol Chem* 280:26483-26490.

77. Bjorkhem, I., and Meaney, S. 2004. Brain cholesterol: long secret life behind a barrier. *Arterioscler Thromb Vasc Biol* 24:806-815.

78. Soccio, R., and Breslow, J. 2004. Intracellular cholesterol transport. *Arterioscler Thromb Vasc Biol* 24:1150-1160.

79. Rader, D.J., and Daugherty, A. 2008. Translating molecular discoveries into new therapies for atherosclerosis. *Nature* 451:904-913.

80. Mahley, R.W., Huang, Y., and Weisgraber, K.H. 2006. Putting cholesterol in its place: apoE and reverse cholesterol transport. *J Clin Invest* 116:1226-1229.

81. Tontonoz, P., and Mangelsdorf, D. 2003. Liver X receptor signaling pathways in cardiovascular disease. *Mol Endocrinol* 17:985-993.

82. Groen, A.K., Oude Elferink, R.P., Verkade, H.J., and Kuipers, F. 2004. The ins and outs of reverse cholesterol transport. *Ann Med* 36:135-145.

83. Linsel-Nitschke, P., and Tall, A.R. 2005. HDL as a target in the treatment of atherosclerotic cardiovascular disease. *Nat Rev Drug Discov* 4:193-205.

84. Mahley, R.W. 1985. Atherogenic lipoproteins and coronary artery disease: concepts derived from recent advances in cellular and molecular biology. *Circulation* 72:943-948.

85. Norlin, M., and Wikvall, K. 2007. Enzymes in the conversion of cholesterol into bile acids. *Curr Mol Med* 7:199-218.

86. Altmann, S.W., Davis, H.R., Jr., Zhu, L.J., Yao, X., Hoos, L.M., Tetzloff, G., Iyer, S.P., Maguire, M., Golovko, A., Zeng, M., et al. 2004. Niemann-Pick C1 Like 1 protein is critical for intestinal cholesterol absorption. *Science* 303:1201-1204.

87. Drover, V.A., Ajmal, M., Nassir, F., Davidson, N.O., Nauli, A.M., Sahoo, D., Tso, P., and Abumrad, N.A. 2005. CD36 deficiency impairs intestinal lipid secretion and clearance of chylomicrons from the blood. *J Clin Invest* 115:1290-1297.

88. Kramer, W., Girbig, F., Corsiero, D., Burger, K., Fahrenholz, F., Jung, C., and Muller, G. 2003. Intestinal cholesterol absorption: identification of different binding proteins for cholesterol and cholesterol absorption inhibitors in the enterocyte brush border membrane. *Biochim Biophys Acta* 1633:13-26.

89. Kruit, J.K., Groen, A.K., van Berkel, T.J., and Kuipers, F. 2006. Emerging roles of the intestine in control of cholesterol metabolism. *World J Gastroenterol* 12:6429-6439.

90. Nassir, F., Wilson, B., Han, X., Gross, R.W., and Abumrad, N.A. 2007. CD36 is important for fatty acid and cholesterol uptake by the proximal but not distal intestine. *J Biol Chem* 282:19493-19501.

91. Mardones, P., Quinones, V., Amigo, L., Moreno, M., Miquel, J.F., Schwarz, M., Miettinen, H.E., Trigatti, B., Krieger, M., VanPatten, S., et al. 2001. Hepatic cholesterol and bile acid metabolism and intestinal cholesterol absorption in scavenger receptor class B type I-deficient mice. *J Lipid Res* 42:170-180.

92. Bietrix, F., Yan, D., Nauze, M., Rolland, C., Bertrand-Michel, J., Comera, C., Schaak, S., Barbaras, R., Groen, A.K., Perret, B., et al. 2006. Accelerated lipid absorption in mice overexpressing intestinal SR-BI. *J Biol Chem* 281:7214-7219.

93. Voshol, P.J., Schwarz, M., Rigotti, A., Krieger, M., Groen, A.K., and Kuipers, F. 2001. Down-regulation of intestinal scavenger receptor class B, type I (SR-BI) expression in rodents under conditions of deficient bile delivery to the intestine. *Biochem J* 356:317-325.

94. Plosch, T., Kok, T., Bloks, V.W., Smit, M.J., Havinga, R., Chimini, G., Groen, A.K., and Kuipers, F. 2002. Increased hepatobiliary and fecal cholesterol excretion upon activation of the liver X receptor is independent of ABCA1. *J Biol Chem* 277:33870-33877.

95. Yu, L., York, J., von Bergmann, K., Lutjohann, D., Cohen, J.C., and Hobbs, H.H. 2003. Stimulation of cholesterol excretion by the liver X receptor agonist requires ATP-binding cassette transporters G5 and G8. *J Biol Chem* 278:15565-15570.

96. Endo, A. 1992. The discovery and development of HMG-CoA reductase inhibitors. *J Lipid Res* 33:1569-1582.

97. Law, M.R., Wald, N.J., and Rudnicka, A.R. 2003. Quantifying effect of statins on low density lipoprotein cholesterol, ischaemic heart disease, and stroke: systematic review and meta-analysis. *BMJ* 326:1423.

98. Furberg, C.D. 1999. Natural statins and stroke risk. *Circulation* 99:185-188.

99. Graham, D.J., Staffa, J.A., Shatin, D., Andrade, S.E., Schech, S.D., La Grenade, L., Gurwitz, J.H., Chan, K.A., Goodman, M.J., and Platt, R. 2004. Incidence of hospitalized rhabdomyolysis in patients treated with lipid-lowering drugs. *JAMA* 292:2585-2590.

100. Barter, P.J., and Rye, K.A. 2006. Cardioprotective properties of fibrates: which fibrate, which patients, what mechanism? *Circulation* 113:1553-1555.

101. Robinson, D.M., and Keating, G.M. 2007. Colesevelam: a review of its use in hypercholesterolemia. *Am J Cardiovasc Drugs* 7:453-465.

102. Kamanna, V.S., and Kashyap, M.L. 2008. Mechanism of action of niacin. *Am J Cardiol* 101:20B-26B.

103. Brown, B.G., and Zhao, X.Q. 2008. Nicotinic acid, alone and in combinations, for reduction of cardiovascular risk. *Am J Cardiol* 101:58B-62B.

104. Garcia-Calvo, M., Lisnock, J., Bull, H.G., Hawes, B.E., Burnett, D.A., Braun, M.P., Crona, J.H., Davis, H.R., Jr., Dean, D.C., Detmers, P.A., et al. 2005. The target of ezetimibe is Niemann-Pick C1-Like 1 (NPC1L1). *Proc Natl Acad Sci U S A* 102:8132-8137.

105. Temel, R.E., Tang, W., Ma, Y., Rudel, L.L., Willingham, M.C., Ioannou, Y.A., Davies, J.P., Nilsson, L.M., and Yu, L. 2007. Hepatic Niemann-Pick C1-like 1 regulates biliary cholesterol concentration and is a target of ezetimibe. *J Clin Invest* 117:1968-1978.

106. Gomez-Garre, D., Munoz-Pacheco, P., Gonzalez-Rubio, M., Aragoncillo, P., Granados, R., and Fernandez-Cruz, A. 2009. Ezetimibe reduces plaque inflammation in a rabbit model of atherosclerosis and inhibits monocyte migration in addition to its lipid-lowering effect. *Br J Pharmacol*.

107. Terasaka, N., Hiroshima, A., Koieyama, T., Ubukata, N., Morikawa, Y., Nakai, D., and Inaba, T. 2003. T-0901317, a synthetic liver X receptor ligand, inhibits development of atherosclerosis in LDL receptor-deficient mice. *FEBS Letters FEBS Lett* 536:6-11.

108. Joseph, S., B, McKilligin, E., Pei, L., Watson, M., A, Collins, A., R, Laffitte, B., A, Chen, M., Noh, G., Goodman, J., Hagger, G., N, et al. 2002. Synthetic LXR ligand inhibits the development of atherosclerosis in mice. *Proceedings of the National Academy of Sciences of the United States of America Proc Natl Acad Sci U S A* 99:7604-7609.

109. Aranda, A., and Pascual, A. 2001. Nuclear hormone receptors and gene expression. *Physiol Rev* 81:1269-1304.

110. Escriva Garcia, H., Laudet, V., and Robinson-Rechavi, M. 2003. Nuclear receptors are markers of animal genome evolution. *J Struct Funct Genomics* 3:177-184.

111. Barish, G.D., Downes, M., Alaynick, W.A., Yu, R.T., Ocampo, C.B., Bookout, A.L., Mangelsdorf, D.J., and Evans, R.M. 2005. A Nuclear Receptor Atlas: macrophage activation. *Mol Endocrinol* 19:2466-2477.

112. Rastinejad, F., Perlmann, T., Evans, R.M., and Sigler, P.B. 1995. Structural determinants of nuclear receptor assembly on DNA direct repeats. *Nature* 375:203-211.

113. Laudet, V., and Gronemeyer, H. 2001. *THE NUCLEAR RECEPTOR facts book*: Academic press.

114. Owen, G.I., and Zelent, A. 2000. Origins and evolutionary diversification of the nuclear receptor superfamily. *Cell Mol Life Sci* 57:809-827.

115. Olefsky, J. 2001. Nuclear receptor minireview series. *J Biol Chem* 276:36863-36864.

116. Germain, P., Staels, B., Dacquet, C., Spedding, M., and Laudet, V. 2006. Overview of nomenclature of nuclear receptors. *Pharmacol Rev* 58:685-704.

117. Shulman, A.I., Larson, C., Mangelsdorf, D.J., and Ranganathan, R. 2004. Structural determinants of allosteric ligand activation in RXR heterodimers. *Cell* 116:417-429.

118. Mangelsdorf, D.J., Thummel, C., Beato, M., Herrlich, P., Schutz, G., Umesono, K., Blumberg, B., Kastner, P., Mark, M., Chambon, P., et al. 1995. The nuclear receptor superfamily: the second decade. *Cell* 83:835-839.

119. Escriva, H., Delaunay, F., and Laudet, V. 2000. Ligand binding and nuclear receptor evolution. *Bioessays* 22:717-727.

120. Szanto, A., Narkar, V., Shen, Q., Uray, I.P., Davies, P.J., and Nagy, L. 2004. Retinoid X receptors: X-ploring their (patho)physiological functions. *Cell Death Differ* 11 Suppl 2:S126-143.

121. Thornton, J.W., and DeSalle, R. 2000. A new method to localize and test the significance of incongruence: detecting domain shuffling in the nuclear receptor superfamily. *Syst Biol* 49:183-201.

122. Otte, K., Kranz, H., Kober, I., Thompson, P., Hoefer, M., Haubold, B., Remmel, B., Voss, H., Kaiser, C., Albers, M., et al. 2003. Identification of farnesoid X receptor beta as a novel mammalian nuclear receptor sensing lanosterol. *Mol Cell Biol* 23:864-872.

123. Robinson-Rechavi, M., Carpentier, A.S., Duffraisse, M., and Laudet, V. 2001. How many nuclear hormone receptors are there in the human genome? *Trends Genet* 17:554-556.

124. Svensson, S., Ostberg, T., Jacobsson, M., Norstrom, C., Stefansson, K., Hallen, D., Johansson, I.C., Zachrisson, K., Ogg, D., and Jendeberg, L. 2003. Crystal structure of the heterodimeric complex of LXRalpha and RXRbeta ligand-binding domains in a fully agonistic conformation. *EMBO J* 22:4625-4633.

125. Heery, D.M., Kalkhoven, E., Hoare, S., and Parker, M.G. 1997. A signature motif in transcriptional co-activators mediates binding to nuclear receptors. *Nature* 387:733-736.

126. Perissi, V., Staszewski, L.M., McInerney, E.M., Kurokawa, R., Krones, A., Rose, D.W., Lambert, M.H., Milburn, M.V., Glass, C.K., and Rosenfeld, M.G. 1999. Molecular determinants of nuclear receptor-corepressor interaction. *Genes Dev* 13:3198-3208.

127. Bannister, A.J., Schneider, R., and Kouzarides, T. 2002. Histone methylation: dynamic or static? *Cell* 109:801-806.

128. Jenuwein, T., and Allis, C.D. 2001. Translating the histone code. *Science* 293:1074-1080.

129. Lee, D.Y., Teyssier, C., Strahl, B.D., and Stallcup, M.R. 2005. Role of protein methylation in regulation of transcription. *Endocr Rev* 26:147-170.

130. Tsukada, Y., Fang, J., Erdjument-Bromage, H., Warren, M.E., Borchers, C.H., Tempst, P., and Zhang, Y. 2006. Histone demethylation by a family of JmjC domain-containing proteins. *Nature* 439:811-816.

131. Yoon, H.G., Chan, D.W., Reynolds, A.B., Qin, J., and Wong, J. 2003. N-CoR mediates DNA methylation-dependent repression through a methyl CpG binding protein Kaiso. *Mol Cell* 12:723-734.

132. Peterson, C.L. 2002. Chromatin remodeling: nucleosomes bulging at the seams. *Curr Biol* 12:R245-247.

133. Rosenfeld, M.G., Lunyak, V.V., and Glass, C.K. 2006. Sensors and signals: a coactivator/corepressor/epigenetic code for integrating signal-dependent programs of transcriptional response. *Genes Dev* 20:1405-1428.

134. McKenna, N.J., Xu, J., Nawaz, Z., Tsai, S.Y., Tsai, M.J., and O'Malley, B.W. 1999. Nuclear receptor coactivators: multiple enzymes, multiple complexes, multiple functions. *J Steroid Biochem Mol Biol* 69:3-12.

135. Torchia, J., Rose, D.W., Inostroza, J., Kamei, Y., Westin, S., Glass, C.K., and Rosenfeld, M.G. 1997. The transcriptional co-activator p/CIP binds CBP and mediates nuclear-receptor function. *Nature* 387:677-684.

136. Chen, J.D., and Evans, R.M. 1995. A transcriptional co-repressor that interacts with nuclear hormone receptors. *Nature* 377:454-457.

137. Horlein, A.J., Naar, A.M., Heinzel, T., Torchia, J., Gloss, B., Kurokawa, R., Ryan, A., Kamei, Y., Soderstrom, M., Glass, C.K., et al. 1995. Ligand-independent repression by the thyroid hormone receptor mediated by a nuclear receptor co-repressor. *Nature* 377:397-404.

138. Perissi, V., and Rosenfeld, M.G. 2005. Controlling nuclear receptors: the circular logic of cofactor cycles. *Nat Rev Mol Cell Biol* 6:542-554.

139. Delmotte, M.H., Tahayato, A., Formstecher, P., and Lefebvre, P. 1999. Serine 157, a retinoic acid receptor alpha residue phosphorylated by protein kinase C in vitro, is involved in RXR.RARalpha heterodimerization and transcriptional activity. *J Biol Chem* 274:38225-38231.

140. Davies, P.J., Berry, S.A., Shipley, G.L., Eckel, R.H., Hennuyer, N., Crombie, D.L., Ogilvie, K.M., Peinado-Onsurbe, J., Fievet, C., Leibowitz, M.D., et al. 2001. Metabolic effects of rexinoids: tissue-specific regulation of lipoprotein lipase activity. *Mol Pharmacol* 59:170-176.

141. Lenhard, J.M., Lancaster, M.E., Paulik, M.A., Weiel, J.E., Binz, J.G., Sundseth, S.S., Gaskill, B.A., Lightfoot, R.M., and Brown, H.R. 1999. The RXR agonist LG100268 causes hepatomegaly, improves glycaemic control and decreases cardiovascular risk and cachexia in diabetic mice suffering from pancreatic beta-cell dysfunction. *Diabetologia* 42:545-554.

142. Mukherjee, R., Davies, P.J., Crombie, D.L., Bischoff, E.D., Cesario, R.M., Jow, L., Hamann, L.G., Boehm, M.F., Mondon, C.E., Nadzan, A.M., et al. 1997. Sensitization of diabetic and obese mice to insulin by retinoid X receptor agonists. *Nature* 386:407-410.

143. Willy, P.J., Umesono, K., Ong, E.S., Evans, R.M., Heyman, R.A., and Mangelsdorf, D.J. 1995. LXR, a nuclear receptor that defines a distinct retinoid response pathway. *Genes Dev* 9:1033-1045.

144. Janowski, B.A., Willy, P.J., Devi, T.R., Falck, J.R., and Mangelsdorf, D.J. 1996. An oxysterol signalling pathway mediated by the nuclear receptor LXR alpha. *Nature* 383:728-731.

145. Costet, P., Luo, Y., Wang, N., and Tall, A.R. 2000. Sterol-dependent transactivation of the ABC1 promoter by the liver X receptor/retinoid X receptor. *J Biol Chem* 275:28240-28245.

146. Repa, J.J., Turley, S.D., Lobaccaro, J.A., Medina, J., Li, L., Lustig, K., Shan, B., Heyman, R.A., Dietschy, J.M., and Mangelsdorf, D.J. 2000. Regulation of absorption and ABC1-mediated efflux of cholesterol by RXR heterodimers. *Science* 289:1524-1529.

147. Schwartz, K., Lawn, R.M., and Wade, D.P. 2000. ABC1 gene expression and ApoA-I-mediated cholesterol efflux are regulated by LXR. *Biochem Biophys Res Commun* 274:794-802.

148. Venkateswaran, A., Repa, J.J., Lobaccaro, J.M., Bronson, A., Mangelsdorf, D.J., and Edwards, P.A. 2000. Human white/murine ABC8 mRNA levels are highly induced in lipid-loaded macrophages. A transcriptional role for specific oxysterols. *J Biol Chem* 275:14700-14707.

149. Venkateswaran, A., Laffitte, B.A., Joseph, S.B., Mak, P.A., Wilpitz, D.C., Edwards, P.A., and Tontonoz, P. 2000. Control of cellular cholesterol efflux by the nuclear oxysterol receptor LXR alpha. *Proc Natl Acad Sci U S A* 97:12097-12102.

150. Li, A.C., and Glass, C.K. 2002. The macrophage foam cell as a target for therapeutic intervention. *Nat Med* 8:1235-1242.

151. Repa, J.J., Liang, G., Ou, J., Bashmakov, Y., Lobaccaro, J.M., Shimomura, I., Shan, B., Brown, M.S., Goldstein, J.L., and Mangelsdorf, D.J. 2000. Regulation of mouse sterol regulatory element-binding protein-1c gene (SREBP-1c) by oxysterol receptors, LXRalpha and LXRbeta. *Genes Dev* 14:2819-2830.

152. Yoshikawa, T., Shimano, H., Amemiya-Kudo, M., Yahagi, N., Hasty, A.H., Matsuzaka, T., Okazaki, H., Tamura, Y., Iizuka, Y., Ohashi, K., et al. 2001. Identification of liver X receptor-retinoid X receptor as an activator of the sterol regulatory element-binding protein 1c gene promoter. *Mol Cell Biol* 21:2991-3000.

153. Zhang, Y., Repa, J.J., Gauthier, K., and Mangelsdorf, D.J. 2001. Regulation of lipoprotein lipase by the oxysterol receptors, LXRalpha and LXRbeta. *J Biol Chem* 276:43018-43024.

154. Joseph, S.B., Laffitte, B.A., Patel, P.H., Watson, M.A., Matsukuma, K.E., Walczak, R., Collins, J.L., Osborne, T.F., and Tontonoz, P. 2002. Direct and indirect mechanisms for regulation of fatty acid synthase gene expression by liver X receptors. *J Biol Chem* 277:11019-11025.

155. Chu, K., Miyazaki, M., Man, W.C., and Ntambi, J.M. 2006. Stearoyl-coenzyme A desaturase 1 deficiency protects against hypertriglyceridemia and increases plasma high-density lipoprotein cholesterol induced by liver X receptor activation. *Mol Cell Biol* 26:6786-6798.

156. Cha, J.Y., and Repa, J.J. 2007. The liver X receptor (LXR) and hepatic lipogenesis. The carbohydrate-response element-binding protein is a target gene of LXR. *J Biol Chem* 282:743-751.

157. Brunham, L.R., Kruit, J.K., Pape, T.D., Parks, J.S., Kuipers, F., and Hayden, M.R. 2006. Tissue-specific induction of intestinal ABCA1 expression with a liver X receptor agonist raises plasma HDL cholesterol levels. *Circ Res* 99:672-674.

158. Repa, J.J., Berge, K.E., Pomajzl, C., Richardson, J.A., Hobbs, H., and Mangelsdorf, D.J. 2002. Regulation of ATP-binding cassette sterol transporters ABCG5 and ABCG8 by the liver X receptors alpha and beta. *J Biol Chem* 277:18793-18800.

159. Lehmann, J.M., Kliewer, S.A., Moore, L.B., Smith-Oliver, T.A., Oliver, B.B., Su, J.L., Sundseth, S.S., Winegar, D.A., Blanchard, D.E., Spencer, T.A., et al. 1997. Activation of the nuclear receptor LXR by oxysterols defines a new hormone response pathway. *J Biol Chem* 272:3137-3140.

160. Joseph, S.B., McKilligin, E., Pei, L., Watson, M.A., Collins, A.R., Laffitte, B.A., Chen, M., Noh, G., Goodman, J., Hagger, G.N., et al. 2002. Synthetic LXR ligand inhibits the development of atherosclerosis in mice. *Proc Natl Acad Sci U S A* 99:7604-7609.

161. Terasaka, N., Hiroshima, A., Koieyama, T., Ubukata, N., Morikawa, Y., Nakai, D., and Inaba, T. 2003. T-0901317, a synthetic liver X receptor ligand, inhibits development of atherosclerosis in LDL receptor-deficient mice. *FEBS Lett* 536:6-11.

162. Torra, I.P., Ismaili, N., Feig, J.E., Xu, C.F., Cavasotto, C., Pancratov, R., Rogatsky, I., Neubert, T.A., Fisher, E.A., and Garabedian, M.J. 2008. Phosphorylation of liver X receptor alpha selectively regulates target gene expression in macrophages. *Mol Cell Biol* 28:2626-2636.

163. Li, X., Zhang, S., Blander, G., Tse, J., Krieger, M., and Guarente, L. 2007. SIRT1 deacetylates and positively regulates the nuclear receptor LXR. *Mol Cell* 28:91-106.

164. Jamroz-Wisniewska, A., Wojcicka, G., Horoszewicz, K., and Beltowski, J. 2007. Liver X receptors (LXRs). Part II: non-lipid effects, role in pathology, and therapeutic implications. *Postepy Hig Med Dosw (Online)* 61:760-785.

165. Laffitte, B.A., Chao, L.C., Li, J., Walczak, R., Hummasti, S., Joseph, S.B., Castrillo, A., Wilpitz, D.C., Mangelsdorf, D.J., Collins, J.L., et al. 2003. Activation of liver X receptor improves glucose tolerance through coordinate regulation of glucose metabolism in liver and adipose tissue. *Proc Natl Acad Sci U S A* 100:5419-5424.

166. Stulnig, T.M., Steffensen, K.R., Gao, H., Reimers, M., Dahlman-Wright, K., Schuster, G.U., and Gustafsson, J.A. 2002. Novel roles of liver X receptors exposed by gene expression profiling in liver and adipose tissue. *Mol Pharmacol* 62:1299-1305.

167. Efanov, A.M., Sewing, S., Bokvist, K., and Gromada, J. 2004. Liver X receptor activation stimulates insulin secretion via modulation of glucose and lipid metabolism in pancreatic beta-cells. *Diabetes* 53 Suppl 3:S75-78.

168. Green, C.D., Jump, D.B., and Olson, L.K. 2009. Elevated Insulin Secretion from Liver X Receptor-Activated Pancreatic Beta-Cells Involves Increased De Novo Lipid Synthesis and Triacylglyceride Turnover. *Endocrinology*.

169. Choe, S.S., Choi, A.H., Lee, J.W., Kim, K.H., Chung, J.J., Park, J., Lee, K.M., Park, K.G., Lee, I.K., and Kim, J.B. 2007. Chronic activation of liver X receptor induces beta-cell apoptosis through hyperactivation of lipogenesis: liver X receptor-mediated lipotoxicity in pancreatic beta-cells. *Diabetes* 56:1534-1543.

170. Kalaany, N.Y., Gauthier, K.C., Zavacki, A.M., Mammen, P.P., Kitazume, T., Peterson, J.A., Horton, J.D., Garry, D.J., Bianco, A.C., and Mangelsdorf, D.J. 2005. LXRs regulate the balance between fat storage and oxidation. *Cell Metab* 1:231-244.

171. Ross, S.E., Erickson, R.L., Gerin, I., DeRose, P.M., Bajnok, L., Longo, K.A., Misek, D.E., Kuick, R., Hanash, S.M., Atkins, K.B., et al. 2002. Microarray analyses during adipogenesis: understanding the effects of Wnt signaling on adipogenesis and the roles of liver X receptor alpha in adipocyte metabolism. *Mol Cell Biol* 22:5989-5999.

172. Joseph, S.B., Castrillo, A., Laffitte, B.A., Mangelsdorf, D.J., and Tontonoz, P. 2003. Reciprocal regulation of inflammation and lipid metabolism by liver X receptors. *Nat Med* 9:213-219.

173. Wang, Y.Y., Dahle, M.K., Agren, J., Myhre, A.E., Reinholt, F.P., Foster, S.J., Collins, J.L., Thiemermann, C., Aasen, A.O., and Wang, J.E. 2006. Activation of the liver X receptor

protects against hepatic injury in endotoxemia by suppressing Kupffer cell activation. *Shock* 25:141-146.

174. Delvecchio, C.J., Bilan, P., Radford, K., Stephen, J., Trigatti, B.L., Cox, G., Parameswaran, K., and Capone, J.P. 2007. Liver X receptor stimulates cholesterol efflux and inhibits expression of proinflammatory mediators in human airway smooth muscle cells. *Mol Endocrinol* 21:1324-1334.

175. Zelcer, N., Khanlou, N., Clare, R., Jiang, Q., Reed-Geaghan, E.G., Landreth, G.E., Vinters, H.V., and Tontonoz, P. 2007. Attenuation of neuroinflammation and Alzheimer's disease pathology by liver x receptors. *Proc Natl Acad Sci U S A* 104:10601-10606.

176. Morello, F., de Boer, R.A., Steffensen, K.R., Gnecchi, M., Chisholm, J.W., Boomsma, F., Anderson, L.M., Lawn, R.M., Gustafsson, J.A., Lopez-Ilasaca, M., et al. 2005. Liver X receptors alpha and beta regulate renin expression in vivo. *J Clin Invest* 115:1913-1922.

177. Janowski, B., Grogan, M., Jones, S., Wisely, G., Kliewer, S., Corey, E., and Mangelsdorf, D. 1999. Structural requirements of ligands for the oxysterol liver X receptors LXRalpha and LXRbeta. *Proc Natl Acad Sci U S A* 96:266-271.

178. Williams, S., Bledsoe, R., Collins, J., Boggs, S., Lambert, M., Miller, A., Moore, J., McKee, D., Moore, L., Nichols, J., et al. 2003. X-ray crystal structure of the liver X receptor beta ligand binding domain: regulation by a histidine-tryptophan switch. *J Biol Chem* 278:27138-27143.

179. Mitro, N., Vargas, L., Romeo, R., Koder, A., and Saez, E. 2007. T0901317 is a potent PXR ligand: implications for the biology ascribed to LXR. *FEBS Lett* 581:1721-1726.

180. Houck, K.A., Borchert, K.M., Hepler, C.D., Thomas, J.S., Bramlett, K.S., Michael, L.F., and Burris, T.P. 2004. T0901317 is a dual LXR/FXR agonist. *Mol Genet Metab* 83:184-187.

181. Quinet, E., M, Savio, D., A, Halpern, A., R, Chen, L., Miller, C., P, and Nambi, P. 2004. Gene-selective modulation by a synthetic oxysterol ligand of the liver X receptor. *Journal of Lipid Research J Lipid Res* 45:1929-1942.

182. Paigen, B. 1995. Genetics of responsiveness to high-fat and high-cholesterol diets in the mouse. *Am J Clin Nutr* 62:458S-462S.

183. Liao, F., Andalibi, A., Lusis, A.J., and Fogelman, A.M. 1995. Genetic control of the inflammatory response induced by oxidized lipids. *Am J Cardiol* 75:65B-66B.

184. Shi, W., Haberland, M.E., Jien, M.L., Shih, D.M., and Lusis, A.J. 2000. Endothelial responses to oxidized lipoproteins determine genetic susceptibility to atherosclerosis in mice. *Circulation* 102:75-81.

185. Rader, D.J., and Pure, E. 2000. Genetic susceptibility to atherosclerosis: insights from mice. *Circ Res* 86:1013-1015.

186. Breslow, J.L. 1996. Mouse models of atherosclerosis. *Science* 272:685-688.

187. Dansky, H.M., Charlton, S.A., Sikes, J.L., Heath, S.C., Simantov, R., Levin, L.F., Shu, P., Moore, K.J., Breslow, J.L., and Smith, J.D. 1999. Genetic background determines the extent of atherosclerosis in ApoE-deficient mice. *Arterioscler Thromb Vasc Biol* 19:1960-1968.

188. Desai, A., Zhao, Y., and Warren, J.S. 2008. Development of atherosclerosis in Balb/c apolipoprotein E-deficient mice. *Cardiovasc Pathol* 17:233-240.

189. Dong, Z.M., Brown, A.A., and Wagner, D.D. 2000. Prominent role of P-selectin in the development of advanced atherosclerosis in ApoE-deficient mice. *Circulation* 101:2290-2295.

190. Zhang, W., Yancey, P.G., Su, Y.R., Babaev, V.R., Zhang, Y., Fazio, S., and Linton, M.F. 2003. Inactivation of macrophage scavenger receptor class B type I promotes atherosclerotic lesion development in apolipoprotein E-deficient mice. *Circulation* 108:2258-2263.

191. Groot, P.H., van Vlijmen, B.J., Benson, G.M., Hofker, M.H., Schiffelers, R., Vidgeon-Hart, M., and Havekes, L.M. 1996. Quantitative assessment of aortic atherosclerosis in APOE*3 Leiden transgenic mice and its relationship to serum cholesterol exposure. *Arterioscler Thromb Vasc Biol* 16:926-933.

192. Westerterp, M., van der Hoogt, C.C., de Haan, W., Offerman, E.H., Dallinga-Thie, G.M., Jukema, J.W., Havekes, L.M., and Rensen, P.C. 2006. Cholesteryl ester transfer protein decreases high-density lipoprotein and severely aggravates atherosclerosis in APOE*3-Leiden mice. *Arterioscler Thromb Vasc Biol* 26:2552-2559.

193. Caligiuri, G., Nicoletti, A., Zhou, X., Tornberg, I., and Hansson, G.K. 1999. Effects of sex and age on atherosclerosis and autoimmunity in apoE-deficient mice. *Atherosclerosis* 145:301-308.

194. Yu, W., Braz, J.C., Dutton, A.M., Prusakov, P., and Rekhter, M. 2007. In vivo imaging of atherosclerotic plaques in apolipoprotein E deficient mice using nonlinear microscopy. *J Biomed Opt* 12:054008.

195. Le, T.T., Langohr, I.M., Locker, M.J., Sturek, M., and Cheng, J.X. 2007. Label-free molecular imaging of atherosclerotic lesions using multimodal nonlinear optical microscopy. *J Biomed Opt* 12:054007.

196. Denk, W., Strickler, J.H., and Webb, W.W. 1990. Two-photon laser scanning fluorescence microscopy. *Science* 248:73-76.

197. Brown, E., McKee, T., diTomaso, E., Pluen, A., Seed, B., Boucher, Y., and Jain, R.K. 2003. Dynamic imaging of collagen and its modulation in tumors in vivo using second-harmonic generation. *Nat Med* 9:796-800.

198. Campagnola, P.J., and Loew, L.M. 2003. Second-harmonic imaging microscopy for visualizing biomolecular arrays in cells, tissues and organisms. *Nat Biotechnol* 21:1356-1360.

199. Parasassi, T., Yu, W., Durbin, D., Kuriashkina, L., Gratton, E., Maeda, N., and Ursini, F. 2000. Two-photon microscopy of aorta fibers shows proteolysis induced by LDL hydroperoxides. *Free Radic Biol Med* 28:1589-1597.

200. Zoumi, A., Yeh, A., and Tromberg, B.J. 2002. Imaging cells and extracellular matrix in vivo by using second-harmonic generation and two-photon excited fluorescence. *Proc Natl Acad Sci U S A* 99:11014-11019.

201. Heinrich, C., Hofer, A., Ritsch, A., Ciardi, C., Bernet, S., and Ritsch-Marte, M. 2008. Selective imaging of saturated and unsaturated lipids by wide-field CARS-microscopy. *Opt Express* 16:2699-2708.

202. Nan, X., Cheng, J.X., and Xie, X.S. 2003. Vibrational imaging of lipid droplets in live fibroblast cells with coherent anti-Stokes Raman scattering microscopy. *J Lipid Res* 44:2202-2208.

203. Potma, E.O., Evans, C.L., and Xie, X.S. 2006. Heterodyne coherent anti-Stokes Raman scattering (CARS) imaging. *Opt Lett* 31:241-243.

204. Freudiger, C.W., Min, W., Saar, B.G., Lu, S., Holtom, G.R., He, C., Tsai, J.C., Kang, J.X., and Xie, X.S. 2008. Label-free biomedical imaging with high sensitivity by stimulated Raman scattering microscopy. *Science* 322:1857-1861.

205. Louw, D.F., Strating, J., and Backer, H.J. 1954. Delta-5-Steroids and provitamin D with branched side chains, III. Preparation and reduction of some delta-5-steroid omega-amines. *Recueil des Travaux Chimiques des Pays-Bas et de la Belgique* 73:667-676.

206. Pfaffl, M., W, Horgan, G., W, and Dempfle, L. 2002. Relative expression software tool (REST) for group-wise comparison and statistical analysis of relative expression results in real-time PCR. *Nucleic Acids Research Nucleic Acids Res* 30:e36-e36.

207. Wang, X., Sato, R., Brown, M.S., Hua, X., and Goldstein, J.L. 1994. SREBP-1, a membrane-bound transcription factor released by sterol-regulated proteolysis. *Cell* 77:53-62.

208. Lowry, O.H., Rosebrough, N.J., Farr, A.L., and Randall, R.J. 1951. Protein measurement with the Folin phenol reagent. *J Biol Chem* 193:265-275.

209. Gagnon, R.F., and Gallimore, B. 1988. Characterization of a mouse model of chronic uremia. *Urol Res* 16:119-126.

210. Greenspan, P., Mayer, E.P., and Fowler, S.D. 1985. Nile red: a selective fluorescent stain for intracellular lipid droplets. *J Cell Biol* 100:965-973.

211. Stojakovic, T., Putz-Bankuti, C., Fauler, G., Scharnagl, H., Wagner, M., Stadlbauer, V., Gurakuqi, G., Stauber, R.E., Marz, W., and Trauner, M. 2007. Atorvastatin in patients with primary biliary cirrhosis and incomplete biochemical response to ursodeoxycholic acid. *Hepatology* 46:776-784.

212. Miyazaki, M., Kim, Y.C., and Ntambi, J.M. 2001. A lipogenic diet in mice with a disruption of the stearoyl-CoA desaturase 1 gene reveals a stringent requirement of endogenous monounsaturated fatty acids for triglyceride synthesis. *J Lipid Res* 42:1018-1024.

213. Shevchenko, A., Wilm, M., Vorm, O., and Mann, M. 1996. Mass spectrometric sequencing of proteins silver-stained polyacrylamide gels. *Anal Chem* 68:850-858.

214. Carr, S., Aebersold, R., Baldwin, M., Burlingame, A., Clauser, K., and Nesvizhskii, A. 2004. The need for guidelines in publication of peptide and protein identification data: Working Group on Publication Guidelines for Peptide and Protein Identification Data. *Mol Cell Proteomics* 3:531-533.

215. Kaneko, E., Matsuda, M., Yamada, Y., Tachibana, Y., Shimomura, I., and Makishima, M. 2003. Induction of intestinal ATP-binding cassette transporters by a phytosterol-derived liver X receptor agonist. *J Biol Chem* 278:36091-36098.

216. D. F. Louw, S., G., and Backer, H.J. 1954.,. 1954. Delta-5-Steroids and provitamins D with branched side chains. III. Preparation and reduction of some delta-5-steroid omega-amines. *Recueil des Travaux Chimiques des Pays-Bas et de la Belgique 73:667-676.*

217. Kaplan, R., Zhang, T., Hernandez, M., Gan, F.X., Wright, S.D., Waters, M.G., and Cai, T.Q. 2003. Regulation of the angiopoietin-like protein 3 gene by LXR. *J Lipid Res* 44:136-143.

218. Laffitte, B.A., Joseph, S.B., Chen, M., Castrillo, A., Repa, J., Wilpitz, D., Mangelsdorf, D., and Tontonoz, P. 2003. The phospholipid transfer protein gene is a liver X receptor target expressed by macrophages in atherosclerotic lesions. *Mol Cell Biol* 23:2182-2191.

219. Li, J.M., Eslami, M.H., Rohrer, M.J., Dargon, P., Joris, I., Hendricks, G., Baker, S., and Cutler, B.S. 2008. Interleukin 18 binding protein (IL18-BP) inhibits neointimal hyperplasia after balloon injury in an atherosclerotic rabbit model. *J Vasc Surg* 47:1048-1057.

220. Kawakami, A., Osaka, M., Tani, M., Azuma, H., Sacks, F.M., Shimokado, K., and Yoshida, M. 2008. Apolipoprotein CIII links hyperlipidemia with vascular endothelial cell dysfunction. *Circulation* 118:731-742.

221. Strassel, C., Nonne, C., Eckly, A., David, T., Leon, C., Freund, M., Cazenave, J.P., Gachet, C., and Lanza, F. 2007. Decreased thrombotic tendency in mouse models of the Bernard-Soulier syndrome. *Arterioscler Thromb Vasc Biol* 27:241-247.

222. Hunter, M., Angelicheva, D., Tournev, I., Ingley, E., Chan, D., Watts, G., Kremensky, I., and Kalaydjieva, L. 2005. NDRG1 interacts with APO A-I and A-II and is a functional candidate for the HDL-C QTL on 8q24. *Biochem Biophys Res Commun* 332:982-992.

223. Okuda, T., Higashi, Y., Kokame, K., Tanaka, C., Kondoh, H., and Miyata, T. 2004. Ndrg1-deficient mice exhibit a progressive demyelinating disorder of peripheral nerves. *Mol Cell Biol* 24:3949-3956.

224. Qi, L., Heredia, J., Altarejos, J., Screaton, R., Goebel, N., Niessen, S., Macleod, I., Liew, C., Kulkarni, R., Bain, J., et al. 2006. TRB3 links the E3 ubiquitin ligase COP1 to lipid metabolism. *Science* 312:1763-1766.

225. Qiang, L., Wang, H., and Farmer, S. 2007. Adiponectin secretion is regulated by SIRT1 and the endoplasmic reticulum oxidoreductase Ero1-L alpha. *Mol Cell Biol* 27:4698-4707.

226. Feige, J., and Auwerx, J. 2007. DisSIRTing on LXR and cholesterol metabolism. *Cell Metab* 6:343-345.

227. Fontaine, C., Rigamonti, E., Pourcet, B., Duez, H., Duhem, C., Fruchart, J.C., Chinetti-Gbaguidi, G., and Staels, B. 2008. The nuclear receptor Rev-erbalpha is a liver X receptor (LXR) target gene driving a negative feedback loop on select LXR-induced pathways in human macrophages. *Mol Endocrinol* 22:1797-1811.

228. Rigamonti, E., Helin, L., Lestavel, S., Mutka, A.L., Lepore, M., Fontaine, C., Bouhlel, M.A., Bultel, S., Fruchart, J.C., Ikonen, E., et al. 2005. Liver X receptor activation controls intracellular cholesterol trafficking and esterification in human macrophages. *Circ Res* 97:682-689.

229. Joseph, S.B., Bradley, M.N., Castrillo, A., Bruhn, K.W., Mak, P.A., Pei, L., Hogenesch, J., O'Connell R, M., Cheng, G., Saez, E., et al. 2004. LXR-dependent gene expression is important for macrophage survival and the innate immune response. *Cell* 119:299-309.

230. Haidar, B., Kiss, R.S., Sarov-Blat, L., Brunet, R., Harder, C., McPherson, R., and Marcel, Y.L. 2006. Cathepsin D, a lysosomal protease, regulates ABCA1-mediated lipid efflux. *J Biol Chem* 281:39971-39981.

231. Arai, S., Shelton, J.M., Chen, M., Bradley, M.N., Castrillo, A., Bookout, A.L., Mak, P.A., Edwards, P.A., Mangelsdorf, D.J., Tontonoz, P., et al. 2005. A role for the apoptosis inhibitory factor AIM/Spalpha/Api6 in atherosclerosis development. *Cell Metab* 1:201-213.

232. Li, Y., Bolten, C., Bhat, B.G., Woodring-Dietz, J., Li, S., Prayaga, S.K., Xia, C., and Lala, D.S. 2002. Induction of human liver X receptor alpha gene expression via an autoregulatory loop mechanism. *Mol Endocrinol* 16:506-514.

233. Chawla, A., Boisvert, W.A., Lee, C.H., Laffitte, B.A., Barak, Y., Joseph, S.B., Liao, D., Nagy, L., Edwards, P.A., Curtiss, L.K., et al. 2001. A PPAR gamma-LXR-ABCA1 pathway in macrophages is involved in cholesterol efflux and atherogenesis. *Mol Cell* 7:161-171.

234. Schmidt, R.J., Ficorilli, J.V., Zhang, Y., Bramlett, K.S., Beyer, T.P., Borchert, K., Dowless, M.S., Houck, K.A., Burris, T.P., Eacho, P.I., et al. 2006. A 15-ketosterol is a liver X receptor ligand that suppresses sterol-responsive element binding protein-2 activity. *J Lipid Res* 47:1037-1044.

235. Ishimoto, K., Tachibana, K., Sumitomo, M., Omote, S., Hanano, I., Yamasaki, D., Watanabe, Y., Tanaka, T., Hamakubo, T., Sakai, J., et al. 2006. Identification of human low-density lipoprotein receptor as a novel target gene regulated by liver X receptor alpha. *FEBS Lett* 580:4929-4933.

236. Lachat, P., Shaw, P., Gebhard, S., van Belzen, N., Chaubert, P., and Bosman, F. 2002. Expression of NDRG1, a differentiation-related gene, in human tissues. *Histochem Cell Biol* 118:399-408.

237. Molloy, E.J. 2009. Triggering Receptor Expressed on Myeloid Cells (TREM) family and the application of its antagonists. *Recent Pat Antiinfect Drug Discov* 4:51-56.

238. Ornatowska, M., Azim, A.C., Wang, X., Christman, J.W., Xiao, L., Joo, M., and Sadikot, R.T. 2007. Functional genomics of silencing TREM-1 on TLR4 signaling in macrophages. *Am J Physiol Lung Cell Mol Physiol* 293:L1377-1384.

239. Sacks, F.M., Alaupovic, P., Moye, L.A., Cole, T.G., Sussex, B., Stampfer, M.J., Pfeffer, M.A., and Braunwald, E. 2000. VLDL, apolipoproteins B, CIII, and E, and risk of recurrent coronary events in the Cholesterol and Recurrent Events (CARE) trial. *Circulation* 102:1886-1892.

240. Chen, W., Chen, G., Head, D.L., Mangelsdorf, D.J., and Russell, D.W. 2007. Enzymatic reduction of oxysterols impairs LXR signaling in cultured cells and the livers of mice. *Cell Metab* 5:73-79.

241. Ma, Y., Xu, L., Rodriguez-Agudo, D., Li, X., Heuman, D.M., Hylemon, P.B., Pandak, W.M., and Ren, S. 2008. 25-Hydroxycholesterol-3-sulfate regulates macrophage lipid metabolism via the LXR/SREBP-1 signaling pathway. *Am J Physiol Endocrinol Metab* 295:E1369-1379.

242. Matsuda, D., Ohte, S., Ohshiro, T., Jiang, W., Rudel, L., Hong, B., Si, S., and Tomoda, H. 2008. Molecular target of piperine in the inhibition of lipid droplet accumulation in macrophages. *Biol Pharm Bull* 31:1063-1066.

243. Bujo, H., and Saito, Y. 2000. Markedly induced expression of LR11 in atherosclerosis. *J Atheroscler Thromb* 7:21-25.

244. Park, Y.M., Febbraio, M., and Silverstein, R.L. 2009. CD36 modulates migration of mouse and human macrophages in response to oxidized LDL and may contribute to macrophage trapping in the arterial intima. *J Clin Invest* 119:136-145.

245. Rojek, A.M., Skowronski, M.T., Fuchtbauer, E.M., Fuchtbauer, A.C., Fenton, R.A., Agre, P., Frokiaer, J., and Nielsen, S. 2007. Defective glycerol metabolism in aquaporin 9 (AQP9) knockout mice. *Proc Natl Acad Sci U S A* 104:3609-3614.

246. Calamita, G., Ferri, D., Gena, P., Carreras, F.I., Liquori, G.E., Portincasa, P., Marinelli, R.A., and Svelto, M. 2008. Altered expression and distribution of aquaporin-9 in the liver of rat with obstructive extrahepatic cholestasis. *Am J Physiol Gastrointest Liver Physiol* 295:G682-690.

247. Leinonen, J.S., Saari, K.A., Seppanen, J.M., Myllyla, H.M., and Rajaniemi, H.J. 2004. Immunohistochemical demonstration of carbonic anhydrase isoenzyme VI (CA VI) expression in rat lower airways and lung. *J Histochem Cytochem* 52:1107-1112.

248. Sugiura, Y., Ichihara, N., Nishita, T., Murakami, M., Amasaki, H., and Asari, M. 2008. Immunohistolocalization and gene expression of secretory carbonic anhydrase isoenzyme CA-VI in canine nasal cavity. *J Vet Med Sci* 70:1037-1041.

249. De Cosmo, S., Prudente, S., Andreozzi, F., Morini, E., Rauseo, A., Scarpelli, D., Zhang, Y., Xu, R., Perticone, F., Dallapiccola, B., et al. 2007. Glutamine to arginine substitution at amino acid 84 of mammalian tribbles homolog TRIB3 and CKD in whites with type 2 diabetes. *Am J Kidney Dis* 50:688-689.

250. Okamoto, H., Latres, E., Liu, R., Thabet, K., Murphy, A., Valenzeula, D., Yancopoulos, G.D., Stitt, T.N., Glass, D.J., and Sleeman, M.W. 2007. Genetic deletion of Trb3, the mammalian Drosophila tribbles homolog, displays normal hepatic insulin signaling and glucose homeostasis. *Diabetes* 56:1350-1356.

251. Li, X., Yang, H.Y., and Giachelli, C.M. 2008. BMP-2 promotes phosphate uptake, phenotypic modulation, and calcification of human vascular smooth muscle cells. *Atherosclerosis* 199:271-277.

252. Emmanuele, L., Ortmann, J., Doerflinger, T., Traupe, T., and Barton, M. 2003. Lovastatin stimulates human vascular smooth muscle cell expression of bone morphogenetic protein-2, a potent inhibitor of low-density lipoprotein-stimulated cell growth. *Biochem Biophys Res Commun* 302:67-72.

253. Cao, W., Bao, C., Padalko, E., and Lowenstein, C.J. 2008. Acetylation of mitogen-activated protein kinase phosphatase-1 inhibits Toll-like receptor signaling. *J Exp Med* 205:1491-1503.

254. Braunersreuther, V., Steffens, S., Arnaud, C., Pelli, G., Burger, F., Proudfoot, A., and Mach, F. 2008. A novel RANTES antagonist prevents progression of established atherosclerotic lesions in mice. *Arterioscler Thromb Vasc Biol* 28:1090-1096.

255. Schultz, J.R., Tu, H., Luk, A., Repa, J.J., Medina, J.C., Li, L., Schwendner, S., Wang, S., Thoolen, M., Mangelsdorf, D.J., et al. 2000. Role of LXRs in control of lipogenesis. *Genes Dev* 14:2831-2838.

256. Klucken, J., Buchler, C., Orso, E., Kaminski, W.E., Porsch-Ozcurumez, M., Liebisch, G., Kapinsky, M., Diederich, W., Drobnik, W., Dean, M., et al. 2000. ABCG1 (ABC8), the human homolog of the Drosophila white gene, is a regulator of macrophage cholesterol and phospholipid transport. *Proc Natl Acad Sci U S A* 97:817-822.

257. Oram, J.F., Lawn, R.M., Garvin, M.R., and Wade, D.P. 2000. ABCA1 is the cAMP-inducible apolipoprotein receptor that mediates cholesterol secretion from macrophages. *J Biol Chem* 275:34508-34511.

258. Oram, J.F., and Vaughan, A.M. 2000. ABCA1-mediated transport of cellular cholesterol and phospholipids to HDL apolipoproteins. *Curr Opin Lipidol* 11:253-260.

259. Repa, J.J., Turley, S.D., Lobaccaro, J.A., Medina, J., Li, L., Lustig, K., Shan, B., Heyman, R.A., Dietschy, J.M., and Mangelsdorf, D.J. 2000. Regulation of absorption and ABC1-mediated efflux of cholesterol by RXR heterodimers. *Science* 289:1524-1529.

260. Berge, K.E., Tian, H., Graf, G.A., Yu, L., Grishin, N.V., Schultz, J., Kwiterovich, P., Shan, B., Barnes, R., and Hobbs, H.H. 2000. Accumulation of dietary cholesterol in sitosterolemia caused by mutations in adjacent ABC transporters. *Science* 290:1771-1775.

261. Lee, M.H., Lu, K., Hazard, S., Yu, H., Shulenin, S., Hidaka, H., Kojima, H., Allikmets, R., Sakuma, N., Pegoraro, R., et al. 2001. Identification of a gene, ABCG5, important in the regulation of dietary cholesterol absorption. *Nat Genet* 27:79-83.

262. Zhu, J., Lee, B., Buhman, K.K., and Cheng, J.X. 2009. A dynamic, cytoplasmic triacylglycerol pool in enterocytes revealed by ex vivo and in vivo coherent anti-Stokes Raman scattering imaging. *J Lipid Res*.

12 Supplemental data

There are several coactivators and corepressors that play important role in the transcriptional machinery that can be activated by nuclear receptors (NR).

Table A. NR coactivators and corepressors
The lists are taken from the book Nuclear receptor facts book by Laudet et al.

Human factors	Synonyms	NID motif	Accession number[a]	Comments
1. Nuclear receptor-binding subunits of coactivator complexes				
Bona fide NR coactivators				
SRC-1a	hERAP160 mNCoA1	Yes	U90661 NM_010881	First identified coactivator; binds NR and CBP/p300; displays acetyltransferase activity and contacts basal transcription factors
SRC-1e		Yes	U19179	Isoform of SRC-1a; lacks the C-terminal NR box of SRC-1a
TIF2	hNCoA2 mGRIP1 SRC-3	Yes	X97674 U39060	Member of the same coactivator family as SRC-1
ACTR	hAIB1 hRAC3 hTRAM1 mpCIP	Yes	U59302 AF000581	Member of the same coactivator family as SRC-1/TIF2
Cointegrators				
CBP	 mCBP	Yes	U47741 sw:P45481	Transcriptional cointegrator for several signaling pathways in addition to those involving NRs (CREB, STATs, AP1, etc.); interacts with pCAF, SRC-1, TIF2 and pCIP; displays acetyltransferase activity
p300		Yes	U01877	Functional homologue of CBP; p300 and CBP functions are not entirely redundant
pCAF			U57317	Similar to hGCN5; interacts with CBP/p300; possesses intrinsic acetyltransferase activity; present in a 2 MDa complex
Others				
SRA	 mSRA		AF092038 AF092039	An RNA molecule, identified by using the N-terminal domain of PR as a bait; the SRA gene does not encode a protein; SRA is proposed to be part of a complex containing SRC-1
2. Nuclear receptor-binding subunits of corepressor complexes				
Bona fide NR corepressors				
N-CoR	hNcoR1 mN-CoR RIP13 (partial)	Yes	NM_006311 U35312	Interacts with and corepresses TR, RAR, COUPTFI and Rev-erb
SMRT	hSMRT hNCoR2 TRAC2 (partial)	Yes	U37146 NM_006312	Corepresses TR and RAR, and has sequence similarity with N-CoR
Sun-CoR	 mSun-CoR		 AF031426	Corepresses TR and Rev-erb

Others

TRUP	SURF-3		M36072	Interacts with the hinge region and the N-terminal portion of the LBD of TR in a hormone-independent manner; exerts its inhibiting activity by interfering with DNA binding of the receptor to this element
TSG101				Interacts with AF-1 of GR and represses transcriptional activity of GR in mammalian and in yeast cells
REA	BAP-37	Unclear		Isolated by interaction with the dominant negative ER receptor (L540Q); interacts also with the antiestrogen-liganded ER; represses transcriptional activity of ER but not of PR, RAR or VP16; contains an LxxLL NR box motif but its function in interaction has not been demonstrated
ALIEN	hALIEN dALIEN		AF120268 U57758	Shows the expected properties of a corepressor of nuclear receptor in *Drosophila*; apparently plays the same role for mammalian nuclear receptors

3.Nuclear receptor-binding subunits of the SRB/mediator containing complex (SMCC)

TRAP220	hDRIP205 hDRIP230	Yes	AF055994	Included in the SMCC complex that interacts with liganded TR and VDR; enhances *in vitro* transcription by these receptors
	hTRIP2 (partial)			
	mPBP		AF000294	mPBP was originally isolated by interaction with PPAR
TRAP100	hDRIP100	Unclear	AF055995	DRIP100 does not interact directly with VDR in a ligand-dependent manner; overexpression leads to coactivation first and then to squelching; NID does not promote direct interaction with NR
TRAP170	hDRIP150 hRGR1 hEXLM1		AF135802	DRIP150 interacts with and coactivates AF-1 of GR; may work in association with DRIP205 (interacts with and coactivates GR AF-2)

4. Nuclear receptor-binding subunits of the SWI/SNF complex

hSNF2a hSNF2b	hbrm BRG1		X72889	Coimmunoprecipitates with GR; both hBRM and BRG1 interact with ER in a ligand-dependent manner in yeast

5. Factors interacting with nuclear receptors

In a ligand- and/or AF-2-dependent manner

RIP140		Yes	sw:P48542	Interacts with and coactivates ER, but corepresses TR2 orphan receptor and retinoid receptors
	hERAP140			
	mRIP140		AF053062	
ARA70		Unclear	L49399	Reported to coactivate AR in DU145 cells; coactivates PPARγ activity in a ligand-dependent manner; possesses one LxxLL motif but this motif is not implicated in the interaction; isoform of hELE1a
	hELE1a			
	hRFG			
	hELE1b			
ARA55			AF116343	Interacts with AR through LIM domain
ARA54			AF049330	Another AR putative coactivator that contains a RING finger domain
TRIP1		Yes	L38810	TRIP1 interacts with RXR, mSUG1 with different members of the NR superfamily; TRIP1 is a component of the 26S proteasome
	mSUG1		Z54219	

ASC-1			AF168418	Interacts with basal transcription factors (TBP and TFIIA), transcription integrators (SRC-1 and CBP/p300) and nuclear receptors. Although the interaction domain with NR seems to be the hinge region, AF-2 integrity is required
ASC-2	AIB3	Unclear	AF177388	Interacts with RAR, TR, ERa and GR and binds also TFIIA, TBP, SRC-1 and CBP/p300; microinjection of anti-ASC-2 antibody abrogated the ligand-dependent transactivation by retinoic acid receptor; is amplified in human cancers; contains two LxxLL motifs but implication in the interaction has not been demonstrated
p120		Unclear	AF016270	Interacts with TR LBD; possesses a LSELL motif in the NR interacting region
TIF1α	mTIF1a	Yes	AF009353 S78221	Interacts with several NR; belongs to the RBCC family of proteins; interacts also with KRAB domain-containing proteins, which are involved in determining heterochromatin structures
NRIF3	EnL and EnS	Yes		Claimed to be a specific coactivator for TR and interacts through a variant of the NID motif LxxLL
Trip230			AAD09135	Binds to and coactivates TR; binds also to Rb
L7	SPA			Interacts with and coactivates RU486-bound PR and enhances its partial agonist activity
Tip60		Unclear	U74667	Interaction with AR LBD enhanced by the ligand; able to coactivate PR and ER in transfections; contains a LxxLL motif but its function has not been demonstrated
RAP250		Yes	AF128458	Ligand-dependent or ligand-enhanced interaction with nuclear receptors; interaction involves the only LxxLL NR box; has intrinsic glutamine-rich activation domain; widely expressed in reproductive organs
FHL2	DRAL	Unclear	NM_001450	Human four and a half LIM domains protein 2 (FHL2); claimed to act as tissue-specific coactivator of the androgen receptor; nuclear protein; expressed in myocardium and prostate epithelium; contains autonomous transactivation function; coactivates AR but not other NRs
In a ligand-independent manner				
MBF1	hMBF1a hMBF1b		AB002282 AB002283	Example of a coactivator conserved throughout evolution; interaction implicates the DBD and increases DNA binding
ARA160	TMF		NM_007114	Interacts with the AB domain of AR; however, the ligand enhances interaction, suggesting that ARA160 may work in association with ARA70 to coactivate AR
ORCA	hORCA		U46751	Factor that binds COUP-TFII *in vitro* and allows COUP-TFII to function as a transcriptional activator in mammalian cells; identical to a recently described ligand of the tyrosine kinase signaling molecule p56(lck), suggesting that it mediates cross-talk between mitogenic and NR signal transduction pathways
PGC-1	mPGC-1	Unclear	AF049330	First report of an inducible coactivator for a nuclear receptor, originally described for PPARγ but interacts also with other NRs; interaction is ligand independent and implicates the DBD and the hinge region of the receptor; NID motif is not required for PPAR binding
PGC-2	mPGC-2		AF017433	Isolated using the AF-1 region of PPARγ as bait; contains a partial SCAN domain; binds to and increases the transcriptional activity of PPARγ, but does not interact with other PPARs or most other nuclear receptors
SNURF	rSNURF		AF022081	Isolated by two-hybrid interaction using AR DBD as bait; interaction is ligand dependent but SNURF is able to stimulate both basal and ligand-induced transcription
NCoA-62			AF045184	Fished out with VDR as bait; interacts with the LBD even in the

				absence of the ligand and coactivates in mammalian cells vitamin D_3-,retinoic acid-, estrogen- and glucocorticoid-mediated gene expression
RAP46	hBAG-1 hBAG-1L		Z35491	Originally identified as a protein able to interact with several nuclear receptors including GR, ER and TR; the ligand was not strictly required for interaction; subsequent cloning of a longer form, BAG-1L that coimmunoprecipitates and coactivates AR in PC3 transfections; RAP46 was described as a negative regulator of GR and RAR
MIP224	TBP7		NM_006503	Isolated using the two-hybrid system and the orphan receptor MB67 as a bait; in transfection experiments MIP224 inhibits the transcriptional activation by MB67; MIP224 is a component of the 26S proteasome
PIAS1		Unclear	AF167160	Binds in yeast the DBD + LBD of AR in a ligand-dependent manner; *in vitro* it binds the isolated DBD; coactivates in mammalian cells AR and PR ligand-dependent transactivation but represses PR; first cloned as an inhibitor of STAT1; contains an LxxLL motif but its role in interaction has not been demonstrated
ARIP3	hPIASxy rARIP3	Unclear	AF044058	Binds the DBD of AR and modulates AR-dependent transcription. Belongs to the PIAS family of proteins; contains an LxxLL motif but its role in interaction has not been demonstrated
p68		Unclear	AF015812	Interacts with the A/B domain of hERα; phosphorylation of hERαSer118 potentiates the interaction with p68; enhances the AF-1 activity; contains an LxxLL motif but its role in interaction has not been demonstrated
With both liganded and non-liganded receptors				
NSD1	mNSD1	Yes	AF064553	Interacts through NID-L with unliganded RAR and TR and through NID + L with liganded RAR, TR, RXR and ER has properties of both a coactivator and a corepressor
zac1b				Variant of zac1, a putative transcriptional activator involved in apoptosis and cell-cycle regulation; isolated as a protein that binds to the C-terminal region of the coactivator TIF2/GRIP1; interacts with CBP, p300 and nuclear receptors in yeast two-hybrid and *in vitro* experiments; contains autonomous transactivation domain; acts as coactivator but in some cell lines and with certain promoters zac1b acts as repressor of nuclear receptor action
	zac1		NM_009538	
6. Other factors that interact directly or indirectly with nuclear receptors				
STAT3	mSTAT3		U30709	Associates with ligand-bound glucocorticoid receptor to form a transactivating/signaling complex, which can function through either an IL-6-responsive element or a glucocorticoid-responsive element
STAT5	mSTAT5		U48730 U21110	GR can act as a transcriptional coactivator for Stat5 and enhance Stat5-dependent transcription
E6-AP	mE6-AP	Unclear	AF016708 U96636	Interacts with and coactivates the transcriptional activity of PR in a ligand-dependent manner; however, in the Angelman syndrome, the phenotype results from the defect in the ubiquitin–proteosome-mediated degradation of E6-AP
cyclinD1		Unclear	M64349	Direct physical binding of cyclin D1 to the LBD increases binding of the receptor to this element and either activates transcription in the absence of estrogen or enhances transcription in its presence
HMG-1	mHMG-1		X12597 U00431	Coregulatory proteins that increase the DNA binding and transcriptional activity of steroid NR
HMG-2	mHMG-2		X62534 U00431	cf HMG-1
Bcl3		Unclear	U05681	Able to interact with RXR both in a ligand-independent manner

				with a fragment comprising the ABC domain and in a ligand-dependent manner with the ligand-binding domain; interacts with the general transcription factors TFIIB, TBP and TFIIA, but not with TFIIEα in the GST pull-down assays and enhances the *9cis*-RA-induced transactivation of RXR; possesses an LxxLL motif but mutation in the motif does not abolish interaction
Vpr		Yes	U71182	Interacts directly with the GR and general transcription factors, acting as a coactivator via a LxxLL signature motif
TLS			AF071213	interaction with the DBD of RXR, ER, TR and GR
dUTPase			U62891	PPARα-interacting protein. Interacts *in vitro* with all three isoforms of mouse PPAR, but not with RXR and TR; this interaction seems to inhibit PPAR/RXR, resulting in an inhibition of PPAR activity in a ligand-independent manner
Smad3	mSmad3		AB004930 AF016189.1t	Specific coactivator for ligand-induced transactivation of VDR by forming a complex with a member of the steroid receptor coactivator-1 protein family
E1A				Interacts directly with TR via the DBD and carboxy-terminal part of the LBD in a ligand-independent manner
hnRNP U	GRIP120 mhnRNP U		NM_004501 AF073992	Scaffold attachment region and RNA-binding protein that coimmunoprecipitates with GR
TIF1β	KAP1		NM_005762	Enhances the transcription of the *agp* gene by GR in a ligand- and GRE-dependent manner, even if the interaction is ligand independent
TDG			NM_003211	Implicated in the reparation of T:G mismatch; interacts through a region containing α-helix1 of the LBD with RAR and RXR
TSC-2			NM_000548	Cloned by interaction with RXR in yeast; coactivates PPARγ and VDR in mammalian cells but no clear demonstration of a direct interaction

12.1 Microarray data

Microarrays were performed with MPM treated with 2.5µM DMHCA or 1 µM T0901317, respectively. Data were compared DMHCA-treated versus control, T0901317-treated versus control, treatment group (DMHCA and T0901317 combined) versus control and DMHCA-treated versus T0901317-treated. For each comparison pathway matching was performed using GeneSpring software.

12.1.1 Gene regulation in DMHCA-treated macrophages versus control-treated macrophages

Table B Pathway analysis: DMHCA-treated compared to control, down upon DMHCA treatment with *FC*≤0.5, p≤0.1; most abundant pathways

Category	Genes in Category	% of Genes in Category	Genes in List in Categorv	% of Genes in List in Category	p-Value
GO:16126: sterol biosynthesis	25	0,183	16	9,816	1,48E-25
GO:16125: sterol metabolism	58	0,425	20	12,27	1,30E-24
GO:6695: cholesterol biosynthesis	22	0,161	13	7,975	2,77E-20
GO:8203: cholesterol metabolism	54	0,395	17	10,43	2,77E-20
GO:6694: steroid biosynthesis	62	0,454	17	10,43	4,01E-19
GO:8202: steroid metabolism	123	0,9	21	12,88	9,59E-19
GO:8610: lipid biosynthesis	182	1,332	20	12,27	4,45E-14
GO:6629: lipid metabolism	481	3,521	28	17,18	2,77E-12
GO:44255: cellular lipid metabolism	387	2,833	25	15,34	4,89E-12

GO:8299: isoprenoid biosynthesis	12	0,0878	6	3,681	2,29E-09
GO:6720: isoprenoid metabolism	22	0,161	6	3,681	1,68E-07
GO:9241: polyisoprenoid biosynthesis	2	0,0146	2	1,227	0,000141
GO:16114: terpenoid biosynthesis	2	0,0146	2	1,227	0,000141
GO:16109: tetraterpenoid biosynthesis	2	0,0146	2	1,227	0,000141
GO:16117: carotenoid biosynthesis	2	0,0146	2	1,227	0,000141
GO:16108: tetraterpenoid metabolism	2	0,0146	2	1,227	0,000141
GO:16116: carotenoid metabolism	2	0,0146	2	1,227	0,000141
GO:16096: polyisoprenoid metabolism	6	0,0439	2	1,227	0,00206
GO:6721: terpenoid metabolism	6	0,0439	2	1,227	0,00206
GO:10025: wax biosynthesis	3	0,022	1	0,613	0,0354
GO:10166: wax metabolism	3	0,022	1	0,613	0,0354

Setting p≤0.1 and *FC*≤0.5 406 genes were downregulated upon DMHCA-treatment in comparison with control cells, whereas p≤0.05 and *FC*≤0.5 led to 194 genes that were differently regulated (Table C).

Table C. Downregulated genes in DMHCA versus control, down in DMHCA for p≤0.05 and FC≤0.5

Gene Name	Fold Change	Common	P-value	Genbank	Description
826570	0,014	Idi1	0,0114	NM_145360.1	isopentenyl-diphosphate delta isomerase
565056	0,0273	Idi1	0,000193	NM_145360.1	isopentenyl-diphosphate delta isomerase
598079	0,0306	Crisp4	0,0122	null	cysteine-rich secretory protein 4
435645	0,0422	Hsd17b7	0,0241	NM_010476.2	hydroxysteroid (17-beta) dehydrogenase 7
634387	0,0607	Cyp51	0,00357	NM_020010.1	cytochrome P450, family 51
640447	0,0613	Dhcr24	0,0391	NM_053272.1	24-dehydrocholesterol reductase
917926	0,0693	Acat2	0,023	NM_009338.1	acetyl-Coenzyme A acetyltransferase 2
340275	0,0695	A730092B10	0,0214	null	null
848334	0,0698	4930543L23Rik	0,0287	NM_183110.1	RIKEN cDNA 4930543L23 gene
515114	0,0699	A930004K21Rik	0,0442	NM_172673.2	RIKEN cDNA A930004K21 gene
529335	0,0742	Sqle	0,00205	NM_009270.2	squalene epoxidase
888038	0,0818	LOC637705|Ifit3	0,00954	NM_001005858.1	interferon-induced protein with tetratricopeptide repeats 3
430706	0,0946	Ldlr	0,0292	null	low density lipoprotein receptor
882896	0,101	6530439I21	0,0288	NM_177837.2	null
730737	0,104	Acat3|Acat2|LOC630106	0,0243	NM_153151.1	acetyl-Coenzyme A acetyltransferase 3|acetyl-Coenzyme A acetyltransferase 2
464308	0,107	Oas2	0,0301	NM_145227.1	2'-5' oligoadenylate synthetase 2
909892	0,113	Hmgcs1	0,0109	NM_145942.2	3-hydroxy-3-methylglutaryl-Coenzyme A synthase 1
537504	0,117	null	0,000682	null	null
542220	0,122	Sc4mol	0,0325	NM_025436.1	sterol-C4-methyl oxidase-like
678760	0,131	Ms4a6b	0,0372	null	membrane-spanning 4-domains, subfamily A, member 6B
552012	0,134	Trim60	0,017	NM_153097.1	tripartite motif-containing 60
730299	0,136	Tm7sf2	0,0368	NM_028454.1	transmembrane 7 superfamily member 2

503224	0,139	Sc5d	0,0115	NM_172769.1	sterol-C5-desaturase (fungal ERG3, delta-5-desaturase) homolog (S. cerevisae)
867196	0,148	BC042761	0,0339	null	cDNA sequence BC042761
829972	0,151	Enpp4	0,0228	null	ectonucleotide pyrophosphatase/phosphodiesterase 4
735288	0,158	Nme4	0,035	null	expressed in non-metastatic cells 4, protein
559603	0,161	Mvd	0,0212	NM_138656.1	mevalonate (diphospho) decarboxylase
342510	0,168	Insig1|LOC625787	0,025	NM_153526.2	insulin induced gene 1
304467	0,176	Cox7a1	0,0422	NM_009944.2	cytochrome c oxidase, subunit VIIa 1
662135	0,176	Cacng8	0,0307	NM_133190.1	calcium channel, voltage-dependent, gamma subunit 8
579184	0,18	null	0,018	null	null
386178	0,183	A730061H03Rik	0,0376	null	RIKEN cDNA A730061H03 gene
434342	0,189	1700020N18Rik	0,0415	null	RIKEN cDNA 1700020N18 gene
508816	0,189	2810051F02Rik	0,0198	NM_028330.1	RIKEN cDNA 2810051F02 gene
917041	0,19	Prlpc3	0,0249	NM_023741.1	prolactin-like protein C 3
827287	0,192	8030475D13Rik	0,0163	null	RIKEN cDNA 8030475D13 gene
429576	0,196	Aldoc	0,0325	NM_009657.1	aldolase 3, C isoform
603979	0,196	Apoc3	0,00665	NM_023114.2	apolipoprotein C-III
866913	0,198	Minpp1	0,0151	null	multiple inositol polyphosphate histidine phosphatase 1
329505	0,204	BC025833	0,0344	null	cDNA sequence BC025833
454396	0,209	null	0,0403	null	null
475398	0,209	Gm97	0,0384	null	gene model 97, (NCBI)
450585	0,211	Perld1	0,0178	null	per1-like domain containing 1
578854	0,211	D930048N14Rik	0,0374	NM_175289.2	RIKEN cDNA D930048N14 gene
370245	0,213	null	0,029	null	null
623195	0,218	C630001G18Rik	0,0194	null	RIKEN cDNA C630001G18 gene
681778	0,219	Gimap9	0,0325	NM_174960.2	GTPase, IMAP family member 9
363166	0,22	Gp1bb	0,00416	NM_001001999.1	glycoprotein Ib, beta polypeptide
694956	0,222	null	0,0345	null	null
714772	0,222	BC055004	0,0195	null	cDNA sequence BC055004
414273	0,226	Sgpp2|LOC639204	0,0046	NM_001004173.1	null
394283	0,227	Fbxl12	0,0207	null	F-box and leucine-rich repeat protein 12
899879	0,228	null	0,0338		null
890231	0,231	Dlc1	0,041	null	deleted in liver cancer 1
349503	0,235	C730036D15Rik|LOC230161	0,0106	NM_145368.2	RIKEN cDNA C730036D15 gene
857500	0,236	Drd4	0,0448	NM_007878.2	dopamine receptor 4
298347	0,238	4930405H06Rik	0,0457	null	RIKEN cDNA 4930405H06 gene
302585	0,238	LOC546866	0,0459	null	null
460449	0,245	Alk	0,045	NM_007439.1	anaplastic lymphoma kinase
688680	0,245	Prodh	0,0108	NM_011172.1	proline dehydrogenase
803828	0,245	null	0,0201	null	null
299744	0,246	4930597O21Rik	0,023	null	RIKEN cDNA 4930597O21 gene
367615	0,246	Pnpt1	0,0365	null	polyribonucleotide nucleotidyltransferase 1
671973	0,246	Oas1c	0,0485	NM_033541.2	2'-5' oligoadenylate synthetase 1C
850068	0,247	Fndc1	0,0416	null	fibronectin type III domain containing 1

636040	0,249	B4galt4	0,0284	NM_019804.1	UDP-Gal:betaGlcNAc beta 1,4-galactosyltransferase, polypeptide 4
746252	0,251	Rab19	0,0438	NM_011226.1	RAB19, member RAS oncogene family
577533	0,254	Dmrta1	0,0319	NM_175647.2	doublesex and mab-3 related transcription factor like family A1
735058	0,256	Phf21a	0,0365	null	PHD finger protein 21A
610337	0,258	4831407H17Rik	0,0107	null	RIKEN cDNA 4831407H17 gene
481867	0,259	4933439K11Rik	0,0124	null	RIKEN cDNA 4933439K11 gene
907925	0,259	Iigp1	0,00681	NM_021792.3	interferon inducible GTPase 1
884333	0,261	Epb4.1l4b	0,0412	NM_019427.1	erythrocyte protein band 4.1-like 4b
404142	0,265	LOC632120	0,0239	null	null
790492	0,265	2310002D06Rik	0,0387	null	RIKEN cDNA 2310002D06 gene
305754	0,267	null	0,0362	null	null
538501	0,272	LOC620400	0,0288	null	null
301554	0,273	Cbfa2t2h	0,0364	NM_172860.1	core-binding factor, runt domain, alpha subunit 2, translocated to, 2 homolog (human)
482490	0,274	C030034L19Rik	0,0289	null	RIKEN cDNA C030034L19 gene
304116	0,277	A830037D11Rik	0,0478	null	RIKEN cDNA A830037D11 gene
741070	0,277	D130051D11Rik	0,0125	null	RIKEN cDNA D130051D11 gene
505568	0,278	D330017J20Rik	0,00792	NM_177204.2	RIKEN cDNA D330017J20 gene
728547	0,279	Gpr112	0,0114	null	G protein-coupled receptor 112
853341	0,28	LOC544710	0,0222	null	null
545195	0,282	1700023D08Rik	0,0238	null	RIKEN cDNA 1700023D08 gene
681040	0,282	RP23-419P16.7	0,0369	null	null
834443	0,282	LOC620153	0,0435	null	null
920843	0,282	Ms4a6b	0,0381	NM_027209.2	membrane-spanning 4-domains, subfamily A, member 6B
467024	0,283	Aqp8	0,0174	NM_007474.1	aquaporin 8
478800	0,286	Cldn2	0,00561	NM_016675.3	claudin 2
928957	0,289	Tac2	0,0476	NM_009312.1	tachykinin 2
632446	0,292	Syt10	0,0197	NM_018803.1	synaptotagmin X
522188	0,299	4930562D21Rik	0,0036	null	RIKEN cDNA 4930562D21 gene
667671	0,299	Maf	0,0104	null	avian musculoaponeurotic fibrosarcoma (v-maf) AS42 oncogene homolog
725464	0,302	Sema7a	0,032	NM_011352.2	sema domain, immunoglobulin domain (Ig), and GPI membrane anchor, (semaphorin) 7A
563722	0,305	Wnt1	0,0339	NM_021279.3	wingless-related MMTV integration site 1
838923	0,306	Plp1	0,0124	NM_011123.1	proteolipid protein (myelin) 1
886901	0,307	Tbx3	0,00287	NM_198052.1	T-box 3
462888	0,308	Aicda	0,0281	NM_009645.1	activation-induced cytidine deaminase
759510	0,308	Npr2	0,0331	NM_173788.2	natriuretic peptide receptor 2
720018	0,311	Sez6	0,00557	NM_021286.2	seizure related gene 6
561156	0,312	null	0,0494	null	null
618781	0,318	D630004D15Rik	0,0359	null	RIKEN cDNA D630004D15 gene
705490	0,319	Gm489	0,0141	null	gene model 489, (NCBI)
476991	0,321	LOC384557|Psg29	0,0323	null	pregnancy-specific glycoprotein 29
620416	0,329	Aqr	0,0455	NM_009702.1	aquarius
441639	0,33	9330174C13Rik	0,0405	null	RIKEN cDNA 9330174C13 gene

607819	0,331	LOC436235|Rgs3	0,0349	NM_134257.1	regulator of G-protein signaling 3
838717	0,333	Ggt6	0,0224	NM_027819.1	gamma-glutamyltransferase 6
528034	0,338	B230118H07Rik	0,0223	null	RIKEN cDNA B230118H07 gene
699522	0,338	null	0,0193	null	null
614268	0,339	null	0,0312	null	null
666381	0,339	null	0,00907	null	null
894638	0,341	Tuba1	0,0346	NM_011653.1	tubulin, alpha 1
351046	0,345	Clec4a1	0,0405	NM_199311.1	C-type lectin domain family 4, member a1
922417	0,348	Dcir2|Clec4a2	0,0208	NM_011999.2	C-type lectin domain family 4, member a2
795835	0,35	0610007P14Rik	0,00981	null	RIKEN cDNA 0610007P14 gene
380830	0,355	5330439C02Rik|LOC544812	0,0353	NM_175453.2	RIKEN cDNA 5330439C02 gene
694533	0,355	9430063H18Rik	0,0294	null	RIKEN cDNA 9430063H18 gene
661344	0,356	9230114K14Rik	0,0162	null	RIKEN cDNA 9230114K14 gene
704123	0,36	null	0,0318	null	null
834092	0,361	1700123J03Rik	0,0135	null	RIKEN cDNA 1700123J03 gene
523824	0,362	Avpi1	0,0298	NM_027106.1	arginine vasopressin-induced 1
544037	0,364	9330140K16Rik	0,0282	NM_183019.2	RIKEN cDNA 9330140K16 gene
402854	0,365	Mgll	0,00723	NM_011844.3	monoglyceride lipase
702135	0,365	Hmgb4	0,00424	NM_027036.1	high-mobility group box 4
332871	0,368	Ppm1e	0,0318	null	protein phosphatase 1E (PP2C domain containing)
908253	0,369	Col3a1	0,0143	NM_009930.1	procollagen, type III, alpha 1
446817	0,371	1700064N11Rik	0,0394	null	RIKEN cDNA 1700064N11 gene
711961	0,372	null	0,0237	null	null
770406	0,374	Fah	0,0216	NM_010176.1	fumarylacetoacetate hydrolase
833590	0,374	Lamb2	0,0373	NM_008483.2	laminin, beta 2
931530	0,374	Srebf2	0,0119	null	sterol regulatory element binding factor 2
532830	0,375	Dync1li2	0,036	null	dynein, cytoplasmic 1 light intermediate chain 2
462848	0,38	null	0,0182	null	null
531120	0,381	Camk1	0,0188	NM_133926.1	calcium/calmodulin-dependent protein kinase I
849249	0,381	9130211I03Rik	0,0181	NM_030060.1	RIKEN cDNA 9130211I03 gene
382334	0,384	null	0,0154	null	null
652680	0,384	Cst11	0,00901	NM_030059.1	cystatin 11
307817	0,385	null	0,00496	null	null
656011	0,385	null	0,049	null	null
688049	0,387	I830077J02Rik	0,026	null	RIKEN cDNA I830077J02 gene
299157	0,388	Rnf32	0,0338	null	ring finger protein 32
720216	0,389	LOC624765	0,0466	null	null
377239	0,392	null	0,0275	null	null
631006	0,392	1700015I17Rik	0,0321	null	RIKEN cDNA 1700015I17 gene
492318	0,393	Olfr1240	0,0277	NM_146808.1	olfactory receptor 1240
355752	0,397	null	0,0286	null	null
753313	0,399	Ccl8	0,00685	NM_021443.1	chemokine (C-C motif) ligand 8
313790	0,402	null	0,00171	null	null
801635	0,41	Dact1	0,00684	NM_021532.2	dapper homolog 1, antagonist of beta-catenin (xenopus)
854333	0,41	null	0,026	null	null

695989	0,412	LOC627766	0,0176	null	null
589801	0,416	Eif5a2	0,00752	NM_177586.4	eukaryotic translation initiation factor 5A2
452059	0,418	Gabbr1	0,00495	null	gamma-aminobutyric acid (GABA-B) receptor, 1
489094	0,419	Selenbp2	0,0227	NM_019414.1	selenium binding protein 2
659186	0,424	9330112M16	0,0295	null	null
863480	0,424	4930448C13Rik	0,039	null	RIKEN cDNA 4930448C13 gene
928427	0,424	Lmo6	0,0149	NM_175097.2	LIM domain only 6
629949	0,425	Syt8	0,00417	NM_018802.2	synaptotagmin VIII
317785	0,426	Ifi47	0,021	NM_008330.1	interferon gamma inducible protein 47
870608	0,426	Vill	0,0385	NM_011700.1	villin-like
373960	0,427	4930427A07Rik	0,00129	null	RIKEN cDNA 4930427A07 gene
367657	0,432	Samd9l	0,0293	NM_177590.1	sterile alpha motif domain containing 9-like
550613	0,433	Sorl1	0,0375	NM_011436.1	sortilin-related receptor, LDLR class A repeats-containing
862528	0,434	Tm4sf20	0,0239	NM_025453.1	transmembrane 4 L six family member 20
432503	0,435	C130061O14Rik	0,0325	null	RIKEN cDNA C130061O14 gene
381228	0,437	Metap2	0,00399	null	methionine aminopeptidase 2
549996	0,438	Lrrc27	0,0367	null	leucine rich repeat containing 27
858328	0,439	Klra3|Klra9	0,0128	NM_010651.2	killer cell lectin-like receptor, subfamily A, member 3|killer cell lectin-like receptor subfamily A, member 9
906988	0,441	Lbr	0,0318	NM_133815.1	lamin B receptor
680282	0,443	null	0,0467	null	null
339169	0,444	Sort1	0,0321	NM_019972.2	sortilin 1
772124	0,45	null	0,0126	null	null
316250	0,451	Traip	0,037	NM_011634.2	TRAF-interacting protein
609726	0,453	Cd9	0,0393	null	CD9 antigen
632559	0,459	A630001O12Rik	0,046	null	RIKEN cDNA A630001O12 gene
929652	0,46	Cdc42ep3	0,0315	NM_026514.1	CDC42 effector protein (Rho GTPase binding) 3
476504	0,463	null	0,0339	null	null
909394	0,467	Thbd	0,00428	NM_009378.1	thrombomodulin
929520	0,471	Hist1h2bc|Hist1h2bg	0,0294	NM_023422.1	histone 1, H2bc|histone 1, H2bg
528156	0,475	D11Ertd759e|LOC629974	0,00638	NM_172949.1	DNA segment, Chr 11, ERATO Doi 759, expressed
672645	0,475	null	0,0135	null	null
360305	0,476	null	0,00978	null	null
668748	0,476	Il1f6	0,0247	NM_019450.2	interleukin 1 family, member 6
491310	0,478	null	0,0254	null	null
336302	0,481	2410089E03Rik	0,033	null	RIKEN cDNA 2410089E03 gene
507782	0,488	Tep1	0,026	NM_009351.1	telomerase associated protein 1
331550	0,489	Mrc1	0,0361	NM_008625.1	mannose receptor, C type 1
607214	0,491	Asf1b	0,0361	null	ASF1 anti-silencing function 1 homolog B (S. cerevisiae)
686289	0,491	Cerkl	0,0388	null	ceramide kinase-like
301819	0,493	Mal	0,00546	NM_010762.2	myelin and lymphocyte protein, T-cell differentiation protein
830012	0,493	Mum1	0,0446	NM_023431.4	melanoma associated antigen (mutated) 1
452618	0,497	4931427F14Rik	0,00819	NM_028892.2	RIKEN cDNA 4931427F14 gene

489525	0,501	Nfam1	0,022	NM_028728.1	Nfat activating molecule with ITAM motif 1
541128	0,505	Eif2ak2	0,0182	NM_011163.2	eukaryotic translation initiation factor 2-alpha kinase 2
630664	0,506	Man1c1	0,0106	NM_207237.1	mannosidase, alpha, class 1C, member 1
907105	0,506	Cd200r1	0,046	NM_021325.2	CD200 receptor 1
922147	0,507	Pbxip1	0,0314	NM_146131.1	pre-B-cell leukemia transcription factor interacting protein 1
419024	0,508	2900078C09Rik	0,0331	null	RIKEN cDNA 2900078C09 gene
637794	0,511	Scamp5	0,0379	NM_020270.2	secretory carrier membrane protein 5
746329	0,512	Pira1	0,00889	null	paired-Ig-like receptor A1
914220	0,512	Nmi	0,0436	NM_019401.1	N-myc (and STAT) interactor
897331	0,514	Cks2|LOC626178|LOC635484|LOC633373	0,0366	NM_025415.1	CDC28 protein kinase regulatory subunit 2
325540	0,515	Vamp5	0,049	NM_016872.1	vesicle-associated membrane protein 5
495444	0,519	null	0,0117	null	null
569769	0,519	Kti12	0,0432	NM_029571.1	KTI12 homolog, chromatin associated (S. cerevisiae)
908563	0,519	Cds1	0,0142	NM_173370.3	CDP-diacylglycerol synthase 1
677926	0,52	1190005I06Rik	0,0122	NM_197988.1	RIKEN cDNA 1190005I06 gene
387753	0,521	Gstm2	0,0213	null	glutathione S-transferase, mu 2
596044	0,521	Fasn	0,041	NM_007988.1	fatty acid synthase
735437	0,522	LOC240055|LOC638857	0,0211	null	null
347824	0,526	null	0,0149	null	null
896842	0,529	Olfr707|LOC630437|Olfr708	0,00798	NM_001011542.1	olfactory receptor 707|olfactory receptor 708
303657	0,536	Arpc1b	0,0491	null	actin related protein 2/3 complex, subunit 1B
896076	0,536	LOC277089|LOC640162	0,0227	null	null
828762	0,539	Nfxl1	0,0297	NM_177007.2	nuclear transcription factor, X-box binding-like 1
869267	0,541	Rarsl	0,0169	NM_181406.2	arginyl-tRNA synthetase-like
898849	0,541	Stmn1	0,0263	null	stathmin 1
905599	0,541	1810009M01Rik	0,023	NM_023056.2	RIKEN cDNA 1810009M01 gene
398481	0,545	Tubb2a	0,0101	null	tubulin, beta 2a
896215	0,546	Ppia	0,0335	NM_008907.1	peptidylprolyl isomerase A
509321	0,548	Pkn1	0,0477	null	protein kinase N1
921450	0,55	Igfbp7	0,0254	NM_008048.1	insulin-like growth factor binding protein 7
908765	0,552	3110001D03Rik	0,0162	NM_025849.2	RIKEN cDNA 3110001D03 gene
487473	0,553	2210415F13Rik	0,0108	NM_027339.1	RIKEN cDNA 2210415F13 gene
487085	0,554	Tpst1	0,0396	NM_013837.1	protein-tyrosine sulfotransferase 1
645643	0,555	Gpr112	0,0352	null	G protein-coupled receptor 112
566195	0,557	Pwwp2	0,0237	null	PWWP domain containing 2
455381	0,558	Nudt2	0,0209	NM_025539.1	nudix (nucleoside diphosphate linked moiety X)-type motif 2
907414	0,558	1810027O10Rik	0,00633	null	RIKEN cDNA 1810027O10 gene
621881	0,559	Ece1	0,000851	NM_199307.1	endothelin converting enzyme 1
933050	0,562	Birc1e	0,0272	NM_010870.1	baculoviral IAP repeat-containing 1e
856998	0,563	4931409D07Rik	0,0147	null	RIKEN cDNA 4931409D07 gene
654132	0,564	Rab31	0,0357	NM_133685.1	RAB31, member RAS oncogene family
758078	0,568	Ptpn6	0,0119	NM_013545.1	protein tyrosine phosphatase, non-receptor type 6

318595	0,569	Ntf5	0,037	NM_198190.1	neurotrophin 5
347580	0,569	3110009E18Rik	0,0157	NM_028439.1	RIKEN cDNA 3110009E18 gene
926820	0,569	Zfp161	0,012	NM_009547.2	zinc finger protein 161
794818	0,571	Atxn7l4	0,0283	NM_028139.1	ataxin 7-like 4
354366	0,574	Glb1	0,0118	null	galactosidase, beta 1
516046	0,575	LOC637404|LOC628525	0,0259	null	null
913679	0,576	Lilrb3|LOC619608	0,0177	NM_011095.1	leukocyte immunoglobulin-like receptor, subfamily B (with TM and ITIM domains), member 3
802579	0,577	2310022M17Rik	0,0244	null	RIKEN cDNA 2310022M17 gene
926875	0,578	4930425N13Rik	0,00749	NM_178388.2	RIKEN cDNA 4930425N13 gene
791682	0,58	Clcn5	0,0195	null	chloride channel 5
804312	0,581	Stxbp1	0,046	NM_009295.1	syntaxin binding protein 1
508555	0,59	1110014D18Rik	0,0263	null	RIKEN cDNA 1110014D18 gene
503137	0,592	2610307O08Rik	0,0344	null	RIKEN cDNA 2610307O08 gene
673420	0,593	Olfr1179	0,0255	NM_146917.1	olfactory receptor 1179
563229	0,594	Osbpl11	0,00531	NM_176840.2	oxysterol binding protein-like 11
932625	0,595	Klf10	0,00944	NM_013692.1	Kruppel-like factor 10
415620	0,596	Txnl4	0,0338	NM_025299.1	thioredoxin-like 4
902329	0,597	Ppia	0,0459	null	peptidylprolyl isomerase A
436770	0,599	BC064078	0,0108	null	cDNA sequence BC064078
459464	0,6	Havcr2	0,034	NM_134250.1	hepatitis A virus cellular receptor 2
567508	0,604	Eef2k	0,0348	null	eukaryotic elongation factor-2 kinase
704921	0,604	1500001M20Rik	0,0338	null	RIKEN cDNA 1500001M20 gene
908701	0,605	S100a13	0,0444	NM_009113.2	S100 calcium binding protein A13
368460	0,606	1110007C02Rik	0,0411	NM_027923.1	RIKEN cDNA 1110007C02 gene
610478	0,606	Gstt3	0,0483	NM_133994.2	glutathione S-transferase, theta 3
801460	0,61	Gpsn2	0,0389	NM_134118.1	glycoprotein, synaptic 2
870208	0,613	2410004N11Rik	0,0213	NM_025888.2	RIKEN cDNA 2410004N11 gene
604623	0,614	Parp3	0,00926	NM_145619.2	poly (ADP-ribose) polymerase family, member 3
925260	0,614	Fyb	0,0167	NM_011815.1	FYN binding protein
312704	0,615	Nostrin	0,0249	NM_181547.2	nitric oxide synthase trafficker
911031	0,615	Mcm4	0,0174	NM_008565.2	minichromosome maintenance deficient 4 homolog (S. cerevisiae)
898854	0,618	Hn1	0,0221	NM_008258.1	hematological and neurological expressed sequence 1
334316	0,619	2410017P09Rik	0,0112	null	RIKEN cDNA 2410017P09 gene
453378	0,619	null	0,0476	null	null
859085	0,622	Gale	0,0244	NM_178389.2	galactose-4-epimerase, UDP
915324	0,623	Anxa1	0,0364	NM_010730.1	annexin A1
603831	0,624	Snx27	0,0254	null	sorting nexin family member 27
910929	0,625	Calm1	0,0231	NM_009790.3	calmodulin 1
726026	0,626	Umps	0,0159	NM_009471.1	uridine monophosphate synthetase
729505	0,627	A830007P12Rik	0,0432	NM_146115.2	RIKEN cDNA A830007P12 gene
673478	0,628	C030004G16Rik	0,0174	null	RIKEN cDNA C030004G16 gene
907901	0,629	1600020H07Rik	0,0264	NM_019975.2	RIKEN cDNA 1600020H07 gene
868762	0,634	Tcfcp2	0,00948	NM_033476.1	transcription factor CP2
537456	0,635	2810048G17Rik	0,0363	NM_133746.2	RIKEN cDNA 2810048G17 gene
312148	0,637	Asb8	0,0256	NM_030121.2	ankyrin repeat and SOCS box-containing protein 8
365500	0,637	null	0,0146	null	null

495799	0,637	Scrn3	0,0312	null	secernin 3
564896	0,638	Rtcd1	0,0316	null	RNA terminal phosphate cyclase domain 1
431994	0,639	Lrrc25	0,0436	NM_153074.2	leucine rich repeat containing 25
528718	0,639	Apex1	0,00844	null	apurinic/apyrimidinic endonuclease 1
727935	0,639	Akr1c19	0,0416	null	aldo-keto reductase family 1, member C19
902685	0,639	Tuba6	0,0383	NM_009448.2	tubulin, alpha 6
353985	0,64	2510042P03Rik	0,00186	null	RIKEN cDNA 2510042P03 gene
440132	0,64	Camkk2	0,011	NM_145358.1	calcium/calmodulin-dependent protein kinase kinase 2, beta
434863	0,642	Cyb5	0,0142	NM_025797.1	cytochrome b-5
494716	0,642	Psen2	0,0189	NM_011183.1	presenilin 2
321554	0,643	Ttyh2	0,0327	null	tweety homolog 2 (Drosophila)
356393	0,645	1110018F16Rik	0,03	null	RIKEN cDNA 1110018F16 gene
754153	0,645	Cugbp2	0,0352	NM_010160.1	CUG triplet repeat, RNA binding protein 2
411586	0,646	2310002B06Rik	0,0014	NM_181649.2	RIKEN cDNA 2310002B06 gene
453235	0,646	Rcbtb2	0,0471	null	regulator of chromosome condensation (RCC1) and BTB (POZ) domain containing protein 2
487148	0,647	3110003A17Rik	0,0239	null	RIKEN cDNA 3110003A17 gene
850994	0,647	4930538D17Rik	0,0228	NM_029186.1	RIKEN cDNA 4930538D17 gene
900913	0,647	LOC631031|LOC627165|Lsm6|LOC635563	0,00383	null	LSM6 homolog, U6 small nuclear RNA associated (S. cerevisiae)
405688	0,65	null	0,0342	null	null
479437	0,652	Vps13d	0,0371	null	vacuolar protein sorting 13D (yeast)
902671	0,653	Actg1|LOC545167	0,015	NM_009609.2	actin, gamma, cytoplasmic 1
767665	0,654	Ralb	0,0118	NM_022327.3	v-ral simian leukemia viral oncogene homolog B (ras related)
803218	0,658	Zfp668	0,0212	NM_146259.2	zinc finger protein 668
883374	0,658	null	0,017	null	null
809382	0,659	null	0,0413	null	null
904378	0,661	Qdpr	0,0251	NM_024236.1	quininoid dihydropteridine reductase
568105	0,663	Lyn	0,0499	null	Yamaguchi sarcoma viral (v-yes-1) oncogene homolog
436393	0,664	Ofcc1	0,0392	NM_172143.1	orofacial cleft 1 candidate 1
437857	0,666	Gsn	0,0268	NM_146120.2	gelsolin
916060	0,666	Ebpl	0,0138	NM_026598.1	emopamil binding protein-like
927665	0,666	2700029M09Rik	0,0118	null	RIKEN cDNA 2700029M09 gene

Pathway matching was also performed for upregulated genes in the comparison of DMHCA-treatment versus control (Figure A, Table D).

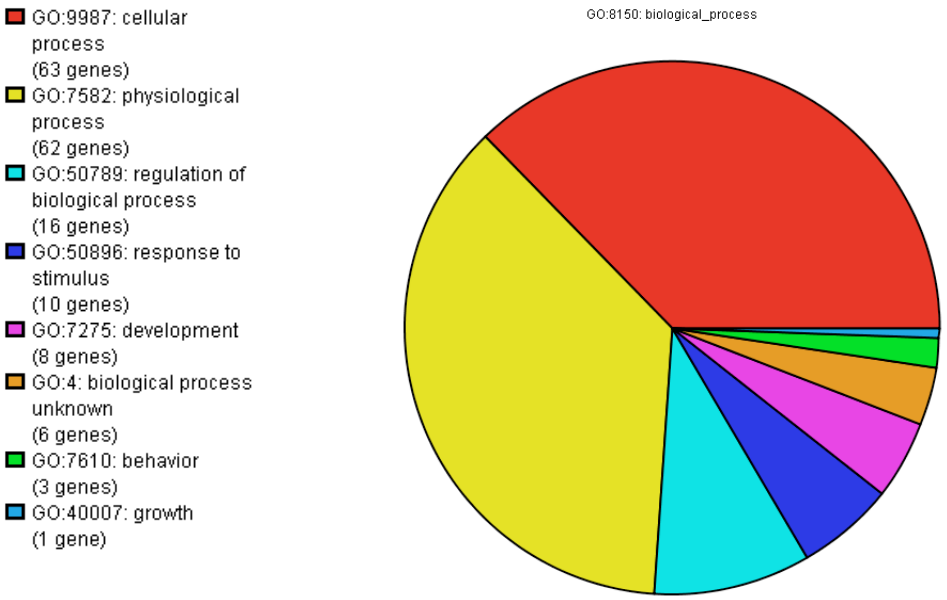

Figure A. DMHCA vs Ctrl, up in DMHCA
The pie chart shows that most genes upregulated with DMHCA play a role in cellular and physiological processes.

Table D. Pathway analysis: DMHCA-treated compared to control, up upon DMHCA treatment with *FC*≥2, p≤0.1; most abundant pathways

Category	Genes in Category	% of Genes in Category	Genes in List in	% of Genes in List in Category	p-Value
GO:6869: lipid transport	61	0,446	5	7,353	1,26E-05
GO:50875: cellular physiological process	9300	68,07	60	88,24	0,0001
GO:6983: ER overload response	4	0,0293	2	2,941	0,000146
GO:6457: protein folding	231	1,691	7	10,29	0,000146
GO:74: regulation of progression through cell cycle	315	2,306	8	11,76	0,000162
GO:15918: sterol transport	7	0,0512	2	2,941	0,000504
GO:30301: cholesterol transport	7	0,0512	2	2,941	0,000504
GO:6984: ER-nuclear signaling pathway	9	0,0659	2	2,941	0,000859
GO:8652: amino acid biosynthesis	43	0,315	3	4,412	0,00126
GO:6888: ER to Golgi transport	57	0,417	3	4,412	0,00285
GO:7049: cell cycle	607	4,443	9	13,24	0,00301
GO:6094: gluconeogenesis	18	0,132	2	2,941	0,00355
GO:9309: amine biosynthesis	62	0,454	3	4,412	0,00362
GO:44271: nitrogen compound biosynthesis	62	0,454	3	4,412	0,00362
GO:6082: organic acid metabolism	406	2,972	7	10,29	0,00396
GO:19752: carboxylic acid metabolism	406	2,972	7	10,29	0,00396
GO:6986: response to unfolded protein	67	0,49	3	4,412	0,0045
GO:19276: UDP-N-acetylgalactosamine metabolism	1	0,00732	1	1,471	0,00498
GO:42789: mRNA transcription from RNA polymerase II promoter	1	0,00732	1	1,471	0,00498
GO:9299: mRNA transcription	1	0,00732	1	1,471	0,00498
GO:6931: substrate-bound cell migration, cell attachment to substrate	1	0,00732	1	1,471	0,00498
GO:6090: pyruvate metabolism	22	0,161	2	2,941	0,00529

GO:46364: monosaccharide biosynthesis	23	0,168	2	2,941	0,00577
GO:19319: hexose biosynthesis	23	0,168	2	2,941	0,00577
GO:46165: alcohol biosynthesis	23	0,168	2	2,941	0,00577
GO:48193: Golgi vesicle transport	75	0,549	3	4,412	0,00617
GO:9064: glutamine family amino acid metabolism	24	0,176	2	2,941	0,00628
GO:6915: apoptosis	469	3,433	7	10,29	0,00856
GO:12501: programmed cell death	478	3,499	7	10,29	0,00945
GO:7527: adult somatic muscle development	2	0,0146	1	1,471	0,00993

The most abundant and most significantly involved pathway in DMHCA-upregulated genes in the comparison of DMHCA with control was the lipid transport. 121 genes were upregulated with DMHCA when DMHCA treatment was compared with control ($p \leq 0.1$ and $FC \geq 2$).

Table E. Upregulated genes in DMHCA versus control, up with DMHCA for p≤0.1 and FC≥2

Fold Change	Common	P-value	Genbank	Description
13,81	Car6	0,0197	NM_009802.1	carbonic anhydrase 6
6,682	Trib3	0,0132	NM_144554.1	tribbles homolog 3 (Drosophila)
5,798	Abca1	0,0521	NM_013454.2	ATP-binding cassette, sub-family A (ABC1), member 1
5,785	Lbp	0,0616	NM_008489.1	lipopolysaccharide binding protein
5,624	Chac1	0,0164	NM_026929.2	ChaC, cation transport regulator-like 1 (E. coli)
5,534	Ddit3	0,046	NM_007837.2	DNA-damage inducible transcript 3
5,499	Il18bp	0,0481	NM_010531.1	interleukin 18 binding protein
4,78	Krtap16-4	0,0761	NM_130873.1	keratin associated protein 16-4
4,42	Asns	0,0278	NM_012055.1	asparagine synthetase
4,246	Ndrg1	0,0131	NM_010884.1	N-myc downstream regulated gene 1
4,216	Serpinb9c	0,0892	NM_011453.2	serine (or cysteine) peptidase inhibitor, clade B, member 9c
4,13	LOC625537| LOC640536	0,0671	null	null
4,112	Mylip	0,039	NM_153789.2	myosin regulatory light chain interacting protein
3,968	C1ql1	0,0684	null	complement component 1, q subcomponent-like 1
3,931	Pck2	0,0209	NM_028994.1	phosphoenolpyruvate carboxykinase 2 (mitochondrial)
3,798	B3galnt2	0,0851	NM_178640.1	UDP-GalNAc:betaGlcNAc beta 1,3-galactosaminyltransferase, polypeptide 2
3,691	Abcg1	0,0657	NM_009593.1	ATP-binding cassette, sub-family G (WHITE), member 1
3,517	Kdelr2	0,0977	NM_025841.1	KDEL (Lys-Asp-Glu-Leu) endoplasmic reticulum protein retention receptor 2
3,51	Arid5a	0,0957	NM_145996.2	AT rich interactive domain 5A (Mrf1 like)
3,468	Fbxo32	0,0481	NM_026346.1	F-box only protein 32
3,416	Faah	0,0179	NM_010173.2	fatty acid amide hydrolase
3,415	3732413I11Rik	0,0239	NM_028862.1	RIKEN cDNA 3732413I11 gene
3,412	Aqp9	0,0194	NM_022026.2	aquaporin 9
3,378	Dusp1	0,000954	NM_013642.1	dual specificity phosphatase 1
3,318	Sqstm1	0,0857	NM_011018.1	sequestosome 1
3,227	Refbp2	0,0556	null	RNA and export factor binding protein 2
3,215	Det1	0,0742	NM_029585.2	de-etiolated homolog 1 (Arabidopsis)

3,178	Fabp2	0,0978	NM_007980.2	fatty acid binding protein 2, intestinal
3,153	Spata5l1	0,0262	null	spermatogenesis associated 5-like 1
3,135	Dnajb9	0,0636	null	DnaJ (Hsp40) homolog, subfamily B, member 9
3,106	Dnajc16	0,0405	NM_172338.1	DnaJ (Hsp40) homolog, subfamily C, member 16
3,085	Pik3cb	0,0364	NM_029094.1	phosphatidylinositol 3-kinase, catalytic, beta polypeptide
3,079	Mthfd2	0,0696	NM_008638.1	methylenetetrahydrofolate dehydrogenase (NAD+ dependent), methenyltetrahydrofolate cyclohydrolase
3,057	Ier3	0,0903	NM_133662.1	immediate early response 3
3,034	Il1a	0,0797	NM_010554.3	interleukin 1 alpha
3,023	Dnaja3	0,0823	NM_023646.2	DnaJ (Hsp40) homolog, subfamily A, member 3
3,003	Ung	0,055	null	uracil DNA glycosylase
2,953	Foxk2	0,0409	null	forkhead box K2
2,931	Gramd1b	0,0889	NM_172768.1	GRAM domain containing 1B
2,9	2810428C21Rik	0,015	null	RIKEN cDNA 2810428C21 gene
2,834	Gadd45a	0,0124	NM_007836.1	growth arrest and DNA-damage-inducible 45 alpha
2,754	Cd2ap	0,0972	NM_009847.2	CD2-associated protein
2,739	null	0,0563	null	null
2,734	BC022687	0,0359	NM_145450.2	cDNA sequence BC022687
2,732	Pltp	0,0159	NM_011125.1	phospholipid transfer protein
2,705	null	0,0375	null	null
2,686	2310026L22Rik	0,0454	null	RIKEN cDNA 2310026L22 gene
2,675	Slc43a3	0,0774	NM_021398.1	solute carrier family 43, member 3
2,653	4732471D19Rik	0,0276	NM_176987.2	RIKEN cDNA 4732471D19 gene
2,619	null	0,0661	null	null
2,616	Wdr67	0,0261	null	WD repeat domain 67
2,615	MGC27770	0,0442	NM_145986.1	null
2,609	Vegfa	0,0765	NM_009505.2	vascular endothelial growth factor A
2,608	Nktr	0,053	null	natural killer tumor recognition sequence
2,599	A930014E10Rik	0,0872	null	RIKEN cDNA A930014E10 gene
2,598	1700003F17Rik	0,082	null	RIKEN cDNA 1700003F17 gene
2,596	1700009P17Rik	0,0656	NM_029301.1	RIKEN cDNA 1700009P17 gene
2,589	Cry1	0,038	NM_007771.3	cryptochrome 1 (photolyase-like)
2,559	Rps27	0,0405	null	ribosomal protein S27
2,519	Tes	0,0944	NM_207176.2	testis derived transcript
2,507	Copb1	0,0896	NM_033370.2	coatomer protein complex, subunit beta 1
2,467	Psat1	0,0126	NM_177420.1	phosphoserine aminotransferase 1
2,449	AW124694	0,0869	null	expressed sequence AW124694
2,434	Herpud1	0,0652	NM_022331.1	homocysteine-inducible, endoplasmic reticulum stress-inducible, ubiquitin-like domain member 1
2,426	Npal3	0,0806	NM_028995.1	NIPA-like domain containing 3
2,405	Ifrd1	0,0113	NM_013562.1	interferon-related developmental regulator 1
2,383	Sec23a	0,00682	null	SEC23A (S. cerevisiae)
2,369	Xpot|LOC639101|LOC634577|LOC625674	0,0538	null	exportin, tRNA (nuclear export receptor for tRNAs)
2,368	Mir16	0,0545	NM_019580.3	membrane interacting protein of RGS16
2,365	Zfp689	0,0727	NM_175163.2	zinc finger protein 689
2,365	null	0,0607	null	null
2,363	LOC236749	0,0963	null	null
2,361	Arfgap3	0,013	NM_025445.2	ADP-ribosylation factor GTPase activating protein 3
2,333	Aldh18a1	0,0033	null	aldehyde dehydrogenase 18 family, member A1

2,326	LOC432832	0,0544	null	null
2,311	Heca	0,029	null	headcase homolog (Drosophila)
2,311	null	0,00912	null	null
2,31	Gramd1b	0,0205	null	GRAM domain containing 1B
2,308	1700019H03Rik	0,0678	null	RIKEN cDNA 1700019H03 gene
2,307	BC025076	0,0906	NM_175002.1	cDNA sequence BC025076
2,277	Skp2	0,0871	NM_013787.1	S-phase kinase-associated protein 2 (p45)
2,277	Mtmr4	0,0635	NM_133215.1	myotubularin related protein 4
2,266	null	0,0924	null	null
2,241	Sec24d	0,0755	NM_027135.2	SEC24 related gene family, member D (S. cerevisiae)
2,234	H13	0,0901	NM_010376.2	histocompatibility 13
2,225	LOC634529|LOC624188|LOC624199|LOC634517|LOC634546	0,02	null	null
2,215	Btg3|LOC640416	0,0207	NM_009770.1	B-cell translocation gene 3
2,205	Cxcl1	0,0116	NM_008176.1	chemokine (C-X-C motif) ligand 1
2,195	Elk4	0,0482	NM_007923.1	ELK4, member of ETS oncogene family
2,192	Kif3a	0,061	NM_008443.2	kinesin family member 3A
2,186	Sec63	0,0598	NM_153055.2	SEC63-like (S. cerevisiae)
2,184	Atf4	0,00569	NM_009716.1	activating transcription factor 4
2,184	Slc39a7	0,0471	NM_008202.1	solute carrier family 39 (zinc transporter), member 7
2,177	Atad2	0,0414	NM_153199.1	ATPase family, AAA domain containing 2
2,168	Nfil3	0,0425	NM_017373.3	nuclear factor, interleukin 3, regulated
2,167	A530079E22Rik	0,0208	NM_177048.2	RIKEN cDNA A530079E22 gene
2,166	LOC628772|LOC621500|LOC636273	0,0428	null	null
2,154	Parp9	0,0342	NM_030253.2	poly (ADP-ribose) polymerase family, member 9
2,135	Hist4h4|LOC632387	0,00224	NM_175652.1	histone 4, H4
2,134	Sec24a	0,0598	NM_175255.2	SEC24 related gene family, member A (S. cerevisiae)
2,127	A430054B03	0,0919	null	null
2,119	Gmppb	0,0309	NM_177910.2	GDP-mannose pyrophosphorylase B
2,092	Met	0,09	NM_008591.1	met proto-oncogene
2,092	Ptgir	0,0717	NM_008967.1	prostaglandin I receptor (IP)
2,073	LOC544815	0,0214	null	null
2,061	null	0,0492	null	null
2,06	Frs3	0,0113	NM_144939.1	fibroblast growth factor receptor substrate 3
2,059	Gtlf3a	0,00656	NM_025293.1	gene trap locus F3a
2,058	Osbpl7	0,0644	null	oxysterol binding protein-like 7
2,054	Rgs1	0,0998	NM_015811.1	regulator of G-protein signaling 1
2,052	Epor	0,04	NM_010149.2	erythropoietin receptor
2,036	null	0,0219	null	null
2,029	Tnfrsf12a	0,0936	NM_013749.1	tumor necrosis factor receptor superfamily, member 12a
2,018	Wdr75	0,0308	null	WD repeat domain 75
2,016	Coasy	0,00346	NM_027896.1	Coenzyme A synthase
2,011	Bbc3	0,0448	NM_133234.1	Bcl-2 binding component 3
2,01	Hspa5	0,0119	NM_022310.2	heat shock 70kD protein 5 (glucose-regulated protein)
2,009	LOC632563|LOC623719	0,0118	null	null
2,007	BC062650	0,0859	null	cDNA sequence BC062650
2,005	LOC633677|Eprs	0,0997	null	glutamyl-prolyl-tRNA synthetase

12.1.2 T0901317-treated macrophages versus control-treated macrophages

Pathway analysis in T0901317-treated MPM versus control-treated cells, upregulated with T0901317, showed the lipid transport to be the most significantly regulated pathway.

Table F Pathway analysis: T0901317-treated compared to control, up after T0901317 treatment with *FC*≥2, p≤0.1; most abundant pathways

Category	Genes in Category	% of Genes in Category	Genes in List in	% of Genes in List in Category	p-Value
GO:6869: lipid transport	61	0,446	4	11,43	1,70E-05
GO:15918: sterol transport	7	0,0512	2	5,714	0,000133
GO:30301: cholesterol transport	7	0,0512	2	5,714	0,000133
GO:6633: fatty acid biosynthesis	55	0,403	3	8,571	0,000369
GO:6631: fatty acid metabolism	135	0,988	4	11,43	0,000376
GO:44255: cellular lipid metabolism	387	2,833	6	17,14	0,000402
GO:16053: organic acid biosynthesis	58	0,425	3	8,571	0,000432
GO:46394: carboxylic acid biosynthesis	58	0,425	3	8,571	0,000432
GO:6801: superoxide metabolism	17	0,124	2	5,714	0,000846
GO:6629: lipid metabolism	481	3,521	6	17,14	0,00126
GO:7144: female meiosis I	1	0,00732	1	2,857	0,00256
GO:7413: axonal fasciculation	2	0,0146	1	2,857	0,00512
GO:42157: lipoprotein metabolism	44	0,322	2	5,714	0,00564
GO:45332: phospholipid translocation	3	0,022	1	2,857	0,00767
GO:15914: phospholipid transport	3	0,022	1	2,857	0,00767
GO:8203: cholesterol metabolism	54	0,395	2	5,714	0,00839
GO:6512: ubiquitin cycle	513	3,755	5	14,29	0,00936
GO:16125: sterol metabolism	58	0,425	2	5,714	0,00963
GO:6800: oxygen and reactive oxygen species metabolism	62	0,454	2	5,714	0,011
GO:8610: lipid biosynthesis	182	1,332	3	8,571	0,0111
GO:30239: myofibril assembly	5	0,0366	1	2,857	0,0127
GO:45214: sarcomere organization	5	0,0366	1	2,857	0,0127
GO:30968: unfolded protein response	5	0,0366	1	2,857	0,0127
GO:50875: cellular physiological process	9300	68,07	30	85,71	0,0152
GO:7143: female meiosis	6	0,0439	1	2,857	0,0153

66 genes were upregulated with T0901317 in the comparison of T0901317-treated MPM versus control-treated cells (p≤0.1 and *FC*≥2)

Table G. Upregulated genes in T0901317 versus control, up in T0901317 with p≤0.1 and FC≥2

Gene Name	P-value	Common	Fold Change	Genbank	Description
575019	0,0319	Scd1	7,29	NM_009127.2	stearoyl-Coenzyme A desaturase 1
797048	0,0939	Il18bp	5,347	NM_010531.1	interleukin 18 binding protein
802990	0,0747	4930428E23Rik	5,072	null	RIKEN cDNA 4930428E23 gene
403608	0,0709	Abca1	4,281	NM_013454.2	ATP-binding cassette, sub-family A (ABC1), member 1
596044	0,0428	Fasn	4,239	NM_007988.1	fatty acid synthase
601840	0,0305	Mylip	4,14	NM_153789.2	myosin regulatory light chain interacting protein
646071	0,00668	Scd2	4,084	NM_009128.1	stearoyl-Coenzyme A desaturase 2
909582	0,0495	Srebf1	3,711	NM_011480.1	sterol regulatory element binding factor 1
391972	0,0186	Mmp27	3,39	null	matrix metallopeptidase 27
637641	0,00527	A930014E01Rik	3,332	null	RIKEN cDNA A930014E01 gene
916686	0,00598	Ndrg1	3,299	NM_010884.1	N-myc downstream regulated gene 1
917377	0,061	S100a16	3,263	NM_026416.2	S100 calcium binding protein A16
410126	0,0936	1700009P17Rik	3,205	NM_029301.1	RIKEN cDNA 1700009P17 gene
573930	0,0353	null	3,188	null	null
532780	0,0886	Abcg1	3,09	NM_009593.1	ATP-binding cassette, sub-family G (WHITE), member 1
392895	0,0637	Ero1l	3,066	NM_015774.2	ERO1-like (S. cerevisiae)
445998	0,0432	5033430I15Rik	2,995	null	RIKEN cDNA 5033430I15 gene
931031	0,0369	Abi3	2,903	NM_025659.1	ABI gene family, member 3
532736	0,0125	2310005P05Rik	2,791	NM_026189.2	RIKEN cDNA 2310005P05 gene
603303	0,053	Apoc1	2,736	NM_007469.2	apolipoprotein C-I
703716	0,0936	Gpr176	2,72	NM_201367.1	G protein-coupled receptor 176
396513	0,0637	C530025M09Rik	2,706	null	RIKEN cDNA C530025M09 gene
443397	0,0425	C130022K22Rik	2,704	NM_172730.1	RIKEN cDNA C130022K22 gene
598999	0,0715	Pltp	2,658	NM_011125.1	phospholipid transfer protein
755030	0,0978	Serpinb9c	2,653	NM_011453.2	serine (or cysteine) peptidase inhibitor, clade B, member 9c
928375	0,0957	Cd5l	2,641	NM_009690.1	CD5 antigen-like
505100	0,0714	4933409L06Rik	2,619	null	RIKEN cDNA 4933409L06 gene
555784	0,0659	Zfp27	2,616	NM_011754.1	zinc finger protein 27
643007	0,0541	null	2,608	null	null
433673	0,0542	2700033H19Rik	2,593	null	RIKEN cDNA 2700033H19 gene
678907	0,0102	Dscr1l2	2,566	NM_022980.2	Down syndrome critical region gene 1-like 2
786761	0,0078	Gdf15	2,55	NM_011819.1	growth differentiation factor 15
325670	0,0286	Zfp11	2,521	NM_172462.1	zinc finger protein 11
884290	0,0991	Celsr3	2,473	NM_080437.1	cadherin EGF LAG seven-pass G-type receptor 3
790904	0,0716	Zfp260|LOC635007	2,458	NM_011981.4	zinc finger protein 260
839063	0,061	Mare	2,431	NM_181569.1	alpha globin regulatory element containing gene
904090	0,00712	null	2,427	null	null
741416	0,0397	Ophn1	2,418	NM_052976.2	oligophrenin 1
932169	0,0922	Dusp6	2,397	NM_026268.1	dual specificity phosphatase 6
438272	0,0111	null	2,386	null	null

926804	0,0309	Mmp11	2,363	NM_008606.1	matrix metallopeptidase 11
453584	0,0828	Acsl3	2,315	NM_028817.1	acyl-CoA synthetase long-chain family member 3
527466	0,0416	Mlh3	2,313	null	mutL homolog 3 (E coli)
543288	0,04	Faah	2,304	NM_010173.2	fatty acid amide hydrolase
576927	0,0285	9830002I17Rik	2,281	NM_029932.1	RIKEN cDNA 9830002I17 gene
859645	0,0124	Surf6	2,274	NM_009298.2	surfeit gene 6
389652	0,0852	D12Wsu118e	2,272	null	DNA segment, Chr 12, Wayne State University 118, expressed
765113	0,0455	Atrnl1	2,262	NM_181415.3	attractin like 1
375946	0,0685	Pcgf6	2,239	NM_027654.1	polycomb group ring finger 6
911606	0,0624	Spire1	2,232	NM_194355.1	spire homolog 1 (Drosophila)
907938	0,0742	3732413I11Rik	2,214	NM_028862.1	RIKEN cDNA 3732413I11 gene
558461	0,0137	1110008J03Rik	2,209	NM_029096.1	RIKEN cDNA 1110008J03 gene
447466	0,0462	Fbxw8	2,198	NM_172721.1	F-box and WD-40 domain protein 8
887658	0,0278	null	2,173	null	null
450952	0,0998	Fbxo32	2,156	NM_026346.1	F-box only protein 32
328511	0,0839	4933425L03Rik	2,142	null	RIKEN cDNA 4933425L03 gene
718639	0,0778	Pdcd11	2,109	NM_011053.2	programmed cell death protein 11
548849	0,0684	3110018I06Rik	2,072	null	RIKEN cDNA 3110018I06 gene
462865	0,0392	Tmem86a	2,068	NM_026436.1	transmembrane protein 86A
527334	0,0421	Entpd4	2,05	NM_026174.1	ectonucleoside triphosphate diphosphohydrolase 4
475354	0,0696	Lrrk1	2,044	NM_146191.3	leucine-rich repeat kinase 1
442176	0,0286	Neurl2	2,028	null	neuralized-like 2 (Drosophila)
588861	0,0392	Gli3	2,028	NM_008130.1	GLI-Kruppel family member GLI3
361480	0,0899	Chac1	2,009	NM_026929.2	ChaC, cation transport regulator-like 1 (E. coli)
604511	0,0695	2410127E18Rik	2,009	NM_029742.1	RIKEN cDNA 2410127E18 gene
535686	0,0443	D530031C13Rik	2,001	null	RIKEN cDNA D530031C13 gene

For downregulated genes upon T0901317 treatment in T0901317 versus control no obvious pathway was highly significantly regulated. This can be seen in Table H, where the p-values do not show high significance (The lower the p-value, the more certain the involvement of a pathway).

Table H. Pathway analysis: T0901317-treated compared to control, down after T0901317 treatment with *FC*≤0.5, p≤0.1; most abundant pathways

Category	Genes in Category	% of Genes in Category	Genes in List in	% of Genes in List in Category	p-Value
GO:7218: neuropeptide signaling pathway	78	0,571	4	3,774	0,00314
GO:7613: memory	13	0,0952	2	1,887	0,0044
GO:7402: ganglion mother cell fate determination	1	0,00732	1	0,943	0,00776
GO:8052: sensory organ determination	1	0,00732	1	0,943	0,00776
GO:42987: amyloid precursor protein catabolism	1	0,00732	1	0,943	0,00776
GO:30575: nuclear body organization and biogenesis	1	0,00732	1	0,943	0,00776
GO:30578: PML body organization and biogenesis	1	0,00732	1	0,943	0,00776
GO:7220: Notch receptor processing	1	0,00732	1	0,943	0,00776
GO:270: peptidoglycan metabolism	18	0,132	2	1,887	0,00841

GO:8544: epidermis development	67	0,49	3	2,83	0,0152
GO:51605: proteolysis during protein maturation	2	0,0146	1	0,943	0,0155
GO:51604: protein maturation	2	0,0146	1	0,943	0,0155
GO:51563: smooth endoplasmic reticulum calcium ion homeostasis	2	0,0146	1	0,943	0,0155
GO:7616: long-term memory	2	0,0146	1	0,943	0,0155
GO:7168: receptor guanylyl cyclase signaling pathway	2	0,0146	1	0,943	0,0155
GO:7398: ectoderm development	71	0,52	3	2,83	0,0177
GO:7154: cell communication	3597	26,33	38	35,85	0,0191

131 genes were downregulated with T0901317 treatment when T0901317-treated MPM were compared with control-treated cells ($p \leq 0.05$, $FC \leq 0.5$).

Table I. Downregulated genes in T0901317 versus control, down with T0901317 for $p \leq 0.05$, $FC \leq 0.5$

Gene Name	P-value	Common	Fold Change	Genbank	Description
848334	0,031	4930543L23Rik	0,118	NM_183110.1	RIKEN cDNA 4930543L23 gene
756978	2,27E-05	null	0,119	null	null
882896	0,0191	6530439I21	0,141	NM_177837.2	null
867196	0,00302	BC042761	0,162	null	cDNA sequence BC042761
462868	0,0349	Cox7b	0,163	null	cytochrome c oxidase subunit VIIb
434336	0,0303	Pfkfb1	0,167	null	6-phosphofructo-2-kinase/fructose-2,6-biphosphatase 1
892253	0,0295	Mrg2	0,179	null	myeloid ecotropic viral integration site-related gene 2
651224	0,0405	6820408C15Rik	0,18	NM_177656.2	RIKEN cDNA 6820408C15 gene
732869	0,0311	Rhpn1	0,186	NM_008164.1	rhophilin, Rho GTPase binding protein 1
327795	0,0205	Hcn2	0,201	NM_008226.1	hyperpolarization-activated, cyclic nucleotide-gated K+ 2
671858	0,0149	LOC631764|LOC620595|LOC239191|Dnmt3b	0,212	NM_001003960.1	DNA methyltransferase 3B
378325	0,0443	Tmprss6	0,217	NM_027902.1	transmembrane serine protease 6
931113	0,0322	Aqp9	0,217	NM_022026.2	aquaporin 9
662135	0,0326	Cacng8	0,222	NM_133190.1	calcium channel, voltage-dependent, gamma subunit 8
476463	0,00139	Myo1e	0,228	NM_181072.2	myosin IE
550392	0,0495	Mapk3	0,23	NM_011952.1	mitogen activated protein kinase 3
746252	0,0337	Rab19	0,233	NM_011226.1	RAB19, member RAS oncogene family
339413	0,016	Gnl3l	0,237	NM_198110.1	guanine nucleotide binding protein-like 3 (nucleolar)-like
400547	0,0147	Mmp17	0,239	NM_011846.3	matrix metallopeptidase 17
532222	0,0191	Kifc2	0,265	NM_010630.1	kinesin family member C2
795225	0,0165	Trem1	0,268	NM_021406.2	triggering receptor expressed on myeloid cells 1
623195	0,0455	C630001G18Rik	0,272	null	RIKEN cDNA C630001G18 gene
829972	0,0399	Enpp4	0,273	null	ectonucleotide pyrophosphatase/phosphodiesterase 4
362079	0,0415	Zfp710	0,275	NM_175433.4	zinc finger protein 710

485202	0,0412	Acp1	0,276	NM_021330.2	acid phosphatase 1, soluble
509062	0,0321	Zfp318	0,277	NM_207671.2	zinc finger protein 318
672645	0,0455	null	0,28	null	null
847962	0,0357	null	0,28	null	null
729451	0,0275	Pik4cb	0,281	NM_175356.1	phosphatidylinositol 4-kinase, catalytic, beta polypeptide
464140	0,00497	Ripk5	0,283	NM_172516.2	receptor interacting protein kinase 5
582299	0,00677	Kbtbd8	0,283	NM_001008785.1	kelch repeat and BTB (POZ) domain containing 8
630898	0,0493	E130114P18Rik	0,285	null	RIKEN cDNA E130114P18 gene
410328	0,0319	null	0,286	null	null
318595	0,00434	Ntf5	0,288	NM_198190.1	neurotrophin 5
434342	0,0366	1700020N18Rik	0,288	null	RIKEN cDNA 1700020N18 gene
380631	0,0461	Bmp2	0,289	NM_007553.1	bone morphogenetic protein 2
322213	0,0153	Gnptab	0,297	NM_001004164.1	null
462888	0,0185	Aicda	0,297	NM_009645.1	activation-induced cytidine deaminase
608848	0,0352	Prr3	0,297	null	proline-rich polypeptide 3
320722	0,0135	4930479M11Rik	0,305	NM_183108.1	RIKEN cDNA 4930479M11 gene
553010	0,0209	1700100I10Rik	0,305	null	RIKEN cDNA 1700100I10 gene
438449	0,0231	Atpbd3	0,306	NM_145582.1	ATP binding domain 3
887478	0,0383	Pml	0,311	null	promyelocytic leukemia
728547	0,0205	Gpr112	0,313	null	G protein-coupled receptor 112
474562	0,023	Serpina3n	0,315	NM_009252.1	serine (or cysteine) peptidase inhibitor, clade A, member 3N
666956	0,0103	Zbtb10	0,319	null	zinc finger and BTB domain containing 10
862528	0,043	Tm4sf20	0,321	NM_025453.1	transmembrane 4 L six family member 20
883173	0,015	Odz4	0,322	null	odd Oz/ten-m homolog 4 (Drosophila)
456283	0,0392	Rhebl1	0,323	NM_026967.3	Ras homolog enriched in brain like 1
481867	0,00956	4933439K11Rik	0,325	null	RIKEN cDNA 4933439K11 gene
916979	0,00692	Gcn1l1	0,327	null	GCN1 general control of amino-acid synthesis 1-like 1 (yeast)
522188	0,0234	4930562D21Rik	0,328	null	RIKEN cDNA 4930562D21 gene
866913	0,0336	Minpp1	0,331	null	multiple inositol polyphosphate histidine phosphatase 1
383046	0,0268	Col15a1	0,332	NM_009928.2	procollagen, type XV
538501	0,018	LOC620400	0,333	null	null
445847	0,0331	Rarres1	0,335	null	retinoic acid receptor responder (tazarotene induced) 1
642595	0,00565	null	0,336	null	null
834228	0,0199	Ceacam1	0,338	null	CEA-related cell adhesion molecule 1
695268	0,0119	Olfr480	0,339	NM_020291.1	olfactory receptor 480
396284	0,00887	1700018A23Rik	0,343	null	RIKEN cDNA 1700018A23 gene
724199	0,0394	V1rc33|LOC434017	0,345	NM_134436.1	vomeronasal 1 receptor, C33
432073	0,0467	BC024386	0,346	null	cDNA sequence BC023486
613984	0,0201	Ythdf3	0,348	NM_172677.2	YTH domain family 3
828662	0,0376	null	0,349	null	null
381530	0,0289	6230429P13Rik	0,35	null	RIKEN cDNA 6230429P13 gene
589307	0,0382	Il4i1	0,35	NM_010215.1	interleukin 4 induced 1
450585	0,0388	Perld1	0,355	null	per1-like domain containing 1

822876	0,015	1110002J07Rik	0,355	null	RIKEN cDNA 1110002J07 gene
385086	0,0459	Tmem52	0,356	null	transmembrane protein 52
801120	0,00962	Rhobtb2	0,358	null	Rho-related BTB domain containing 2
454396	0,0378	null	0,359	null	null
476264	0,00716	LOC433565|LOC636299	0,36	null	null
498083	0,00238	Cd79b	0,371	NM_008339.1	CD79B antigen
801635	0,00705	Dact1	0,371	NM_021532.2	dapper homolog 1, antagonist of beta-catenin (xenopus)
319089	0,00492	Gpr147	0,374	null	G protein-coupled receptor 147
918490	0,0418	Kctd16	0,375	null	potassium channel tetramerisation domain containing 16
472648	0,00874	Crhbp	0,38	NM_198408.1	corticotropin releasing hormone binding protein
416270	0,00848	Arrdc5	0,381	null	arrestin domain containing 5
828538	0,0244	1810064L21Rik	0,383	NM_176946.2	RIKEN cDNA 1810064L21 gene
722795	0,0177	Olfr399	0,386	NM_147004.1	olfactory receptor 399
441270	0,0455	Pcdh7	0,391	null	protocadherin 7
462848	0,0181	null	0,391	null	null
725442	0,0312	4931406C07Rik	0,391	NM_133732.1	RIKEN cDNA 4931406C07 gene
674079	0,011	4632427E13Rik	0,392	null	RIKEN cDNA 4632427E13 gene
301877	0,0234	Slc25a14	0,393	NM_011398.1	solute carrier family 25 (mitochondrial carrier, brain), member 14
366102	0,00392	null	0,394	null	null
509895	0,00727	Upb1	0,395	NM_133995.1	ureidopropionase, beta
337568	0,0367	null	0,396	null	null
614102	0,00465	BC021381	0,396	NM_145382.2	cDNA sequence BC021381
917041	0,0399	Prlpc3	0,396	NM_023741.1	prolactin-like protein C 3
490817	0,0435	4930480K23Rik	0,397	null	RIKEN cDNA 4930480K23 gene
558201	0,0284	LOC229005|LOC622647|LOC638740	0,397	null	null
547181	0,0318	Cdca8	0,399	NM_026560.2	cell division cycle associated 8
896881	0,0211	Zfp352	0,399	NM_153102.1	zinc finger protein 352
628216	0,0337	Ednra	0,402	NM_010332.1	endothelin receptor type A
638287	0,0356	D830044I16Rik	0,404	null	RIKEN cDNA D830044I16 gene
860746	0,0482	Speer2	0,404	null	spermatogenesis associated glutamate (E)-rich protein 2
380830	0,0378	5330439C02Rik|LOC544812	0,405	NM_175453.2	RIKEN cDNA 5330439C02 gene
495600	0,00747	null	0,406	null	null
306837	0,0427	Mrpl41	0,415	null	mitochondrial ribosomal protein L41
806556	0,00994	Gm1420	0,416	null	gene model 1420, (NCBI)
365817	0,0122	LOC634435|LOC624098	0,418	null	null
666984	0,035	null	0,421	null	null
819042	0,047	null	0,421	null	null
504336	0,0289	null	0,422	null	null
545195	0,0317	1700023D08Rik	0,425	null	RIKEN cDNA 1700023D08 gene
371229	0,0215	Rgl2	0,429	NM_009059.2	ral guanine nucleotide dissociation stimulator-like 2
849874	0,00487	null	0,43	null	null

465651	0,0411	Fga	0,431	NM_010196.1	fibrinogen, alpha polypeptide
907925	0,0108	Iigp1	0,431	NM_021792.3	interferon inducible GTPase 1
767150	0,0354	LOC210583	0,438	null	null
900420	0,0408	LOC545886	0,438	null	null
659186	0,0358	9330112M16	0,439	null	null
604621	0,0487	9330169B04Rik	0,441	null	RIKEN cDNA 9330169B04 gene
365177	0,0217	Vgll2	0,442	NM_153786.1	vestigial like 2 homolog (Drosophila)
478454	0,0194	null	0,442	null	null
618195	0,0221	null	0,443	null	null
316370	0,0406	7530428D23Rik	0,446	null	RIKEN cDNA 7530428D23 gene
301819	0,0305	Mal	0,449	NM_010762.2	myelin and lymphocyte protein, T-cell differentiation protein
851897	0,0159	Fbxw11	0,455	null	F-box and WD-40 domain protein 11
331841	0,0145	null	0,456	null	null
459961	0,00205	Spata1	0,462	NM_027617.1	spermatogenesis associated 1
513596	0,0349	Sctr	0,468	null	secretin receptor
304479	0,0316	AA408296	0,469	NM_145415.2	expressed sequence AA408296
919619	0,00407	Pcgf2	0,471	NM_009545.1	polycomb group ring finger 2
921902	0,0461	Ggt1	0,475	NM_008116.1	gamma-glutamyltransferase 1
862650	0,0279	LOC628772|LOC621500 |LOC636273	0,479	null	null
336196	0,0419	6530401D17Rik	0,482	NM_029541.1	RIKEN cDNA 6530401D17 gene
816217	0,0351	null	0,49	null	null
854005	0,0484	Olfr1447	0,494	NM_146703.1	olfactory receptor 1447
569233	0,00791	null	0,499	null	null

12.1.3 Treated (combination of DMHCA and T0901317) macrophages versus control-treated macrophages

When the treatments with both ligands were combined to the treatment group and compared with control-treated cell, the most significantly regulated pathways were the lipid transport and the unfolded protein response.

Table J. Pathway analysis: Treated (DMHCA combined with T0) compared to control, up in treatment for *FC*≥2, p≤0.1; most abundant pathways

Category	Genes in Category	% of Genes in Category	Genes in List in	% of Genes in List in Category	p-Value
GO:6869: lipid transport	61	0,446	5	11,9	1,13E-06
GO:30968: unfolded protein response	5	0,0366	2	4,762	9,17E-05
GO:15918: sterol transport	7	0,0512	2	4,762	0,000192
GO:30301: cholesterol transport	7	0,0512	2	4,762	0,000192
GO:6984: ER-nuclear signaling pathway	9	0,0659	2	4,762	0,000328
GO:42157: lipoprotein metabolism	44	0,322	3	7,143	0,000328
GO:19276: UDP-N-acetylgalactosamine metabolism	1	0,00732	1	2,381	0,00307
GO:6679: glucosylceramide biosynthesis	1	0,00732	1	2,381	0,00307

GO:42789: mRNA transcription from RNA polymerase II promoter	1	0,00732	1	2,381	0,00307
GO:9299: mRNA transcription	1	0,00732	1	2,381	0,00307
GO:6678: glucosylceramide metabolism	1	0,00732	1	2,381	0,00307
GO:15721: bile acid transport	1	0,00732	1	2,381	0,00307
GO:15722: canalicular bile acid transport	1	0,00732	1	2,381	0,00307
GO:7050: cell cycle arrest	35	0,256	2	4,762	0,00515
GO:42158: lipoprotein biosynthesis	36	0,264	2	4,762	0,00544
GO:7413: axonal fasciculation	2	0,0146	1	2,381	0,00614

85 genes were upregulated with the treatment when the treatment (DMHCA and T0901317 combined) was compared to control (p≤0.1, FC≥2).

Table K. Uregulated genes in treatment (DMHCA and T0 combined) compared to control, up in treatment for p≤0.1, FC≥2

Gene Name	P-value	Common	Fold change (upInTreate	Genbank	Description
607840	0,0939	Lbp	6,10	NM_008489.1	lipopolysaccharide binding protein
856939	0,0436	LOC632433|Arl4c	5,92	NM_177305.2	ADP-ribosylation factor-like 4C
797048	0,0827	Il18bp	5,43	NM_010531.1	interleukin 18 binding protein
403608	0,00666	Abca1	4,98	NM_013454.2	ATP-binding cassette, sub-family A (ABC1), member 1
802990	0,0473	4930428E23Rik	4,41	null	RIKEN cDNA 4930428E23 gene
601840	0,0537	Mylip	4,13	NM_153789.2	myosin regulatory light chain interacting protein
916686	0,000241	Ndrg1	3,75	NM_010884.1	N-myc downstream regulated gene 1
402090	0,0119	Rtn1	3,72	NM_001007596.1	reticulon 1
901980	0,0755	Srm	3,58	NM_009272.2	spermidine synthase
932912	0,0221	BC040823	3,46	NM_177727.2	cDNA sequence BC040823
392895	0,00258	Ero1l	3,40	NM_015774.2	ERO1-like (S. cerevisiae)
532780	0,00253	Abcg1	3,38	NM_009593.1	ATP-binding cassette, sub-family G (WHITE), member 1
361480	0,024	Chac1	3,36	NM_026929.2	ChaC, cation transport regulator-like 1 (E. coli)
755030	0,0492	Serpinb9c	3,34	NM_011453.2	serine (or cysteine) peptidase inhibitor, clade B, member 9c
511921	0,0756	Myd116	3,33	NM_008654.1	myeloid differentiation primary response gene 116
861450	0,0278	6720487G11Rik	3,30	NM_175676.2	RIKEN cDNA 6720487G11 gene
752774	0,00663	C1ql1	3,19	null	complement component 1, q subcomponent-like 1
818447	0,0128	null	3,19	null	null
422947	0,0485	Ddit3	3,06	NM_007837.2	DNA-damage inducible transcript 3
573930	0,0335	null	2,89	null	null
410126	0,0714	1700009P17Rik	2,88	NM_029301.1	RIKEN cDNA 1700009P17 gene
754351	0,0468	Arid5a	2,87	NM_145996.2	AT rich interactive domain 5A (Mrf1 like)
543288	0,00249	Faah	2,81	NM_010173.2	fatty acid amide hydrolase
910111	0,0346	Asns	2,76	NM_012055.1	asparagine synthetase
907938	0,0104	3732413I11Rik	2,75	NM_028862.1	RIKEN cDNA 3732413I11 gene
584563	0,0169	Ddx49	2,74	null	DEAD (Asp-Glu-Ala-Asp) box polypeptide 49
450952	0,0437	Fbxo32	2,73	NM_026346.1	F-box only protein 32

591232	0,0288	B3galnt2	2,73	NM_178640.1	UDP-GalNAc:betaGlcNAc beta 1,3-galactosaminyltransferase, polypeptide 2
932169	0,0036	Dusp6	2,72	NM_026268.1	dual specificity phosphatase 6
303607	0,0158	Tnfaip3	2,71	NM_009397.2	tumor necrosis factor, alpha-induced protein 3
395181	0,0333	Ung	2,70	null	uracil DNA glycosylase
598999	0,00624	Pltp	2,70	NM_011125.1	phospholipid transfer protein
391972	0,0464	Mmp27	2,68	null	matrix metallopeptidase 27
595893	0,0936	Il1a	2,68	NM_010554.3	interleukin 1 alpha
643007	0,068	null	2,67	null	null
603303	0,017	Apoc1	2,63	NM_007469.2	apolipoprotein C-I
433673	0,0293	2700033H19Rik	2,59	null	RIKEN cDNA 2700033H19 gene
555784	0,0288	Zfp27	2,54	NM_011754.1	zinc finger protein 27
928375	0,099	Cd5l	2,51	NM_009690.1	CD5 antigen-like
899622	0,0539	null	2,49	null	null
548849	0,00533	3110018I06Rik	2,46	null	RIKEN cDNA 3110018I06 gene
905471	0,0404	Ier3	2,43	NM_133662.1	immediate early response 3
621581	0,0651	Prr6	2,43	null	proline-rich polypeptide 6
309377	0,0693	Cars	2,41	NM_013742.2	cysteinyl-tRNA synthetase
315710	0,0284	Pik3cb	2,40	NM_029094.1	phosphatidylinositol 3-kinase, catalytic, beta polypeptide
765113	0,0105	Atrnl1	2,37	NM_181415.3	attractin like 1
328511	0,0377	4933425L03Rik	2,35	null	RIKEN cDNA 4933425L03 gene
917377	0,0223	S100a16	2,34	NM_026416.2	S100 calcium binding protein A16
617536	0,0981	Zdhhc3	2,33	NM_026917.4	zinc finger, DHHC domain containing 3
648975	0,0757	Yif1b	2,33	null	Yip1 interacting factor homolog B (S. cerevisiae)
497453	0,0255	Spata5l1	2,31	null	spermatogenesis associated 5-like 1
643952	0,0103	2810428C21Rik	2,31	null	RIKEN cDNA 2810428C21 gene
443397	0,0381	C130022K22Rik	2,30	NM_172730.1	RIKEN cDNA C130022K22 gene
337648	0,0299	Refbp2	2,29	null	RNA and export factor binding protein 2
703180	0,0284	null	2,28	null	null
474703	0,00576	null	2,27	null	null
496423	0,00572	Gadd45a	2,27	NM_007836.1	growth arrest and DNA-damage-inducible 45 alpha
532736	0,00635	2310005P05Rik	2,26	NM_026189.2	RIKEN cDNA 2310005P05 gene
541496	0,059	5930434B04Rik|LOC636316	2,26	NM_029862.1	RIKEN cDNA 5930434B04 gene
784252	0,0945	5730411O18Rik	2,26	NM_177370.2	RIKEN cDNA 5730411O18 gene
931031	0,0136	Abi3	2,26	NM_025659.1	ABI gene family, member 3
397477	0,0631	Ugcg	2,24	NM_011673.2	UDP-glucose ceramide glucosyltransferase
792174	0,0954	Pck2	2,21	NM_028994.1	phosphoenolpyruvate carboxykinase 2 (mitochondrial)
839063	0,0379	Mare	2,20	NM_181569.1	alpha globin regulatory element containing gene
860650	0,024	Gramd1b	2,20	NM_172768.1	GRAM domain containing 1B
646949	0,0677	Ids	2,19	NM_010498.1	iduronate 2-sulfatase
859800	0,0515	Fabp2	2,19	NM_007980.2	fatty acid binding protein 2, intestinal
653822	0,0822	AW124694	2,16	null	expressed sequence AW124694
884290	0,0771	Celsr3	2,16	NM_080437.1	cadherin EGF LAG seven-pass G-type receptor 3
682978	0,0888	Kdelr2	2,15	NM_025841.1	KDEL (Lys-Asp-Glu-Leu) endoplasmic reticulum protein retention receptor 2

594656	0,0668	Abcc3	2,11	null	ATP-binding cassette, sub-family C (CFTR/MRP), member 3
911548	0,082	Sqstm1	2,10	NM_011018.1	sequestosome 1
555515	0,0721	B430201A12Rik	2,08	null	RIKEN cDNA B430201A12 gene
431426	0,0626	2210011C24Rik	2,07	null	RIKEN cDNA 2210011C24 gene
912952	0,00178	Gramd1b	2,07	null	GRAM domain containing 1B
604511	0,0118	2410127E18Rik	2,07	NM_029742.1	RIKEN cDNA 2410127E18 gene
877424	0,0465	A530079E22Rik	2,06	NM_177048.2	RIKEN cDNA A530079E22 gene
798345	0,0451	1110033M05Rik	2,05	null	RIKEN cDNA 1110033M05 gene
360325	0,0724	Foxk2	2,04	null	forkhead box K2
505100	0,0914	4933409L06Rik	2,04	null	RIKEN cDNA 4933409L06 gene
501314	0,0184	Btbd3	2,03	NM_145534.1	BTB (POZ) domain containing 3
759375	0,00219	Cxcl1	2,02	NM_008176.1	chemokine (C-X-C motif) ligand 1
462361	0,024	MGC27770	2,00	NM_145986.1	null
569199	0,0114	Wdr75	2,00	null	WD repeat domain 75
629919	0,00928	null	2,00	null	null

For downregulated genes in the treatment group in comparison with control the most significantly regulated pathways were cell communication and signal transduction.

Table L. Pathway analysis: Treated (DMHCA combined with T0) compared to control, down in treatment for *FC*≤0.5, p≤0.1; most abundant pathways pathway

Category	Genes in Category	% of Genes in Category	Genes in List in	% of Genes in List in Category	p-Value
GO:7154: cell communication	3597	26,33	59	35,76	0,00456
GO:7165: signal transduction	2998	21,94	49	29,7	0,0119
GO:7402: ganglion mother cell fate determination	1	0,00732	1	0,606	0,0121
GO:8052: sensory organ determination	1	0,00732	1	0,606	0,0121
GO:42994: cytoplasmic sequestering of transcription factor	1	0,00732	1	0,606	0,0121
GO:51220: cytoplasmic sequestering of protein	1	0,00732	1	0,606	0,0121
GO:45840: positive regulation of mitosis	1	0,00732	1	0,606	0,0121
GO:281: cytokinesis after mitosis	1	0,00732	1	0,606	0,0121
GO:40001: establishment of mitotic spindle localization	1	0,00732	1	0,606	0,0121
GO:51293: establishment of spindle localization	1	0,00732	1	0,606	0,0121
GO:45217: intercellular junction maintenance	1	0,00732	1	0,606	0,0121

99 genes were downregulated in the treatment group when the treatment was compared with control-treated cells (p≤0.01, FC≤0.5).

Table M. Downregulated genes in treatment (DMHCA and T0 combined) compared to control, down in treatment for p≤0.01, FC≤0.5

Gene Name	P-value	Common	Fold change (downInTre	Genbank	Description

848334	0,00184	4930543L23Rik	0,091	NM_183110.1	RIKEN cDNA 4930543L23 gene
756978	0,000649	null	0,098	null	null
882896	0,000537	6530439I21	0,119	NM_177837.2	null
537504	0,00813	null	0,140	null	null
867196	0,000101	BC042761	0,155	null	cDNA sequence BC042761
795225	0,00531	Trem1	0,187	NM_021406.2	triggering receptor expressed on myeloid cells 1
671858	0,00177	LOC631764|LOC620595|LOC239191|Dnmt3b	0,196	NM_001003960.1	DNA methyltransferase 3B
662135	0,00187	Cacng8	0,198	NM_133190.1	calcium channel, voltage-dependent, gamma subunit 8
829972	0,00999	Enpp4	0,203	null	ectonucleotide pyrophosphatase/phosphodiesterase 4
827287	0,00632	8030475D13Rik	0,206	null	RIKEN cDNA 8030475D13 gene
366263	0,000712	Gpr133	0,228	null	G protein-coupled receptor 133
434342	0,000889	1700020N18Rik	0,233	null	RIKEN cDNA 1700020N18 gene
363166	0,00441	Gp1bb	0,241	NM_001001999.1	glycoprotein Ib, beta polypeptide
623195	0,00799	C630001G18Rik	0,244	null	RIKEN cDNA C630001G18 gene
370245	0,00188	null	0,247	null	null
299744	0,000235	4930597O21Rik	0,249	null	RIKEN cDNA 4930597O21 gene
866913	0,00561	Minpp1	0,256	null	multiple inositol polyphosphate histidine phosphatase 1
607990	0,00273	Wdfy3	0,262	null	WD repeat and FYVE domain containing 3
803828	0,00641	null	0,263	null	null
603979	0,0054	Apoc3	0,266	NM_023114.2	apolipoprotein C-III
450585	0,00787	Perld1	0,274	null	per1-like domain containing 1
454396	0,00337	null	0,274	null	null
917041	0,00748	Prlpc3	0,274	NM_023741.1	prolactin-like protein C 3
635108	0,00766	Dzip1l	0,275	NM_028258.1	DAZ interacting protein 1-like
750537	0,00689	null	0,279	null	null
883173	0,000816	Odz4	0,285	null	odd Oz/ten-m homolog 4 (Drosophila)
481867	0,000358	4933439K11Rik	0,290	null	RIKEN cDNA 4933439K11 gene
782734	0,00834	Grin1	0,296	NM_008169.1	glutamate receptor, ionotropic, NMDA1 (zeta 1)
610337	0,00299	4831407H17Rik	0,296	null	RIKEN cDNA 4831407H17 gene
728547	0,00856	Gpr112	0,296	null	G protein-coupled receptor 112
462888	0,00232	Aicda	0,302	NM_009645.1	activation-induced cytidine deaminase
582299	0,0011	Kbtbd8	0,303	NM_001008785.1	kelch repeat and BTB (POZ) domain containing 8
798950	0,00941	A730090H04Rik	0,309	null	RIKEN cDNA A730090H04 gene
522188	0,000582	4930562D21Rik	0,313	null	RIKEN cDNA 4930562D21 gene
478800	0,000244	Cldn2	0,314	NM_016675.3	claudin 2
538665	0,00282	LOC434031|Igk-V38	0,317	null	immunoglobulin kappa chain variable 38(V38)
456283	0,00344	Rhebl1	0,319	NM_026967.3	Ras homolog enriched in brain like 1
320722	0,00151	4930479M11Rik	0,321	NM_183108.1	RIKEN cDNA 4930479M11 gene
853341	0,0026	LOC544710	0,321	null	null
505568	0,000674	D330017J20Rik	0,321	NM_177204.2	RIKEN cDNA D330017J20 gene
810380	0,00541	Chrac1	0,325	null	chromatin accessibility complex 1
886901	0,00106	Tbx3	0,325	NM_198052.1	T-box 3
685400	0,00773	null	0,331	null	null

568233	0,008	Zan	0,332	NM_011741.1	zonadhesin
907925	0,00326	Iigp1	0,334	NM_021792.3	interferon inducible GTPase 1
364111	0,00853	null	0,345	null	null
545195	0,00196	1700023D08Rik	0,347	null	RIKEN cDNA 1700023D08 gene
759510	0,00182	Npr2	0,347	NM_173788.2	natriuretic peptide receptor 2
632446	0,00618	Syt10	0,352	NM_018803.1	synaptotagmin X
488598	0,0072	1700063D05Rik	0,354	null	RIKEN cDNA 1700063D05 gene
642595	0,00182	null	0,357	null	null
472648	0,000713	Crhbp	0,361	NM_198408.1	corticotropin releasing hormone binding protein
900420	0,00224	LOC545886	0,361	null	null
476264	0,00167	LOC433565|LOC636299	0,362	null	null
416270	0,00829	Arrdc5	0,364	null	arrestin domain containing 5
672645	0,00653	null	0,364	null	null
720018	0,00438	Sez6	0,365	NM_021286.2	seizure related gene 6
694533	0,00352	9430063H18Rik	0,365	null	RIKEN cDNA 9430063H18 gene
432073	0,00168	BC024386	0,366	null	cDNA sequence BC023486
366102	0,00024	null	0,366	null	null
811585	0,006	null	0,369	null	null
828538	0,00259	1810064L21Rik	0,371	NM_176946.2	RIKEN cDNA 1810064L21 gene
520850	0,0049	Gfap	0,372	null	glial fibrillary acidic protein
504336	0,00654	null	0,373	null	null
862528	0,00603	Tm4sf20	0,373	NM_025453.1	transmembrane 4 L six family member 20
493777	0,00874	C130021I20	0,379	NM_177842.2	null
656151	0,0099	6530421E24Rik	0,380	NM_207280.1	RIKEN cDNA 6530421E24 gene
476991	0,0041	LOC384557|Psg29	0,381	null	pregnancy-specific glycoprotein 29
313790	8,81E-05	null	0,382	null	null
509895	0,00565	Upb1	0,383	NM_133995.1	ureidopropionase, beta
724199	0,00116	V1rc33|LOC434017	0,388	NM_134436.1	vomeronasal 1 receptor, C33
801635	0,00262	Dact1	0,390	NM_021532.2	dapper homolog 1, antagonist of beta-catenin (xenopus)
661344	0,00421	9230114K14Rik	0,392	null	RIKEN cDNA 9230114K14 gene
801120	0,000817	Rhobtb2	0,401	null	Rho-related BTB domain containing 2
771748	0,00402	E030024N20Rik	0,403	NM_176911.2	RIKEN cDNA E030024N20 gene
429119	0,00558	2610318N02Rik	0,403	null	RIKEN cDNA 2610318N02 gene
711961	0,00804	null	0,406	null	null
452059	0,000426	Gabbr1	0,411	null	gamma-aminobutyric acid (GABA-B) receptor, 1
722795	0,00818	Olfr399	0,421	NM_147004.1	olfactory receptor 399
854333	0,00931	null	0,422	null	null
603474	0,00569	null	0,426	null	null
498083	0,00846	Cd79b	0,427	NM_008339.1	CD79B antigen
659186	5,26E-05	9330112M16	0,431	null	null
800583	0,00983	Fscn2	0,434	NM_172802.1	fascin homolog 2, actin-bundling protein, retinal (Strongylocentrotus purpuratus)
786266	0,0061	Glis2	0,435	NM_031184.2	GLIS family zinc finger 2
446817	0,00414	1700064N11Rik	0,438	null	RIKEN cDNA 1700064N11 gene
834092	0,00499	1700123J03Rik	0,439	null	RIKEN cDNA 1700123J03 gene

382334	0,00373	null	0,445	null	null
331841	0,00287	null	0,445	null	null
539613	0,0018	B230114P17Rik	0,450	null	RIKEN cDNA B230114P17 gene
373960	0,00317	4930427A07Rik	0,452	null	RIKEN cDNA 4930427A07 gene
569233	0,00168	null	0,457	null	null
498074	0,00958	Phc1	0,465	NM_007905.1	polyhomeotic-like 1 (Drosophila)
301819	9,60E-05	Mal	0,470	NM_010762.2	myelin and lymphocyte protein, T-cell differentiation protein
329286	0,00541	Ptprk	0,476	null	protein tyrosine phosphatase, receptor type, K
495530	0,00634	LOC628890|LOC546148|Cd209c|LOC433000|LOC433002	0,478	NM_130903.2	CD209c antigen
306849	0,00273	null	0,482	null	null
735437	0,000816	LOC240055|LOC638857	0,488	null	null

12.2 DMHCA-treated macrophages versus T0901317-treated macrophages

When DMHCA-treated MPM were compared with T0901317-treated cells, it was most striking that sterol and lipid biosynthesis were significantly regulated-

Table N. Pathway analysis: DMHCA-treated compared to T0901317-treated, down in DMHCA for *FC*≤0.5, p≤0.1; most abundant pathways

Category	Genes in Category	% of Genes in Category	Genes in List in Category	% of Genes in List in Category	p-Value
GO:16126: sterol biosynthesis	25	0,183	14	9,272	8,82E-22
GO:16125: sterol metabolism	58	0,425	17	11,26	2,93E-20
GO:8610: lipid biosynthesis	182	1,332	22	14,57	5,34E-17
GO:6694: steroid biosynthesis	62	0,454	15	9,934	1,32E-16
GO:6695: cholesterol biosynthesis	22	0,161	11	7,285	1,32E-16
GO:8203: cholesterol metabolism	54	0,395	14	9,272	4,89E-16
GO:8202: steroid metabolism	123	0,9	18	11,92	1,41E-15
GO:44255: cellular lipid metabolism	387	2,833	27	17,88	1,40E-14
GO:6629: lipid metabolism	481	3,521	29	19,21	5,71E-14
GO:6066: alcohol metabolism	211	1,544	20	13,25	1,71E-13
GO:8299: isoprenoid biosynthesis	12	0,0878	5	3,311	1,15E-07
GO:9058: biosynthesis	1123	8,22	32	21,19	4,99E-07
GO:6720: isoprenoid metabolism	22	0,161	5	3,311	3,49E-06
GO:9241: polyisoprenoid biosynthesis	2	0,0146	2	1,325	0,000121
GO:16114: terpenoid biosynthesis	2	0,0146	2	1,325	0,000121
GO:16109: tetraterpenoid biosynthesis	2	0,0146	2	1,325	0,000121
GO:16117: carotenoid biosynthesis	2	0,0146	2	1,325	0,000121
GO:46246: terpene biosynthesis	2	0,0146	2	1,325	0,000121
GO:16108: tetraterpenoid metabolism	2	0,0146	2	1,325	0,000121
GO:16116: carotenoid metabolism	2	0,0146	2	1,325	0,000121

GO:6952: defense response	680	4,977	18	11,92	0,000512
GO:9607: response to biotic stimulus	711	5,204	18	11,92	0,00086
GO:6721: terpenoid metabolism	6	0,0439	2	1,325	0,00177
GO:42214: terpene metabolism	6	0,0439	2	1,325	0,00177
GO:16096: polyisoprenoid metabolism	6	0,0439	2	1,325	0,00177
GO:6082: organic acid metabolism	406	2,972	12	7,947	0,00184
GO:19752: carboxylic acid metabolism	406	2,972	12	7,947	0,00184
GO:44237: cellular metabolism	6427	47,04	89	58,94	0,0021
GO:8152: metabolism	6804	49,8	93	61,59	0,00225
GO:6897: endocytosis	171	1,252	7	4,636	0,00291
GO:7169: transmembrane receptor protein tyrosine kinase signaling pathway	129	0,944	6	3,974	0,00308
GO:6633: fatty acid biosynthesis	55	0,403	4	2,649	0,00316
GO:16053: organic acid biosynthesis	58	0,425	4	2,649	0,00383
GO:46394: carboxylic acid biosynthesis	58	0,425	4	2,649	0,00383
GO:6631: fatty acid metabolism	135	0,988	6	3,974	0,00385
GO:19748: secondary metabolism	32	0,234	3	1,987	0,00519
GO:6955: immune response	558	4,084	13	8,609	0,00895

163 genes were downregulated upon DMHCA-treatment when DMCHA-treated MPM were compared with T0901317-treated cells (*FC≤0.5*, p-value≤0.05).

Table O. Downregulated in DMHCA-treated compared to T09013117-treated, down in DMHCA for FC≤0.5, p-value≤0.05

P-value	Common	FC	Genbank	Description
0,0483	Idi1	0,018	NM_145360.1	isopentenyl-diphosphate delta isomerase
0,0126	Idi1	0,028	NM_145360.1	isopentenyl-diphosphate delta isomerase
0,00516	Hsd17b7	0,046	NM_010476.2	hydroxysteroid (17-beta) dehydrogenase 7
0,0388	null	0,046	null	null
0,00533	Acat2	0,049	NM_009338.1	acetyl-Coenzyme A acetyltransferase 2
0,0384	Dhcr24	0,057	NM_053272.1	24-dehydrocholesterol reductase
0,039	Crisp4	0,069	null	cysteine-rich secretory protein 4
0,00393	Sqle	0,069	NM_009270.2	squalene epoxidase
0,00576	Ldlr	0,069	null	low density lipoprotein receptor
0,0431	Oas2	0,092	NM_145227.1	2'-5' oligoadenylate synthetase 2
0,04	LOC637705|Ifit3	0,093	NM_001005858.1	interferon-induced protein with tetratricopeptide repeats 3
0,000892	Hmgcs1	0,100	NM_145942.2	3-hydroxy-3-methylglutaryl-Coenzyme A synthase 1
0,03	Acat3|Acat2|LOC630106	0,107	NM_153151.1	acetyl-Coenzyme A acetyltransferase 3|acetyl-Coenzyme A acetyltransferase 2
0,0125	Sc5d	0,113	NM_172769.1	sterol-C5-desaturase (fungal ERG3, delta-5-desaturase) homolog (S. cerevisae)
0,0289	A730092B10	0,114	null	null
0,0204	Sc4mol	0,116	NM_025436.1	sterol-C4-methyl oxidase-like

0,00411	H2-DMa	0,116	NM_010386.2	histocompatibility 2, class II, locus DMa
0,0105	Tm7sf2	0,117	NM_028454.1	transmembrane 7 superfamily member 2
0,00469	Insig1|LOC625787	0,122	NM_153526.2	insulin induced gene 1
0,0217	Fasn	0,123	NM_007988.1	fatty acid synthase
0,0453	Mvd	0,129	NM_138656.1	mevalonate (diphospho) decarboxylase
0,0342	Scd2	0,132	NM_009128.1	stearoyl-Coenzyme A desaturase 2
0,0274	Aldoc	0,132	NM_009657.1	aldolase 3, C isoform
0,0461	Scd1	0,134	NM_009127.2	stearoyl-Coenzyme A desaturase 1
0,0346	1500005P14Rik	0,148	null	RIKEN cDNA 1500005P14 gene
0,031	Lsm6	0,157	null	LSM6 homolog, U6 small nuclear RNA associated (S. cerevisiae)
0,0204	Nme4	0,171	null	expressed in non-metastatic cells 4, protein
0,00961	null	0,172	null	null
0,0331	null	0,175	null	null
0,0459	Ier5l	0,177	NM_030244.2	immediate early response 5-like
0,0313	null	0,179	null	null
0,0154	Acsl3	0,192	NM_028817.1	acyl-CoA synthetase long-chain family member 3
0,0142	Usmg4	0,192	null	upregulated during skeletal muscle growth 4
0,00974	Trim16	0,200	NM_053169.1	tripartite motif protein 16
0,0118	null	0,206	null	null
0,0361	Cxcl10	0,209	NM_021274.1	chemokine (C-X-C motif) ligand 10
0,0492	null	0,212	null	null
0,0248	null	0,215	null	null
0,0222	Apxl	0,216	null	apical protein, Xenopus laevis-like
0,00863	4930477O03Rik	0,225	null	RIKEN cDNA 4930477O03 gene
0,0441	null	0,227	null	null
0,013	D130051D11Rik	0,229	null	RIKEN cDNA D130051D11 gene
0,015	Pkd2	0,232	null	polycystic kidney disease 2
0,0461	LOC638238|2810417H13Rik	0,237	NM_026515.1	RIKEN cDNA 2810417H13 gene
0,0448	Twist1	0,241	null	twist gene homolog 1 (Drosophila)
0,00822	null	0,245	null	null
0,0388	null	0,252	null	null
0,045	Nfe2	0,262	NM_008685.2	nuclear factor, erythroid derived 2
0,0359	null	0,265	null	null
0,0287	null	0,267	null	null
0,0195	Fbxl10	0,268	NM_013910.2	F-box and leucine-rich repeat protein 10
0,0293	Defb3	0,269	NM_013756.1	defensin beta 3
0,048	null	0,271	null	null
0,0124	C730036D15Rik|LOC230161	0,274	NM_145368.2	RIKEN cDNA C730036D15 gene
0,0213	Exoc3	0,274	null	exocyst complex component 3
0,0229	Camk1	0,277	NM_133926.1	calcium/calmodulin-dependent protein kinase I
0,00667	null	0,277	null	null
0,0121	Cox10	0,282	null	COX10 homolog, cytochrome c oxidase assembly protein, heme A: farnesyltransferase (yeast)

0,0395	2810051F02Rik	0,283	NM_028330.1	RIKEN cDNA 2810051F02 gene
0,0188	Mt1	0,285	NM_013602.2	metallothionein 1
0,0162	2310020A21Rik	0,285	NM_175249.2	RIKEN cDNA 2310020A21 gene
0,00698	null	0,288	null	null
0,0323	Apcdd1	0,293	NM_133237.1	adenomatosis polyposis coli down-regulated 1
0,0171	null	0,298	null	null
0,0369	Slc2a6	0,301	NM_172659.1	solute carrier family 2 (facilitated glucose transporter), member 6
0,0174	4930534H03Rik	0,301	null	RIKEN cDNA 4930534H03 gene
0,031	null	0,303	null	null
0,0171	Bag2	0,303	NM_145392.1	Bcl2-associated athanogene 2
0,0411	Srebf1	0,304	NM_011480.1	sterol regulatory element binding factor 1
0,0246	Echdc3	0,306	NM_024208.3	enoyl Coenzyme A hydratase domain containing 3
0,0412	4930505H01Rik	0,310	null	RIKEN cDNA 4930505H01 gene
0,0477	Usp18	0,313	NM_011909.1	ubiquitin specific peptidase 18
0,0337	0610007P14Rik	0,313	null	RIKEN cDNA 0610007P14 gene
0,00438	Maf	0,316	null	avian musculoaponeurotic fibrosarcoma (v-maf) AS42 oncogene homolog
0,0291	Echdc1	0,320	NM_025855.2	enoyl Coenzyme A hydratase domain containing 1
0,0482	Map2k7	0,326	NM_011944.1	mitogen activated protein kinase kinase 7
0,0468	Ppfia4	0,333	null	protein tyrosine phosphatase, receptor type, f polypeptide (PTPRF), interacting protein (liprin), alpha 4
0,0136	Lbr	0,335	NM_133815.1	lamin B receptor
0,0293	Lamb2	0,340	NM_008483.2	laminin, beta 2
0,0442	Rnf32	0,341	null	ring finger protein 32
0,0315	Pbxip1	0,347	NM_146131.1	pre-B-cell leukemia transcription factor interacting protein 1
0,039	Hist1h2bk	0,367	NM_175665.1	histone 1, H2bk
0,0337	Cps1	0,368	null	carbamoyl-phosphate synthetase 1
0,0427	null	0,370	null	null
0,0244	Fah	0,370	NM_010176.1	fumarylacetoacetate hydrolase
0,0125	null	0,378	null	null
0,0241	Sdc3	0,380	NM_011520.2	syndecan 3
0,0444	Prc1	0,392	NM_145150.1	protein regulator of cytokinesis 1
0,00355	Olfr470	0,399	NM_146425.1	olfactory receptor 470
0,0267	Nrtn	0,399	NM_008738.1	neurturin
0,0351	Klra3	0,403	NM_010648.1	killer cell lectin-like receptor, subfamily A, member 3
0,0464	1110020L19Rik	0,403	NM_207104.1	RIKEN cDNA 1110020L19 gene
0,00597	Gstm2	0,404	null	glutathione S-transferase, mu 2
0,0011	D11Ertd759e|LOC629974	0,416	NM_172949.1	DNA segment, Chr 11, ERATO Doi 759, expressed
0,0458	Selenbp2	0,416	NM_019414.1	selenium binding protein 2
0,0313	9830130M13Rik	0,418	NM_177713.2	RIKEN cDNA 9830130M13 gene
0,0113	Acot2	0,419	NM_134188.2	acyl-CoA thioesterase 2
0,012	4930448C13Rik	0,420	null	RIKEN cDNA 4930448C13 gene
0,0222	Clstn1	0,420	null	calsyntenin 1
0,0352	null	0,420	null	null

0,0389	Mgll	0,421	NM_011844.3	monoglyceride lipase
0,0317	Arpc1b	0,423	null	actin related protein 2/3 complex, subunit 1B
0,0451	Nxn	0,424	NM_008750.2	nucleoredoxin
0,0365	D530035G10Rik	0,424	null	RIKEN cDNA D530035G10 gene
0,00601	Thbd	0,427	NM_009378.1	thrombomodulin
0,00232	null	0,428	null	null
0,0209	Glb1	0,429	null	galactosidase, beta 1
0,0471	Plekha7	0,431	null	pleckstrin homology domain containing, family A member 7
0,0218	Sort1	0,435	NM_019972.2	sortilin 1
0,00588	Cysltr1	0,435	NM_021476.2	cysteinyl leukotriene receptor 1
0,00328	AW548124	0,436	NM_134117.1	expressed sequence AW548124
0,0309	Alk	0,438	NM_007439.1	anaplastic lymphoma kinase
0,0165	Ifi47	0,438	NM_008330.1	interferon gamma inducible protein 47
0,0315	Mum1	0,438	NM_023431.4	melanoma associated antigen (mutated) 1
0,0202	4930538D17Rik	0,439	NM_029186.1	RIKEN cDNA 4930538D17 gene
0,0459	null	0,440	null	null
0,0476	Clec4a1	0,442	NM_199311.1	C-type lectin domain family 4, member a1
0,0053	Ece1	0,442	NM_199307.1	endothelin converting enzyme 1
0,0265	Avpi1	0,443	NM_027106.1	arginine vasopressin-induced 1
0,0257	Saa1	0,444	null	serum amyloid A 1
0,0475	5830427D03Rik	0,445	NM_175232.2	RIKEN cDNA 5830427D03 gene
0,0485	Scamp5	0,447	NM_020270.2	secretory carrier membrane protein 5
0,0374	D230050A05	0,447	NM_177585.2	null
0,049	1810014L12Rik	0,447	NM_133706.1	RIKEN cDNA 1810014L12 gene
0,0182	Cds1	0,453	NM_173370.3	CDP-diacylglycerol synthase 1
0,00775	Tpst1	0,454	NM_013837.1	protein-tyrosine sulfotransferase 1
0,0392	A130092J06Rik	0,454	NM_175511.2	RIKEN cDNA A130092J06 gene
0,037	null	0,455	null	null
0,0252	LOC552905	0,458	null	null
0,0351	Mrc1	0,459	NM_008625.1	mannose receptor, C type 1
0,0395	Pgpep1	0,459	null	pyroglutamyl-peptidase I
0,0394	Lrrc25	0,460	NM_153074.2	leucine rich repeat containing 25
0,00708	Ttyh2	0,468	null	tweety homolog 2 (Drosophila)
0,00766	Pwwp2	0,469	null	PWWP domain containing 2
0,0392	4933440H19Rik	0,470	null	RIKEN cDNA 4933440H19 gene
0,02	Sorl1	0,470	NM_011436.1	sortilin-related receptor, LDLR class A repeats-containing
0,0262	Gale	0,471	NM_178389.2	galactose-4-epimerase, UDP
0,0465	Wnt1	0,471	NM_021279.3	wingless-related MMTV integration site 1
0,0282	Dync1li2	0,472	null	dynein, cytoplasmic 1 light intermediate chain 2
0,0402	Lsp1	0,473	NM_019391.1	lymphocyte specific 1
0,0157	Cdc42ep3	0,475	NM_026514.1	CDC42 effector protein (Rho GTPase binding) 3
0,0218	Snx27	0,475	null	sorting nexin family member 27
0,0423	Cd9	0,476	null	CD9 antigen
0,0438	Lxn	0,477	NM_016753.2	latexin

0,0171	LOC633079|LOC622629	0,478	null	null
0,0344	null	0,479	null	null
0,00335	null	0,480	null	null
0,044	Mnda|Ifi205	0,480	NM_172648.2	myeloid cell nuclear differentiation antigen|interferon activated gene 205
0,0246	Hist1h2bc|Hist1h2bg	0,480	NM_023422.1	histone 1, H2bc|histone 1, H2bg
0,0261	Samd9l	0,481	NM_177590.1	sterile alpha motif domain containing 9-like
0,0224	Nmi	0,482	NM_019401.1	N-myc (and STAT) interactor
0,00769	Arpc1b	0,483	NM_023142.1	actin related protein 2/3 complex, subunit 1B
0,0492	null	0,485	null	null
0,0205	Clcn5	0,487	null	chloride channel 5
0,04	0910001L09Rik	0,487	null	RIKEN cDNA 0910001L09 gene
0,0156	E130306D19Rik	0,493	null	RIKEN cDNA E130306D19 gene
0,0285	Hist2h2be	0,494	NM_175666.1	histone 2, H2be
0,00348	Man1c1	0,494	NM_207237.1	mannosidase, alpha, class 1C, member 1
0,0197	C030044C12Rik	0,495	null	RIKEN cDNA C030044C12 gene
0,0486	Vamp5	0,496	NM_016872.1	vesicle-associated membrane protein 5
0,00179	LOC634163|Pcdha4	0,497	NM_007766.1	protocadherin alpha 4
0,00425	Actg1|LOC545167	0,497	NM_009609.2	actin, gamma, cytoplasmic 1
0,0424	Osgep	0,499	NM_133676.1	O-sialoglycoprotein endopeptidase

Pathway analysis for upregulated genes with DMHCA-treatment, DMHCA versus T0901317, showed no highly significant pathway regulation.

Table P. Pathway analysis: DMHCA-treated compared to T0901317-treated, up in DMHCA for *FC*≥2, p≤0.1; most abundant pathways

Category	Genes in Category	% of Genes in Category	Genes in List in	% of Genes in List in Category	p-Value
GO:42789: mRNA transcription from RNA polymerase II promoter	1	0,00732	1	1,695	0,00432
GO:9299: mRNA transcription	1	0,00732	1	1,695	0,00432
GO:47497: mitochondrion transport along microtubule	1	0,00732	1	1,695	0,00432
GO:7155: cell adhesion	543	3,975	7	11,86	0,00859
GO:42474: middle ear morphogenesis	2	0,0146	1	1,695	0,00862
GO:30903: notochord development	2	0,0146	1	1,695	0,00862
GO:46381: CMP-N-acetylneuraminate metabolism	2	0,0146	1	1,695	0,00862
GO:30503: regulation of cell redox homeostasis	2	0,0146	1	1,695	0,00862
GO:6730: one-carbon compound metabolism	39	0,285	2	3,39	0,0123
GO:35051: cardiac cell differentiation	3	0,022	1	1,695	0,0129
GO:6529: asparagine biosynthesis	3	0,022	1	1,695	0,0129
GO:6528: asparagine metabolism	3	0,022	1	1,695	0,0129
GO:48012: hepatocyte growth factor receptor signaling pathway	3	0,022	1	1,695	0,0129

163 genes were upregulated with DMHCA when DMHCA-treated MPM were compared with T0901317-treated cells (*FC*≥2, p≤0.05)

Table Q. Upregulated genes in DMHCA-treated compared to T0901317, up in DMHCA for p≤0.05 and *FC*≥2

P-value	Common	FC	Genbank	Description
0,0232	Car6	22,831	NM_009802.1	carbonic anhydrase 6
0,00747	Aqp9	15,699	NM_022026.2	aquaporin 9
0,00298	Olfr740	11,186	NM_146667.1	olfactory receptor 740
0,0345	LOC631403	6,667	null	null
0,0231	4632415K11Rik	6,410	null	RIKEN cDNA 4632415K11 gene
0,0319	Zc3h7a	5,618	NM_145931.1	zinc finger CCCH type containing 7 A
0,0191	Trib3	5,587	NM_144554.1	tribbles homolog 3 (Drosophila)
0,0194	BC062650	5,181	null	cDNA sequence BC062650
0,0207	Lrrc8a	4,975	NM_177725.2	leucine rich repeat containing 8A
0,00512	Zbtb10	4,975	null	zinc finger and BTB domain containing 10
0,00261	Kptn	4,950	NM_133727.1	kaptin
0,0488	Pcdh7	4,739	null	protocadherin 7
0,0125	LOC628772|LOC621500|LOC636273	4,525	null	null
0,0258	Bmp2	4,484	NM_007553.1	bone morphogenetic protein 2
0,0245	T	4,444	NM_009309.1	brachyury
0,0483	Maml3	4,274	null	mastermind like 3 (Drosophila)
0,016	null	4,098	null	null
0,0323	Akr1e1	4,082	null	aldo-keto reductase family 1, member E1
0,0241	Met	4,000	NM_008591.1	met proto-oncogene
0,0471	Mrg2	3,937	null	myeloid ecotropic viral integration site-related gene 2
0,0318	Cdr2	3,906	NM_007672.1	cerebellar degeneration-related 2
0,0209	LOC432675	3,831	null	null
0,0387	null	3,831	null	null
0,0183	Cmah	3,817	NM_007717.1	cytidine monophospho-N-acetylneuraminic acid hydroxylase
0,0161	Gcn1l1	3,788	null	GCN1 general control of amino-acid synthesis 1-like 1 (yeast)
0,00496	Olfr1106	3,584	NM_146752.1	olfactory receptor 1106
0,0483	4930511J11Rik	3,546	NM_029070.1	RIKEN cDNA 4930511J11 gene
0,0115	Dusp8	3,497	NM_008748.1	dual specificity phosphatase 8
0,0269	null	3,448	null	null
0,0329	Pck2	3,155	NM_028994.1	phosphoenolpyruvate carboxykinase 2 (mitochondrial)
0,0259	Fancd2	3,096	null	Fanconi anemia, complementation group D2
0,049	Foxn2	3,067	NM_180974.1	forkhead box N2
0,034	Ctsf	3,030	NM_019861.1	cathepsin F
0,015	Pabpc1	2,985	null	poly A binding protein, cytoplasmic 1
0,0147	Ift140	2,915	null	intraflagellar transport 140 homolog (Chlamydomonas)
0,00782	Mycbp	2,899	NM_019660.1	c-myc binding protein
0,00175	Dusp1	2,890	NM_013642.1	dual specificity phosphatase 1
0,0239	LOC620760	2,882	null	null
0,0385	LOC243423	2,874		null
0,0231	Chac1	2,801	NM_026929.2	ChaC, cation transport regulator-like 1 (E. coli)

0,0485	Wnk2	2,755	null	WNK lysine deficient protein kinase 2
0,028	A830021K08Rik	2,747	null	RIKEN cDNA A830021K08 gene
0,0264	Tmprss7	2,717	NM_172455.1	transmembrane serine protease 7
0,0287	C230076A16Rik	2,710	null	RIKEN cDNA C230076A16 gene
0,0164	LOC630318|LOC637592	2,703	null	null
0,0214	4930567K20Rik	2,695	null	RIKEN cDNA 4930567K20 gene
0,0478	Grpel2	2,632	NM_021296.1	GrpE-like 2, mitochondrial
0,0258	Trim55	2,611	null	tripartite motif-containing 55
0,0114	null	2,551	null	null
0,0362	C130057N11Rik	2,525	null	RIKEN cDNA C130057N11 gene
0,0186	Tcf15	2,519	NM_009328.1	transcription factor 15
0,0435	Col9a2	2,513	NM_007741.1	procollagen, type IX, alpha 2
0,0246	AA408296	2,494	NM_145415.2	expressed sequence AA408296
0,0241	LOC625123|2310042E22Rik	2,451	NM_025634.1	RIKEN cDNA 2310042E22 gene
0,0259	Slc25a14	2,439	NM_011398.1	solute carrier family 25 (mitochondrial carrier, brain), member 14
0,0462	Ptgir	2,433	NM_008967.1	prostaglandin I receptor (IP)
0,00311	null	2,381	null	null
0,0239	null	2,364	null	null
0,0393	Prr3	2,326	null	proline-rich polypeptide 3
0,0267	AI790205	2,299	null	expressed sequence AI790205
0,0294	C3	2,273	NM_009778.1	complement component 3
0,0126	9330123L03Rik	2,273	null	RIKEN cDNA 9330123L03 gene
0,0355	null	2,262	null	null
0,0484	null	2,262	null	null
0,0472	Mass1	2,232	null	monogenic, audiogenic seizure susceptibility 1
0,0279	R3hdm1	2,208	NM_181750.2	R3H domain 1 (binds single-stranded nucleic acids)
0,0205	Pir	2,174	NM_027153.1	pirin
0,00681	null	2,110	null	null
0,0325	null	2,105	null	null
0,026	9430015G10Rik	2,092	null	RIKEN cDNA 9430015G10 gene
0,00605	Rpl18	2,070	null	ribosomal protein L18
0,0352	Wdr67	2,066	null	WD repeat domain 67
0,0296	Elk4	2,045	NM_007923.1	ELK4, member of ETS oncogene family

Table R. Upregulated in D vs T, FC at least 2, p-value at least 0.01

P-value	Common	FC	Genbank	Description
0,00747	Aqp9	15,699	NM_022026.2	aquaporin 9
0,00298	Olfr740	11,186	NM_146667.1	olfactory receptor 740
0,00512	Zbtb10	4,975	null	zinc finger and BTB domain containing 10
0,00261	Kptn	4,950	NM_133727.1	kaptin
0,00496	Olfr1106	3,584	NM_146752.1	olfactory receptor 1106
0,00782	Mycbp	2,899	NM_019660.1	c-myc binding protein
0,00175	Dusp1	2,890	NM_013642.1	dual specificity phosphatase 1

0,00311	null	2,381	null	null
0,00681	null	2,110	null	null
0,00605	Rpl18	2,070	null	ribosomal protein L18

12.3 Additional LXRE

LXR bindings sites were detected with application of an *in silico* search program (Rephex) from Phenex Pharmaceuticals within the human and mouse promoter region of target genes.

Table S. LXR response elements with perfect match (0), 1 mismatch (1) and two mismatches (2) for human and mouse DUSP1, SORL1, CAR6, AQP9, SREBF1(SREBP1), and SREBF2 (SREBP2)

Name	Sequence	MM
human DUSP1		
Dual specificity protein phosphatase 1 (EC 3.1.3.48) (EC 3.1.3.16) (MAP kinase phosphatase 1) (MKP-1)		
-17625	AGATCACCTGAGGTCG	2
-11994	ACTTCAGCCCAGGTGA	2
-10176	AGATCACCTGAGGTCA	1
-9158	GGATCACTTGAGGTCA	2
-6896	TGGACAAGTCAGTTCA	2
2441	AGGCCACGGGAGGTGA	2
2551	ACTTCACCCGAGTTCC	2
8543	AGGTCTACGGAGTTGA	2
9237	AGATCACCTGAGTTCA	1
-13303	AGATCACTTGAGGCCA	2
-2505	AGGTCACTGCAAGCCA	2
1226	AGGACCAGCAAGTTCA	2
2606	AGTTCAGCAAATGTCT	2
3739	AGCTCACACCAGTACA	2
mouse DUSP1		
dual specificity phosphatase 1		
-17175	AGGCCAAGGTAGTTCA	1
-3825	AGGACTGTTGAGGTCA	2
2325	AGTTCCACTGAGTTCC	2
-14653	AGGCTAGAGGAGGTCA	2
-3063	AGTTCAAAGGAGAGCA	2
335	AGTTCAGCGTTGGGCA	2
2370	AGTTCAGCAAATGTCT	2
human SORL1		
Sortilin-related receptor precursor (Sorting protein-related receptor containing LDLR class A repeats) (SorLA) (SorLA-1) (Low-density lipoprotein receptor relative with 11 ligand-binding repeats) (LR11).		
-19076	GGATCACCTGAGGTCA	2
-14678	AGGTCATATTCTGTCA	2
-12101	AGATCACTTGAGGTCA	1
-3112	AGGACAGAGGAGGGCA	2
-1859	AGGTGACAGTGGTTCA	2
3519	GGATCACTTGAGGTCA	2
1595	AGTCAAGCAAAGGTCA	2
2458	AGTACAGGGAAGTTCT	2
7933	AGGTCACATCAGTTAC	2
mouse SORL1		
sortilin-related receptor, LDLR class A repeats-containing		
-11639	GGGTCACATAAGGCCA	2
-6083	AGGTCAAGAGGTTTCA	2
-1586	AGCTCATAGGAGGTCT	2
-1368	AGGTCAGATCATGACA	2
-17258	TGATCATCCAAGGTCA	2
-1032	ATTTCATCCTAGGTCT	2
human CA6		
Carbonic anhydrase 6 precursor (EC 4.2.1.1) (Carbonic anhydrase VI)		
-16429	AGGTCAGCTTTGTCCA	2
-13706	AGATCACTCGAGCTCA	2
-8328	GGATCACCTCAGGTCA	2
-7385	AGTTTAATAAAATTCA	2
-517	GGATCACCTGAGGTCA	2
1729	AGATCACCTGAGGTCA	1
6064	AGGTCATGCCACTGCA	2
6736	GGATCACTTGAGGTCA	2
7173	GGATCACTTGAGGTCA	2
8797	GGTTCAGGCAAGGTCC	2

-19636	TGATCACTTGAGGTCA	2
-18306	AGATCACCTGAGGTCA	1
-17894	GGATCATTTGAGGTCA	2
-16835	GGATCACCTGAGGTCA	2
-15976	AGATCACTTAAGTCCA	2
-14927	AGGCCAAGGTAGATCA	2
-12279	AAATCACCTGAGGTCA	2
-7584	GGATCACCTGAGGTCA	2
-3606	ATTTCATATCCGGTCA	2
-2997	AGATCACCTAAGGTCA	1
-2231	GGATCACTTGAGGTCA	2
948	AGATAACTTGAGGTCA	2
3102	GGATCACTTGAGGTCA	2
4482	GGGTCACTCTGGTTCA	2
5130	AGATCACTTGAGGTCA	1
5540	AGATCACCTGAGGTCA	1
8958	AGATCATGCCACTTCA	2
9133	GGATCACTTGAGGTCA	2
9601	AGTTCATAGAAATTCA	1
mouse CA6		
carbonic anhydrase 6		
-14995	ATTTCTCAGAAGTTCA	2
-14820	AGTTCACCCTACATCA	2
-10961	AGGTCAGAAGAGGGCG	2
3390	TGGTCACCTAAGGGCA	2
-13716	AGTTCACAGAGGTCCA	2
-3934	AGGTGAGCACAGGTGA	2
-3924	AGATCAAGGAAGGTGA	2
6766	AGTTTATTTTGGTTCA	2
human AQP9		
Aquaporin-9 (AQP-9) (Small solute channel 1),		
-19978	AGGTCATTGTAGTATA	2
-18567	GGATCACTTGAGGTCA	2
-18001	AGGTTTTCTTAGTTCA	2
-17271	AGGTGAGGTGAGTACA	2
-16923	GGATCACTTGAGGTCA	2
-16287	ATGTCAAAGGAGTTCT	2
-15149	AGGTCACCTTTGTTCA	1
-8544	AGTTCTGGCCAGGGCA	2
-3250	AGGGGAAGTGAGGTCA	2
5053	AGGACAAGAGAGGGCA	2
5063	AGGGCAAAGGAGGTTA	2
6999	GGATCACCTAAGGTCA	2
-4327	GGATCACCCAAGGTCA	2
3235	AGGGCACTGAAGGTAA	2
mouse aqp9		
-19004	AGGTCACGTCAGTAGA	2
-17374	AGATGACTGGAGTTCA	2
-6036	ACTTCCAGAAAGGTCA	2
-5673	AGGTCAGAAGAGATTA	2
-5597	AGGTCAGACGAGTTGC	2
-4217	AGGTCAGTGGAACTCA	2
8992	AGGACAGAGAATTTCA	2
-9238	AGTTCATGTGTTGTCA	2
-343	AATTTAGAATAGTTCA	2
1250	GGCTCACACCAGTTCA	2
7155	AGTTCTCAGTAGGTCC	2
SREBF1		
Sterol regulatory element-binding protein 1 (SREBP-1)		
-19921	AGCCCAGGGGAGTTCA	2
-17773	AGATCATTTGAGGCCA	2
-15036	AGGTGATTAAGGGTCA	2
-9240	AGGTCAGCACAGGTTC	2
-2026	GGATCACCTAAGGTCA	2
57	AGGCCAGGGCAGGACA	2
668	AGGTTACTCACGGTCA	2
-15653	AGATCACCTGAGGTCA	1
-2523	AGGTAAGACAAGGTCA	1
1683	AGGGCAGTGAAGGACA	2
3228	AGATCACCTGAGCTCA	2
mouse SREBF1		
sterol regulatory element binding factor 1		
-19118	AGGTCAGCCTAGGGAA	2
381	AGTTCACCAAAATTCC	2
-17241	AGGTCACATCAGGTAG	2
-16693	AGGACAAGGAAGGCCA	2
-7414	AGTTCACAAGAGTTGA	1

-7404	AGGACAGGACAGTTCA	1
-7081	AGGTCCCTCTAGGGCA	2
-4345	AGGCCACAGGAGTTCT	2
3715	AGTTAATTAAAAGTCA	2
5098	TGGTCACCTAAGCTCA	2

SREBF2

Sterol regulatory element-binding protein 2 (SREBP-2)

-18771	GGATCACCTGAGGTCA	2
-1135	AATTAACCCAAGGTCA	2
4221	GGATCACCTGAGGTCA	2
5396	GGATCACCCGAGGTCA	2
-9659	AGATCACTTGAGGTCA	1
-7800	AGGTCAGCCAGAGTCA	2
-1698	AGATCATTTGAGGTCA	1

mouse SREBF2

sterol regulatory element binding factor 2

-11981	AGGTGAAGTCAGGTCA	1
-1863	AGGTCAGAGAACTTCT	2
-1812	GGTTGATTTCAGGTCA	2
-17315	AGGCCACAGGAGGACA	2
-10569	AGGTCAACCTGGGTTA	2
-8747	GGGTCAACCCGGTTCA	2
-5300	AGAACAGGACAGGTCA	2
-4472	AGTTTAATTAAGCTCA	2
-4262	AGGTCAGAAAAGGGCA	1
-766	CCTTCAGACAAGGTCA	2
4859	AGTTGAACTCAGGTCC	2
7947	AGGCCAGAAGAGGACA	2
9133	AGGCCAGAAGAGGACA	2

12.4 Protein determination by two dimensional gel electrophoresis

After two dimensional gel electrophoresis was performed, proteins with at least 2-fold deregulation between DMHCA-treated and control-treated wild type mice were picked and analyzed with LC/MS.

Table T. Liver proteins up- or downregulated after 6 days i.p. injection of DMHCA (50mg/kg BW/day in 1.3% Tween80 and 0.25% carboxymethylcellulose) versus control for FC≥2

FC: Treated vs WT	protein name	ID number GI	ID # pept / % sequ2	Description
-2,28	glutathione S-transferase, mu3	33468899	11_46	Conjugation of reduced glutathione to a wide number of exogenous and endogenous hydrdophobic electrophils
-2,21	glutathione S-transferase, mu1	28386202	10_42	
2,37	Ribonuclease/angiogenin inhibitor 1 (u.p.p)	74203197	3_7	RNA catabolism; forms a tight complex with Rnase-inhibition of pancreatic Rnase and angiogenin
2,48	Aldolase 2, B isoform	21707669	10_24	Glykolyse, Gluconeogenese; fructose-bisphosphate,homotetramer,fructose metabolism,induced after feeding a carbohydrate diet,energy pathway,same affinity for F-1-P and F-1,6-P
	Alcoholdehydrogenase 1 (class I)	32449839	4_9	
-2,15	Proteasome (prosome, macropain) subunit, alpha type 1	13543191	2_9	The proteasome is a multicatalytic proteinase complex (at least 15 subunits) which is characterized by its ability to cleave peptides with Arg, Phe, Tyr, Leu, and Glu adjacent to the leaving group at neutral or slightly basic pH.
2,06	Dicarbonyl L-xylulose reductase u.p.p	74152058	7_30	Catalyzes the NADPH-dependent reduction of several pentoses, tetroses, trioses,alpha-dicarbonyl compounds and L- xylulose. Participates in the uronate cycle of glucose metabolism. May play a role in the water absorption and cellular osmoregulation in the proximal renal tubules by producing xylitol, an osmolyte, thereby preventing osmolytic stress from occurring in the renal tubules
	2810007J24 Rik protein u.p.p	26341170	4_15	
	cytochromeC-1 u.p.p	12833077	3_12	
2,55	hypoxiaup-regulated 1 u.p.p	74219123	21_22	Has a pivotal role in cytoprotective cellular mechanisms triggered by oxygen deprivation. May play a role as a molecular chaperone and participate in protein folding.
	PREDICTED: carbamoyl-phosphate synthetase 1 isoform 1	82879179	9_7	Involved in the urea cycle of ureotelic animals where the enzyme plays an important role in removing excess ammonia from the cell
-2,23	PREDICTED: carbamoyl-phosphate synthetase 1 isoform 1	82879179	18_12	
	threonyl-tRNAsynthetase u.p.p	26326983	10_15	Belongs to the class-II aminoacyl-tRNA synthetase family
	Transferrin	18606172	10_14	Transferrins are iron binding transport proteins which can bind two Fe(3+) ions inassociation with the binding of an anion, usually bicarbonate. It is responsible for the transport of iron from sites of absorption and heme degradation to those of storage and utilization. Serum transferrin may also have a further role in stimulating cell proliferation
	Lppprotein, hypothetical LOC288010 [Rattus	62078463	4_8	protein binding, metal ion binding, molecular function unknown

	norvegicus]			
-2,5	Transferrin	18606172	14_20	
	PREDICTED: carbamoyl-phosphate synthetase 1 isoform 1	82879179	13_10	
	threonyl-tRNAsynthetase u.p.p	26326983	5_7	
-2,36	Stress-70protein, mitochondrial precursor, u.p.p	74204605	12_17	
	albumin1, u.p.p	74137565	10_19	binds FA, negative regulation of apoptosis
-2,26	albumin1, u.p.p	74137565	18_32	
	Kars	20072717	6_8	lysyl tRNA synthetase
	Hemopexin	18044757	5_10	Binds heme and transports it to the liver for breakdown and iron recovery, after which the free hemopexin returns to the circulation
-2,17	albumin1, u.p.p	74137565	8_15	
	PREDICTED: similar to Plastin-3 (T-plastin) [Rattus norvegicus].	109510539	6_11	
-1,66	albumin1, u.p.p	74137565	17_28	
	Kars	20072717	11_13	
	gamma-glutamylcysteine synthetase	1815762	6_10	
	Aldh1l1 protein	23271467	5_6	Aldehyd dehydrogenase 1 family, member 1
	Hemopexin	18044757	5_10	
	TNF receptor-associated protein 1 [Rattus norvegicus]	54035509	5_6	Chaperone that expresses an ATPase activity
-2,28	albumin1, u.p.p	74137565	11_20	
	Hemopexin	18044757	5_10	
	Complement component 3	28175786	3_1	
-2,71	albumin1, u.p.p	74137565	20_35	
	Hemopexin	18044757	3_6	
	Kars	20072717	2_3	
-2,26	hypothetical protein LOC72361(carboxylesterase precursor) NM197	37574080	7_12	
	PREDICTED: similar to 60 kDa heat shock protein, mitochondrial precursor (Hsp60) (60 kDa chaperonin)	51766670	16_11	Implicated in mitochondrial protein import and macromolecular assembly. May facilitate the correct folding of imported proteins. May also prevent misfolding and promote the refolding and proper assembly of unfolded polypeptides generated under stress conditions in the mitochondrial matrix
	albumin1, u.p.p	74137565	5_9	
	Carboxylesterase 6	19354488	5_8	
-1,06	T-complexprotein1 (TCP-1), u.p.p	74220827	4_7	Molecular chaperone; assists the folding of proteins upon ATP hydrolysis. Known to play a role in vitro in the folding of actin and

				tubulin
	Carboxylesterase 6	19354488	4_8	
-2,03	Vinculin	14250200	40_44	Involved in cell adhesion. May be involved in the attachment of the actin-based microfilaments to the plasma membrane
	heterogenous nuclear ribonucleoprotein U, u.p.p	74186692	6_9	Binds to pre-mRNA. Has high affinity for scaffold- attached region (SAR) DNA. Binds to double- and single-stranded DNA and RNA
	PREDICTED: similar to Carbamoyl-phosphate synthase [ammonia], mitochondrial precursor (Carbamoyl-phosphate synthetase I)	94363632	6_4	
-2,54	PREDICTED: similar to Carbamoyl-phosphate synthase [ammonia], mitochondrial precursor (Carbamoyl-phosphate synthetase I)	94363632	34_30	
-2,4	Transferrin	20330802	32_48	
	PREDICTED: similar to Carbamoyl-phosphate synthase [ammonia],mitochondrial precursor (Carbamoyl-phosphate synthetase I)	94365161	9_7	
-2,37	Rho GDP dissociation inhibitor (GDI) alpha	56541074	3_19	Regulates the GDP/GTP exchange reaction of most Rab proteins by inhibiting the dissociation of GDP from them, and the subsequent binding of GTP to them
	RAN binding protein 1	6755284	3_11	Inhibits GTP exchange on Ran. Forms a Ran-GTP-RANBP1 trimeric complex. Increase GTPhydrolysis induced by the Ran GTPase activating protein RANGAP1. May act in an intracellular signaling pathway which may control the progression through the cell cycle by regulating the transport of protein and nucleic acids across the nuclear membrane

Table U. Proteins in macrophages, up- or downregulated after 6 days i.p. injection of DMHCA (50mg/kg BW/day in 1.3% Tween80 and 0.25% carboxymethylcellulose) versus control for FC≥2

FC: Treated vs WT	protein name	ID number GI	ID # pept / % seq	Description
2,55	Heat shock 90kDa protein 1, beta	51859516	7_11	Molecular chaperone. Has ATPase activity, protein binding, ATP binding
	Cathepsin D, u.p.p	26354406	6_16	Acid protease active in intracellular protein breakdown. Involved in the pathogenesis of several diseases such as breast cancer and possibly Alzheimer's disease, proteolysis, lysosome, mitochondrion
	Eno1 protein [Rattus norvegicus]	38649320	4_12	Multifunctional enzyme, glycolysis, growth control, hypoxia tolerance, allergic responses; may function in the intravascular and pericellular fibrinolytic system-serves as a receptor and activator of plasminogen on the cell surface
2,52	cathepsin B, u.p.p	74213457	5_15	Thiol protease, which is believed to

				participate in intracellular degradation and turnover of proteins. Has also been implicated in tumor invasion and metastasis
	PREDICTED: similar to Histone H2B 291B [Rattus norvegicus], Hist2h4protein	109504977	4_12	central role in nucleosome formation
	gamma actin, PREDICTED: similar to myosin VIIb [Rattus norvegicus].	109506410	3_1	motor activity, ATP binding
	u.p.p, 14-3-3 protein gamma	74215924	3_10	inhibitor of apoptosis through inhibiting the activation of p38 MAP kinase
2,9	protective protein for beta-galactosidase isoform a	84042525	7_16	
	PREDICTED: similar to FK506-binding protein 4 (Peptidyl-prolyl cis-trans isomerase)	109472679	5_6	May play a role in the intracellular trafficking of hetero-oligomeric forms of steroid hormone receptors
	PREDICTED: similar to heat shock protein 8	83001113	3_7	chaperone, increases cell survival by inhibting the apoptotic programme
	similar to Glyceraldehyde-3-phosphate dehydrogenase (GAPDH) [Mus musculus].	82893986	3_7	glycolysis, gluconeogenesis
-2,84	PREDICTED: desmoplakin isoform 1	82950147	9_4	
	Gliamaturationfactor, beta	29165811	2_23	This protein causes differentiation of brain cells, stimulation of neural regeneration, and inhibition of proliferation of tumor cells
	Junction plakoglobin	26252155	2_3	Common junctional plaque protein
-3,09	peptidyloropylisomerase (cyclophilin_ABH_like), u.p.p	12846244	7_30	
	Rho GDP dissociation inhibitor (GDI) alpha	56541074	4_22	anti-apoptotic
	peroxiredoxinV	6644338	4_25	Reduces hydrogen peroxide and alkyl hydroperoxides with reducing equivalents provided through the thioredoxin system. Involved in intracelular redox signaling
2,12	ATPase, H+ transporting, V0 subunit D isoform 1 [Rattus norvegicus].	58865424	3_7	exact function is unknown
2,25	PREDICTED: similar to myosin VIIb [Rattus norvegicus], u.p.p	109506410	5_2	
	PREDICTED: similar to Histone H2B 291B [Rattus norvegicus]	109504977	3_10	
	PREDICTED: similar to 40S ribosomal protein S20 [Rattus norvegicus].	62648896	3_25	
	u.p.p, similar to ubiquitin-conjugating enzyme E2	12838544	3_17	glycolysis
	PREDICTED: similar to coactosin-like 1 [Rattus norvegicus]	34851815	3_11	
2,24	PREDICTED: desmoplakin isoform 1	82950147	4_2	
	CathepsinD, u.p.p	26354406	2_6	
2,43	PREDICTED: similar to Histone H2B 291B [Rattus norvegicus]	109504977	4_13	
	PREDICTED: similar to coactosin-like 1 [Rattus norvegicus].	34851815	3_11	actin binding, enzyme binding, biological process unknown
2,12	LOC433182 protein, Eno1protein	53734652	4_13	
	u.p.p, Biliverdin reductase A	12832065	2_9	Heme metabolism
-2,19	LOC433182 protein, Eno1protein	53734652	13_38	MBP1 binds to the c-myc promoter

				and acts as a transcriptional repressor. May be a tumor suppressor
	u.p.p, Arginase family, Arginase1-liver	74146247	7_25	Arginine degradation via the urea cycle; first step
	Proteasome (prosome, macropain) 26S subunit, non-ATPase, 14	13277672	6_30	
	Pyrophosphatase (inorganic) 2	15030287	4_17	
2,17	u.p.p, lactate dehydrogenase1, A-chain	74217959	8_25	
-2,26	PREDICTED: desmoplakin isoform 1	82950147	9_3	
	Junction plakoglobin	26252155	5_7	
2,41	u.p.p, CathepsinB	74213457	8_30	response to oxidative stress, mitochondrion, peroxidase activity
	Chloride intracellular channel 1	13435562	8_43	seems to act as a chloride ion channel
	PREDICTED: similar to myosin VIIb [Rattus norvegicus]	109506410	6_2	
3,7	u.p.p, valosin containing protein	74198702	12_19	transitional endoplasmic reticulum ATPase, complexing with clathrin, and heat-shock protein Hsc70
	u.p.p, CathepsinB	74213457	8_30	
	u.p.p, Chloride intracellular channel 1	74198647	4_24	
-2,99	PREDICTED: similar to myosin VIIb [Rattus norvegicus]	109506410	5_2	
	u.p.p, BiP, Hsp70	74198293	5_9	
	u.p.p, vimentin	74199770	5_13	biological process unknown, cell motility, oxygen transport
	u.p.p., CathepsinD	26354406	4_15	
	u.p.p, Prolyl4-hydroxylase, beta polypeptide (thioredoxin, thyroid hormone binding protein	54777	4_9	
2,61	Rho GDP dissociation inhibitor (GDI) alpha	56541074	3_19	
	RAN binding protein 1	6755284	3_11	
-2,66	tyrosine 3-monooxygenase/tryptophan 5-monooxygenase activation protein, zeta polypeptide [Rattus norvegicus]	62990183	12_48	14-3-3 zeta, proteinkinase C inhibitor protein
	u.p.p, vimentin	74199770	11_23	
	u.p.p, AnnexinV	74151976	10_33	
	u.p.p, ribonuclease/angiogenin inhibitor 1	74203197	5_12	
2,19	Aconitase 2, mitochondrial	63101587	3_5	
3,11	Protein-arginine deiminase type-4	13542680	11_20	Anticoagulant protein acting as an indirect inhibitor of the thrombo-plastin-specific complex, which is involved in the blood coagulation cascade
	SAM domain and HD domain, 1	45501315	7_12	
-3,15	Transketolase	33244005	16_31	pentose-phosphate pathway
2,55	Tumor rejection antigen gp96 (predicted) [Rattus norvegicus].	51858886	13_18	Molecular chaperone that functions in the processing and transport of secreted proteins, Hsp90
	Junction plakoglobin	26252155	6_9	
-2,33	TOAD-64 [Rattus rattus].	599966	5_12	
	u.p.p.,ATPase, H+ transporting, V1 subunit A, isoform 1	74184909	4_9	
4,35	PREDICTED: similar to Actin, cytoplasmic 2 (Gamma-actin), Rat	109507063	9_21	?
	PREDICTED: similar to Histone H2B 291B [Rattus	109504977	7_20	

	norvegicus]			
	u.p.p., heat shock 70kD protein 5	74198293	6_12	
	u.p.p., CNDP dipeptidase 2 (metallopeptidase M20 family)	74182267	6_14	
3,67	keratin oder desmoplakin isoform 1???????			
2,52	u.p.p, CathepsinB	74213457	5_15	
	PREDICTED: similar to myosin VIIb [Rattus norvegicus].	109506410	3_1	DR4: AGGGCATCTACGGGCA, AGGTCAGGAGGGTCCA
	PREDICTED: similar to Histone H2B 291B [Rattus norvegicus]	109504977	4_12	
	u.p.p., 14-3-3 protein gamma	74215924	3_10	5 DR4
2,9	protective protein for beta-galactosidase isoform a,Cathepsin A	84042525	7_16	
	PREDICTED: similar to FK506-binding protein 4	109472679	5_6	
	PREDICTED: similar to heat shock protein 8	94387987	3_7	
-2,84	PREDICTED: desmoplakin isoform 1	82950147	9_4	
	Glia maturation factor, beta	29165811	2_23	
	Junction plakoglobin	26252155	2_7	
-3,09	u.p.p., cyclophilin_ABH_like	12846244	7_30	
	Rho GDP dissociation inhibitor (GDI) alpha	56541074	4_22	
	peroxiredoxin V	6644338	4_25	
2,12	PREDICTED: ATPase, H+ transporting, V0 subunit D isoform 1, (predicted) [Rattus norvegicus]	62665162		
	PREDICTED: desmoplakin isoform 1	82950147	3_0	
2,25	PREDICTED: similar to myosin VIIb [Rattus norvegicus].	109506410	5_2	
	PREDICTED: similar to Histone H2B 291B [Rattus norvegicus].	109504977	3_10	
	PREDICTED: similar to 40S ribosomal protein S20 [Rattus norvegicus].	62648896	3_25	
	u.p.p., putative ubiquitin-conjugating enzyme E2N	12838544	3_17	
2,24	PREDICTED: desmoplakin isoform 1	82950147	4_2	
	Cathepsin D, u.p.p	26354406	2_6	
2,43	PREDICTED: similar to Histone H2B 291B	109504977	4_13	
	PREDICTED: similar to myosin VIIb [Rattus norvegicus]	109506410	3_1	
	PREDICTED: similar to coactosin-like 1 [Rattus norvegicus]	34851815	3_11	
2,08	t-complex protein 1, u.p.p	74195576	14_33	protein folding, transport
	Protein disulfide isomerase associated 3	23958822	7_15	
	mKIAA0098 protein, Chaperonin GroEL (HSP60 family)	37359776	3_7	
	TOAD-64 [Rattus rattus]	599966	3_7	
-2,06	glucose-6-phosphate dehydrogenase X-linked, full insert sequence, u.p.p	74138546	23_43	Carbohydrate degradation; pentose phosphate pathway
	coronin, actin binding protein 1A [Rattus norvegicus]	18426834	4_9	
2,46	BiP, heat shock 70kD protein 5 (glucose-regulated)	74198974	19_34	anti-apoptotic
	PREDICTED: similar to myosin VIIb [Rattus norvegicus]	109506410	12_4	
	ATPase, H+ transporting, V1 subunit B, isoform 2, u.p.p.	74195936	7_16	
	Atp5b protein, ATP synthase, H+ transporting	23272966	6_14	

	mitochondrial F1 complex, beta subunit			
	PREDICTED: similar to Histone H2B 291B [Rattus norvegicus]	109506410	6_15	
	CNDP dipeptidase 2, (metallopeptidase M20 family), MNCb-1930 protein	74182267	5_13	
	PREDICTED: similar to tubulin, beta 2 [Rattus norvegicus]	109504787	3_5	
	ATP synthase, H+ transporting, mitochondrial F1 complex, alpha subunit, isoform 1 [Rattus norvegicus]	38512279	3_7	
2,06	TOAD-64 [Rattus rattus]	599966	9_20	
	peptidase 4	6679279	7_15	
	BiP, heat shock 70kD protein 5 (glucose-regulated protein)	74198974	6_12	
	ATPase, H+ transporting, V1 subunit B, isoform 2, u.p.p.	74195936	5_11	
	Coronin, actin binding protein 1A	31418362	3_9	
2,06	aldehyde dehydrogenase 2, u.p.p.	74213579	19_48	glycolysis, FA metabolism
	RuvB-like protein 1 [Rattus norvegicus]	55824715	9_25	
	Chaperonin subunit 2 (beta)	13938629	4_9	
	uridine monophosphate synthetase	33859498	4_10	
	sphingomyelin phosphodiesterase, acid-like 3A	74198753	3_8	
-2,9	M2-type pyruvate kinase [Mus musculus]	1405933	17_39	glycolysis, gluconeogenesis
	Unknown (protein for MGC:116262) [Rattus norvegicus] ,region ABC_SMC6_euk	71051822	3_5	
2,44	mKIAA0573 protein, Thioredoxin domain containing 4	50510531	9_25	Inhibits the calcium channel activity of ITPR1
	u.p.p., CathepsinD	26354406	9_26	
	plasma cell-specific thioredoxin-related protein; PC-TRP	37936005	6_18	
	u.p.p., p105 coactivator	74179806	5_5	
	Atp5b protein	23272966	5_11	
	u.p.p, prolyl 4-hydroxylase, beta-polypeptide, thyroid hormone binding protein-like	54777	4_9	
	u.p.p., CNDP dipeptidase 2	74182267	4_9	
	protein disulfide isomerase-associated 6 , TRX-domain	58037267	3_10	
	u.p.p., heat shock protein 1, alpha	74147334	3_4	
2,95	u.p.p., PREDICTED: similar to Actin, cytoplasmic 2 (Gamma-actin) [Rattus norvegicus]	109507063	10_23	
	u.p.p., cathepsin B	74213457	9_35	
	u.p.p., cathepsin D	26354406	6_19	
	Serine (or cysteine) peptidase inhibitor, clade B, member 6a, PAI-2	13879569	6_19	
	u.p.p., PAI-2 (Plasminogen Activator Inhibitor-2),serine protease inhibitor 8	26331716	6_18	
2,57	PREDICTED: similar to Actin, cytoplasmic 2 (Gamma-actin) [Rat]	109507063	10_23	
	Chloride intracellular channel 1	13435562	10_28	
	u.p.p., cathepsin B	74213457	9_34	
	PREDICTED: similar to Histone H2B 291B [Rattus norvegicus]	109504977	6_18	
	Protein disulfide isomerase associated 3	23958822	3_6	

	u.p.p., Annexin A5	74151976	3_8	Anticoagulant protein acting as an indirect inhibitor of the thrombo-plastin-specific complex, which is involved in the blood coagulation cascade
2,37	Capping protein (actin filament), gelsolin-like	13097498	8_30	
	protein disulfide isomerase-associated 6, TRX-domain	58037267	6_16	
	LOC433182 protein ,similar to enolase 1, alpha non-neuron	53734652	6_18	
	annexin A7 [Rattus norvegicus]	18426844	6_15	
	u.p.p., Annexin A1	74183811	2_7	
2,91	vimentin	31982755	16_35	
	Tumor rejection antigen gp96 (predicted) [Rattus norvegicus]	51858886	8_11	
	u.p.p., cathepsin B	74213457	6_24	
	interleukin 1, beta	6680415	4_16	
	u.p.p, lectin, galactoside-binding, 90K protein precursor	74212546	3_6	
	Phosducin-like 3 [Rattus norvegicus]	68533843	3_12	
-4,11	u.p.p., Annexin A5	74151976	10_32	Anticoagulant protein acting as an indirect inhibitor of the thrombo-plastin-specific complex, which is involved in the blood coagulation cascade
	PREDICTED: similar to Actin, cytoplasmic 2 (Gamma-actin) [Rattus norvegicus]	109507063	7_15	
	chitinase 3-like 3, u.p.p.	74210387	5_17	
	PREDICTED: similar to 60 kDa heat shock protein, mitochondrial precursor	94391428	5_11	
	tyrosine 3-monooxygenase/tryptophan 5-monooxygenase activation protein, zeta polypeptide	74187552	3_13	
	u.p.p., vimentin	74199770	3_6	
-3,73	PREDICTED: similar to myosin VIIb [Rattus norvegicus]	109506410	10_4	actin binding, ATP binding, motor activity
	u.p.p., Prolyl 4-hydroxylase, beta polypeptide, thyroid hormone binding protein	54777	9_27	
	heat shock 70kD protein 5 (glucose-regulated protein), 78kDa glucose-regulated protein, u.p.p	74198293	7_13	
	Bcl2-associated athanogene 1	110611812	7_21	has anti-apoptotic activity
	tyrosine 3-monooxygenase/tryptophan 5-monooxygenase activation protein, zeta polypeptide, u.p.p	74187552	6_30	
	gelsolin	28916693	6_8	
	u.p.p., Cathepsin D	26354406	5_17	
	u.p.p., valosin containing protein	74198702	3_5	
2,55	Serine (or cysteine) peptidase inhibitor, clade B, member 1a	74354376	7_22	
	u.p.p., Cathepsin D	26354406	4_10	
	mKIAA1258 protein, guanine deaminase	50510861	3_6	purine metabolism
-2,98	Glutathione S-transferase, mu 1	28386202	8_38	
-2,5	mKIAA1258 protein, guanine deaminase	50510861	9_20	
	PREDICTED: similar to myosin VIIb [Rattus	109506410	7_3	

	norvegicus].			
	tyrosine 3-monooxygenase/tryptophan 5-monooxygenase activation, protein, zeta polypeptide [Rattus norvegicus].	62990183	6_30	
	mKIAA1027 protein [Mus musculus], talin 1 ?	49022858	4_2	
	eukaryotic translation initiation factor 4A2	7305019	3_7	
	u.p.p, fibrinogen, gamma polypeptide	74143561	3_6	
-2,05	PREDICTED: similar to myosin VIIb [Rattus norvegicus]	109506410	8_4	
	mKIAA1258 protein, guanine deaminase	50510861	8_20	
	LOC433182 protein, Eno1protein	53734652	5_14	
	M2-type pyruvate kinase	1405933	5_12	
	u.p.p., Cathepsin D	26354406	4_15	
2,2	AHNAK nucleoprotein isoform 1	61743961	4_3	
	u.p.p.; tubulin,beta 3	74223783	3_7	
3,63	PREDICTED: desmoplakin isoform 1	82950147	3_1	
	PREDICTED: similar to SET and MYND domain-containing protein 1	109472157	3_4	
-3,25	Annxa1	70912321	14_47	$^{Ca2+}$ and PL binding protein which promotes membrane fusion and is involved in exocytosis
	u.p.p., eukaryotic translation elongation factor 2	74181334	8_13	
	alpha-N-acetyl-galactosaminidase	19547877	6_12	
	M2-type pyruvate kinase	94405226	3_5	
2,27	PREDICTED: similar to heterogeneous nuclear ribonucleoprotein A3 (rat)	94373120	3_9	
	u.p.p., Cathepsin D	26354406	3_6	
-2,84	Transketolase, Thiamine pyrophosphate (TPP) family	33244005	17_35	pentose-phosphate pathway
	PREDICTED: similar to myosin VIIb [Rattus norvegicus]	109506410	4_1	
	u.p.p., Annexin A1	74183810	3_9	
	PREDICTED: similar to Histone H2B 291B [Rattus norvegicus]	109504977	3_7	
-2,37	Transketolase	33244005	11_23	
-2,26	M2-type pyruvate kinase	1405933	10_27	glycolysis
-2,73	LOC433182 protein, similar to enolase 1, alpha non-neuron	53734652	11_33	
	coronin, actin binding protein 1A [Rattus norvegicus]	18426834	4_8	Present in macrophages. May be a crucial component of the cytoskeleton of highly motile cells, functioning both in the invagination of large pieces of plasma membrane, as well as in forming protrusions of the plasma membrane involved in cell locomotion
3,62	Eukaryotic translation elongation factor 1 alpha 1	13278382	8_17	
2,53	put. beta-actin	49868	8_32	
	serpin (Plasminogen Activator Inhibitor-2 (PAI-2))	2398729	6_21	
	Heat shock 90kDa protein 1, beta [Rattus norvegicus]	51859516	4_6	
	mKIAA0051 protein, IQ motof containing GTPase activating protein	37359752	3_2	
2,6	u.p.p., aldo-keto reductase family 1, member A4 (aldehyde reductase)	74226780/79	10_35	

-3,2	u.p.p., tubulin, beta 5	74141821	3_8	
-3,4	Malate dehydrogenase 2, NAD (mitochondrial)	19484047	11_42	
	PREDICTED: similar to tubulin, beta 2 [Rattus norvegicus]	109504787	11_16	
	PREDICTED: similar to Actin, cytoplasmic 2 (Gamma-actin) [Rattus norvegicus]	109507063	10_23	
	Tubulin, alpha 1 [Rattus norvegicus]	38328248	9_29	
	Atp5b protein, ATP synthase, H+ transporting mitochondrial F1 complex, beta subunit	23272966	9_23	
	ATP synthase, H+ transporting, mitochondrial F1 complex, alpha subunit, isoform 1 [R. norvegicus]	38512279	7_16	
	ATPase, Na+/K+ transporting, alpha 1 polypeptide [Rattus norvegicus]	6978543	6_8	
	tyrosine 3-monooxygenase/tryptophan 5-monooxygenase activation protein [Rattus norvegicus]	13928824	5_21	!!!
	PREDICTED: similar to Histone H2B 291B [Rattus norvegicus]	109504977	5_12	
2,46	u.p.p., cathepsin B preprotein	74213457	7_29	
	PREDICTED: similar to myosin VIIb [Rattus norvegicus]	109506410	5_2	
2,12	annexin II; calpactin 1 [Rattus sp.]	9247200	6_20	
	aldose reductase	786001	4_13	
2,37	Mus musculus myosin, heavy polypeptide 1, skeletal muscle, adult (Myh1)	82524273	47_25	62656256removed (rat)
	PREDICTED: similar to Actin, cytoplasmic 2 (Gamma-actin) [Rattus norvegicus]	109507063	15_30	62657474 removed
	u.p.p., tropomyosin 1, alpha	26346649	9_29	
	u.p.p., cathepsin D	26354406	7_21	
	Myosin light chain 1, skeletal muscle isoform (MLC1F) (A1 catalytic) [Rattus norvegicus]	127131	5_38	
	creatine kinase, muscle	6671762	4_14	
	enolase 3, beta muscle	6679651	4_12	
-3,08	vimentin	31982755	14_32	
3,26	Annexin A2	13097099	10_33	Ca^{2+} and PL binding protein,calpactin 1,involved in exocytosis, annexin A2 inhibits PCSK9 function
	u.p.p., aldo-keto reductase family 1, member B3 (aldose reductase)	74226524	7_20	
	u.p.p., pre-B-cell colony-enhancing factor 1, nicotinamide phosphoribosyltransferas	74147564	4_10	
2,61	u.p.p., cathepsin D	26354406	4_10	
3,59	u.p.p., EIA homolog, Serpinb1a protein	26345114	6_18	
	u.p.p., septin 2	74195946	3_11	
	u.p.p., cathepsin D	26354406	3_8	
2,45	PREDICTED: similar to RAN, member RAS oncogene family	94368195	2_8	
-2,16	Proteasome (prosome, macropain) subunit, beta type 3	15928628	7_39	
	Triosephosphate isomerase 1	28436836	5_26	
-2,05	PREDICTED: similar to myosin VIIb [Rattus norvegicus]	109506410	2_0	
-2,82	gelsolin	28916693	4_7	